The Effect of Microorganisms on the Surface Properties of Chalcopyrite

by

Yi Yang
(M. Sc.)

Mineral Resources
CSIRO
School of Chemical & Physical Sciences
Flinders University

September 2014

Thesis submitted to Flinders University for Degree of Doctor of Philosophy (Chemistry)

TABLE OF CONTENT

Declaration

I declare that this thesis does not incorporate without acknowledgement any material previously submitted for a degree or diploma in any university. To the best of my knowledge this thesis does not contain materials previously published or written by another person except where due reference is made in the text.

……

Yi Yang

List of Publications

The following publications or manuscripts have arisen from work completed by the candidate for the present thesis.

Yang, Y., Liu, W., Chen, M., 2013. A copper and iron K-edge XANES study on chalcopyrite leached by mesophiles and moderate thermophiles. Minerals Engineering 48, 31-35.

Yang, Y., Harmer, S., Chen, M., 2014. Synchrotron X-ray photoelectron spectroscopic study of the chalcopyrite leached by moderate thermophiles and mesophiles. Minerals Engineering, 69, 185-195.

Yang, Y., Liu, W., Chen, M., 2014 XANES and XRD study of the effect of ferrous and ferric ions on chalcopyrite bioleaching at 30 ^{o}C and 48 ^{o}C. Minerals Engineering (Accepted)

Yang, Y., Harmer, S., Chen, M. Synchrotron-based XPS and NEXAFS study of surface chemical species during electrochemical oxidation of chalcopyrite. Submitted to Hydrometallurgy (in revision)

Yang, Y., Harmer, S., Tan, S.N, de Jonge, M., Paterson, D., Spiers, K., Chen, M. μ-XRF and Raman study of the galvanic assisted chalcopyrite bioleaching with extreme thermophile and mesophiles. Submitted to Hydrometallurgy (in revision)

Yang, **Y.**, Tan S.N, Glenn, M., Harmer, S., Chen, M. A direct observation of bacterial population dynamics and film formation of *Acidithiobacillus ferrooxidans* at chalcopyrite and pyrite surfaces. In preparation

Acknowledgements

First of all, I would like to give my sincere thanks to my supervisor Dr. Miao Chen who was always available to offer supervision, support and inspiration with thoughtful ideas and excellent skills in the last three years. I wish to thank my principal supervisor Dr. Sarah Harmer, for her support in all aspects, especially for her professional guidance in challenging synchrotron experiments.

The work of this project was done in Mineral Resources Flagship of CSIRO. I wish to thank Mineral Resources Flagship of CSIRO for providing the resources and funds for my research and stipend throughout the project and the University of South Australia and Flinders University for the cover of international student tuition fee.

I wish to thank Su Nee Tan for her help and training in daily lab work and AFM measurement, as well as her inspirative suggestions.

I wish to acknowledge Dr. Weihua Liu for his help in XAS experiment, for his patient and professional help during the proposal preparation, data collection and analysis. I wish to acknowledge my gratitude to Dr. Victor Qu for the training in electrochemical measurement and Dr. Adrian Trinchi for his training and assist in Raman measurement. Acknowledges also are made to Dr Sam Yang, Dr Mayo Sherry, Ms Ruru Li for training in CT tomography data collection and analysis. Acknowledges are extended to the beamline scientists and staff in Australian synchrotron and KEK for their kind assistance.

Sincere thanks to my group members, Guohua Gu, Lianxiang Yu, Qinyou Liu, Mikko Vepsalainen, Rachel Brokenshire and Yan Jin who have been part of the research family and accompanied me.

Finally, thanks must also go to my father and my mother, for their loving, supporting and understanding which help bring my thesis to life.

List of Figures

List of Tables

Table 7-2 The fitting results of Fe K-edge XANES analysis of leached residue collected after 14 and 31 days of leaching (wt%)

Abstract

To understand the chalcopyrite dissolution and passivation mechanism during bioleaching, the leaching kinetics, surface species, mineralogy and bacteria-mineral interaction under different conditions (temperature, Eh, pyrite, Ag^+ and bacteria species) have been investigated. X-ray photoelectron spectroscopy (XPS), X-ray absorption spectroscopy (XAS), Powder X-ray diffraction (XRD), Raman spectroscopy, X-ray fluorescence microscopy (XFM) and Electron backscatter diffraction (EBSD) have been applied in this study.

The results indicate thermophiles significantly enhanced the leaching efficiency, which was mostly caused by the increased abiotic reaction rate. Cu K-edge XANES analysis indicated the formation of CuS_n-like species in the early stages of leaching. XPS results show a sulfur-rich layer developed with time which is likely to be the rate limiting factor of the surface reaction. There is no significant difference on surface sulfur speciation between the chalcopyrite bioleached at 48 or 30 ^oC.

The electrochemical studies show that there was an activated region in the middle of two passive regions for chalcopyrite dissolution. In the active region, between 550 to 630 mV (vs. Ag/AgCl), S_n^{2-}/S^0, S_2^{2-} species and covellite were found by XPS and Raman. XPS study suggested a thin sulfur rich layer formed in the first passive region (530 mV). At 650 mV, S_2^{2-} species and covellite started to dissolve, leaving a highly metal deficient polysulfide layer.

Bacterial concentration at the mineral surfaces increased to about 5-7% coverage in 24 hrs. Raman spectroscopy showed the presence of organic species in the colourful film covered areas, which confirmed the formation of biofilm. From EBSD and optical images analysis, no significant difference in selectivity of bacterial attachment was found on crystal orientation of chalcopyrite.

Low Eh (350-480 mV vs. Ag/AgCl) significantly promoted the chalcopyrite (bio)leaching. The leaching results and quantitative XRD and XANES analysis show jarosite and elemental sulfur did not primarily account for the passivation of chalcopyrite. Secondary mineral covellite was detected in chalcopyrite dissolution.

Chalcopyrite leaching was significantly enhanced by pyrite addition. Chalcopyrite was selctively leached in chemical leaching as a result of galvanic effect. The favourable influence of galvanic effect and to chalcopyrite leaching is at least partially because of its function on Eh control. However, in bioleaching pyrite dissolution was significant which decreased the chalcopyrite leaching efficiency. μ-XRF and Raman studies suggest a sulfur-rich layer developed inhomogenously on mineral. The galvanic effect was also verified in column leaching of low grade chalcopyrite, which increased the yield of copper by a factor of about 3 in bioleaching.

The bioleaching effeciency of chalcopyrite was enhanced at low concentration of Ag^+ but decreased at high concentration of Ag^+. AgCuS species was found in the leaching residue. The solution pH of the case with high concentration of Ag^+ increased significantly in bioleaching but not in chemical leaching, which caused the formation of hematite.

Introduction

As high grade copper resources are depleted, the exploitation of low grade, complex copper ores becomes increasingly important. In many cases, those ores are not economically profitable to be processed by conventional pyrometallurgy technologies, while biohydrometallurgy provides an alternative (Brierley, 2010; Brierley, 2008). Biohydrometallurgy possesses several advantages over pyrometallurgy technology, for instance, it consumes less energy and is more environmental-friendly. Biohydrometallurgy has been successfully applied into commercial use for secondary copper sulfide recovery. However, for chalcopyrite, the most abundant copper sulfide mineral in terms of availability, its leaching rate in application is still not economically feasible. The dissolution mechanism of chalcopyrite in bioleaching process needs to be better understood in order to enhance the chalcopyrite leaching rate, in order to apply it in commercial scale.

So far, the dissolution mechanism of chalcopyrite is generally considered via polysulfide pathway as indirect mechanism, in which chalcopyrite is attacked and dissolved by the Fe^{3+} and H^{+} generated by bacteria (Sand et al., 2001). In this process, various species containing Fe, Cu, and S are generated at the mineral surface (Rodríguez et al., 2003; Sandström et al., 2005; Sasaki et al, 2009). These surface chemical products carry information about the chalcopyrite decomposition mechanism, which is not clear in the presence of bacteria. Besides the oxidative decomposition described above, an alternative mechanism has been proposed by Hiroyoshi et al (2000), which considers the reduction of chalcopyrite to secondary minerals at low Eh values, and needs to be further understood.

The surface chemistry and the mineralogy changes during chalcopyrite bioleaching also prominently affect the kinetics of chalcopyrite bioleaching. Passivation is one of the major issues that retards the application of chalcopyrite bioleaching, and this is apparently related some of the leaching products. Unfortunately, the nature of the passivation layer is still in debate (Klauber, 2008; Liang et al., 2010; Rodríguez et al., 2003; Sandström et al., 2005; Sasaki et al, 2009). The surface chemical species are influenced by various conditions such as pH, Eh, temperature, impurities and bacteria species, and related to the

kinetics variation (Rodr ́guez et al., 2003; Vilcaez et al., 2008, 2009; Liang et al., 2010). Those connections are of vital importance in establishing an improved model of chalcopyrite leaching.

Although it is generally accepted there is no direct enzymatic attack from microorganisms to chalcopyrite, studies indicate the cell attachment and biofilm is important for mineral dissolution (Sand and Gehrke, 2006). The physical attachment of bacteria to mineral surfaces has also been proposed to accelerate leaching. The biofilm formation at mineral surfaces upon bacteria-mineral attachment provides a reaction space enriched in ferric ions. It is worthy to study the behaviour of the bacteria attachment and biofilm formation to determine how the microorganisms interact with chalcopyrite.

Therefore, this thesis aims to understand the surface species and properties changes in chalcopyrite bioleaching in response to the different environment conditions (temperature, Eh, pyrite, catalyst and bacteria species) as well as the interaction between bacteria and chalcopyrite, by which a deeper understanding to chalcopyrite dissolution mechanism and facilitates the establishment of a connection among the surface change, leaching kinetics, and environmental conditions, which further helps to establish a better control for chalcopyrite bioleaching. To achieve this purpose, the combination of solution and surface properties will be carried out. The surface characterization will be endeavoured to be carried out in inert atmosphere. With the combination of leaching study and electrochemical study, a range of state-of-art methods such as XPS, XAS, XRD and Raman and the morphologic techniques such as AFM, XFM played a key role in this project.

Chapter 1 Literature review

1.1 Chalcopyrite structure

1.1.1 Crystal structure

Chalcopyrite is a covalent copper sulfide that is isostructural with sphalerite (ZnS) (Li et al., 2013). The chalcopyrite structure may be derived from the structure of zinc blende by ordering of the two cations of copper and iron alternately on the cation sublattice and the cubic symmetry of the ZnS structure is replaced by a tetragonal symmetry (Petiau, 1988; Miller et al., 1981). The unit cell dimensions of chalcopyrite are a = b = 5.2890 Å and c = 10.4230 Å (Hall and Stewart, 1973). In chalcopyrite crystal, each sulphur atom is tetrahedrally coordinated to four metal atoms (2 Cu and 2 Fe) and each metal atom is tetrahedrally coordinated to four sulphur atoms. The S-Fe-S angle is 109.47 °with an Fe-S interatomic spacing of 2.257 Å, while the tetrahedron centered on the copper atoms is slightly distorted and the S-Cu-S angles vary from 108.68 ° to 111.06 ° with a Cu-S distance of 2.302 Å (Jones, 2006) (Fig. 1-1).

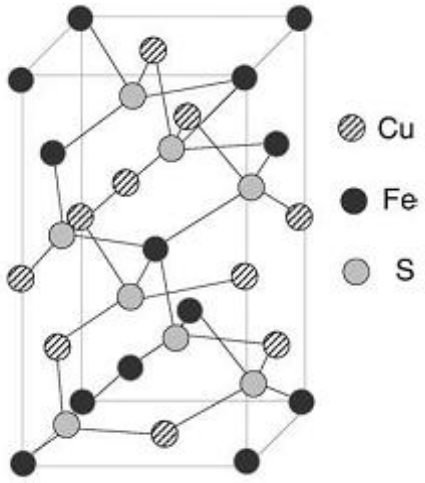

Fig. 1-1 Crystal structure of chalcopyrite (reprinted from Sand et al., 2001)

1.1.2 Oxidation state

The oxidation state of metals in chalcopyrite has been extensively studied in order to understand their fundamental crystal chemical properties and the processes of mineral formation and breakdown. Generally, the oxidation state of chalcopyrite is considered in

the form of $Cu^{I}Fe^{III}S_2^{II-}$. Using Mössbauer spectroscopy, iron atoms have been recognized in the Fe(III) state (Rai et al., 1968; Mussel et al., 2007). X-ray photoelectron spectroscopy (XPS) and X-ray absorption spectroscopy (XAS) have led to the same conclusion, showing that copper is likely to be monovalent (Nakai et al., 1978; God et al., 2006; Petiau, 1988). With the results from *2p* XPS, L-edge XANES and Mössbauer spectroscopy, Pearce et al. (2006) classified chalcopyrite into the monovalent copper category, and identify formal valency formula for chalcopyrite as $Cu^{I}Fe^{III}S_2^{II-}$ with the "d count" in the copper compounds between d^9 and d^{10}. Mikhlin et al. (2005) found Cu L_3-edge presented a strong pre-edge peak and a small post-edge peak shifted to higher energy. The pre-edge peak was proposed to be due to the electron transition from Cu 2p to 3d at 931 eV indicating a minor occurrence of Cu $3d^9$. The intensity of the Cu^{2+} main XAS peak is 25 times greater than that of Cu^{+} (Pearce et al., 2006), which means that a minor amount of Cu^{2+} may present.

1.2 Microorganisms in bioleaching

1.2.1 Diversity of acidophilic microbes

Extremely acidophilic microbes are the most predominant metal-sulfide-dissolving species used in bioleaching industry, which thrive at pH values below 3 and are able to oxidize either inorganic sulfur compounds and/or iron(II) ions (Rohwerder et al., 2003). Although the acidophiles live in very extreme environment, which has high acidity and low concentration of nutrient with harsh temperatures in some cases, they still show a microbial diversity with at least 11 putative prokaryotic divisions living at AMD sites (Baker and Banfield 2003; Hallberg and Johnson 2001; Johnson 1998; Rohwerder et al., 2003). According to the growth temperatures, they can be classified into mesophiles (<40^{o}C), moderate thermophiles (40-60^{o}C) and extreme thermophiles (>60^{o}C).

Acidithiobacillus genus (formerly known as *Thiobacillus*) is the most classic bioleaching species (Kelly and Wood, 2000), which includes *Acidithiobacillus ferrooxidans* (*A.f*), *Acidithiobacillus thiooxidans* (*A.t*) and *Acidithiobacillus albertensis* (*A.b*). *A. ferrooxidans* is the first isolated extremely acidophilic sulfur- and/or iron(II)-oxidizing bacteria. For many years it was considered as the most important microorganism in the bioleaching of sulphide ores operating at temperature lower than 40 ^{o}C (Brierley, 1982; Kelly and Wood, 2000; Lundgren and Silver, 1980), therefore it is also the most researched bioleaching species from genetic to industrial levels (Valdés et al., 2008).

Leptospirillum is another important genus in bioleaching industry. Important members of this genus include *Leptospirillum ferrooxidans* and *Leptospirillum ferriphilum* only oxidize iron(II) (Hippe 2000; Coram and Rawlings 2002). Using the analysis of the 16 S rDNA amplification products of total DNA, current researches show that the iron-oxidising *L. ferrooxidans* have been found as the dominant populations in bioleaching tanks that contain nickel ores with low iron content at the end of the experiments, in copper ores leached at low ferrous iron concentration and in a continuous flow biooxidation tank for the treatment of gold-bearing arsenopyrite concentrates (Falco et al., 2003; Rawlings et al., 1999). Compared to *A. ferrooxidans*, *L. ferrooxidans* has a greater affinity for ferrous iron and is less sensitive to inhibition by ferric iron (Norris *et al.*, 1988). '*Leptospirillum* '-like bacteria have also been reported to be more acid resistant than *A. ferrooxidans*, which can grow at a pH of 1.2 (Norris, 1983). With regard to temperature, *L. ferrooxidans* has been reported to have an upper limit of around 45 ^{o}C, which is more tolerant of high temperatures than *A. ferrooxidans* (Norris et al., 1986; Rawlings et al., 1999).

Other leaching proteobacteria are species of the genus *Acidiphilium* such as *A. acidophilum* (Hiraishi et al. 1998). Members in this group can grow heterotrophically using organic compounds such as glucose, and can improve the growth of chemotropic microorganism such as *A. ferrooxidans* by consuming the organic waste produced by metabolism (Yang et al., 2013). There are also reports about the mesophilic and acidophilic iron(II)-oxidizing archaea. Two species belong to the Thermoplasmales, *Ferroplasma acidiphilum* and *F. acidarmanus* have been reported to have iron(II)-oxidizing ability (Edwards et al. 2000; Golyshina et al. 2000; Rohwerder et al., 2003)

Most of the moderately thermophilic species are from *Acidimicrobium*, *Ferromicrobium*, and *Sulfobacillus*, which are gram-positive leaching bacteria (Rohwerder et al., 2003). Members of *Sulfobacillus* spp. such as *Sulfobacillus thermosulfidooxidans* are typical moderate thermophiles, which was firstly isolated from thermal areas in Iceland and can be used for bioleaching in conditions where the temperature is in the 50–55 ℃ range. (Le Roux et al., 1977; Golovacheva and Karavaiko, 1978; Brierley 2008). They are able to oxidize ferrous ions but require the addition of 0.02% (w/w) yeast extraction (Brierley and Le Roux, 1977). The studies by Norris et al.(1980) and Norris and Barr (1985) indicate these microbes cannot use sulfate as a source of sulfur and the yeast extract or reduced forms of sulfur are required a source of organic sulfur for growth of the bacteria.

A. caldus is a moderately thermophilic species of *Acidithiobacillus* spp. The study of Dopson and Lindstrom (2003) show the amount of elemental sulfur was less in the bioleaching of arsenic pyrite with a mixture of *A.caldus* and *S. thermosulfidooxidans* than with pure *S. thermosulfidooxidans*, which indicates *A. caldus* is able to oxidize reduced sulfur compounds more effectively.

Most of the extreme thermophiles are Achaea, which can oxidize reduced inorganic sulfur compounds and/or Fe(II) ions in aerobic condition, or reduce iron(III) ion anaerobically coupled by the oxidation of sulfur compounds or hydrogen (Brock et al., 1972; Kurosawa et al., 1998; Segerer et al., 1991). The habitat of extreme thermophiles is stringently restricted. They can usually been found in acidic hot spring (>60^{o}C) or hydrothermal vents. *Sulfolobus* is one of the most studied genus in extreme thermophiles. They can grow chemotropically or heterotrophically using reduced sulfur compounds and/or simple organic compounds with an optimum temperature of 60-70 ^{o}C and pH around 1.5 (Brock et al., 1972). In bioming with temperature over 70^{o}C, *Sulfolobus metalicus* has been found to be the most prominent species (Rawlings et al., 2005). Archaea belong to the genus *Acidianus* such as *A. brierley*, *A. ambivalensi* or *A. infernu*s are also capable of growing at high temperature (Fuchs et al., 1996; Konishi et al., 2001; Segerer et al., 1986). Other extreme thermophiles from *Metallosphaera* spp., *Stygiolobus* spp., *Sulfurisphaera* spp. have also been reported (Kurosawa et al., 1998; Segerer et al., 1991).

1.2.2 Roles of the bacteria

There are two hypothesis proposed for the role of bacteria in bioleaching -- direct and indirect mechanisms. The direct mechanism concerns the adhesion of bacteria to the surface of sulfide minerals, inducing the oxidation process (Brierley, 1978; Sharma et al., 2003). The assumption is the action of a metal sulfide-attached cell oxidizing the mineral by an enzyme system with oxygen to sulfate and metal cations. The sulfur moiety of the mineral is supposed to be biologically oxidized to sulfate without any detectable intermediate occurring (Sand et al., 2001). However, so far there is not report on the hypothesized enzyme system yet.

In contrary, indirect mechanism suggest the bioleaching is mainly a chemical process in which ferric iron and protons are responsible for the leaching reactions. According this mechanism, iron (II) ions and elemental sulfur which form in the process of bioleaching are bacterially oxidized to iron(III) and sulfate. The role of the microorganisms is to

generate the leaching chemicals and to create the space in which the leaching reactions take place (Sand et al., 2001; Sharma et al., 2003). The overall role of microbes could described by following equations (Qiu et al., 2007; Rohwerder et al., 2003):

$$2\ Fe^{2+} + 1/2\ O_2 + 2\ H^+ \xrightarrow{\text{bacteria}} 2\ Fe^{3+} + H_2O \qquad (1\text{-}1)$$

$$2S + 3O_2 + 2H_2O \xrightarrow{\text{bacteria}} 2SO_4^{2-} + 4H^+ \qquad (1\text{-}2)$$

1.2.3 Iron and sulfur oxidation pathways of acidophiles

As the leaching of minerals is considered to be a chemical process that results from the action of ferric iron and/or acid, iron and sulfur oxidizing abilities of the leaching microbes directly affect the leaching efficiency. As the main energy sources of leaching microbes, the iron(II) irons and sulfur serve as electron donors during respiration (Rawlings, 2005).

1.2.3.1 Iron oxidation

In aerobic condition, Fe(II) irons serve as an electron donor and O_2 molecules sever as final electron acceptor. As the difference in redox potential between the $Fe^{2+/}Fe^{3+}$ (+770 mV at pH 2) and O_2/H_2O (+820 mV at pH 7) is small and because only one mole of electrons is released per mole of iron oxidized, vast amounts of ferrous iron need to be oxidized to produce small amount of energy. (Rawlings, 2005; Vera et al., 2013).

The mechanism of iron oxidation has been most extensively studied for the bacterium *A. ferrooxidans* (Rawlings, 2005). A model for iron oxidation is shown in Fig. 1-2. Electrons are firstly transferred from the membrane-located cytochrome c2 to rusticyanin (Yarzábal et al., 2002). The Electrons then can either be transported along a “downhill” or an “uphill” pathway (Vera et al., 2013).The downhill path is via cytochrome c4 (Cyt1) to cytochrome aa3 or the uphill via cytochrome c4 (CytA1) to a bc1 I complex and a NADH-Q oxidoreductase (Rawlings, 2005). In the last few years, more information about the redox chains of aerobic iron(II)-oxidizing bacteria has been revealed (Blake and Griff, 2012). On the basis of spectroscopic biochemical and “omics” analyses, it can be stated that the iron(II)-oxidizing systems of the other acidophilic iron-oxidizing bacteria have different redox components and therefore have alternative iron oxidation mechanisms (Bonnefoy and Holmes, 2011).

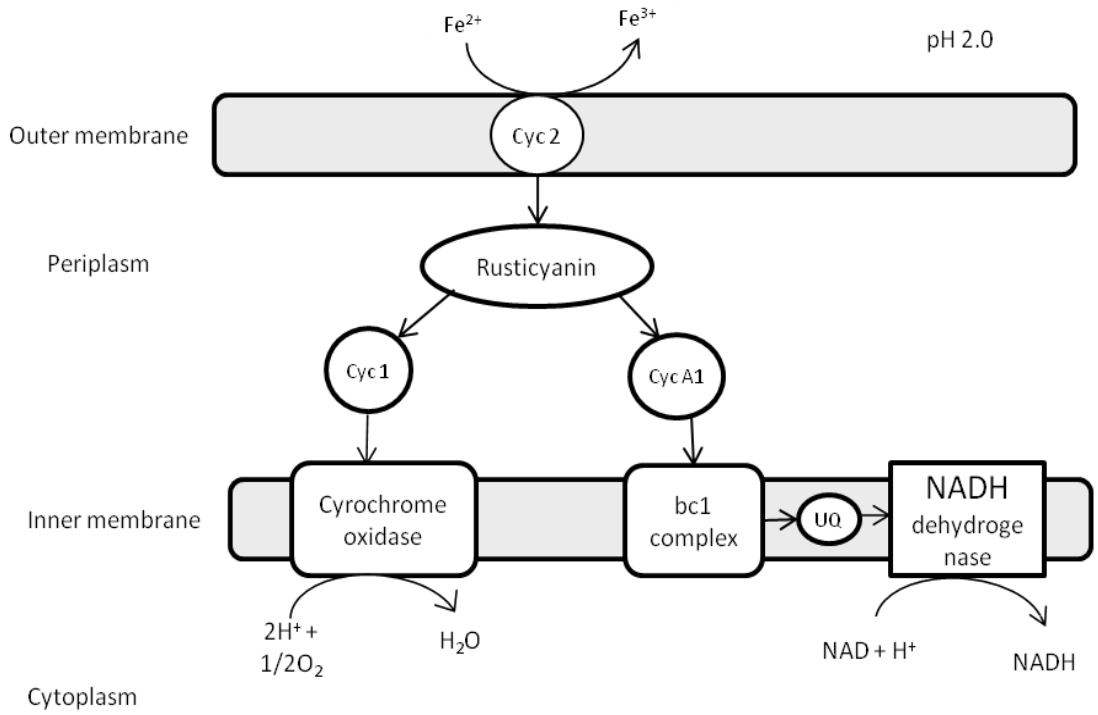

Fig. 1-2 The Model of electron transport in *Acidithiobacillus ferrooxidans*. (Cyc: cyctochrome c; UQ: ubiquinone. Redrawn from Johnson and Hallberg, 2009; Rawlings, 2005)

1.2.3.2 Sulfur oxidation

The pathways involved in sulfur oxidation by acidophilic bacteria are less understood compared to iron (Rawlings, 2005). The study of Rohwerder and Sand (2003) found S_8 ring will be attacked by GSH forming a linear monoorganylpolysulfane compounds (GS_nH, n>1) (Eq. (3). The GS_nH species react with each other or with excess GSH to form GSSG or its higher homologous bisorganylpolysulfanes (GS_nG, n>2) and H_2S (Eq. (4)). They proposed extracellular elemental sulfur is mobilized by thiol groups of special outer-membrane proteins and transported into the periplasmic space. The chain-like sulfur is then oxidized by periplasmic sulfur dioxygenase (SDO). In the further step, the sulfite is oxidized to sulfate by sulfite:acceptor oxidoreductase (SOR). At the same time, free sulfide is oxidized by a separate dehydrogenase (SQR), which uses quinones (Q) as electron acceptors. This mechanism is summaried in Fig. 1-3. The study of Rohwerder and Sand (2003) also indicates the sulfide oxidation requires the disulfide of glutathione to react non-enzymatically with sulfide to give glutathione persulfide prior to enzymic oxidation. At the same time, free sulfide can also be oxidized to elemental sulfur by a sulfide:quinone oxidoreductase, located in the periplasmic site of the cytoplasmic

membrane. One of function of the thiol groups of the outer-membrane proteins is to keep the zero valence sulfur not precipitating.

However, they suggest there are two critical issues unsolved with the sulfur oxidation pathway for *Acidithiobacillus* spp (Rohwerder and Sand, 2007). Firstly, the enzyme, termed sulfur diooxygenase (SDO), has not been characterized yet, although its activity was demonstrated in several studies and partial purification was achieved (Rohwerder and Sand, 2007); secondly, the thiol-bearing membrane proteins have not been identified yet, though some proteins such the sulfide-binding protein isolated from *A. ferrooxidans* AP19-3 (Sugio et al., 1991) and several outer-membrane proteins associated with sulfur oxidation in *A. ferrooxidans* (Ohmura et al., 1996) may possibly to be the candidate (Rohwerder and Sand, 2007).

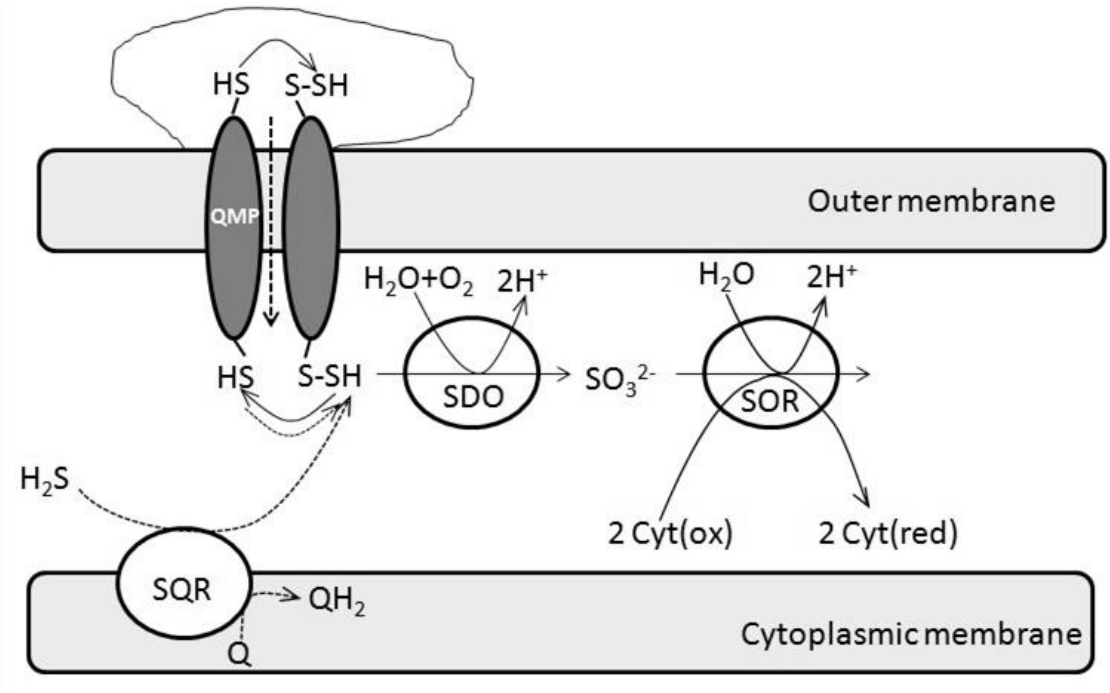

Fig. 1-3 Proposed model for sulfur oxidation in *Acidithiobacillus ferrooxidans*. (SDO: periplasmic sulfur dioxygenase; Cyt: cytochrome; SOR: oxidoreductase; SQR: dehydrogenase; Q: quinones; OMP: outer-membrane proteins. Redrawn from Rohwerder and Sand (2003))

1.3 Bacterial attachments to mineral

Attachment of bacterial cells onto the mineral surface is essential for the contact and cooperative mechanisms. The physical attachment of bacteria to mineral surfaces has also been proposed to accelerate leaching. Biofilm formation at mineral surfaces upon

bacteria-mineral attachment provides a reaction space enriched in ferric ions (Sand and Gehrke, 2006). Studies show more than 80% of the bacteria could attach to the mineral surface within 24 h of inoculation (Gehrke et al. 1998; Harneit et al. 2006; Vera et al., 2013). The attachment process is predominantly mediated by the extracellular polymeric substances (EPS) surrounding the cells, which also provided a micro-enviroment for the Fe^{3+} attack on the metal sulfide (Fig. 1-4). Sand and the coworkers thoroughly studied the characteristics and composition of EPS excreted by *A. ferrooxidans* and its relationship with cell attachment. Primary attachment occurs mainly by electrostatic interactions between positively charged cells with the negatively charged pyrite surface (Vera et al., 2013). Also, hydrophobic interactions contribute somewhat to the attachment to metal sulfide surfaces (Gehrke et al. 1998; Sampson et al. 2000), although this applies especially to very hydrophobic surfaces, e.g. of elemental sulfur. The amount and composition of EPS are significantly impacted by the substrate the cells grown on. For instance, cells grown on different elemental sulfur contain considerably less sugars and uronic acids and most importantly complexed iron(III) ions, but much more fatty acids than EPS from pyrite-grown cells (Gehrke et al. 1998).

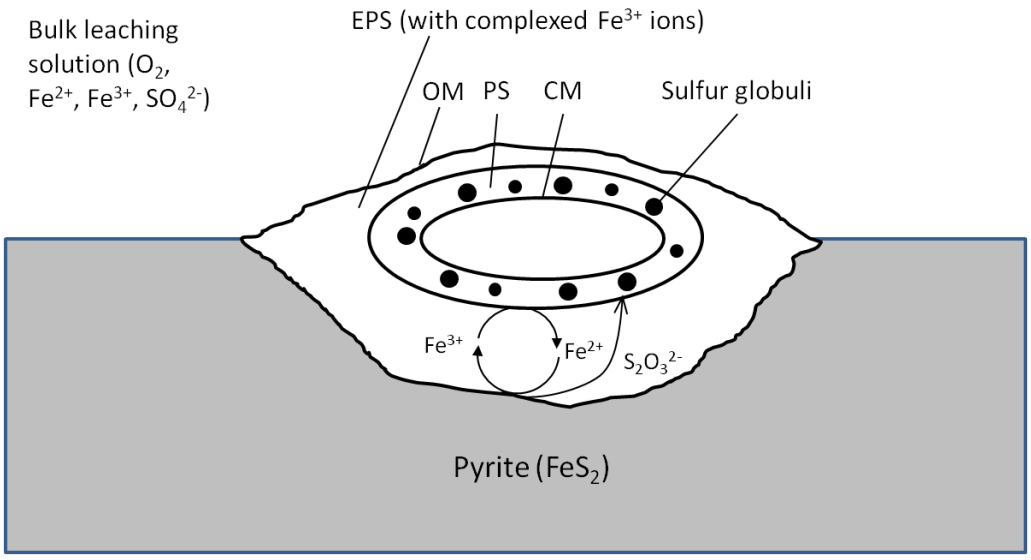

Fig. 1-4 Model for the contact leaching mechanism catalyzed by a cell of *A. ferrooxidans*. (CM: Cytoplasmic membrane, PS: periplasmic space, OM: outer Membrane. Redrawn from Rohwerder et al., 2003)

The sites of attachment have been extensively studied in the case of pyrite (Vera et al., 2013). Selective attachment of bacteria to defective surfaces of mineral was reported previously (Sand et al., 2001). For example, atomic force microscopy (AFM) as well as

confocal laser microscopy (CLSM) images demonstrate that cells of *A. ferrooxidans* preferentially (>80 %) attach to sites with visible surface imperfections (scratches, etc.) (Vera et al., 2013).

In an sense of electrochemistry, dissolution of metal sulfide occurs at local anodes, bringing iron(II) ions and thiosulfate in solution in the case of FeS_2. Vera et al. (2013) pointed out that the micro-anode and cathode may be a result of imperfections in the crystal lattice where the iron-to-sulfur ratio is not exactly 1:2. As several strains of *A. ferrooxidans* and *L. ferrooxidans* are chemotaxic to iron(II)/(III) ions and thiosulfate (Acuña et al. 1992; Meyer et al. 2002), it may be speculated that the cells are chemotactically attracted to the local anodes.

Meanwhile, Ndlovu and coworkers have published a series of paper studying the influence of crystal orientation on the initial rate of bacterial dissolution of pyrite (Ndlovu and Monhemius, 2003; Ndlovu and Monhemius, 2004; Ndlovu and Monhemius, 2005). They have reported a difference in surface corrosion pattern when pyrite was leached chemically and biotically, suggesting the surface film formed at mineral surfaces due to bacterial attachment contributed to the enhancement in leaching of pyrite. The iron terminated 111 plane showed the least overall leaching enhancement by bacteria and the absence of bacterial colonization.

For chalcopyrite, different crystal orientations have different surface atomic arrangements, and one orientation also contains different surfaces. For instance, in S-terminated ((001)-S) surface, there are eight S atoms in the first atomic layer and four Fe and four Cu atoms in the second layer in a two unit cell supercell. In contrast, for the (001)-M surface, in the two-unit cell model, there are four Fe and four Cu atoms in the first layer with eight S atoms in the next layer (de Oliveira and Duarte, 2010). In the (111)-M (metal terminated) surface, there are two Fe and two Cu in the first layer in the one unit cell model, although these four metal atoms are not exactly in the same plane (de Oliveira et al., 2012). In contrast, the (012) plane is the only surface consisting of an equal number of metal atoms (Cu and Fe) and S atoms (Von Oertzen et al., 2006). Recent studies by Cai and coworkers reported selective leaching of chalcopyrite in the 001 and 112 plane in the presence of hydrochloric acid (Cai et al., 2012). The chloride ions can penetrate the structure of chalcopyrite to remove sulfur from these planes.

1.4 Studies on mechanisms of chalcopyrite dissolution

1.4.1 General aspects

Chalcopyrite is acid soluble (Sand et al., 2001). Its dissolution is generally considered happen under the attack of Fe^{3+} and H^{+} via polysulfide mechanism (Fig. 1-5). In this model chalcopyrite is oxidized by Fe^{3+}, and the surface sulfur species change to sulphate via a chain of polysulfide derivations. For this model the overall reaction could be described as equation 1-3 and 1-4.

$$CuFeS_2 + 4Fe^{3+} \rightarrow Cu^{2+} + 5Fe^{2+} + 2S \quad (1\text{-}3)$$

$$2S + 3O_2 + 2H_2O \xrightarrow{\text{bacteria}} 2SO_4^{2-} + 4H^{+} \quad (1\text{-}4)$$

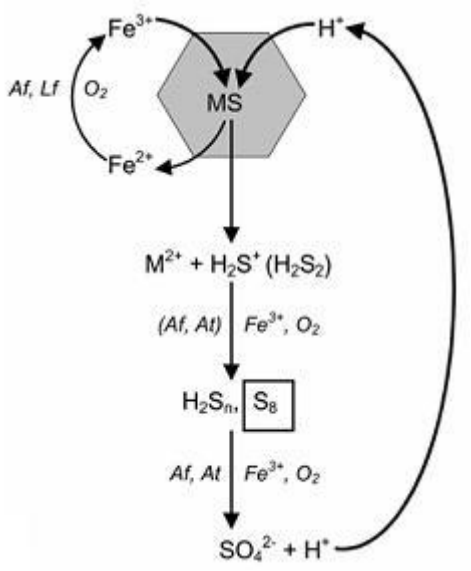

Fig. 1-5 Scheme of polysulfide mechanism in bioleaching of acid-soluble metal sulphides (Sand et al., 2001)

1.4.2 Surface studies

To further understand the detailed mechanisms of chalcopyrite oxidation and dissolution, substantial efforts have been made through spectroscopy studies.

England el al. (1999) examined the oxidation of chalcopyrite using Fe and Cu K-edge EXAFS spectroscopy. On the oxidized chalcopyrite surfaces, the development of Fe-O and Cu-O species was observed and the changes of the Fe-S, Cu-S bond length were detected. These structural changes may have influence on the mineral chemical states and thus the leaching properties; however the relevant studies are quite limited, especially in bioleaching system. Buckley and Woods (1984) observed the exposure of a chalcopyrite

fracture surface to air resulted in a decrease in the surface concentrations of copper and sulfur relative to iron, which became concentrated at the surface as a hydroxide/oxide. They also found copper remained bonded to sulfur as Cu (I) in the initial stages of oxidation, but Cu (II) appeared along with sulfate after 10 days, suggesting that copper sulfate was formed.

Previous studies indicate metal irons in chalcopyrite will be firstly removed, leaving a sulfur rich layer in leaching. In an early XPS study conducted by Buckley and Woods (1984), the authors found the presence of $Cu_{1.3}FeS_{2.7}$ when the freshly fractured chalcopyrite was immerse in 0.2 M acetic acid media for 1 h whilst $Cu_{1.4}FeS_3$ formed after 24 hours. A surface composition of near $Cu_{0.8}S_2$ formed on leaching of freshly fractured chalcopyrite in 0.2 M acetic acid media for 40 days. In addition, when the samples leached in acetic acid was further immersed in hydrogen peroxide (H_2O_2) for 5 min, a surface layer containing S^0 as well as Fe-deficient Cu sulfide formed.

Hackl et al. (1995) performed XPS and Auger electron spectroscopy (AES) on O_2 pressure leached chalcopyrite identifying a CuS_n layer approximately l μm thick. This layer, with a stoichiometry close to CuS_2, was proposed to be leach-rate determining. A similar result has been found by Todd et al. (2003), who proposed that CuS_n ($n > 2$) was the main component in the surface layer resulting from the leaching process.

Harmer et al. (2006) studied the chemical leaching process of chalcopyrite by XPS, and a 3 step-leaching was proposed: The initial oxidation step involves the release of Cu and Fe into solution and the polymerisation of monosulfide (S^{2-}) to polysulfide S_n^{2-}. The subsequent reduction step does not result in the release of cations to solution but does result in the reformation of surface $S^{2-}$and other short chain polysulfides, which then on further oxidation restructure to form crystalline elemental sulfur (S^0). Relevantly, in Raman study by Parker (2008), the short chain of S-S was also confirmed. On the other hand, Klauber et al. (2001) and Parker et al. (2003) dismissed the possibility of S_n^{2-} formation claiming that only the sulfur species S^{2-}, S_2^{2-} (disulfide), S^0 (elemental sulfur) and SO_4^{2-} (sulfate) are detectable on leached $CuFeS_2$ surfaces.

Some secondary mineral have also been detected or proposed in chalcopyrite dissolution. Covellite has been detected by a several authors using Raman, XANES, and XRD (Córdoba et al. 2008a; Sasaki et al., 2009; Zhu et al., 2011). Córdoba et al. (2008a) found the presence of CuS in the leaching products at short times by using XRD. They

suggested the formation of covellite was more likely to be an intermediate during chalcopyrite oxidation. Sasaki et al. (2009) studied bioleaching of chalcopyrite with *A. ferrooxidans* using Raman spectroscopy, they found the presence of covellite when Eh was over 700 mV. Those results suggest covellite is most likely to form in an oxidation process. Chalcopyrite firstly oxidizes, forming CuS as an intermediary product:

$$CuFeS_2 \rightarrow 0.75CuS + 1.25S^0 + 0.25Cu^{2+} + Fe^{2+} + 2.5e^- \qquad (1\text{-}5)$$

Then, covellite is oxidized by ferric sulphate, releasing Cu^{2+} ions:

$$CuS \rightarrow S^0 + Cu^{2+} + 2e^- \qquad (1\text{-}6)$$

In the same time, Arce and González (2002), Velásquez et al. (2005) proved the chalcocite is a possible intermediate in chalcopyrite oxidation through electrochemical method. Thus, the investigation of Cu, Fe and S species on chalcopyrite surface in bioleaching under different conditions provides information of the critical substances and their formation condition thus enables a deeper understanding of chalcopyrite dissolution mechanism.

1.4.3 Electrochemical study on chalcopyrite bioleaching

In chalcopyrite oxidation, some of the intermediate deputed according to the present theories are transparent and unstable, thus they cannot be studied via the common leaching experiment. Online measurements should be employed to understand the leaching process.

Electrochemical method can provide sensitive information to the reaction of chalcopyrite oxidation, thus can be used to analyze the possible intermediates. The electrochemical method also provides information of the controlling steps, passivation process, etc. Parker et al. (1981) studied the electrochemical process of chalcopyrite and attribute the metal – deficient layer as the barrier to Cu^{2+} and Fe^{2+} diffusion. Arce and González (2002) also found non-stoichiometric compound rather than covellite. Nava and González (2006) studied the dissolution mechanism of chalcopyrite, and the potential range on passivation by carbon paste electrodes with chalcopyrite, the results indicate the initial dissolution produced a non-stoichiometric polysulfide ($Cu_{1-r}Fe_{1-s}S_{2-t}$) at $0.615\ V \leq E_{anod} < 1.015\ V$ versus SHE. At $1.015\ V \leq E_{anod} < 1.085\ V$, the non-stoichiometric polysulfide converted into a porous form that allowed the diffusional transport of charged species and the dissolution of the mineral. In the region of $1.085\ V \leq E_{anod} < 1.165\ V$ versus SHE,

formation of covellite (CuS) was identified, which gives rise to complete dissolution of the chalcopyrite in a further enhancement of potential. In a reduction process, Nava et al. (2008) reported in the potential range of 0.115≥Ecat≥−0.085 V the formation of a product with the composition between chalcopyrite and bornite, and when potential was lower than -0.085V, it will be reduced to bornite; in the range of −0.085 to −0.285 V, bornite partially decomposed into chalcocite. As the most recent research, Ghahremaninezhad et al. (2010) investigated a massive chalcopyrite electrode electrochemical behaves in 0.5 M sulfuric acid solution. They prompted a thin layer of $Cu_{1-x}Fe_{1-y}S_2$ ($y \gg x$) formed on the surface from OCP to 100 mV (vs. MSE); At higher potentials 100-300 mV (vs. MSE) the previously formed surface layer partially dissolved and a second passive layer ($Cu_{1-x-z}S_2$) formed; at a potential over 500 mV (vs. MSE), another pseudo-passive CuS layer formed. Some authors reported there are distinct passive and active regions, in a potentiodynamic curve (Ghahremaninezhad et al., 2010; Majuste et al., 2012).

As electrochemical methods only provide indirect evidence of the surface chemistry, a combination of electrochemical methods and the sensitive surface analysis methods such as XPS, XANES and Raman spectroscopy could be helpful for researchers to identify the product of the reaction (Velásquez et al., 2005; Nava et al, 2008, Liang et al. 2011). Velásquez et al (2005) applied surface analysis techniques (XPS and SEM/EDX) together with electrochemical techniques to study chalcopyrite dissolution in a pH 9.2 electrolytic solution. The presence of Cu(II) is not detected in XPS for potentials lower than 0.30 V vs. SCE in positive-going potential sweep (PGPS), but Fe(III) species containing oxygen are always present, which confirmed the initial state of the electro-oxidation of chalcopyrite an iron-deficient chalcopyrite phase is formed. At more positive potentials, XPS data show the presence of Cu(II), Fe(III), and sulfur species containing oxygen.

In acidic solutions, Mikhlin et al. (2004) indicated the production of covellite or covellite - like structure at 0.6 V vs. Ag/AgCl (3M KCl) according to the lower copper binding energy (931.8 eV). Also by XPS, Yin et al. (1995) claimed that CuS_2* (which stands for a metastable phase existing at the electrode surface which has the composition of Cu:2S) was formed in oxidation process. By using synchrotron small angle X-ray diffraction (S-SAXRD) and Raman spectroscopy, Majuste et al. (2012) found the evidence of elemental sulfur (S_8) and covellite (CuS) when chalcopyrite on chalcopyrite after chronoamperometry at 0.80 V vs. SHE. Liang et al. (2011) studied the reduction process of chalcopyrite at 65 ℃ in pH 1.5 9k solution. The results indicate chalcopyrite is

reduced to bornite in the potential range of -0.1 to 0.1 V, which is the initial and rate-limiting step of the successive chalcopyrite reduction. The reduction of bornite and chalcopyrite to chalcocite take place in the potential range of -0.1 to -0.56 V, while the formation of elemental copper was found at potentials more negative than -0.5 V.

1.5 Mechanisms of chalcopyrite passivation

Over the past decades, many authors have addressed the issue of the slow kinetics of bioleaching chalcopyrite and the passivation layer formed in the process. There are various products that are suggested by different researchers for different leaching conditions, most important ones including jarosite, polysulfide, and elemental S (Klauber, 2008). The presence of covellite as intermediate product has also been widely reported but not considered as a factor of passivation layer because of its higher leaching kinetics (Hackl et al., 1995).

1.5.1 Elemental sulfur

Chalcopyrite surface oxidation leads to the formation of an intermediate (in terms of oxidation state) sulfide layer on the surface, which through progressive reaction forms elemental S (Sand et al., 2001). It is considered as passivation factor in some studies especially in chemical leaching (Rodr ́guez et al., 2003). It has been suggested in the literature that elemental sulfur can hinder ion transport and the dissolution process (Dutrizac, 1989). Dutrizac reported that the surface of chalcopyrite was enveloped by a layer of elemental sulfur which became progressively thicker with leaching time. Rodr ́guez et al. (2003) found elemental sulfur formed on the chalcopyrite surface, and caused an important barrier effect at low temperature (35 ^{o}C).

On the other hand, a lot of researchers consider elemental sulfur is not a primary passivation factor in bioleaching. Firstly, in the presence of sulfur oxidizing bacteria the accumulation of elemental sulfur will be eliminated to a large extent (Klauber, 2008). Some researchers believe even without sulfur oxidizing bacteria, the porous elemental sulfur layer will not really hinder the chalcopyrite leaching (Parker et al., 1981; Linger, 1976). In the work of Parker et al. (1981), elemental sulfur on the electrode was removed by dipping the electrode in the solvent of CS_2. As the electrode behaved similarly with that simply suspended in a nitrogen atmosphere, the authors concluded the passivating film was not sulfur. Sandstr ̈om et al. (2005) conducted a series of chemical and bioleach experiments and concluded that S^0 and jarosite form under different electrochemical

conditions and it was the jarosite that passivates the surface. Large amounts of elemental S^0 were found on leach residues from low Eh chemical leach experiments, where the chalcopyrite leaching was fast. Since large amounts of elemental S were found on leach residues from the fastest leach experiments (low Eh), elemental S was not considered as a primary passivating species.

1.5.2 Jarosite

In bioleaching, Fe^{3+} and SO_4^{2-} was produced via bacterial oxidation, they are readily to precipitate out in the form of jarosite precipitation occurs (Reaction (1-7)) which also coats on the surface of chalcopyrite. The rate of jarosite formation increases significantly with temperature and ferric concentration; jarosite formation is also promoted at pH 2 and depressed at pH < 1 or > 3 (Dutrizac, 1983; Dutrizac and Jambor, 2000).

$$3\,Fe^{3+} + 2\,SO_4^{2-} + 6H_2O + M^+ \rightarrow MFe_3(SO_4)_2(OH)_6 + 6\,H^+ \qquad (1\text{-}7)$$

where M represents K^+, NH_4^+ or H^+

The inhibition of chalcopyrite leaching due to jarosite formation is widely discussed in the literature (e.g. (Córdoba et al., 2008b; Córdoba et al., 2009)). Córdoba et al. (2008a) studied the chalcopyrite (bio)leaching in the presence of ferric or ferrous ions, they found when the initial redox potential is very high, that tendency to equilibrium favors rapid precipitation of ferric ion as jarosite and consequently passivation of chalcopyrite. Sasaki et al. (2009) studied the of bioleaching chalcopyrite with *A. ferrooxidans* using Raman spectroscopy together with Fourier transform infrared (FT-IR) and XRD and found potassium jarosite was first found prior to the formation of ammonio-jarosite, which accounted for the slow Cu leaching rate.

However, some researchers found the formation did not passivate chalcopyrite dissolution especially in leaching with thermophiles (D'Hugues et al., 2002). In an experiment conducted by Stott et al. (2002), the authors removed jarosite coated chalcopyrite samples with moderate thermophiles under anoxic conditions, yielding no improvement of leaching rates. Recent studies by Yu et al. (2011) also found that below 650 mV vs. SHE, jarosite effects on bioleaching were negligible. Therefore, it is helpful to study the how the formation of jarosite affects the leaching kinetics to reveal the passivation effect of jarosite.

1.5.3 Metal-deficient (poly)sulfides

As reviewed in the previous section sulfur rich layer forms in chalcopyrite dissolution, this layer often contains metal-deficient sulfides or polysulfides. This layer is also proposed as passivation layer in literatures. Hackl et al. (1995) suggested that the rate determining step in chalcopyrite leaching is the decomposition of the copper polysulfide to cupric ions and elemental sulfur, with the polysulfide chains restructuring to form S_8 rings. The elemental sulfur is porous enough that the rate is not limited by reactant/product diffusion through sulfur. Increasing the temperature increases the CuS_n decomposition rate until at 200 ℃, when no passivation was observed. In an earlier study, Parker et al. (1981b) concluded that the early stages of oxidation are limited by mass transport through an unstable film of metal-deficient "polysulphide".

In an electrochemical study of chalcopyrite carried out by Rodríguez et al. (2003), the authors found a prewave, which occurred at about +500 mV and linked to the formation of a metal-deficient passive species. Similarly, Lazaro and Nicol (2003) also identified a transient anodic pre-wave for chalcopyrite, which indicates an initial iron-deficient and copper-rich surface. They conclude that dissolution is inhibited (implying passivation) by the slow solid-state diffusion of both copper and iron through that layer. In a recently study conducted by Ghahremaninezhad et al. (2010), the authors analyzed the passivation of chalcopyrite using EIS. They also concluded the passivation of chalcopyrite through the formation of $Cu_{1-x}Fe_{1-y}S_2$ and $Cu_{1-x-z}S_2$ passive layers based on the resistance analysis and the surface layers modelling.

1.6 Parameters that affects chalcopyrite (bio)leaching

1.6.1 Temperature and bacteria type

Temperature is one key factor to chalcopyrite leaching. A favorable influence of an elevated temperature has been observed by a large number of studies (Rodríguez et al., 2003; Sandström et al., 2005; He et al., 2009). In chemical leaching of chalcopyrite in 1.5 M H_2SO_4 solution, Sokic et al. (2009) found that dissolution was enhanced from 28% to 70% within 240 min when the temperature was increased from 70 to 90 ℃. In an oxygen pressure leaching tests, the results of Hackl et al. (1995) show copper extraction was only 43-47% after 3 hours at 110 ℃, while copper dissolution increased to 98.6% at 200 ℃ and 99.3% at 220 ℃. The analysis of leach residues revealed little or no elemental sulfur at high temperatures, indicating the sulfides had been oxidized entirely to sulfate.

In the case of bioleaching, the copper extraction was only around 20% in 30 days and often incomplete because of passivation in the presence of mesophiles (Konishi et al., 1999; Mehta et al., 1982). In the case of bioleaching with thermophiles and extremely thermophiles, the copper extraction from chalcopyrite could be more than 90%. d'Hugues et al. (2002) have carried out a continuous bioleaching of chalcopyrite using a novel extremely thermophilic microbial mixed culture (78 ^{o}C) using one 50 L operating capacity. They reported a copper recovery greater than 90% being achieved in a 5-day residence time using a continuous slurry feed at 12% (w/w) solids' concentration. In a pilot scale columns leaching, Petersen and Dixon (2002) coated a chalcopyrite concentrate onto inert support rocks (the GEOCOAT process) and increased the temperature gradually to 70 ^{o}C with successively introducing various mesophile and thermophile cultures. Copper extractions in excess of 90% were achieved within 100 days.

The favourable influence of an elevated temperature of bioleaching may be explained by several reasons. In an elevated temperature the chemical reaction kinetics increases as the function of temperature, which may compensate the passivation effect to a large extent. Researches also indicate at high temperature, there is absent of passivation layer or only forms unstable passivaton layer on chalcopyrite surface (Rodriguez et al., 2003; Hackl et al., 1995). In an electrochemical study of chalcopyrite carried out by Rodr ́guez et al. (2003), the authors found a prewave, which occurred at about +500 mV and linked to the formation of a sulfur-rich passive species. That prewave was weaker at when temperature was raised to 68 ^{o}C. Based on this finding, the authors concluded that at high temperatures the accumulation of intermediate sulfur species (which may be CuS, sulfur-rich non-stoichiometric copper sulfide or polysulphides) will be impaired and will not constitute a diffusion barrier. Hackl et al. (1995) suggested increased leach temperature increased the passivation layer (CuS_n) decomposition rate, which no longer passivates chalcopyrite at 200 ℃. Specifically to bioleaching, another reason could be related to better iron and sulfur oxidation capacities of the thermophiles, which could reproduce Fe^{3+} and/or eliminate elemental sulfur at a higher rate (Zhu et al., 2011).

Different types of bioleaching microbes also have different impacted in bioleaching. For instance, thermophiles have better performance over mesophiles, which could be partially related better iron and sulfur oxidation capacities as reviewed above. On the other hand, microbes with same or similar optimal temperature also have different roles in bioleaching because of their difference in metabolism. Bevilaqua et al. (2002) showed

that the pure culture of *A. thiooxidans* did not oxidise $CuFeS_2$ and the Cu dissolution rate was similar to that of chemical control. This is mainly because of the lack of iron oxidation capacity of *A. thiooxidans*. *A. ferrooxidans* was found to have a higher bioleaching capacity than *L. ferrooxidans* by Akcil et al. (2007), which may be related to the sulfur oxidizing capacity of *A. ferrooxidans*. On the other hand, in industrial applications, *L. ferrooxidans* rather than *A. ferrooxidans* was found to dominant iron-oxidizing bacteria in many commercial processes (Rawlings et al. 1999). At the same time, Akcil et al. (2007) reported a 62.1% copper extraction in leaching with *A. ferrooxidans, L. ferrooxidans* and *A. thiooxidans* which is better than the pure cultures (50.3% using *A. ferrooxidans* and 38.8% Cu using *L. ferrooxidans*).

1.6.2 Eh

As reviewed in previous sections, chalcopyrite dissolution is generally considered to occur via the attack of Fe^{3+} and H^+ through the formation of polysulfide (Sand et al, 2001). According to the overall reaction (1-3), Fe^{3+} is the primary impetus of chalcopyrite dissolution, thus the presence of Fe^{3+} will be favourable to the leaching kinetics. However, some studies show that the addition of ferrous ion can significantly improve the chalcopyrite dissolution kinetics over the addition of ferric ion (Hiroyoshi et al., 1997; Hiroyoshi et al., 2001; Third et al., 2000; Third et al., 2002). This phenomenon may relate to the low solution potentials as a result of Fe^{2+} addition (Sandström et al., 2005; Vilcáez and Inoue, 2009). In a number of chalcopyrite leaching studies, the results have shown that the leaching rate of chalcopyrite is enhanced when leaching is performed at low redox potentials (Sandström et al., 2005; Third et al., 2000; Velásquez-Yévenes et al. 2010). The studies indicated that there is an optimal potential range for chalcopyrite leaching, which has been widely reported in between 350-470 mV, and when the potential was greater than that, the leaching rate slowed (Kametani and Aoki, 1985; Velásquez-Yévenes et al., 2010). Because of the Eh effect, high bacterial concentration could even lead to inhibition of leaching (Third et al., 2000), which indicates that solution potential is far more important than cell concentration and activity in dictating leaching kinetics of chalcopyrite.

The mechanism of the promotion of chalcopyrite leaching kinetics by low redox potential and why there is an optimal Eh range is not clear yet. Chalcopyrite dissolves via a range of intermediates. Present studies show various species such as impermeable sulfur

(Muñoz et al., 1978), insoluble iron salts (Dutrizac, 1978), metal deficient sulfide (Linge, 1976), copper rich polysulfide layer CuS_x (Hackl et al., 1995; Parker et al., 1981), and secondary copper sulphide (Sasaki et al., 2009) may form in chalcopyrite dissolution. It is suspected that the solution potential may influence the speciation of the intermediates, which further influence on the chalcopyrite leaching kinetics. An attempt to explain the ferrous-induced promotion of chalcopyrite leaching was made by Hiroyoshi et al (2000). In their two-step dissolution model, at low Eh, chalcopyrite is reduced ferrous ions to form chalcocite, which is more soluble at cathode (Reaction (1-8)), and the formed chalcocite is oxidized in the second step by ferric ions at anode (Reaction (1-9)).

$$CuFeS_2 + 3Cu^{2+} + 3Fe^{2+} \rightarrow 2Cu_2S + 4Fe^{3+} \quad (1\text{-}8)$$

$$2Cu_2S + 8Fe^{3+} \rightarrow 4Cu^{2+} + 8Fe^{2+} + 2S^0 \quad (1\text{-}9)$$

This model explains why there is an optimum range of the redox potential in which oxidation of chalcopyrite takes place. Reaction (1-8) indicates that in low potential ranges and in the presence of Cu^{2+}, chalcopyrite is reduced to chalcocite (Cu_2S). Compared to chalcopyrite, the intermediate Cu_2S is more easily oxidised by Fe^{3+} (Reaction (1-9)) and this results in the improved copper leaching rate observed at the low potentials (Hiroyoshi et al., 2000).

This two-step reaction takes place only when solution redox potential *E* satisfies the condition $Ec > E > Eox$, where *Ec* and *Eox* correspond to the equilibrium redox potential of the reactions in Equations 1-1 and 1-2. At 1 atm and 298 K, they are expressed as (Hiroyoshi et al., 2008):

$$Ec = 0.681 + 0.059\log([Cu^{2+}]^{0.75}/[Fe^{2+}]^{0.25}) \quad (1\text{-}1)$$

$$E_{ox} = 0.561 + 0.059\log[Cu^{2+}]^{0.5} \quad (1\text{-}2)$$

When $E_{ox} > E$, the intermediate Cu_2S is not oxidized and Cu extraction stops. When $E > E_c$, intermediate Cu_2S is not formed and the chalcopyrite leaching is slow.

However, Hiroyoshi et al. (2000) arrived at this conclusion merely based on solution analysis, and so far there is still lack of clear support from a mineralogical perspective. Furthermore, it is also important to study whether there are other secondary copper ores that can be accounted for by this model. Therefore, a detailed study that examines the

variation of mineralogy and chalcopyrite surface species in the presence of ferrous and ferric ions will help to reveal mechanism of the ferrous-promoted chalcopyrite leaching.

1.6.3 Catalysts

To enhance the leaching rate of chalcopyrite, researchers have investigated the possibility of using catalysts. So far, several chemicals such as active carbon, chloride ions and silver ions have been reported favourably affect the chalcopyrite leaching rate.

1.6.3.1 Activated carbon

Several studies suggest the addition of activated carbon can facilitate the chalcopyrite dissolution. Wan et al. (1984) suggested the dissolution of chalcopyrite in the ferric sulfate solution was accelerated because of the formation of chalcopyrite/carbon aggregates, which changed the conductivity of the reaction product layer. Nakazawa et al. (1998) and Zhang and Gu (2007) found the addition of activated carbon could enhance chalcopyrite bioleaching by mesophiles. In a bioleaching test with extreme thermophile *Acidianus manzaensis*, Liang et al. (2010) found the copper extraction from chalcopyrite was enhanced from 64% to 95% by adding 2 g/L activated carbon.

The catalytic effect of activated carbon on chalcopyrite bioleaching are mainly attributed the galvanic interaction between activated carbon and chalcopyrite, in which activated carbon acted as the cathode and accelerated the anodic dissolution of chalcopyrite (Nakazawa et al., 1998). Meanwhile, Vargas et al. (2009) suggested activated carbon could reduce ferricions to ferrous ions, providing energy to iron(II)-oxidizing bacteria. When chalcopyrite was leached with activated carbon, the solution Eh was also found lower and in the optiamal Eh range (Liang et al., 2010), which also could contribute to the rapid chalcopyrite dissolution.

1.6.3.2 Sodium chloride

Previous studies indicate the dissolution rate of chalcopyrite in chloride-containing media is faster than that in sulfate-containing media (Kinnunen and Puhakka, 2004; Lu et al., 2000). The results of Carneiro and Leão (2007) show copper extractions reached 91% in oxygenated ferric sulphate solution with 2 mol/L NaCl as compared to 45% copper extraction in the absence of NaCl. Liang et al (2012) studied the effect of NaCl on chalcopyrite bioleaching with *A. manzaensis* at 65 ^{o}C, they found the addition of 0.66 g/L NaCl increased the concentration of copper ions in leaching solution from 2.37 g/L to 2.67 g/L.

Several mechanisms have been proposed to explain the effect of chloride ions. Dutrizac (1981) found that the activation energy for chalcopyrite dissolution in chloride solution was 42 kJ/mol, which is much lower than that in sulfate-containing solution (75 kJ/mol). Some researchers also found that chloride ions can increase the surface area and porosity of solid products and promote the formation of crystalline and porous elemental sulfur layers on the mineral surface which favor the dissolution of chalcopyrite (Kinnunen and Puhakka, 2004; Lu et al., 2000). Liang et al. (2012) found the addition of chloride ions eliminated elemental sulfur in leaching residue. They proposed that the removal of the elemental sulfur from the mineral surface in the presence of sodium chloride resulted from the formation of a porous crystalline sulfur layer, which was readily oxidized to sulfuric acid by *A. manzaensis*.

1.6.3.3 Silver ions

Silver has been proven high effective in catalysing chalcopyrite leaching (Blázquez et al., 1999; Hu et al., 2002; Muñoz et al, 2007). Pawlek (1976) investigated the effect of silver ions on the leaching of chalcopyrite at 110 °C and 100 kPa. After 30 min, 40% of copper was dissolved in the absence of silver compared to the complete dissolution of chalcopyrite in the presence of silver. In a chemical leaching with ferric sulfate at 35 ^{o}C, copper dissolution was negligible without silver (3%) at 600 mV vs. Ag/AgCl, while the presence of 1 g Ag/kg the copper extraction was higher than 90% in the presence of an adequate concentration of Fe^{3+} in the leaching medium (Córdoba, et al. 2008c). In bioleaching, with low grade chalcopyrite ores, Muñoz et al. (2007) found small amounts of silver (14.7 g Ag/kg Cu) dramatically accelerated the copper dissolution process while large amounts (294.12 g Ag/kg Cu) had an inhibitory effect. Their results indicate 93.8% of copper was recovered in 15 days of bioleaching with mesophiles in the presence of 14.7 g/kg Cu silver compared to 17.8% in the absence of silver.

Miller and portillo (1979) proposed a model to for silver catalysis. Silver interacts with the chalcopyrite as Reaction (1-10). Silver sulphide is formed on the mineral surface by means of a chemical reaction involving an interchange between the silver and the copper and iron from the chalcopyrite structure. This reaction does not depend on the microorganisms present. The silver sulphide dissolves in the presence of an oxidising agent such as ferric ion (Reaction (1-11)). The S formed via this pathway is more porous and will not hinder the mass transfer on the solution-solid interface (Córdoba et al., 2009).

$$CuFeS_2+4Ag^+ \rightarrow Cu^{2+}+Fe^{2+}+2Ag_2S \quad (1\text{-}10)$$

$$2Ag_2S+4Fe^{3+} \rightarrow 4Ag^+ +4Fe^{2+}+2S \quad (1\text{-}11)$$

Price and Warren (1986) studied the electrochemical behaviour of chalcopyrite electrodes in H_2SO_4 solutions with and without silver. The cyclic voltammetry for $CuFeS_2$ electrodes in the presence of silver ion indicates the formation of Ag_2S and metallic silver on the chalcopyrite surface. They also found additions of Ag^+ up to an optimum of approximately 10^{-3} M result in higher anodic currents for $CuFeS_2$ electrodes. In an electrochemical study, López-Juárez et al. (2006) found in bioleached electrodes, the anodic and cathodic current signals in presence of Ag^+ ions were bigger than that without Ag^+ ions. The electrochemical results indicate the catalysis occurs through a change in morphology or conductivity of the normally protective sulfur layer which forms on $CuFeS_2$ through reactions involving Ag_2S or elemental silver.

However, the passivation by elemental sulfur is still in debate. Many results argued S^0 is not a real passivation layer in both bioleaching and chemical leaching (Klauber, 2008). Therefore, the formation of high porous sulfur may be not the only reason for a 4-5 times increase of copper extraction. Hiroyoshi et al. (2002) based on their previous two-step model consider Ag^+ helps the formation of Cu_2S (Reaction (1-12) and Reaction (1-13). However, this model still lacks of support by work from other groups.

$$2CuFeS_2 + 6H^+ + 2e^- \rightarrow Cu_2S + 2Fe^{2+} + 3H_2S \quad (1\text{-}12)$$

$$2Ag^+ + H_2S \rightarrow Ag_2S + 2H^+ \quad (1\text{-}13)$$

An interesting phenomenon is the catalytic effect of silver is most obvious in leaching with mesophiles. In bioleaching with moderate thermophiles or extreme thermophiles, the presence of silver ions improved the copper recovery in a less obviously manner or even impact bioleaching adversely (Blázquez et al., 1999). Blázquez et al. (1999) reported in a thermophilic bioleaching system the silver on the mineral surface was identified as elemental silver rather than Ag_2S, which may indicate a different reaction pathway for high-temperature leaching. However, there is still a lack of research into the mechanisms associated with silver catalysts in the presence of moderate thermophiles or extreme thermophiles.

1.6.4 Galvanic effects

Galvanic corrosion is an electrochemical process whereby when two minerals are put in contact with each other in a conducting media, the less noble one will preferentially undergo corrosion while the other one is protected. The difference in the rest potentials between the two mineral determines the selectivity in corrosion. In chalcopyrite bioleaching, the most common galvanic system is chalcopyrite-pyrite system, in which, pyrite possessing a higher rest potential, acts as a cathode, and chalcopyrite with a lower rest potential acts as the anode, and chalcopyrite will be corroded preferentially.

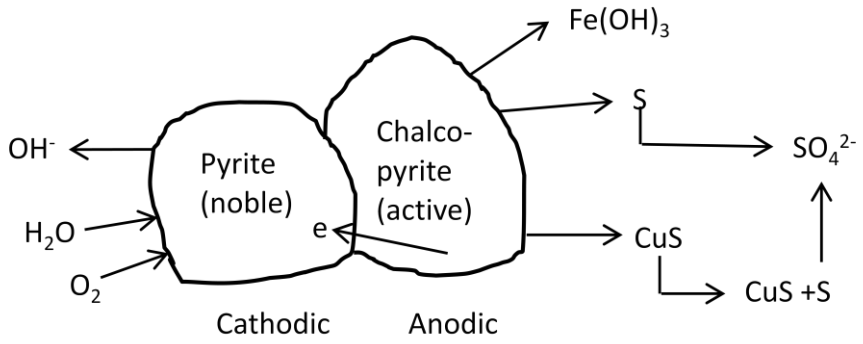

Fig. 1-6 The proposed model of gavanic effect between chalcopyrite and pyrite.(Redrawn from Ekmekqi and Demirel, 1997)

Case studies show that the presence of pyrite can significantly promote the chalcopyrite leaching rate. Acceleration of chalcopyrite leaching by a factor of 2 to 15 has been reported when pyrite was added to the leaching media (Mehta et al., 1982; Mehta and Murr, 1983). The Galvanox^{TM} process is a novel galvanic assisted atmospheric leaching technology developed at the University of British Columbia (Dixon et al., 2008). Pyrite was intentionally added to chalcopyrite concentrate in the absence of bacteria. The optimal weight ratio of pyrite to chalcopyrite for galvanic assisted leaching is in the range of 2:1 and 4:1 (Dixon et al., 2008; Mehta and Murr, 1983). Copper recoveries of more than 98% can be achieved at 80℃ in four hours at solution potential of 470 mV. The presence of microorganisms commonly used in bioleaching (such as *acidithiobacillus ferrooxidans*, *leptospirillum ferriphilum*) can influence the leaching efficiency of chalcopyrite. Copper leaching efficiency was improved more than 10 times has been reported when chalcopyrite and pyrite were leached in the presence of microorganisms at 30℃ (Mehta et al., 1982). On the other hand, no significant advantage of bioleaching

over chemical leaching was observed when the temperature was increased to 55 ℃ in the terms of galvanic leaching.

Enhanced leaching kinetics of chalcopyrite in the presence of pyrite has been confirmed via electrochemical investigations where an increase in current density (i.e., faster dissolution) was reported (Holmes et al., 1995; Lou et al., 2007). However, how the increased current affects the mineralogy in a bioleaching system is still not clear.

Elemental sulfur is a common product in chalcopyrite bioleaching (Klauber, 2008). Its impact on chalcopyrite dissolution has been widely studied as reviewed in the previous sections, the majority of the researchers tend to believe it does not have a significantly negative effect on the bioleaching rate, as the elemental sulphur formed on chalcopyrite surface is porous enough not to hinder the diffusion of oxidizers and the mineral-solution interaction and it also could be effectively removed by sulfur-oxidizing microbe (Klauber, 2008; Hackl et al., 1995; Liang et al., 2012). However, in galvanic leaching, the elemental sulfur that covers minerals may increase the resistance between chalcopyrite-pyrite couple, hindering the galvanic effects.

In an ideal galvanic leaching experiment, chalcopyrite will be selectively leached while pyrite can be recovered and recycled for further processing. The leaching selectivity of galvanic system has not been investigated in detail. Mehta and Murr noted a drop in solution pH and an increase in solution redox potential during microbial leaching of chalcopyrite and pyrite mixtures (Mehta and Murr, 1983). These behaviours may be linked to the biooxidation behaviour of bacteria and dissolution of pyrite, though it has not been explicitly mentioned in the paper. This is a common observation during pyrite leaching (Schippers et al., 1996). A later study on heap bioleaching of copper-gold concentration using the Geocoat technology by Petersen and Dixon (2006) suggested that significant pyrite dissolution occurred during bioleaching at 30 ℃. They attributed the pyrite dissolution to the high solution redox potential.

Galvanic assisted (bio)leaching is not only important for cases where pyrite (or other minerals) is intentionally added to chalcopyrite concentrates, it can also play an important role in the leaching of naturally occurring ore. For example, chalcopyrite is commonly present in ores with impurities such as pyrite and bornite for instance, and these impurities can potentially act as a galvanic couple for (bio)leaching which may accelerate or retard the leaching rate of chalcopyrite. On the other hand, the dissolution rate of

chalcopyrite is remarkably decreased in the presence of sulfide minerals with smaller rest potentials such as sphalerite and galena (Li et al., 2013).

1.7 Bioleaching of low grade chalcopyrite

For low grade chalcopyrite or other metal sulphide ores, the most common technology is heap leaching. It has the advantages of simple equipment request, low investment and operation cost, and reasonable yields over a period of recirculation (Pradhan et al., 2008). In heap bioleaching, bacteria solution is irrigated to (waste) ore that is piled onto an impermeable base supplied with an efficient leach liquor distribution and collection system. The microbes growing on the mineral surfaces of the heap produce the ferric iron and acid that result in mineral dissolution and metal solubilisation. The metal-containing solution is regularly collected and sent for metal recovery using solvent extraction and electrowinning (SX/EW) (Pradhan et al., 2008).

An excellent example of a current commercial bioleach application is the Quebrada Blanca operation in northern Chile located on the Alti Plano at an elevation of 4400 m (Brierley and Brierley, 2001). This facility processes 17300 tonnes/day of sulfide ore to produce 206 tonnes of London Metal Exchange (LME) grade cathode copper. Sulfide ore from the mine is crushed in three stages to 100% smaller than 9 mm. The crushed ore is fed to a 1500 tonne surge bin that includes a steam-to-ore heat exchanger to increase the temperature of the ore. The ore is then agglomerated in rotating drums with sulfuric acid and hot water. The agglomerate is then distributed by a stacker uniformly in an arc to form a 6-6.5 m high continuous pile. Bacterial activity is facilitated by aeration using an array of airlines installed beneath the heap and low-pressure fans. The Quebrada Blanca bioleaching illustrates the successful evolution of biohydrometallurgy in the mining industry.

However, because of the low leaching rate of chalcopyrite, the commercially application of heap leaching for Cu recovery is still most based on copper oxide or/and secondary copper sulphide (Waltling, 2006).

To enhance the leaching rate of chalcopyrite heap leaching, it is necessary to study the relationship between leaching rate and a range of parameters. Conditions like humidity, pH, temperature, energy sources and nutrients will significantly affects the microbe growth. Correct chemical and physical conditions such as ore particle size, access of

oxygen and humidity to the mineral surfaces, heap scale, aeration and irrigation are also crucial to heap leaching (Pradhan et al., 2008).

Optimizing parameters directly on a full-scale heap is uneconomic and also difficult to operate. To understand the behaviour of heap leaching at a lower cost, studies to pilot column leaching are widely applied to low grade chalcopyrite or other metal sulfides and the effects of factors such as pH, temperature, energy sources, microbes, aeration and irrigation have been reported (Muñoz et al., 2007; Norris et al., 2012; Ahonen and Tuovinen, 1995; Darezereshki et al., 2011).

Muñoz et al. (2007) studied the effect of silver on chalcopyrite column leaching. The results show the copper extraction low-grade copper ores was enhanced. More than 70% copper was leached out in 350 days using low concentrations of silver (1.4 g Ag/kg Cu). On the contrary aeration did not significant affect the bioleaching process. In a column leaching of copper sulphide with thermophiles, Norris et al. (2012) found the activity of microbes and the release of copper were influenced by addition of ferric irons to the irrigation solution, by imposed anoxic conditions and, particularly at higher temperatures, by precipitation of oxidized iron compounds. At the same time, aeration of these previously anoxic columns resulted in rapid oxidation of the ferrous iron and some stimulation of the rate of copper release. Ahonen and Tuovinen (1995) studied column bioleaching of a complex sulfide ore material, with varying proportions of pyrrhotite, pyrite, quartzite (low acid consumption) and skarn (high acid consumption). There results show acid consumption was highest under low pH and low redox potential conditions. The leaching rates of Cu (from chalcopyrite) had a tendency to increase with dissolved ferric iron concentration, while the leaching of Ni (from pyrrhotiteand pentlandite) did not correlate with the concentration of ferric iron. Their study also shows trickle-leaching conditions yielded higher acid production and redox-potential values compared to flood leaching. The effect of agglomeration has also been studied in column leaching. The results of Darezereshki et al. (2011) indicates agglomeration could enhance the heap homogeneity and fluid distribution which in turn helps the process optimization, which enhanced the copper yield up to 10%.

1.8 Objective of this study

The surface speciation and properties of chalcopyrite are directly related to the chalcopyrite leaching mechanism, each impacts the leaching process in a different manner.

With the combination of bioleaching, electrochemical and surface studies, the Fe, Cu, S speciation transformation of chalcopyrite was studied. A deeper understanding of chalcopyrite leaching mechanism was achieved. A comprehensive understanding of the relationship between chalcopyrite surface properties in various environmental conditions and their impacts on chalcopyrite leaching was developed, which may help the industrial application of chalcopyrite bioleaching has been proposed.

Chapter 2 of this thesis summarised the materials and techniques used in this study, as well as the standard experiment conditions. Chapter 3 studied the chalcopyrite surface chemistry evolution in chemical and bacterial leaching at different temperatures, which provided information on chalcopyrite dissolution and passivation mechanisms. Chapter 4 is a study of surface chemistry of chalcopyrite in an electrochemical oxidation process. Chapter 5 investigated population behaviour of *Acidithiobacillus ferrooxidans* on chalcopyrite and the biofilm formation and their relationship to mineral sites, and the crystal orientations. Chapter 6, 7 and 8 studied the effect of Eh, pyrite addition and silver ions addition, respectively. Their impact on the kinetics of chalcopyrite leaching and mineral surface chemistry and mineralogy were revealed.

Chapter 2 Experimental and techniques

2.1 Introduction

To obtain a better understanding of chalcopyrite dissolution mechanism and the connection between the surface alteration, leaching kinetics, and environmental conditions, a study of surface chemical species, mineralogy changes in chalcopyrite bioleaching and microbe-mineral interaction was necessary. To achieve this aim, the combination of solution characterisation and surface properties was carried out. With the combination of leaching and electrochemical studies, a range of state-of-art surface sensitive spectroscopic and the morphologic techniques played a key role in this project.

2.2 Material

2.2.1 Minerals

Chalcopyrite and pyrite were obtained from Mt Lyll, Australia and North Dakota, USA, respectively. Chemical analysis revealed the impurity present in the minerals was less than 4%. The chemical analysis of copper, iron and sulfur concentrations in chalcopyrite and pyrite concentrate is listed in table 2-1. The XRD results of the original minerals are shown in Fig. 2-1. The results suggest that the concentrates are primarily chalcopyrite and pyrite, respectively. The chalcopyrite for electrochemical studies was hand picked from the bulk chalcopyrite specimen and the only detectable phase by XRD is chalcopyrite (Fig. 2-2).

Table 2-1 Chemical analysis of pyrite and chalcopyrite concentrate (%)

	Cu	Fe	S	Zn
Chalcopyrite	33.6	30.5	33.7	0.04
Pyrite	0.18	45.0	51.0	-

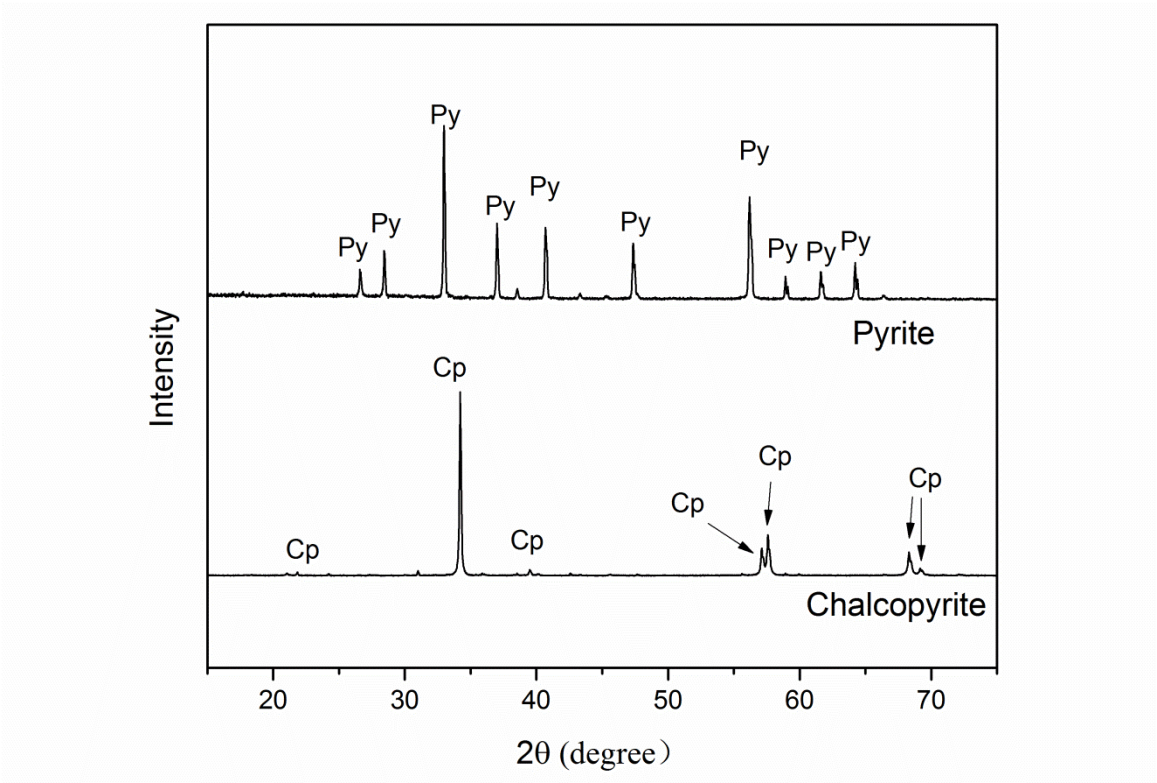

Fig. 2-1 XRD analysis of chalcopyrite and pyrite samples used in leaching studies

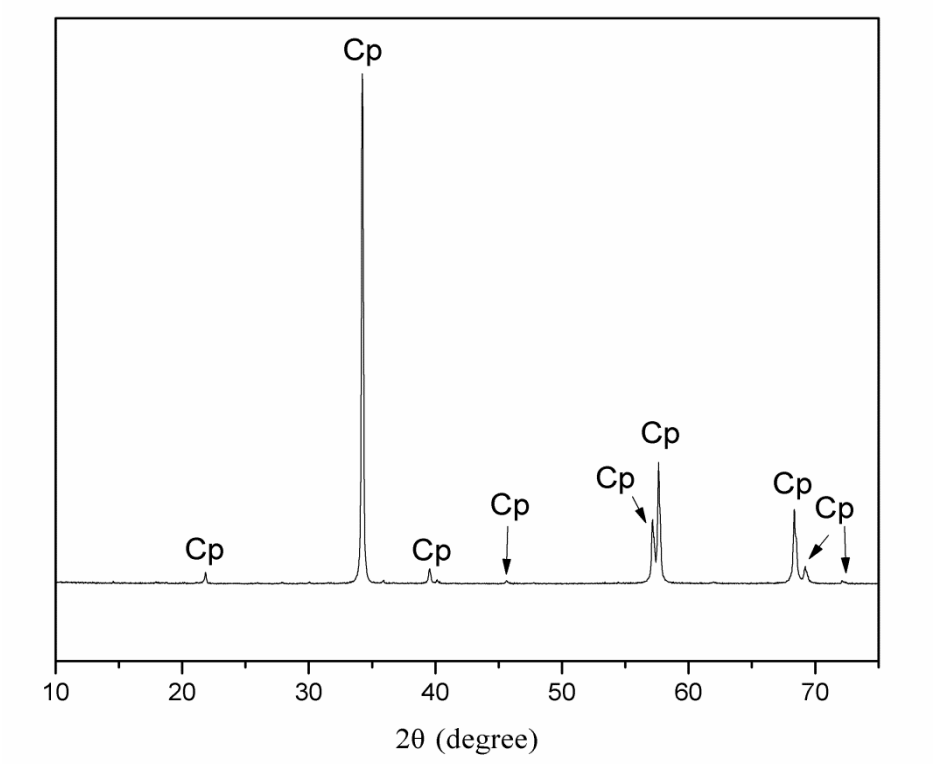

Fig. 2-2 XRD analysis of chalcopyrite sample used in electrochemical studies

Low grade ores are provided by Rio Tinto and the elemental concentration is shown in summarised in table 2-2. The XRD analysis (table 2-3) indicates the copper exists in the ore in the form of chalcopyrite.

Table 2-2 The element analysis of low grade chalcopyrite ore from Rio Tinto Company

Composition	Cu	Fe	S	SiO_2	Al_2O_3	CaO	MgO	K_2O	Na_2O
Content/%	0.60	3.14	1.01	62.3	10.8	3.38	3.62	4.86	0.89

Table 2-3 The composition of low grade chalcopyrite ore from Rio Tinto analysed by XRD

Phase	formula
Quartz	SiO_2
Orthoclase	$K(AlSi_3)O_8$
Calcite	$CaCO_3$
Albite	$(Na_{0.}84Ca_{0.16})Al_{1.16}Si_{2.84}O_8$
Montmorillonite	$Ca_{0.2}(Al, Mg)_2Si_4O_{10}(OH)_2 \cdot x\ H_2O$
Chalcopyrite	$CuFeS_2$
Muscovite	$K(Al_4Si_2O_9(OH)_3)$
Pyrite	FeS_2
Gypsum	$Ca(SO_4)\ (H_2O)_2$

2.2.2 9K basic salt solution

9K basic salt medium was used in this study. This contained $(NH_4)_2SO_4$ (3.0 g/L), $MgSO_4 \cdot 7H_2O$ (0.5 g/L), K_2HPO_4 (0.5 g/L), KCl (0.1 g/L) and $Ca(NO_3)_2$ (0.01 g/L) (Silverman and Lundgren, 1959).

2.2.3 Standards synthesis

Jarosite used in this study was synthesized according to the method of Dutrizac (1976). CuS_n was prepared using the method described by Bowden et al. (1984). Sodium polysulfide (Na_2S_n) was prepared by reacting $Na_2S \cdot 9H_2O$ aqueous solution with excess elemental S for 72 h under N_2 atmosphere. After filtering the unreacted S, the filtrate was mixed with excess $CuSO_4$ aqueous solution, which produced a precipitate. After about 30 min, the precipitate was filtered, washed with water and then washed three times with acetone, yielding a pale-colour CuS_n powder.

2.2.4 Microorganisms

Three strains of mesophiles were used in this study. *Acidithiobacillus ferrooxidans* (*A. ferrooxidans*), *Leptospirillum ferrooxidans* (*L. ferrooxidans*) and *Acidithiobacillus thiooxidans* (*A. thiooxidans*). The mesophiles were cultured in 9K media at 30 ℃ in the absence of $FeSO_4.7H_2O$. 10 g/L of chalcopyrite was used as energy source for culturing *A. ferrooxidans* and *L. ferrooxidans*, while 10 g/L sulfur was used as energy source for culturing *A. thiooxidans*.

In this thesis, the mixed mesophilical culture (30 ^oC) consist of *Acidithiobacillus ferrooxidans*, *Leptospirillum ferrooxidans* and *Acidithiobacillus thiooxidans* with a even initial proportion unless otherwise stated.

The moderate thermophile mixture were enriched from Acid mine drainage (AMD) locations at several chalcopyrite mines in China (Zhou et al., 2009). The major microorganisms in the moderate consortia are *Acidithiobacillus caldus*, *Leptospirillum ferriphilum*, *Sulfobacillus thermosulfidooxidans* and *Sulfobacillus acidophilus* (Zeng et al., 2010). The moderate thermophilic mixture was pre-cultured in 9K media at 48 ^oC using chalcopyrite as energy source.

The extreme thermophile used in this work was *Sulfolobus metallicus* (*S. Metallicus*), which was purchased from purchased from the German Collection of Microorganisms and Cell Cultures (DSMZ). It was pre-cultured in 9K media with addition of 0.02wt% yeast extract at 60 ^oC using chalcopyrite as energy source.

All chemicals used for this thesis were analytical grade reagents. Water purified by MilliQ system (Millipore) was used throughout.

2.3 Sample preparation

2.3.1 Mineral crushing

For batch leaching high grade chalcopyrite and pyrite were grounded into -200 mesh before use. For column leaching, low grade ores and high purity pyrite were crushed to a size 0.5-1.0 cm.

2.3.2 Mixed Cp/Py samples

Coupon samples for μ-XRF, μ-XANES and Raman analyses were prepared by embedding a 50/50 % mixture of chalcopyrite and pyrite in epoxy resin (Epo Fix resin and hardener).

The samples were cut into approximately 1.5 mm thick slices and levelled using 600 and 1200 SiC polishing paper. The samples were then polished with 6, 3 and 1 μm diamond pads for 5 mins each (Beuhler Beta grinder/polisher).

2.3.3 EBSD Samples

For the electron backscattered diffraction (EBSD) study, chalcopyrite powder was prepared by crushing a large crystal, several millimetres across, into a powder with crystallite sizes ranging from a few micrometres to hundreds of micrometres. The chalcopyrite powder was then set in a high edge retention, conductive Bakelite resin, and polished to 0.25 μm using colloidal SiO_2. The polishing was the finished using the following sequence: 400, 600, 800 and 1200 grit SiC paper under water, followed by metallographic polishing using 6, 3, 1 and 0.25 μm diamond abrasive pads and finished with colloidal SiO_2 polishing for a period of 20 mins. After the final step, the sample was ultrasonically cleaned in a bath of ethanol for 2 mins and dried with a jet of dry nitrogen.

2.3.4 Coupon samples

For electrode preparation, the high grade chalcopyrite was cut into pieces approximately 2x2x0.3 cm. After coarse polishing, before each measurement, the electrode surface was polished on 1200-grit silicon carbide paper lubricated with ultrapure water, and then rinsed with deoxygenated deionised water. Finally, a fine polish was achieved with a diamond suspension of 1 μm particle size in a figure-8 pattern, followed by ultrasonically cleaning in Millipore quality water. The coupon samples for cell attachment test were prepared as above following curving the surface with knife to make defeat sites.

2.4 Standard leaching conditions

2.4.1 Batch leaching

For standard batch leaching, 250 ml flasks were used filled with 150 mL 9K basic solution. The flasks were added appropriate amount of minerals and other chemicals (e.g. ferrous sulfate, ferric sulfate and silver nitrite) according to calculation. The initial pH was adjusted 1.8, and the initial cell concentration was $1x10^7$ cell/mL for bioleaching. The leaching experiments were then carried out at 170 rpm in a shaker at appropriate temperature. Solution and solid samples were taken periodically for analysis.

2.4.2 Column leaching

The setup of column leaching was shown in Fig. 2-3. Double layered columns were used in this study. The inner diameter of the column is 10 cm and the height is 30 cm. The water jacket between inner and outer walls of the column provided precise temperature control. Heated water was circulated through column jackets to maintain temperatures which were monitored with thermocouples in the centre of each ore column.

2.8 kg of low grade ore was loaded to the column and an additional 0.6 kg of pyrite was used in the cases of galvanic leaching. 7 L 9K solution was initially added into the reservoir and irrigated onto minerals via peristaltic pump at a speed of 1.6 mL/min. The initial pH was adjusted to 1.8 and the acid consumption (mainly a result of $CaCO_3$ dissolution) was compensated by sulfuric acid. Aeration was from the base of the columns at a rate of approximately 50 mL min^{-1}. An acid leaching pre-treatment for 7 days with 9K basic medium was started to stabilize pH.

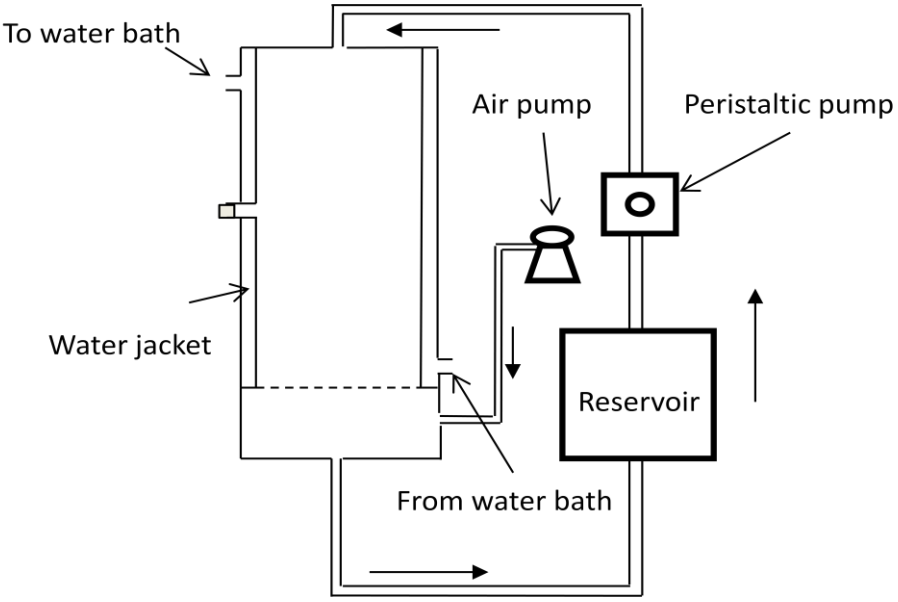

Fig. 2-3 The schematic of column leaching setup

For column leaching at 30 ^{o}C, a mixed culture of *A. ferrooxidans*, *L. ferrooxidans* and *A. thiooxidans* with even initial proportion was inoculated to the column, with an initial bacteria concentration of 1.0 x10^{7} cells/mL. The leaching at 48 ^{o}C was conducted using the same condition as in 30 ^{o}C with replacing the bacteria to thermophilic mixture. Losses of solution due to evaporation were compensated with distilled water to a total

recirculating volume of 7 L per column. Periodically, pH was readjusted to 1.8 with 1:1 (v/v) H_2SO_4.

2.4.3 Cell attachment

The leaching tests were carried out by immersing a test sample in a 10 day old *A. ferrooxidans* culture. The sample was incubated in an incubator-shaker (Bioline) at 30 ℃ and 10 rpm for a fixed period of time (24, 48, 72, 96 hours) before rinsing in iron free 9K solution at pH 1.8.

2.5 Leaching solution studies

Solution tests were conducted by monitoring the bacteria concentration, pH value, metal ion concentration (Fe^{2+}, Fe_{tot} and Cu^{2+}) and redox potentials. Cell growth was monitored by using a Thomas counting chamber (Zeng et al., 2010); Eh was measured by a platinum electrode with Ag/AgCl reference; total copper and iron were measured using inductively coupled plasma atomic emission spectrometry (ICP-AES) and ferrous concentration was determined by the 1,10-phenanthroline method (Tamura et al., 1974).

2.6 Electrochemical studies

2.6.1 Background

Electrochemical studies are commonly used for reactions in conjunction with other surface techniques. Cyclic voltammetry is the most widely used electrochemical study method. Through changes in current with an applied voltage, it gives the information of oxidation and reduction reactions taking place at electrode surface. Using the peak shapes and peak areas of an oxidation peak and its counterpart in reduction process, the reversibility of a reaction could be determined (Bevilaqua, 2007).

2.6.2 Experiment setting

The area of electrode exposed to the electrolyte was approximately 0.2 cm^2. Pt electrode was used as the counter electrode, and an Ag/AgCl electrode (3M KCl) in a lugging capillary as the reference electrode. 9K basic salt medium was used as electrolyte. The medium was adjusted to pH 1.8 with 1 mol/L of sulfuric acid. For study of electrochemical properties of chalcopyrite with silver ions, 5-20 mg/L Ag^+ was added into the electrolyte.

Electrochemical experiments were carried out using a PARSTAT 2273 Potentiostat (US) with Power-Suite Software. The electrode potential was allowed to stabilize for 10 min

before starting the measurements. In order to ensure reproducibility, the error of OCP between measurements was controlled within ±10 mV. CV Cycles were performed from 0 to 800 mV (positive-going potential scan), then to −800 mV (negative-going potential scan), and back to 0 mV (positive-going potential scan), at a scan rate of 5 mV/s. Potentiodynamic polarization study was carried out at the range of 0.1 to 1.2 V at a scan rate of 0.5 mV s^{-1}.

Potentiostatic modification was performed according to the polarization curve at specific potentials for 7200 s, respectively. The chalcopyrite sample after electrochemical treatment was rinsed in diluted sulfuric acid (pH 1.8) and sealed in a vial purged with nitrogen and frozen by dry ice for SXPS, NEXAFS and Raman analysis.

2.7 X-ray Photoelectron Spectroscopy (XPS)

2.7.1 Background

XPS is an ultra-high vacuum technique that has been used extensively in chalcopyrite surface studies (Buckley and Woods, 1984; Hackl et al., 1995; Parker et al., 2003; Sandström et al., 2005; Harmer et al., 2006, Yin et al., 1995). The most commonly used X-ray sources are Mg Kα (1253.6 eV) and Al Kα (1486.6 eV). To reduce peak width of the X-ray source, a monochromators is often used and a reduction inline witdth of about 0.2 eV has been achieved in conventional XPS (Yang, 2004).

XPS gives the binding energy of the electrons that is related to the elements and chemical state. In general the probe depth of XPS is up to 10 nm (Buckley, 1994), can provide very surface sensitive information on chalcopyrite surface, which is ideal to the chalcopyrite decomposition mechanism study.

XPS sampling depth is determined by the IMFP of the electrons which is a function of their kinetic energy. From Fig. 2-4 it is clear that the kinetic energy for which electrons have a minimum free path is around 30-50 eV. With laboratory based XPS, which usually uses energy source such as Al Kα and Mg Kα, the kinetic energy for peaks of interest are usually higher (expecially for low binding energy spectra as S *2p* it will be over 1000 eV), clearly not the optimized energy for maximising surface sensitivity (Laajalehto et al., 1997). As the exciting energy in synchrotron XPS is tuneable, it is possible to tune x-ray photon energies to optimum values for each photoemission peak and thus attain maximum surface sensitivity. This also makes a comparison of XPS data with different

surface sensitivity possible. Another benefit of SR-XPS is by tuning the photo energy, it is possible to avoid interfere from auger peaks and obtain the best signal-noise ratio.

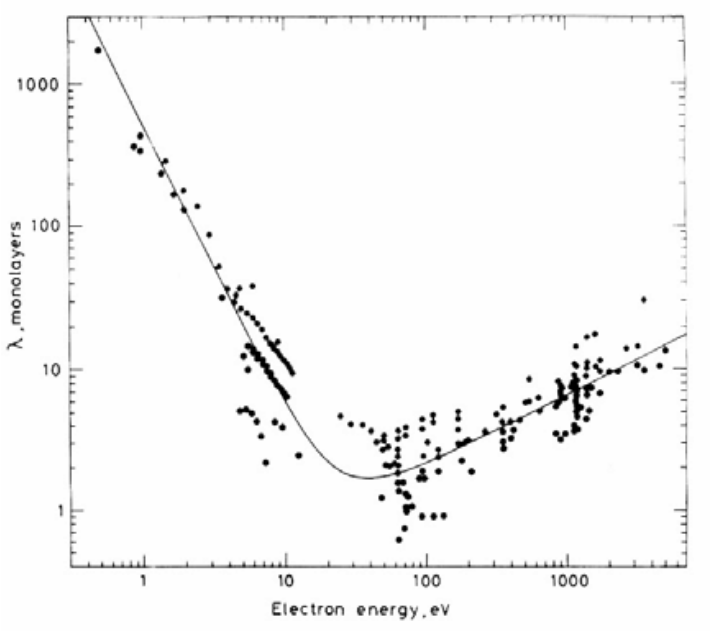

Fig. 2-4 Universal IMFP Curve (Briggs and Seah, 1990)

2.7.2 Experiment setting

Synchrotron XPS (SXPS) measurements were implemented at the Soft X-ray Spectroscopy beamline (14ID) (90–2600 eV) at the Australian Synchrotron. The resolution was about 0.24 eV at photon energy 1487 eV and 0.037 eV at 400 eV. For the Fe *2p* line, the resolution was approximately 0.08 eV. The soft X-ray beamline consists of an elliptically polarized undulator and plane grating monochromator, using a grating of 1200 l/m. The flux (at 400 eV) was between 3×10^{12} and 5×10^{11} photons/s/200mA at the sample, with a beam size of 0.6×0.6 mm (nominal). The current of the storage ring was operated in decay mode.

The spectra were collected with the sample at 90 °to the electron analyzer. Samples were mounted as slurries on carbon tape and dried under vacuum in the loadlock (Smart, 1991). The analysis chamber vacuum was 5×10^{-9} Torr or better. Sample cooling was not available during the measurement. The survey spectra (photon energy 1487 eV) were collected from 1100 eV to -10 eV using a pass energy of 50 eV and a step of 0.5 eV. For the high resolution S *2p* spectra with photon energy 1487 eV and 400 eV (more surface sensitive), the data were collected with a pass energy of 5 eV (chapter 3) or 10 eV (chapter 4) and an energy step of 0.025 eV from 180 to 155 eV. The Fe *2p* spectra were

acquired at a photon energy of 1470 eV (chapter3) or 1487 eV (chapter 4) with a pass energy of 20 and a step size of 0.1 eV (chapter 3) or 0.05 eV (chapter 4). No evidence of beam damage (peak broadening, change in line shape) was observed between sweeps (20-30 sweeps at 100 ms dwell time for S *2p*, 40-60 sweeps at 100 ms dwell for Fe *2p*) or after subsequent scans. The Cu *2p* spectra were acquired at photon energy of 1487 eV with a pass energy of 20 eV and a step width of 0.05 eV. In most of the samples no differential charging was observed. For samples after long term leaching, a small charge shift was observed and compensated using an electron flood gun.

The jarosite Fe 2*p* spectrum was collected using a Kratos Axis Ultra fitted with a delay-line detector, a monochromated Al Kα source (1486.6 eV) operating at 10 KV and 13 mA, utilizing a spot size of 300 μm. The spectrometer was calibrated to Au $4f_{7/2}$ at 84.0 eV. The Fe *2p* spectrum was acquired with a step size of 0.05 eV with a pass energy of 20 eV.

2.7.3 XPS data analysis

The XPS data was processed with software Casa XPS software. All spectra were calibrated by aligning C *1s* peak to 284.8 eV (Metson, 1999) and Au $4f_{7/2}$ peak to 84.0 eV. Atomic concentrations of major elements detected were calculated according the sensitivity factors used in CasaXPS (Fairley, 2009). Sulfur *2p* peaks occur as doublets (S $2p_{3/2}$ and S $2p_{1/2}$) as a result of spin orbit splitting. The S $2p_{3/2}$ peaks are twice of the intensity of the corresponding S $2p_{1/2,}$ which is 1.19 eV higher in binding energy (Schaufuss et al., 1998; Nesbitt and Muir, 1998). For clarity, only the S $2p_{3/2}$ peaks are displayed. The background of high resolution S *2p* spectra was fitted using a Shirley background (Shirley, 1972). The high resolution S *2p* spectra were fitted using a Gaussian–Lorentzian (G/L) function, with a weighting of 50% Gaussian and 50% Lorentzian. The fitting parameters were set according to previous publications (Harmer et al., 2006; Acres et al., 2010a). There may be several polysulfide species with different chain lengths on chalcopyrite surface which are difficult to resolve individually (Smart, 1991). In addition, elemental sulfur can also overlap with the polysulfide, which is difficult to be distinguished (Smart, 1991; Harmer et al., 2006). In this thesis, a broad peak was used to represent both of them. In addition to the S *2p* doublets, an energy loss feature has been fitted, which relates to charge transfers to S *3p*-Fe *3d* overlapping states (Fujisawa et al., 1994; Harmer et al. 2004; Acres et al 2010a).

2.8 X-ray absorption spectroscopy

2.8.1 Background

X-ray absorption spectroscopy (XAS) is a powerful tool to study the composition and structure of material. When the X-ray energy is scanned through the binding energy of a core shell, there is an abrupt increase in absorption cross-section, which gives rise to a so-called absorption edge (Penner-hahn, 2004). Beyond the absorption edge, the spectra displays a complicated oscillation, which is caused by the scattering of the ejected photoelectron by the adjacent atoms, and therefore carries on the chemical and geometrical information of an atom cluster of several shells with the absorption atom as the central (Rehr and Albers, 2000).

At lower energies than the absorption edge, there may be pre-edge peaks, which represent the transition of electrons between molecular orbitals of the absorption atom. They also carry important structure information, and are often of great interest in transition metal studies.

The absorption edge is commonly divided into two regions, i.e, XANES (also referred as NEXAFS in the soft X-ray and surface science communities) (within ca. 50 eV of the edge) which caused by multiple scattering and EXAFS (for several hundred to >1,000 eV above the edge) which is caused by single scattering and multiple scattering when the photoelectron already possesses significant kinetic energy. XANES region carries the information of oxidation state of the absorbing atom and its neighbouring structure (Pattrick et al., 1997). As this technology does not require long range ordering, it is sensitive to both crystal and non-crystal structures (Koningsberger et al., 2000). For mixed compounds, such as leached chalcopyrite, the overall spectrum is a weighted sum of individual components. This feature enables analysis of the composition of complex samples by linear combination (LC) fitting with the assistance of standards (Xia et al., 2010). The EXAFS region is used for quantitative determination of bond length and coordination number (Penner-hahn, 2004).

2.8.2 Cu, Fe K-edge XANES

X-ray absorption spectra were recorded at the BL-20B beamline (Australian National Beamline Facility, ANBF) at the Photon Factory or the X-ray Absorption Spectroscopy (XAS) beamline at Australian synchrotron. The details of beamline and experiments have been described in corresponding chapters.

Fe and Cu K-edge XANES data was calibrated according to the spectra of Fe and Cu foil, respectively, and normalized to the edge jump. LC fitting was then carried out with standard compounds to determine the composition of the leached chalcopyrite samples. All the calibration, normalization and fitting were processed using Athena software, ifeffit package (Newvile, 2001).

2.8.3 S K-edge and Fe, Cu L-edge NEXAFS

S K-edge, Fe, Cu L-edge NEXAFS spectra were taken at the Soft X-ray Spectroscopy beamline (14ID) at the Australian Synchrotron. NEXAFS spectra were recorded by the Phoibos-Hsa3500 using electron analyser using Partial Electron Yield (PEY) mode and Total Electron Yield (TEY) mode. The data of Fe $L_{2,3}$-edge NEXAFS spectra were collected between 695 and 740 or 730 eV by a step width of 0.1 eV and dwell time of 0.5 s (chapter 3) or 1 s (chapter 4) with pass energy of 40 eV. The Cu L_3-edge spectra was recorded from 890 to 960 eV by a step width of 0.1 eV and dwell time of 1 s with pass energy of 40 eV, while S K-edge spectra were recorded from 2460 to 2515 eV with a step width of 0.1 eV and dwell time of 1 s and a pass energy of 40 eV. The resolution for Fe $L_{2,3}$-edge spectra, Cu L_3-edge spectra and S K-edge spectra were 0.08, 0.12, 0.55 eV, respectively. All the data process was performed with iffefit software package (Newville, 2001).

2.9 Powder X-ray diffraction (XRD)

2.9.1 Background

Powder X-ray diffraction (XRD) is a rapid analytical technique primarily used for phase identification of a crystalline material and are widely used in bioleaching study (Córdoba et al., 2008a; Harmer et al., 2006; Majuste et al., 2012; Zhu et al., 2011). The analysed material is finely ground, homogenized, and average bulk composition is determined. X-ray powder diffraction is most widely used for the identification of unknown crystalline materials (e.g. minerals, inorganic compounds), as well as the composition of known crystalline materials in a complex sample.

X-ray diffraction is based on constructive interference of monochromatic X-rays and a crystalline sample. These X-rays are generated by a cathode ray tube, filtered to produce monochromatic radiation, collimated to concentrate, and directed toward the sample. Sharp intensity maxima (constructive interference) emerge from the sample only at the special angles where conditions satisfy Bragg's Law (Fig. 2-5):

$$n\lambda = 2d \sin\theta \qquad (2\text{-}1)$$

where d is the distance of parallel lattice planes, 2θ is the diffraction angle, the angle between the incoming and outgoing X-ray beams, λ is the wavelength of incident X-ray, and n equals 0, ±1, ±2, ... (Dinnebier and Billinge, 2008)

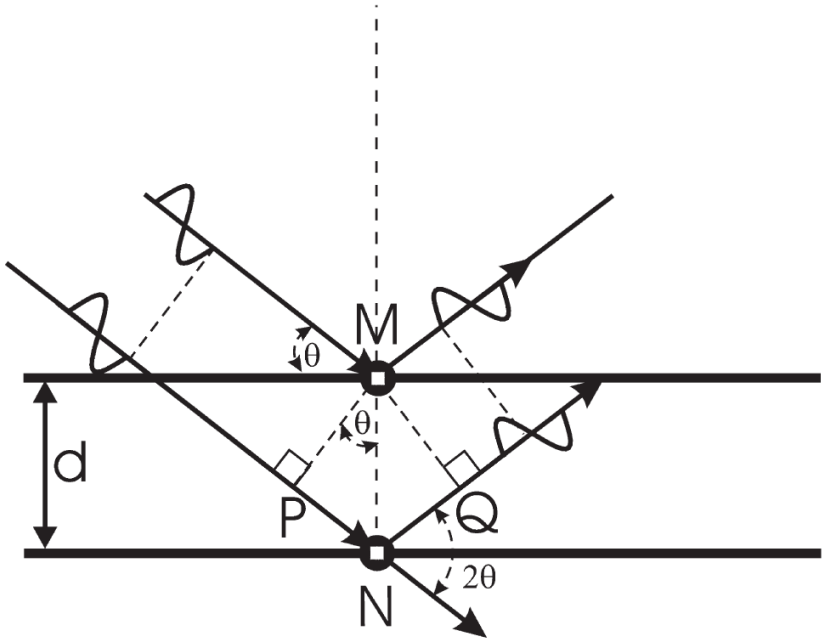

Fig. 2-5 Illustration of the geometry used for the simplified derivation of Bragg's law (Dinnebier and Billinge, 2008)

The diffracted X-rays are then detected, processed and counted. By scanning the sample through a range of 2θ angles, all possible diffraction directions of the lattice should be attained due to the random orientation of the powdered material. Conversion of the diffraction peaks to d-spacings allows identification of the mineral because each mineral has a set of unique d-spacings. Typically, this is achieved by comparison of d-spacings with standard reference patterns.

Quantification of powder diffraction data is to determine the contribution of each component in a mixture to the overall pattern. Commonly used methods can be divided into two distinct groups: ''single peak'' methods which rely on the measurement of a peak, or group of peaks. Whole pattern methods which rely on the comparison of wide range diffraction data with a calculated pattern formed from the summation of individual phase components. Whole pattern (especially Rietveld-based) methods have the potential to produce more accurate and precise results than those obtained from conventional single

peak methods, because all of the peaks in the pattern contribute to the analysis and the impact of some sample related effects, such as preferred orientation, are minimized by the inclusion of all reflections (Madsen and Scarlett, 2008).

2.9.2 Experiment procedure

Powder XRD data were collected in Bragg-Brentano geometry on finely ground samples using a Phillips X'Pert diffractometer fitted with a Co long-fine-focus tube operated at 40 kV and 40 mA, and a curved graphite post-diffraction monochromator. The beam path was defined using $1°$ divergence, 0.3 mm receiving and $1°$ scatter slits. Data were collected over the range $5° < 2\theta < 120°$ in steps of $0.02°$ 2θ. The relative proportions of the crystalline phases in each sample was determined using Rietveld-based quantitative phase analysis (QPA) using TOPAS (Version 4.2.) (Bruker, 2009).

2.10 Raman spectroscopy

2.10.1 Background

Raman spectroscopy is a spectroscopic method commonly used by inorganic chemists. When a monochromatic beam of light from a laser is focused on to a vibrating molecule, majority of the light will be scattered elastically, which is referred to as a Rayleigh scattering. The reminder of the incident laser radiation is scattered inelastically, with frequencies either more or less (Stokes signals) than the frequency of the incident radiation and derives anti-Stokes lines and Stokes lines respectively. The wave number variation between Rayleigh line and Stokes line (or anti-Stoke line) is referred to as a Raman shift, which carries the vibrational and structural information of the molecule (Warner and Butle, 2004). It provides important information about the vibrations of the molecules in the gaseous, liquid, and solid states. Furthermore, it gives clear differences in the compounds with same chemical composition but different structures (for instance linear sulfur and crystal sulfur) (Eckert and Steudel, 2003).

2.10.2 Experiment procedure

The Raman spectroscopic study was performed using a Renishaw Invia Raman Microscope with 514 nm laser source. Before the test, the equipment was calibrated using a silicon standard. To protect the sample from being damaged, a low intensity laser of energy 1 mW was used throughout the experiment. The Raman spectra were recorded at step width of 0.1 cm^{-1} between appropriate data range.

2.11 X-ray fluorescence microscopy (XFM) and μ-XANES

2.11.1 Background

X-ray fluorescence microscopy uses focused X-rays (up to submicron sizes) to perform a raster scanning of the specimen and acquire the X-ray fluorescence spectrum of each pixel, which yields chemical maps for a wide range of elements (Elisabeth et al., 2011; Fahrni, 2009).

When atoms are exposed to hard X-rays, ejection of core-shell electron may happen. The removal of an electron in this way makes the electronic structure of the atom unstable, and electrons in higher orbitals "fall" into the lower orbital to fill the hole left behind. This process results in emission of a photon whose energy is equal to the difference in binding energies of the two shells involved in the transition. Because the binding energy is proportional to the squared nuclear charge, the emitted photon energy is characteristic for each element (Fahrni, 2007). In XFM , hard X-rays is focused to submicron spot sizes, either through a Kirkpatrick-Baez mirror system, refractive lenses or with a Fresnel zone plate (Fahrni, 2007). For instance, in X-ray fluorescence microprobe beamline of Australian synchrotron, the X-ray could be focused at 2-micron length scales for applications requiring high flux using KB mirror microscope and at the 100-nm length scale for extremely high-resolution maps using a zone-plate microscope.

XFM is often coupled with μ-XANES, which has the same basic principal of conventional XANES but could give the localized chemical and structural information in submicron level as a result the focused incident X-rays.

Given these exquisite capabilities, SXRF imaging and microprobe XANES have found widespread applications in geochemistry, cosmochemistry, environmental sciences, as well as materials and polymer sciences (Bertsch et al., 2001).

2.11.2 Experiment procedure

μ-XRF and μ-XANES measurements were taken using the X-ray fluorescence microprobe beamline in the Australian synchrotron (Paterson et al., 2011). The X-ray used in XFM beamline was produced by an in-vacuum undulator filtered by a Si(111) monochromator. In this study, X-rays with an energy of 10 KeV and flux of 4×10^{11} were used. A pair of Kirkpatrick-Baez mirrors was used to form a focus of 2 μm ×2 μm on the sample. The fluorescence signal was recorded using a Vortex detector with 0.2 sec dwell.

Fe K-edge μ-XANES measurements were taken at points of interest identified from the μ-XRF maps. The XANES spectra were recorded from 7.07 to 7.295 KeV. The step width was made 0.5 eV from 7.07 to 7.108 KeV, 0.3 eV from 7.108 to 7.17 KeV and 2.5 eV from 7.17 to 7.295 KeV. The dwell time was 1 sec. The data were processed in MAPS (Vogt, 2003) and the μ-XANES results were processed in Athena software (Newville, 2001).

2.12 Electron Backscatter Diffraction (EBSD)

For SEM analysis the sample was set on a standard 25 mm stub using conductive carbon paint and inserted into the instrument, which was a FEI, Quanta 400, field emission, environmental scanning electron microscope. Some initial secondary and backscattered electron images were collected, then an orientation map was collected using a Bruker, e-Flash EBSD detector. For the map, a resolution of 800 × 690 pixels was selected which covered a sample area of approximately 2.6 × 2.2 mm. A beam energy of 20 KeV, a probe current of 25.1 nA, a stage tilt of 70 °, a dwell time of 10 ms and a diffraction pattern resolution of 160 × 120 pixels (4 × 4 binning) were also used.

Post processing of the map was done using Bruker, Esprit software which allowed the identification of (h, k, l) indices for planes parallel to the plane of polish in selected grains from the sample. A range of grains were selected which covered a number of different orientations in the sample.

2.13 Atomic Force Microscopy (AFM)

2.13.1 Principals

AFM allows the imaging of surface morphology, in some cases with atomic resolution (Butt et al., 2005). When the tip moves horizontally, the short range repulsive forces between surface and tip vary, and the tip is deflected which results the subsequent deflection of the cantilever. As a result, the reflected laser beam diverges from its original position and this divergence is measured by a position sensitive detector and the deflection of the cantilever is recorded. A topographic image of the sample then could be obtained by plotting the deflection of the cantilever versus its position on the sample.

2.13.2 Experiment procedure

AFM studies of chalcopyrite coupons before and after bioleaching were performed on an Agilent Technology 5500 Scanning Probe Microscope. The experiment was carried out in

tapping mode at a speed of 0.5 Hz. The spring constant and the resonant frequency of the probe (nonoScience) were 40 N/m and 300 kHz, respectively.

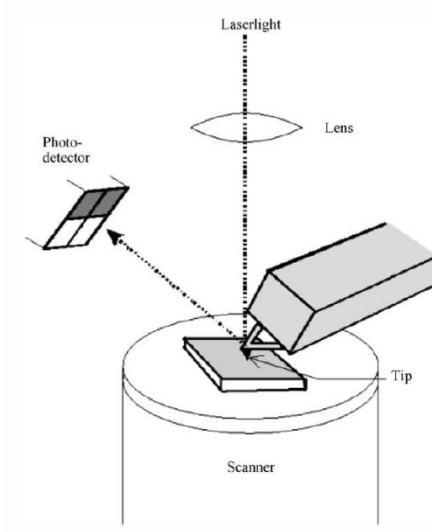

Fig. 2-6 Schematic of an atomic force microscope (Butt H et al., 2005)

2.14 X-ray Tomography (CT)

CT study was performed in Imaging and Medical beamline at Australian synchrotron. The light source was an Advanced Photon Source (APS) type A permanent-magnet wiggler, with 28X8.5 cm periods (total length 2.4 m) (Stevenson et al., 2012). A float-zone Si monolithic double-crystal monochromator was used with a vertical plane of diffraction (Stevenson et al., 2012).

The low grade ore was polished to a rod with a diameter of approximately 1 mm and mounted to the sample chamber as vertical as possible. The distance between sample and detector was approximately 1 cm. Measurements were taken at 30 KeV and 40 KeV, respectively. For each energy, one image was taken with an exposure of 3 sec at 0.075^{o} rotation, which made a sum of 2400 images for an 180^{o} scan. The pixel size of the detector was 6.5 μm and a 10X magnification was used which made the effective pixel size as 0.65 μm. The image size was 2560X2160 pixels (1.664 X1.404 mm^2). A CSIRO developed software package entitled X-Tract was used to do slice reconstruction (http://www.ts-imaging.net/Services/AppInfo/X-TRACT.aspx). The tomographic slices were then imported into the DCM (data constrained modelling) software for the prediction of the internal chemical phases within the sample (Yang et al., 2008).

Chapter 3 The surface species study of chalcopyrite bioleached at different temperatures

3.1 Introduction

As reviewed in chapter 1, chalcopyrite bioleaching kinetics is affected by temperature and bacteria type (Rodríguez et al., 2003; Sandström et al., 2005; He et al., 2009). To understand how the temperature and bacteria type impact on the chalcopyrite dissolution and passivation mechanisms, the mineralogy and surface species evolution during chalcopyrite bioleaching was investigated by SXPS, Cu and Fe K-edge XANES, L-edge NEXAFS and Raman.

3.2 Experimental

3.2.1 Leaching experiment

For the 30 ^{o}C leaching study, the chalcopyrite was leached with pure *L. ferrooxidans* and a mixed culture of *A. ferrooxidans*, *L. ferrooxidans* and *A. thiooxidans* in equal proportions. A 9K basic salt medium was used in this study. The leaching conditions were described in section 2.4.1. The leaching experiment with moderate thermophiles was carried out with the same conditions at 48 ^{o}C. Sterile controls were also performed for comparison.

Solution samples were withdrawn at regular interval for leaching parameter measurements as described in Section 2.5 and solid samples were collected for Cu, Fe K-edge XANES and XRD studies (Samples for SXPS, L-edge NEXAFS, Raman studies were collected from another leaching experiment carried out under same conditions). The solid samples (including original chalcopyrite) were washed with pH 1.8 sulfuric acid three times mixed using a vortex mixer followed by centrifuging at 3000 rpm to remove most of the attached cells. As each sample was from a separated experiment, all samples were taken just shortly before surface analysis.

3.2.2 Surface species characterization

SXPS, NEXAFS and Raman spectroscopy were performed to characterize the surface species of leached chalcopyrite according to the details described in section 2.7, 2.8.3 and 2.10, respectively.

3.2.3 Cu and Fe K-edge XANES studies

X-ray absorption spectra were recorded at BL-20B beamline (Australian National Beamline Facility, ANBF) at the Photon Factory, High Energy Accelerator Reseach Organization (KEK), Japan. BL-20B is a bending magnet beamline equipped with Si(111) monochromator, with an energy resolution (E/ΔE) of 2400. The slit used in this study was 3 mm by 1 mm. The incident beam intensity I_0 was measured with an ionisation chamber filled with N_2 at atmospheric pressure. More than 70% of the X-rays were absorbed within 30 μm around iron and copper K-edge.

Data was acquired in fluorescence mode with a 36-element solid state Ge detector. The near-edge part of the Fe K-edge X-ray absorption spectra that has been used in this study was collected from 7088 to 7152 eV with step size of 0.25 eV and dwell time of 2 s. That of the Cu K-edge X-ray absorption spectra was collected from 8970 to 9020 eV with the same step size and dwell time as for iron. Data processing was performed as described in section 2.8.2.

3.3 Result and discussion

3.3.1 Solution studies

Fig. 3-1 shows the copper and iron concentration changes during leaching. After bioleaching with thermophile for 35 days, 1.37 g/L of copper was released into solution, compared to 0.17 g/L in chemical leaching at 48 ℃ and 0.54 g/L in bioleaching with *L. ferrooxidans* at 30 ℃. These results clearly demonstrate that moderate thermophiles accelerated the copper release. Relatively, the iron concentrations at 48 ℃ were much higher than those leached with mesophiles. The favourable influence of an elevated temperature has also been observed by other researchers (Rodríguez et al., 2003; Sandström et al., 2005; He et al., 2009). The mixed culture of iron and sulfur-oxidizing bacteria did not show an advantage over the pure iron-oxidizing bacteria in this study, which is not in consensus with some studies (Akcil et al., 2007; Battaglia-Brunett et al., 1998). This may be explained by the capacity of strains vary significantly from case to case regarding to their origin, pre-adaption to mineral, the solution pH values and bacteria

growth conditions. Nevertheless, this result indicates the synergistic effect of microorganism with different metabolic pathway does not play an important role in comparison to temperature in bioleaching in the condition of this study. In bioleaching, the most important role of bacteria is to reproduce Fe^{3+} (Sand et al., 2001). Compared to *A. ferrooxidans*, *L. ferrooxidans* has a greater affinity for ferrous iron and is less sensitive to inhibition by ferric iron (Rawlings et al., 1999). Study indicates *L. ferrooxidans* prevails *A. ferrooxidans* in iron oxidation efficiency at redox potential higher than about 480 mV vs Ag/AgCl. In this study, the redox potential exceeded this value before day 7. Actually, in many commercial bioleaching/biooxidation processes, *L. ferrooxidans* was found to be the dominate species rather than *A. ferrooxidans* (Falco et al., 2003; Rawlings et al., 1999). The leaching result indicates the synergistic effect of microorganism with different metabolic pathway does not play an important role as temperature in bioleaching, considering they may have different optimal conditions.

The Fe_{tot} of the former one was higher than that of the latter one in the initial stages, which reached the maximum of 0.53 g/L after 19 days of leaching. However, the total iron in leaching with *L. ferrooxidans* dropped to 0.4 g/L and lower than that with mixed culture at day 35 because of iron precipitation.

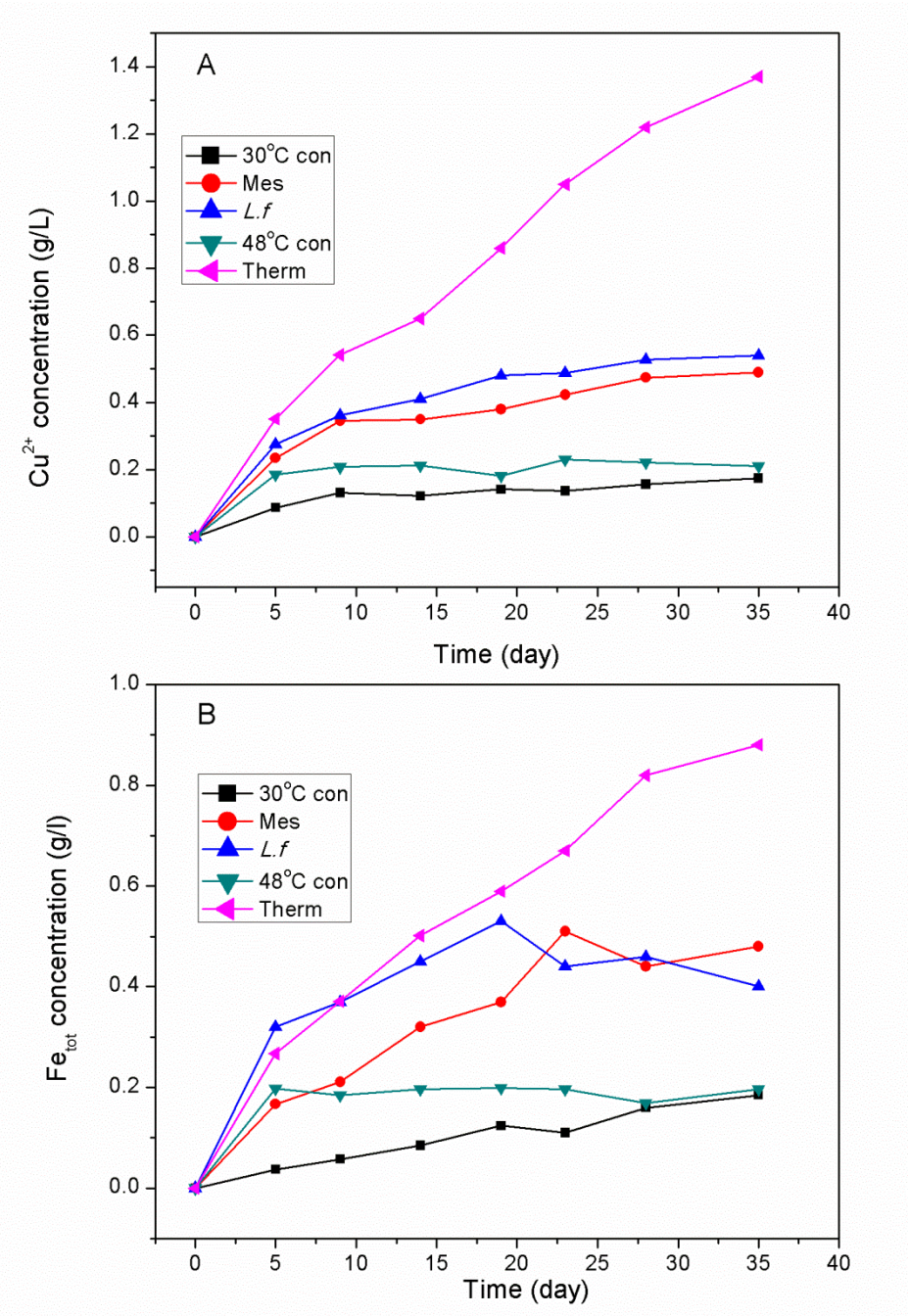

Fig. 3-1 Copper (A) and iron (B) concentration changes in chalcopyrite leaching at 30 and 48 ^{o}C

At the same time, the Fe^{2+} concentrations were low in all cases, which could not be detected accurately. The Equation 1 provided an alternative to roughly assess the $[Fe^{3+}]/[Fe^{2+}]$ ratio at 25 ^{o}C (Hiroyoshi et al., 2001).

$$E = 0.670 + 0.059 \log ([Fe^{3+}]/[Fe^{2+}]) \qquad (3\text{-}1)$$

Where, $[Fe^{3+}]$ and $[Fe^{2+}]$ indicate the concentrations of ferric ions and ferrous ions, and *E* is the solution potential vs. SHE. For this study, the slopes are 0.060 and 0.064 V at 30 ^{o}C and 48 ^{o}C, respectively. From Fig 3-2 it is clear that the Eh values in sterile controls remained low even after long leach times, which were 355 mV (vs. Ag/AgCl electrode, the same for the following Eh values unless otherwise stated) and 383 mV for leaching at 48 ^{o}C and 30 ^{o}C at the end of experiments, respectively. In bioleaching, Eh values rose rapidly over the values in chemical leaching at day 5 and continued rising to 650 mV or higher. According to Equation 1, the $[Fe^{3+}]/[Fe^{2+}]$ ratio in bioleaching were 4-5 orders of magnitude higher than that in sterile control.

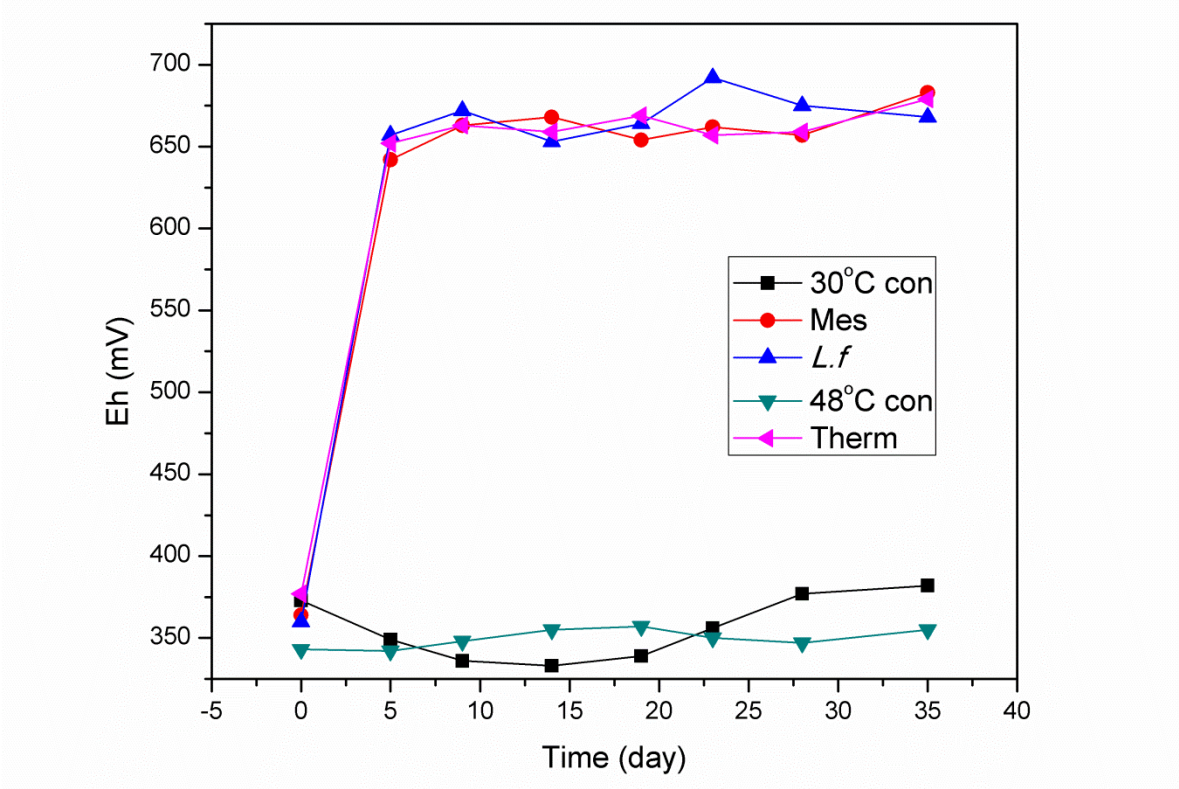

Fig. 3-2 Eh changes in chalcopyrite leaching at 30 and 48 ^{o}C

The Eh of the solution with *L. ferrooxidans* was slightly higher than that with mixed culture in the early stage. This result indicates *L. ferrooxidans* could reach high iron-oxidizing capacity more rapidly after inoculation. This may also explain the higher copper release rate with *L. ferrooxidans*. A higher ferrous oxidation capacity of bacteria resulted in a higher $[Fe^{3+}]/[Fe^{2+}]$ ratio, and subsequently help reach a higher leaching rate. However, this effect may be minor compared the impact of different temperatures (Berry et al., 1978).

The pH changes are shown in Fig. 3-3. The pH in the cases of chemical leaching and the initial stages of bioleaching increased over time, which is a result of the consumption of protons (Sand et al., 2001). In bioleaching with mesophilic mixture and thermophiles the pH increased decreased in the late stages, which could be partially caused by the oxidation of elemental sulfur by bacteria.

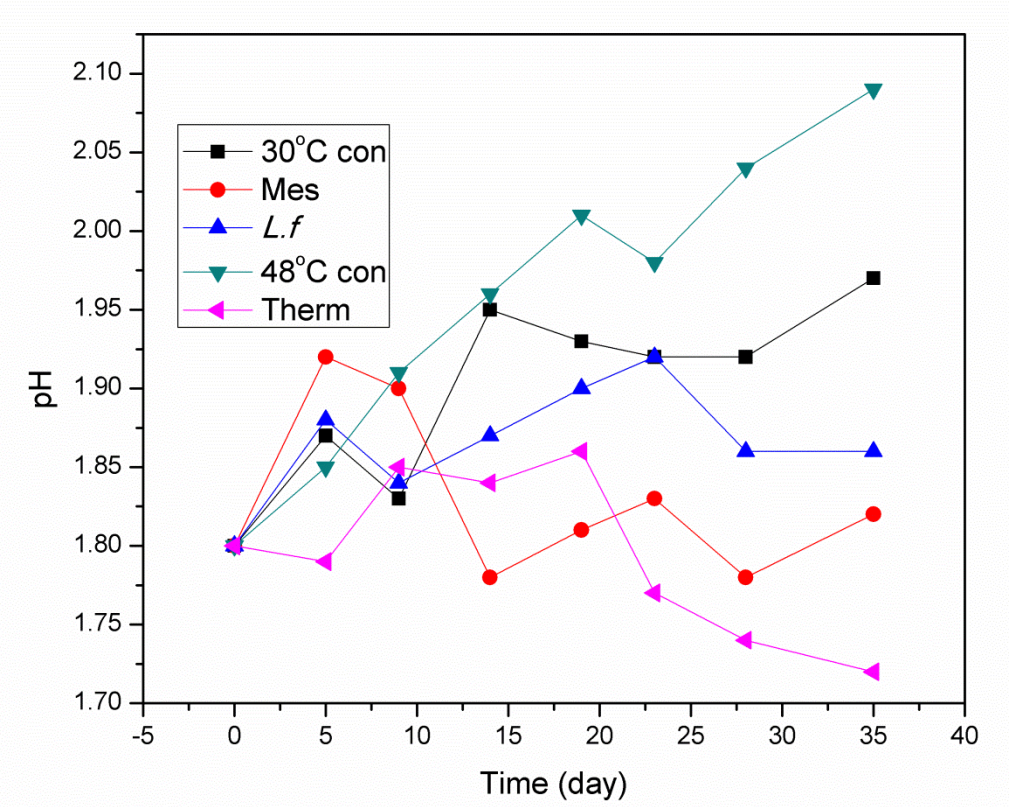

Fig. 3-3 pH changes in chalcopyrite leaching at 30 and 48 °C

The cell growth curves in Fig. 3-4 show that there was a lag phase for the growth of both thermophiles and mesophiles. However, the former one grew faster in the log phase started at day 9, probably because of more rapid chalcopyrite dissolution. At the end of leaching, the concentration of thermophiles was twice as higher as that of mesophiles. On the other hand, the growth curves of *L. ferrooxidans* and mesophilic mixture are similar.

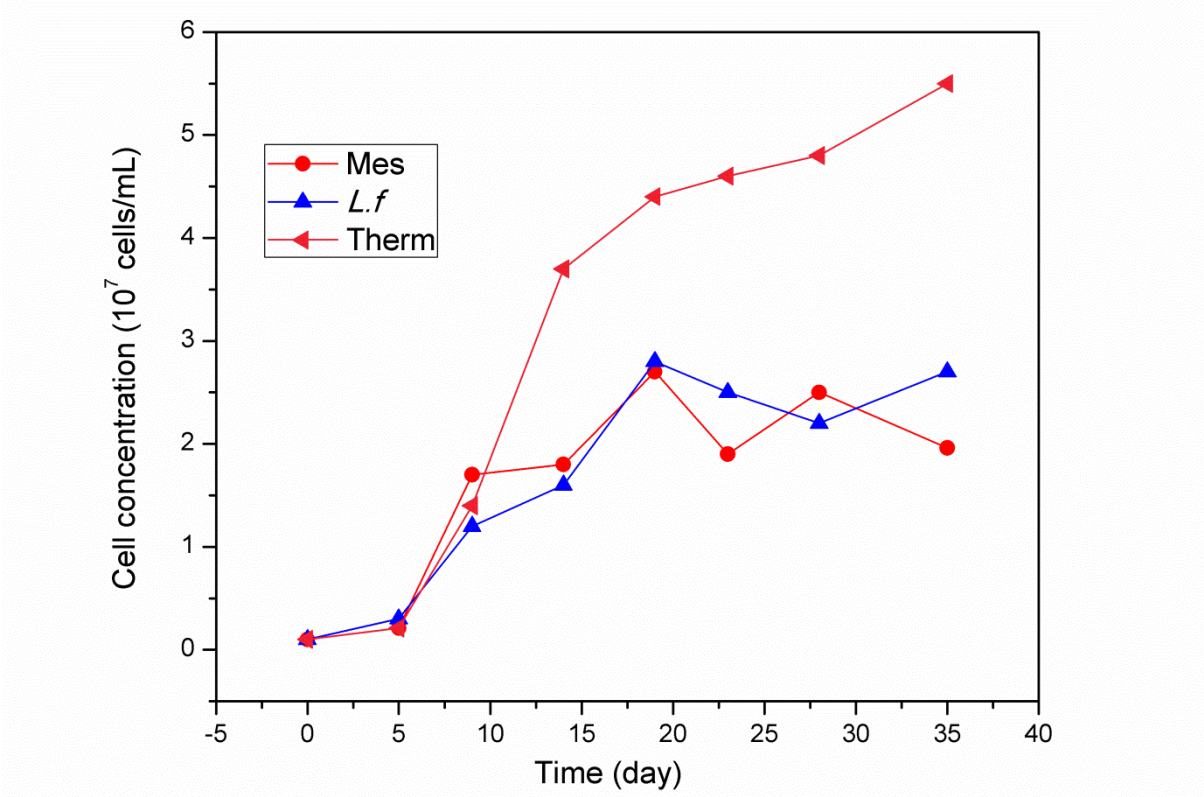

Fig. 3-4 Bacteria growth curves in chalcopyrite leaching at 30 and 48 ^{o}C

3.3.2 SXPS and NEXAFS analysis

3.3.2.1 Surface element concentration studies

The atomic concentrations generated from the survey spectra for each sample are shown in table 3-1 and 3-2 for experiments at 48 ℃ and 30 ℃. The survey scan spectrum of chalcopyrite bioleached at 48 ℃ for 25 days is shown in Fig. 3-5 as an example. At 48 ℃, the most abundant element in the samples is carbon, which contributed to 40-60% of the surface elements. Most of the carbon was adventitious carbon but there may be small amount of carbon from bacteria in long term leached samples. Oxygen is the second most abundant element, which may come from various sources including oxides, hydroxides, attached and absorbed water (Harmer et al., 2006). A slight increase of oxygen was observed in the sample bioleached for 25 days together with a slight increase of phosphorous, nitrogen and iron. The relative concentration of copper decreased with time. A similar result was observed for iron concentration in chemical leaching and early stage of bioleaching. Relatively, a slightly increased S/(Fe+Cu) ratio was detected in both chemical leaching and bioleaching. According to the results above, it could be inferred that the metal atoms on the chalcopyrite surface were depleted preferentially, leaving a

sulfur-rich layer on the surface. This phenomenon was also observed by other authors during the chalcopyrite chemical and electrochemical oxidation (Buckley and Woods, 1984; Ghahremaninezhad et al., 2010). The iron concentration increased at day 25, confirming the iron precipitation occured in the late stage. Nitrogen was detected in both bacterial and chemically leached samples. The source of nitrogen may come from the attached cells or ammonia jarosite precipitate, considering the medium contained abundant NH_4^+ ion. Phosphorus was found in bioleached samples. As no phosphorus was detected from the chemical leaching experiments, it seems not coming from the solution species dried down on the surface but the attached bacteria or/and iron phosphate precipitate (Al-Sogair et al., 2002).

Table 3-1 Atomic concentration (%) of elements on the surface of chalcopyrite chemically (sterile control) and bacterially leached at 48 ^oC ($h\nu$ = 1487 eV)

	C	O	N	S	Fe	Cu	P
Original Cp	46.2	22.7	-	15.1	7.2	8.6	-
Sterile 3 d	51.5	15.7	1.5	16.1	6.9	8.2	-
Sterile 25 d	59.1	21.7	1.2	9.3	4.6	4.0	-
7 d	46.6	22.1	2.6	15.9	6.8	7.1	-
25 d	38.6	26.8	3.4	15.7	8.1	5.7	1.6

Table 3-2 Atomic concentration (%) of elements on the surface of chalcopyrite chemically (sterile control) and bacterially leached at 30 ^oC ($h\nu$ = 1487 eV)

	C	O	N	S	Fe	Cu	P
Control 35 d	40.8	22.9	0.7	18.2	9.2	8.1	-
L.f 7 d	51.1	30.0	5.3	6.1	5.1	2.2	-
L.f 35 d	49.0	32.6	3.0	6.1	4.8	1.8	2.3
Mix 7 d	48.4	29.1	2.8	9.7	5.6	3.2	1.3
Mix 7 d	56.0	28.9	1.7	5.8	4.1	1.7	1.9

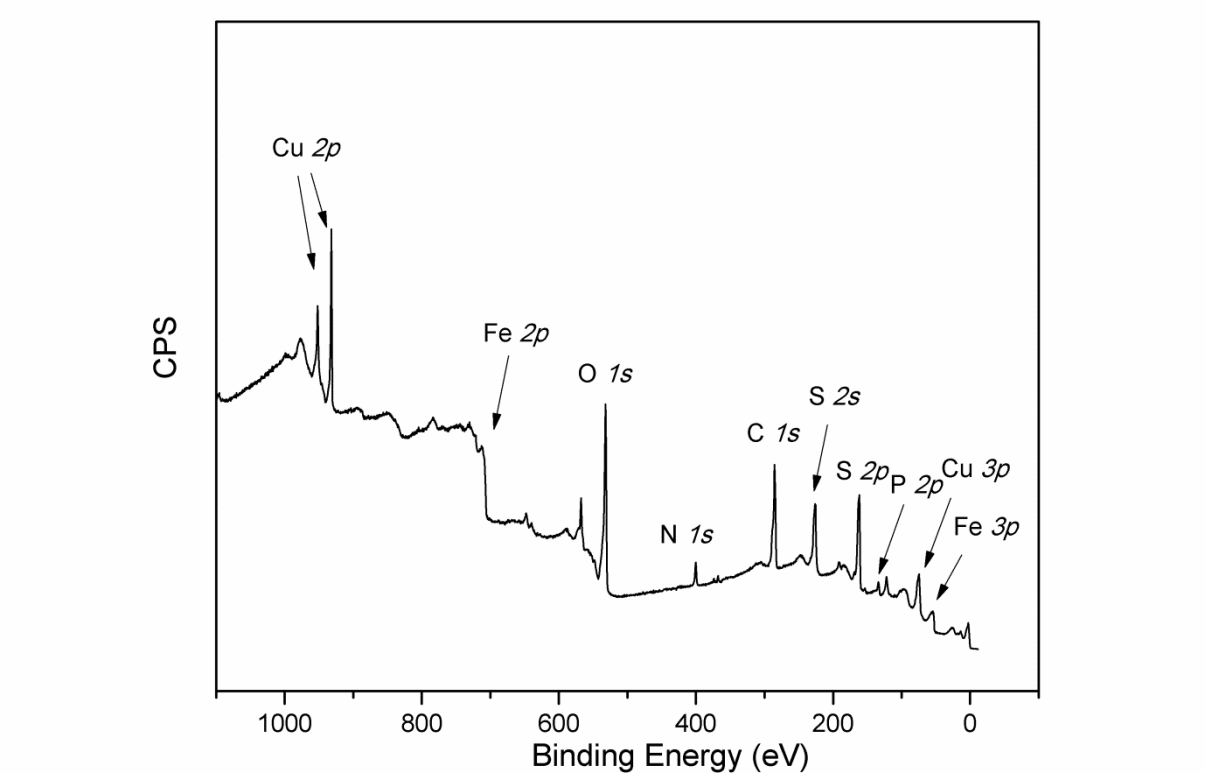

Fig.3-5 The survey scan spectra of chalcopyrite bioleached at 48 ^{o}C for 25 days

The elemental concentration trends at 30 ^{o}C were generally similar with that at 48 ℃. An increase in oxygen and nitrogen was observed in bioleached samples, accompanied with high Fe/Cu ratio, indicating iron(III) oxyhydroxides or jarosite also precipitated in leaching at 30 ^{o}C. Comparing samples from the mixed culture and *L. ferrooxidans*, a slightly higher amount Fe was detected in the presence of *L. ferrooxidans*, which may resulted from higher iron oxidation efficiency of *L. ferrooxidans*. The results indicate the chalcopyrite dissolution at different temperatures has similar mechanisms.

3.3.2.2 S *2p* spectra

High resolution sulfur 2*p* spectra of chalcopyrite leached at 48 ^{o}C collected at a photon energy of 1487 eV are displayed in Fig 3-6. Fig 3-6A displays the features of original chalcopyrite, with the strong S $2p_{3/2}$ peak at 161.4 eV originates from bulk monosulfide. The intensity at higher binding energies are indicative of disulfides at 162.4 eV and S_n^{2-} /S^0 in the range of 163-163.9 eV. The chalcopyrite surface is mildly oxidized (Buckley and Woods, 1984; Harmer et al., 2006). The results also show there was no significant amount of SO_4^{2-} brought to the sample surface during washing with sulfuric acid, because the SO_4^{2-} feature of original chalcopyrite was very weak (Fig. 3-6A).

Fig. 3-6B and Fig.3-6C display the S *2p* spectra generated from the chemically leached chalcopyrite surface. After leaching, the amount of sulfur species with higher binding energy increased, of which majorly originates from S_n^{2-} (Buckley and Woods, 1984; Smart et al, 1999). In the bioleaching group (Fig. 3-6D and 3-6E), similar spectral changes were observed but in a more prominent manner, indicating that more significant oxidation had occured. Compared to the spectra of original chalcopyrite, the intensity of peak of SO_4^{2-} at 168.5 eV increased in spectra of bioleached or chemically leached residuals, which may be an indicative of jarosite (Sandström et al., 2005).

The spectra taken at 400 eV show higher amount of oxidized sulfur species than their counterparts taken at 1487 eV. According to the universal IMFP curve, at 400 eV, the approximate maximum depth probed is 8 monolayers with approximately 40% of the signal originating from the first 3-4 monolayers, which is more sensitive than XPS experiment carried out at photon energy 1487 eV, which collects information from approximately first 15 monolayers (Tanuma et al., 1991; Seah, 1990). This result indicates the oxidized sulfur species (such as S_n^{2-} and S^0) were on the surface of bulk chalcopyrite. It is also noteworthy that the binding energy of S_n^{2-}/S^0 in the spectra taken at 400 eV was higher than that taken at 1487 eV for 0.1-0.2 eV in many cases. This result also indicates the sulfur was more polymerized on the surface than in the bulk.

Parker et al (2003) proposed the oxidized sulfur species contains no polysulfide but merely elemental sulfur. However, Mycroft et al., (1990) found the presence of both polysulfide and elemental sulfur on an oxidized pyrite electrode using Raman, and the XPS analysis indicate the S $2p_{3/2}$ binding energy of oxidized species was between 163.3 and 163.7 eV, which is similar to the spectral interpretation in this study. The binding energy of S_n^{2-}/S^0 S $2p_{3/2}$ peak of the spectra taken at 400 eV photon energy, shows a binding energy of 163.2 eV for original chalcopyrite, increased to 163.3 and 163.4 eV after bioleaching for 7 days and 25 days, respectively. This result suggests increasing polymerisation of sulfur bonding during bioleaching, which further supported the presence of polysulfide in the samples. In addition, as the sublimation of sulfur in the UHV environment at room temperature, most of the oxidized species are likely to be polysulfides.

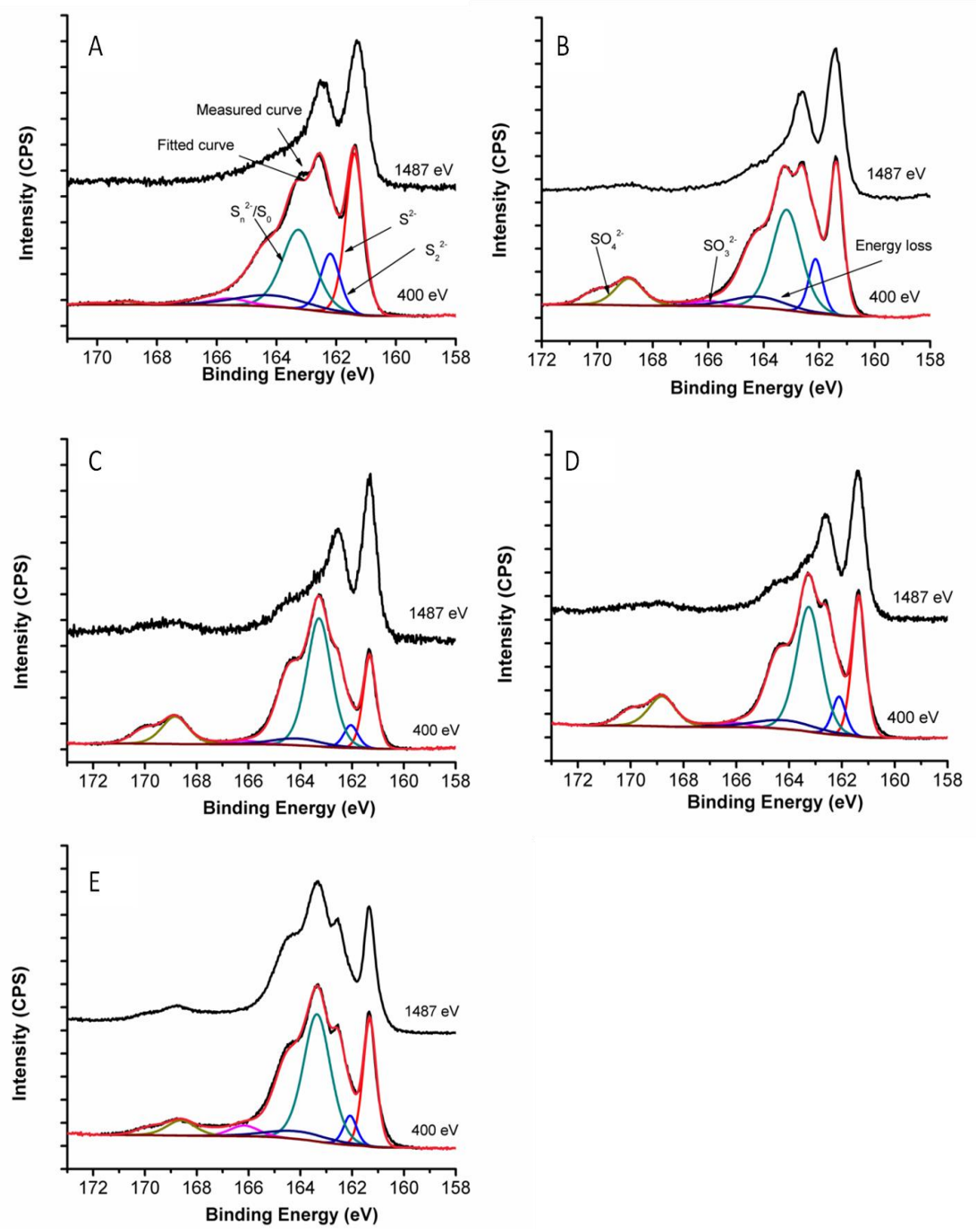

Fig. 3-6 The evolution of chalcopyrite surface sulfur layer leached by moderate thermophiles (A, original chalcopyrite; B, chemical leached for 3days; C, chemical leached for 25 days; D, bioleached for 7 days; E, bioleached for 25 days)

The result of the quantification of sulfur species is shown in table 3-3. The S^{2-} species, which represents bulk chalcopyrite, decreased with time from 38.6% to 26.0% (Atomic percent; hv=400eV. Same for all S *2p* data in the following text unless specifically stated). While S_n^{2-}/S^0, which could be regarded as the result of oxidation, increased from

34.2% to 53.1%. In sterile controls, the same trend was observed which suggests the surface sulfur species evolution may undergo a same pathway regardless of whether bacteria are present or not. The proposed indirect mechanism of bioleaching suggests bacteria produce Fe^{3+} and H^{+} to oxidize the minerial rather than mediate a direct enzymatic attack (Sand et al., 2001).

From atomic concentrations, it can be concluded that copper and iron on the chalcopyrite dissolved more rapidly, while a sulfur-rich surface layer was formed. According to the sulfur *2p* study, this sulfur-rich layer was mostly composed of S_n^{2-}/S^0.

Table 3-3 Percentages of different surface sulfur components in total sulfur on chalcopyrite leached at 48 ^oC

	S^{2-}		S_2^{2-}		S_n^{2-} / S^0		SO_3^{2-}		SO_4^{2-}		Energy loss	
S $2p_{3/2}$ BE (eV)	161.3		162.4		163.0-163.4		165.5-166.2		168.5		164.1	
Photon energy (eV)	1487	400	1487	400	1487	400	1487	400	1487	400	1487	400
Original Cp	60.3	38.6	7.8	15.3	18.8	34.2	-	3.4	1.8	1.2	11.3	7.2
Control 3 d	53.7	29.6	6.6	10.8	25.3	41.3	-	2.2	4.4	10.5	10.0	5.5.
Control 25 d	53.7	21.1	3.2	5.7	26.6	54.7	-	1.8	6.4	12.7	10.0	3.9
Thermophile 7 d	54.4	27.9	3.7	7.7	25.1	45.6	-	4.6	6.6	12.0	10.2	5.2
Thermophile 25 d	43.9	26.0	8.8	6.0	33.9	53.1	-	3.4	5.10	6.7	8.2	4.9

Fig. 3-7 show the S *2p* spectra of chalcopyrite leached at 30 ℃ at photon energies of 1487 eV and 400 eV, respectively. The results of fitting are summarised in table 3-4. In the sterile control, the contribution of S_n^{2-}/S^0 species reached over 40%, which indicated significant surface modification of the chalcopyrite surface. However, only 2.9% sulfate was found, which may imply only very small amount of jarosite was formed at 30 ^oC, when bacteria were not added.

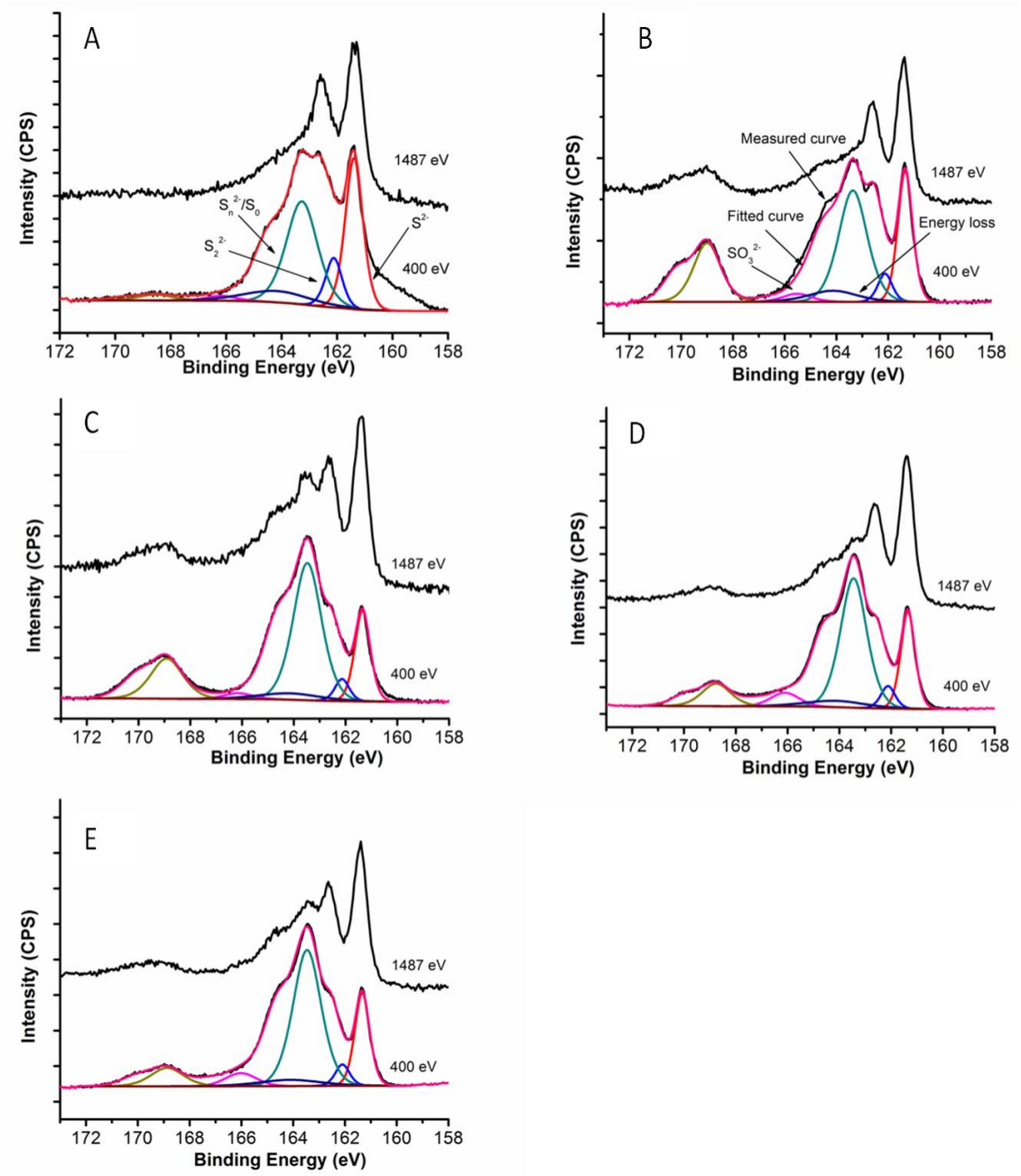

Fig. 3-7 Comparative study of chalcopyrite surface sulfur layer leached by *L. ferrooxidans* and mesophilic mixed culture (A, sterile control; B, leached by *L. ferrooxidans* for 7 days; C, leached by *L. ferrooxidans* for 35 days; D, leached by mixed culture for 7 days; E, leached by mixed culture for 35 days)

Compared to the control group at 48 ^{o}C, the chalcopyrite in sterile control at 30 ^{o}C did not change significantly. The proportion of S^{2-} was 35.4% and that of S_n^{2-}/S^0 was only 42.5% at the end of leaching, while their counterparts at 48 ^{o}C were 21.1% and 54.7%, respectively. However, when microoganisms were added, the differences became more ambigous. At day 7, S^{2-} was 24.9% and S_n^{2-}/S^0 was 41.3% on chalcopyrite leached with *L.*

ferrooxidans, while their counterparts in experiments with moderate thermophiles were 27.9% and 45.6%. At the end of leaching, the 20.4% S^{2-} and 53.1% S_n^{2-}/S^0 were found on chalcopyrite leached with *L. ferrooxidans*, while 26.0% S^{2-} and 53.1% S_n^{2-}/S^0 were detected with thermophiles. Similar results could be found by comparing the sulfur species between leaching with thermophile and mesophilic mixture. Within the experimental error, it could be concluded that the relative concentration of bulk chalcopyrite and S_n^{2-}/S^0 species did not change significantly due to temperature change. The spectra of chalcopyrite leached for 7 days (Fig. 3-7B) can not be well fitted. This is most likely due to slight charging effect has not been compensated. The C *1s* line is a little distorted on the high binding energy side. The splitting is the same distance from the C peak (3 eV) as the peak required to fit the S *2p* shoulder.

Table 3-4 Percentages of different surface sulfur components in total sulfur on chalcopyrite leached at 30 °C

	S^{2-}		S_2^{2-}		S_n^{2-}/S^0		SO_3^{2-}		SO_4^{2-}		Energy loss	
S $2p_{3/2}$ BE (eV)	161.3		162.4		163.2-163.5		165.5-166.2		168.5		164.1	
Photon energy (eV)	1487	400	1487	1487	1487	400	1487	400	1487	400	1487	400
Control 35 d	55.5	35.4	8.0	10.8	23.2	42.5	-	2.0	2.9	2.7	10.4	6.6
L.f 7 d	49.0	24.9	4.2	5.2	24.5	41.3	-	3.0	14.9	20.8	9.2	4.6
L.f 35 d	38.8	20.4	3.3	4.7	33.8	53.1	6.1	2.3	10.7	17.6	7.2	3.5
Mix 7 d	47.9	22.0	3.8	5.1	28.9	54.1	2.7	4.4	7.8	10.3	8.9	4.1
Mix 35 d	41.8	20.3	4.2	4.5	33.7	56.6	4.0	5.8	8.3	8.9	7.8	3.8

In an electrochemical study of chalcopyrite carried out by Rodríguez et al. (2003), the authors found a prewave, which occurred at about +500 mV and linked to the formation of a sulfur-rich passive species. That prewave was weaker at when temperature was arised to 68 °C. Based on this change the author pointed out the passivation was impaired, which may explain the rapid chalcopyrite dissolution at high temperatures. However, according this study, although the leaching of chalcopyrite was considerably accelerated, there is no significant difference on surface S/metal ratio and sulfur speciation between the chalcopyrite bioleached at 48 °C and 30 °C.

Eh is another important factor to chalcopyrite dissolution, the reported optimal Eh range was around 430-470 mV, which provided an obvious avantage for chalcopyrite leaching over that at high Eh (over 600 mV) (Hiroyoshi et al., 2001; Sandström et al., 2005). In this study, when bacteria were added, Eh increased to a high value within a short time. The Eh values in the experiments with bacteria addition were very close and a 5-10 times

increase of copper concentration at 48 ^{o}C should also not be a result of Eh variation. Based on the above analysis, it is clear that the increased leaching rate at high temperature is mostly caused by the increased abiotical reaction rate.

A contribution around 166.5 eV was found in some spectra, which arises from the presence sulfur oxy species such as sulfite (Sartz et al., 1971). The fitting results (table 3-3 and table 3-4) show that a small amount of sulfite species in all the spectra taken at 400 eV but not identified in most of the spectra taken at 1487 eV. This result indicates this species was on the most surface of the sample.

3.3.2.3 Fe 2*p* spectra and Fe L-edge NEXAFS

The Fe 2*p* spectra of the original and leached chalcopyrite are displayed in Fig. 3-8 and 3-9. The peak at 708.2 eV could be assigned to Fe(III)-S (McIntyre and Zetaruk, 1977, Nesbitt et al., 2000), which represents the bulk chalcopyrite. In the oxidized samples, an additional feature around 711 eV appeared. According to the standard Fe *2p* spectrum of jarosite, this feature may be an indication of the jarosite (Sandström et al., 2005; Parker et al., 2003). Interestingly, all the samples showed an increased feature at 711 eV also had a higher amount of N and O (table 3-3 and table 3-4). As in this study, no definitive evidence of K was found in the XPS survey spectra, it is speculated ammonia jarosite could be one of the major components of the iron precipitate. This peak could also be assigned to iron(III)-O-OH species such as iron (III) oxyhydroxides (McIntyre and Zetaruk, 1977; Nesbitt and Muir, 1994) or iron(III) phosphate (Annapragada and Gulari, 1990; Yu et al., 2007). However, Fe oxyhyroxides or/and iron phosphate is expected to have a small contribution to the iron precipitation in the 9k solution at pH 1.8 (Al-Sogair et al., 2002; Acres et al., 2010b).

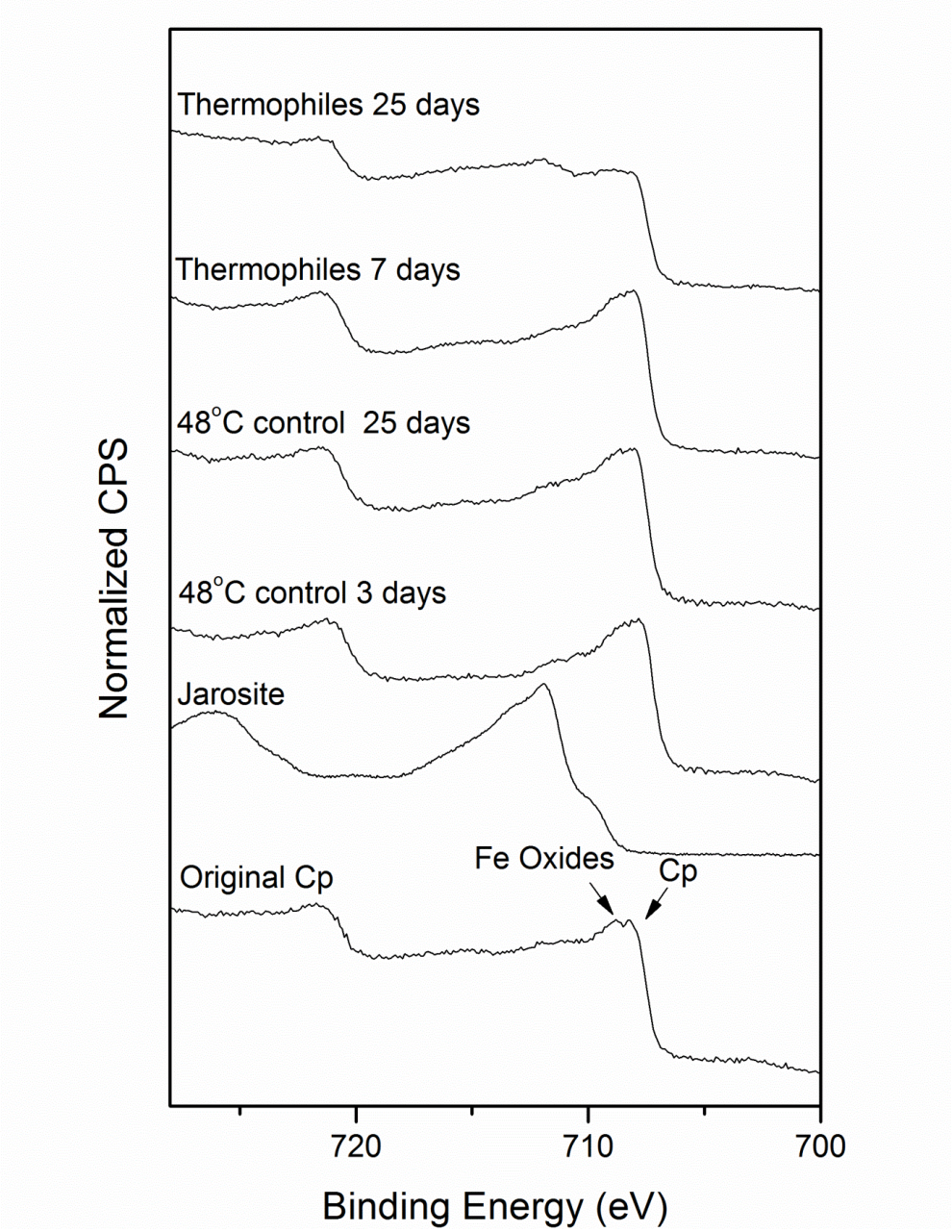

Fig. 3-8 Fe *2p* Spectra of chalcopyrite surface iron species leached by moderate thermophiles (*hv* = 1486.6 eV for jarosite; *hv* = 1470 eV for other spectra)

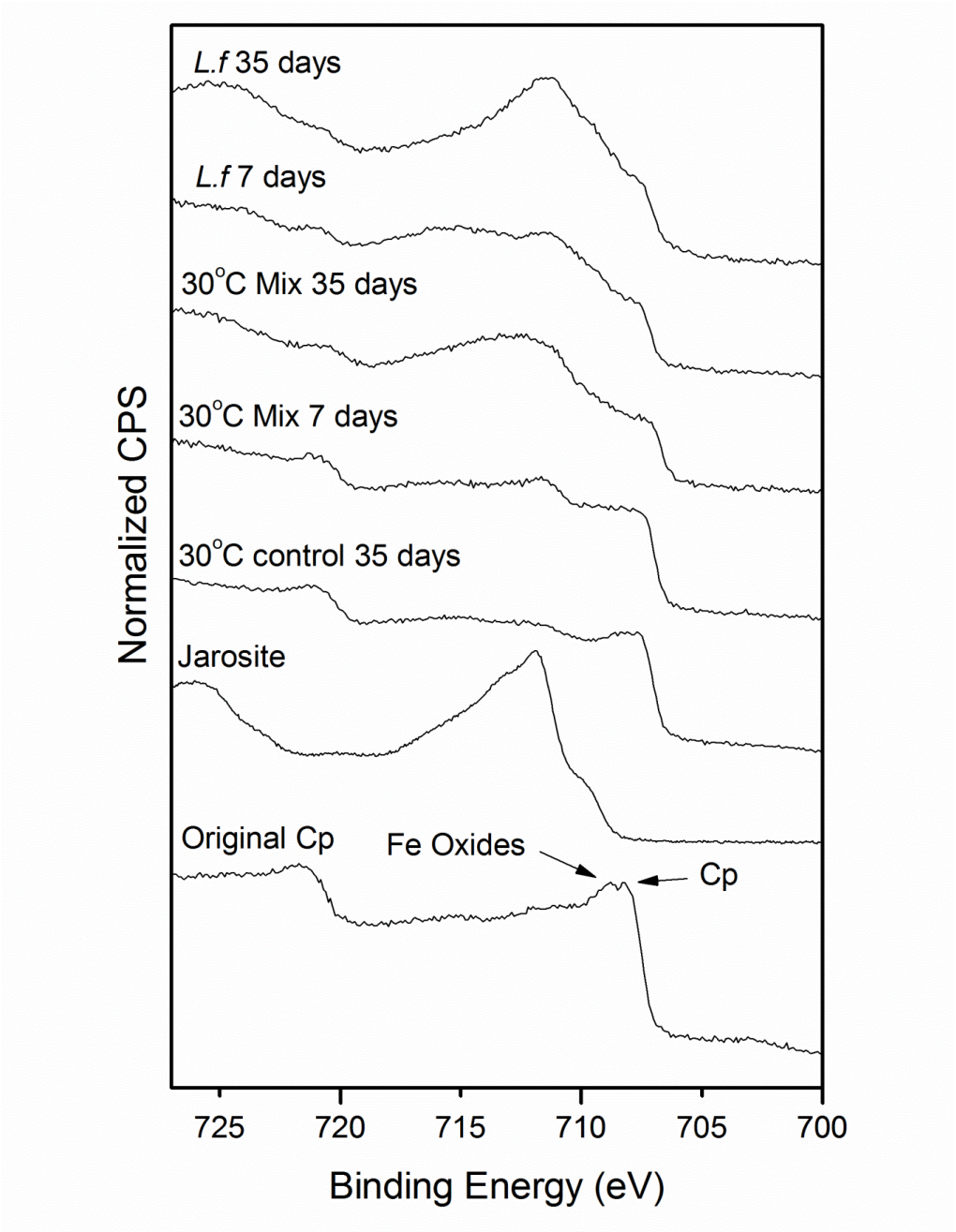

Fig. 3-9 Comparative Fe *2p* study of chalcopyrite surface iron species leached by *L. ferrooxidans* and mesophilic mixed culture (*hv* = 1486.6 eV for jarosite; *hv* = 1470 eV for other spectra)

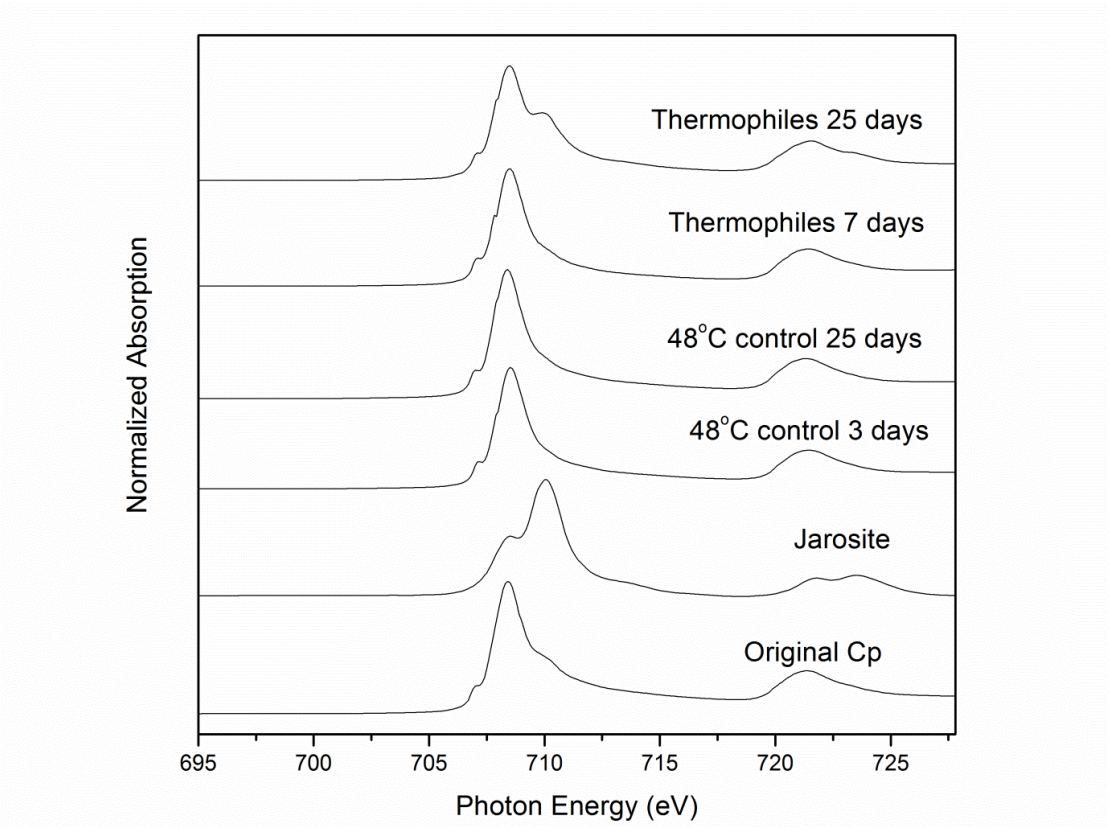

Fig. 3-10 Fe $L_{2,3}$-edge NEXAFS study of chalcopyrite surface iron species leached by moderate thermophiles

Fe $L_{2,3}$-edge NEXAFS data are shown in Fig. 3-10 and 3-11 for chalcopyrite leached at 48 ^{o}C and 30 ^{o}C, respectively. The NEXAFS results gave similar information to the Fe *2p* spectra. The original unoxidised mineral shows only a single peak at 708.5 eV that came from high-spin Fe(III) in chalcopyrite (Pearce et al., 2006). In the sterile control, there was no visible change, indicating no significant iron species precipitated on the minerals surface, which is in consensus with other results of this study. In bioleached samples, there was a new peak increasing with reaction time. The peak indicates the deposition of surface layers, which progressively formed during leaching. This new peak may come from some Fe(III)-OOH species (Pearce et al., 2006), and is similar to that of jarosite standard. Combining above analysis, it is reasonable to claim the growing iron layer majorly came from jarosite precipitation. Compared to Fe $L_{2,3}$-edge NEXAFS spectra, the Cu $L_{2,3}$-edge spectra indicate only Cu(I) present in the samples as evidenced by the peak at at 932.5 eV (Acres et al., 2010a) (Fig. 3-12).

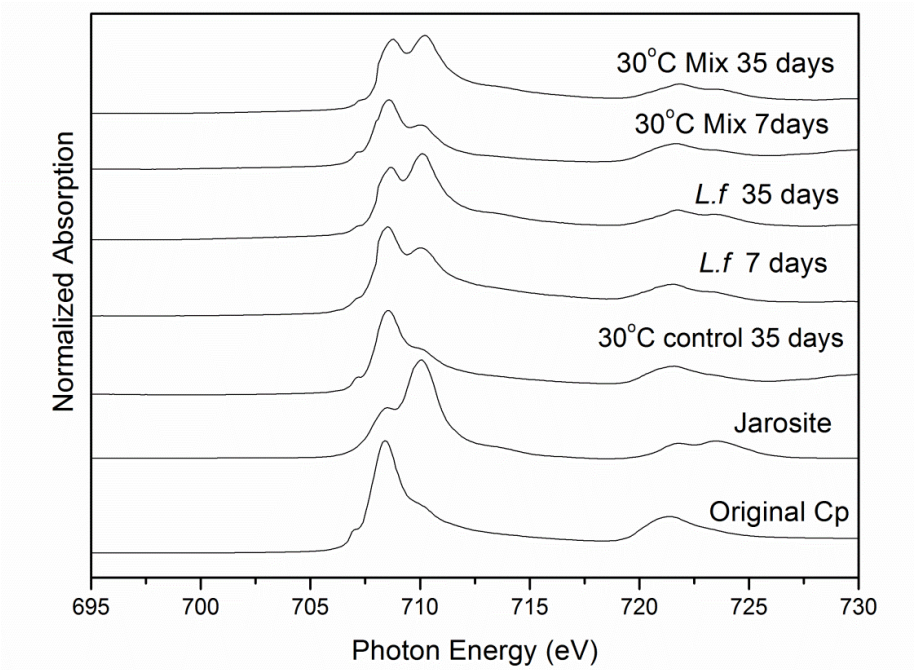

Fig. 3-11 Comparative Fe $L_{2,3}$-edge NEXAFS study of chalcopyrite surface iron species leached by *L. ferrooxidans* and mesophilic mixed culture

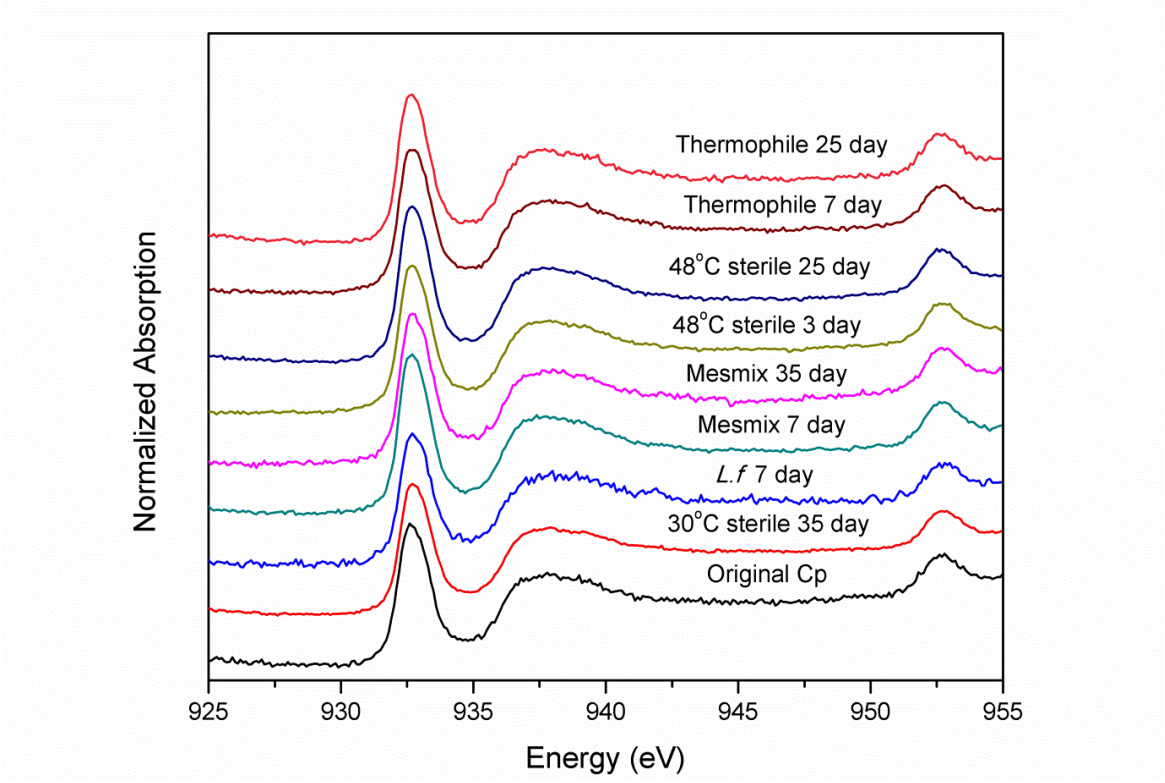

Fig. 3-12 Cu L-edge NEXAFS spectra of chalcopyrite leached in different conditions

3.3.3 Raman studies

Raman spectra of residuals leached at 48 ^{o}C and 30 ^{o}C are shown in Fig. 3-13 and Fig. 3-14, respectively. Compared to the XPS study, the Raman spectra do not show significant changes, which may be explained by the poorer surface sensitivity of Raman. Nevertheless, the Raman spectra provided important supporting evidence to XPS. In Fig. 3-13, the Raman spectra of original mineral only displayed the three peaks at 292 cm^{-1}, 320 cm^{-1}, 353 cm^{-1}, which originate from chalcopyrite (Mernagh and Trudu, 1993; Ohrendorf et al., 1999). In Fig. 3-14, besides the strong chalcopyrite features in all spectra,

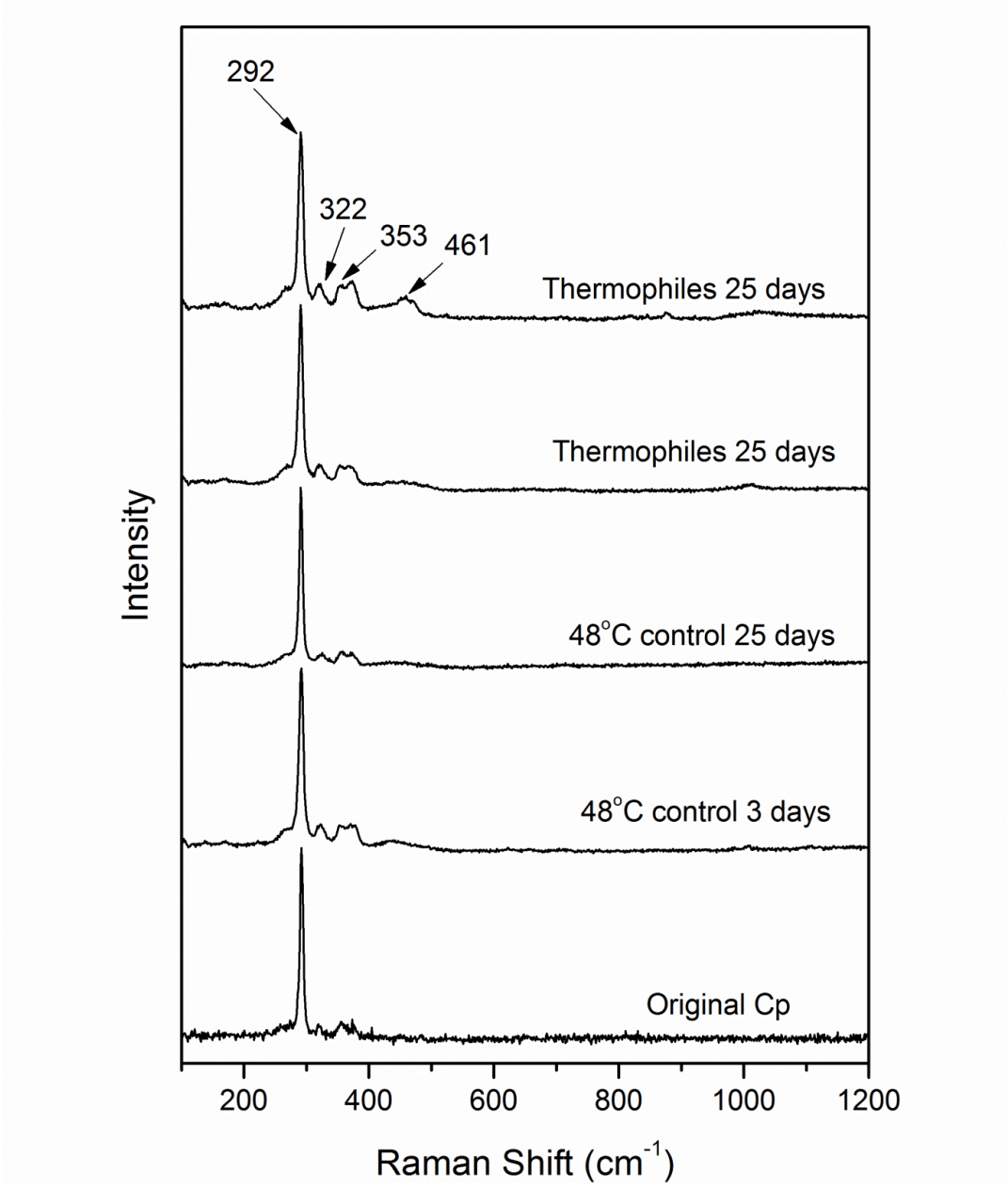

Fig. 3-13 Raman study of chalcopyrite surface species leached by moderate thermophiles

a few new peaks appeared in the leached residuals. The new peaks at 153 cm^{-1}, 220 cm^{-1} and 471 cm^{-1} in the spectra of chalcopyrite leached with *L. ferrooxidans* for 35 days could be assigned to crystalline elemental sulfur (Eckert and Steudel, 2003). In the spectra of chalcopyrite with *L. ferrooxidans* for 7 days, these bands are very weak but still visible. While in other spectra, there were no evidence of the formation of crystalline S_8. To improve the leaching kinetics, Rodr ǵuez et al. (2003) have made an attempt to eliminate elemental sulfur formed on the mineral surface of the bioleached residue using carbon disulfide (CS_2). In that experiment, they found carbon disulfide was inefficient in dissoving the elemental sulfur layer, which indicated the sulfur was not crystalline but plastic and amorphous. However, according to this study and previous results (Parker et al., 2008; Sasaki et al., 2009), crystalline elemental sulfur should be at least one major presenting form of the elemental sulfur on both bioleached and chemically leached chalcopyrite.

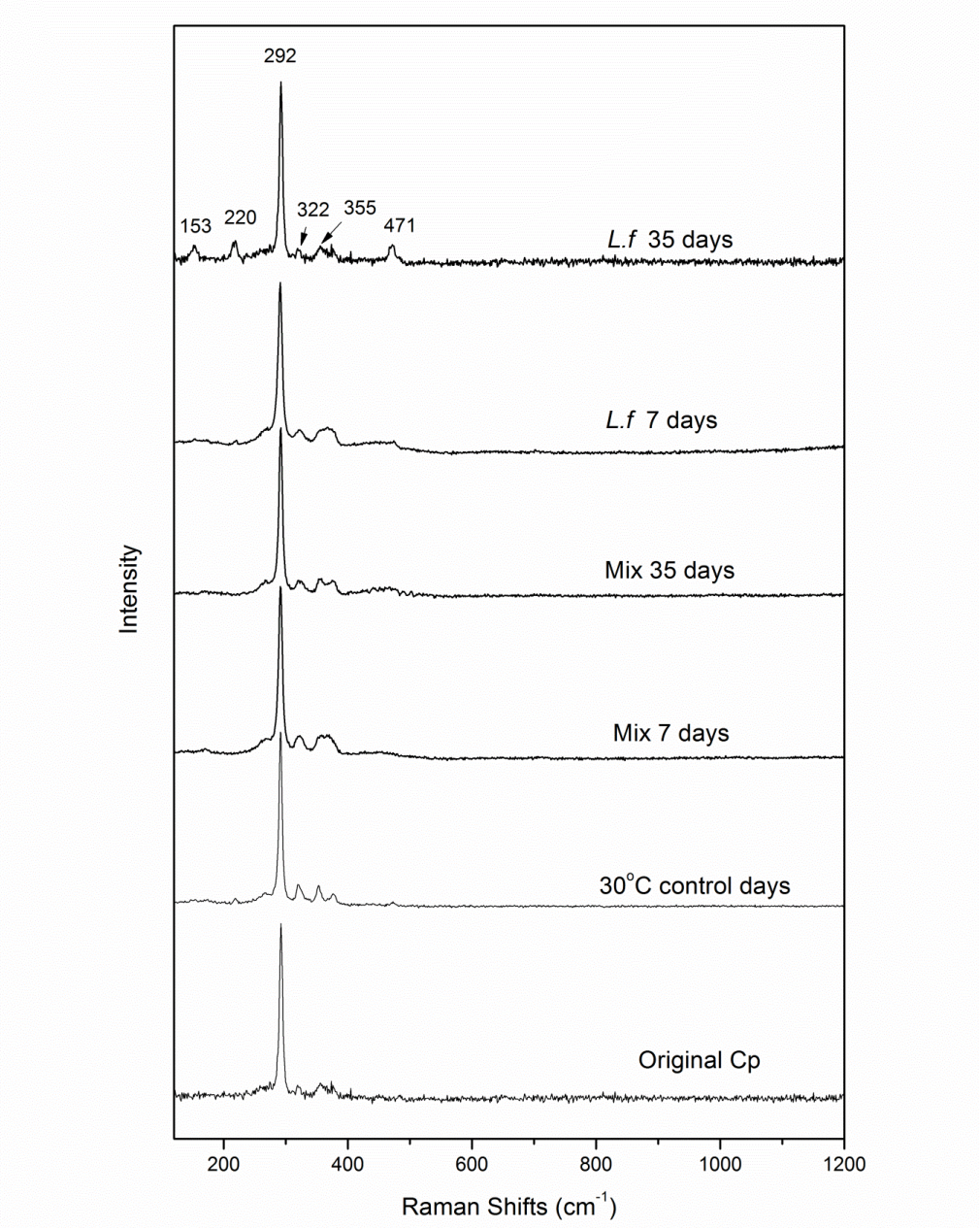

Fig. 3-14 Comparative Raman study of chalcopyrite surface species leached by *L. ferrooxidans* and mesophilic mixed culture

As the Raman spectra only give the information at specific points and the leached chalcopyrite surface is not completely homogenous, the absent of sulfur peaks does not rule out the possibility of the existence of elemental sulfur. However, the fact that the evidence of elemental sulfur was found only in leaching with *L. ferrooxidans* at least indicates more elemental sulfur formed in this case. Combining the results of Raman and S *2p* spectra, it could be concluded that elemental sulfur produced during the leaching was efficiently oxidised by sulfur-oxidizing bacteria. This finding is similar to previous studies. Schippers et al. (1996) investigated the elemental sulfur accumulation via ethanol

extraction and high-pressure liquid chromatography quantification and found more elemental sulfur accumulated on pyrite surface leached by *L. ferrooxidans* than that leached by *A. ferrooxidans*.

The use of mixed culture did not show better leaching result, which as discussed previous section may relate to the inferior iron oxidation ability of *A. ferrooxidans* at high potential. It also indicate elemental sulfur is not a passivation factor, which is in consistent with previously studies (Parker et al., 1981; Sandström et al., 2005). The thermophile showed considerably advantage over the *L. ferrooxidans*, but it should be considered as result of the increased abiotic dissolution kinetics rather than the absent of elemental sulfur. This suggests that the formation of elemental sulfur does not hinder the leaching significantly.

3.3.4 XRD studies

Fig. 3-15, 3-16 and 3-17 show XRD patterns of chalcopyrite bacterially or chemically leached for 7, 20 and 35 days. In most of the samples, only chalcopyrite and a small amount of quartz were identified by XRD. There was no evidence of any copper species other than chalcopyrite could be identified from the XRD patterns, which indicate no crystalline copper compounds present in the samples. The XRD results also show no jarosite or other iron precipitates formed in sterile controls at 30 ^{o}C and bioleaching with mesophilic mixture. In bioleaching at 48 ^{o}C, no jarosite formation was found in early stages, however massive iron precipitation was found after 35 days (Fig 3-17). The iron precipitates that found by XPS in bioleaching at 30 ^{o}C were not peaked up by XRD, which is because XRD is a bulk analysis method. In addition, the peaks of elemental sulfur was only identified in chalcopyrite after 35 day's leaching, which indicate more severe oxidation of chalcopyrite in the presence of thermophiles.

.

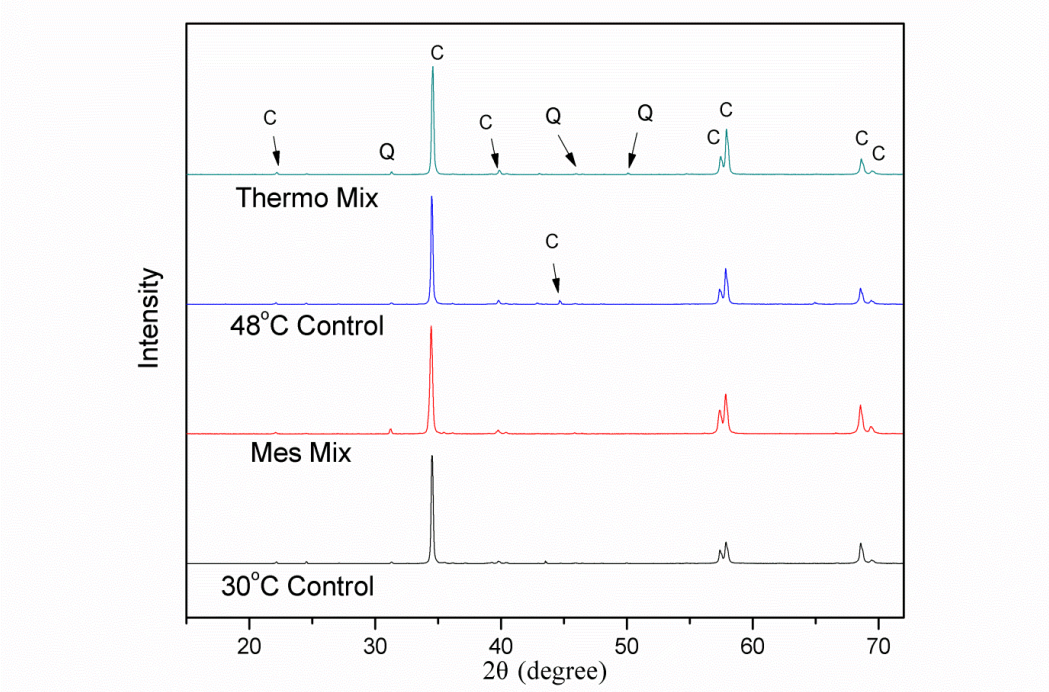

Fig. 3-15 XRD patterns of chalcopyrite leached for 7 days (C: chalcopyrite; Q: quartz)

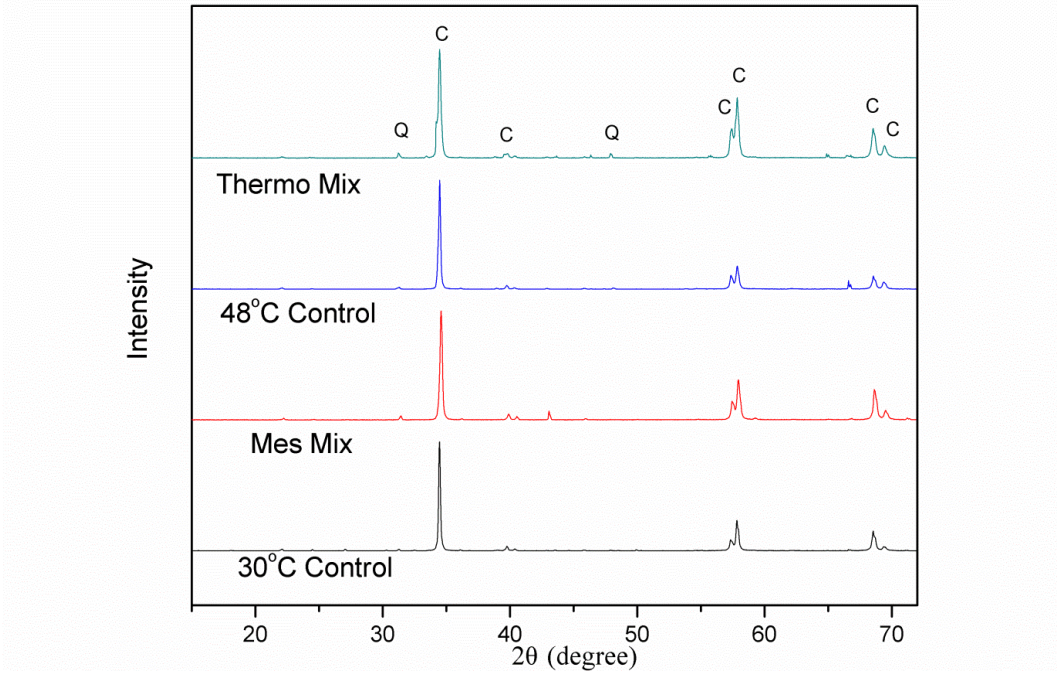

Fig. 3-16 XRD patterns of chalcopyrite leached for 20 days (C: chalcopyrite; Q: quartz)

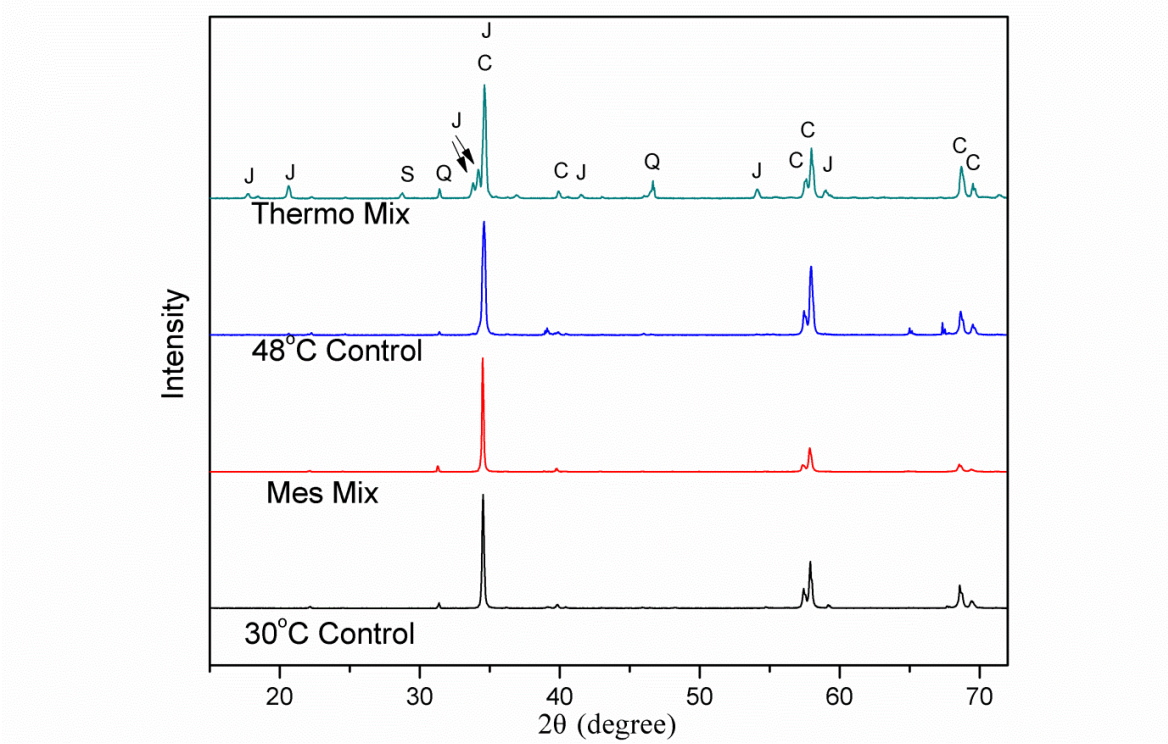

Fig. 3-17 XRD patterns of chalcopyrite leached for 35 days (C: chalcopyrite; Q: quartz; S:S_8)

3.3.5 XANES studies of leached chalcopyrite

3.3.5.1 Copper K-edge studies

Fig. 3-18 shows the Cu K-edge spectra of some typical copper compounds. By comparing the spectra of synthesized CuS_n to other standards, it could be concluded that this standard is not a copper sulfide or copper oxide, which may form in the process of CuS_n synthesis if the conditions are not properly controlled. The peak at 8983.7 eV in the spectra of the original chalcopyrite is indicative of tetrahedrally coordinated Cu, while the smooth profile of CuS_n suggests the existence of distorted triangular coordinated Cu (Pattrick et al., 1997).

The Cu K-edge XANES data for 30 ^oC leaching is shown in Fig. 3-19. In Fig. 3-19A, the spectra of some leached samples shifted towards CuS_n in the first 7 days and changed back to chalcopyrite at later stage (Fig. 3-19). Chalcopyrite leached for 35 days almost had the same spectra as the original one. On the other hand, in sterile controls, the most significant shift of the spectra to CuS_n was observed at day 20 rather than at day 7 (Fig. 3-19B). It is noteworthy that no copper species other than chalcopyrite was found in XRD, which indicate the new copper species that cause the spectra shift is amorphous, such as CuS_n-like species.

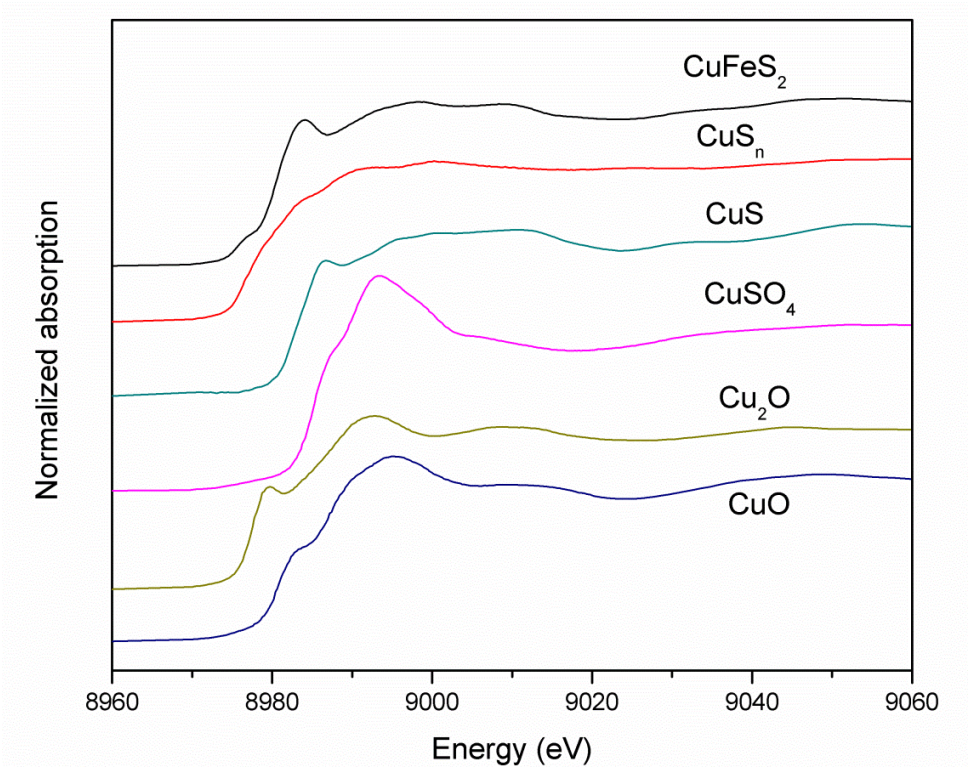

Fig. 3-18 Cu K-edge XANES spectra of some copper standards

To retrieve quantified information from the changes in the spectra, LC fitting was done. The LC fitting was run at first with several references including chalcopyrite, CuS_n, CuS and Cu_2S. However, CuS and Cu_2S were found not to be a likely solution of LC fitting. The best fitting results are summarized in Fig.3-20. With mesophilic mixture, the proportion of CuS_n decreased continuously from 43% at day 7 onwards to 2% at day 35. In leaching with *L. ferrooxidans*, an increase of CuS_n-like species was found in the first 20 days which decreased to 12.1 after 35 days of leaching. In sterile controls, only at day 20, a significant amount of CuS_n-like species was found. The CuS_n-like species accumulated more slowly in sterile controls, indicating microbes sped up the surface reaction of chalcopyrite.

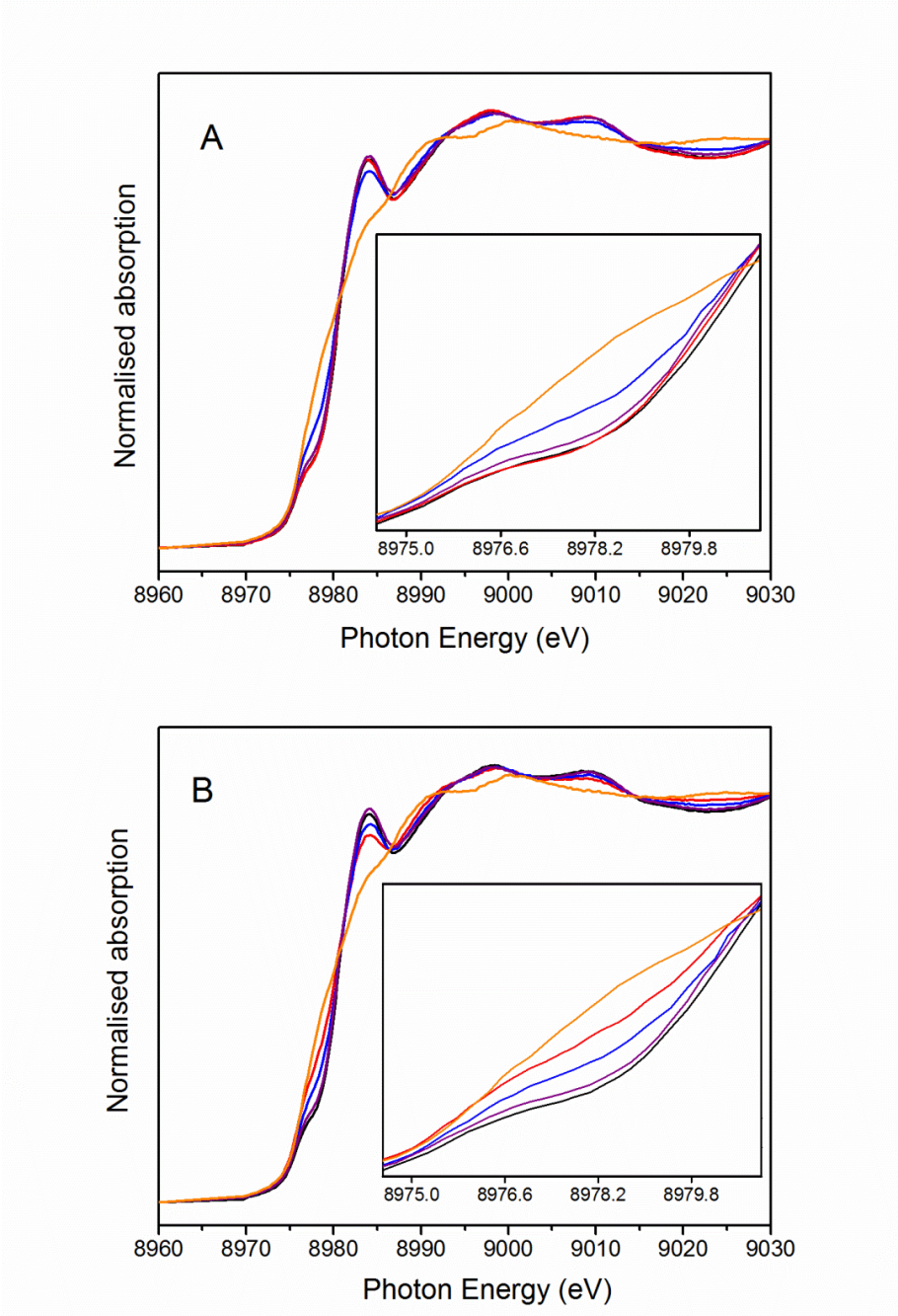

Fig. 3-19 Cu K-edge XANES spectra of chalcopyrite A) bioleached by mesophilic mixture and B) chemical leached at 30 ^{o}C (Original chalcopyrite — black; CuS_n — orange; chalcopyrite leached for 7 d — red, 20 d — blue, 35 d— purple.)

At 48 ^{o}C, a similar trend was detected. However, the shift from CuS_n to $CuFeS_2$ was faster than that at 30 ^{o}C (Fig. 3-20), indicating that higher temperature facilitated copper release and the formation of high S/Cu ratio polysulfides. A higher amount CuS_n-like species was detected at day 35. In sterile controls, the proportion of CuS_n-like species remained fairly constant over time and there was about as much that on day 20 of the 30 ^{o}C control test.

Based on these results, it is likely that the elevated temperatures accelerated both the formation and dissolution of CuS_n-like species.

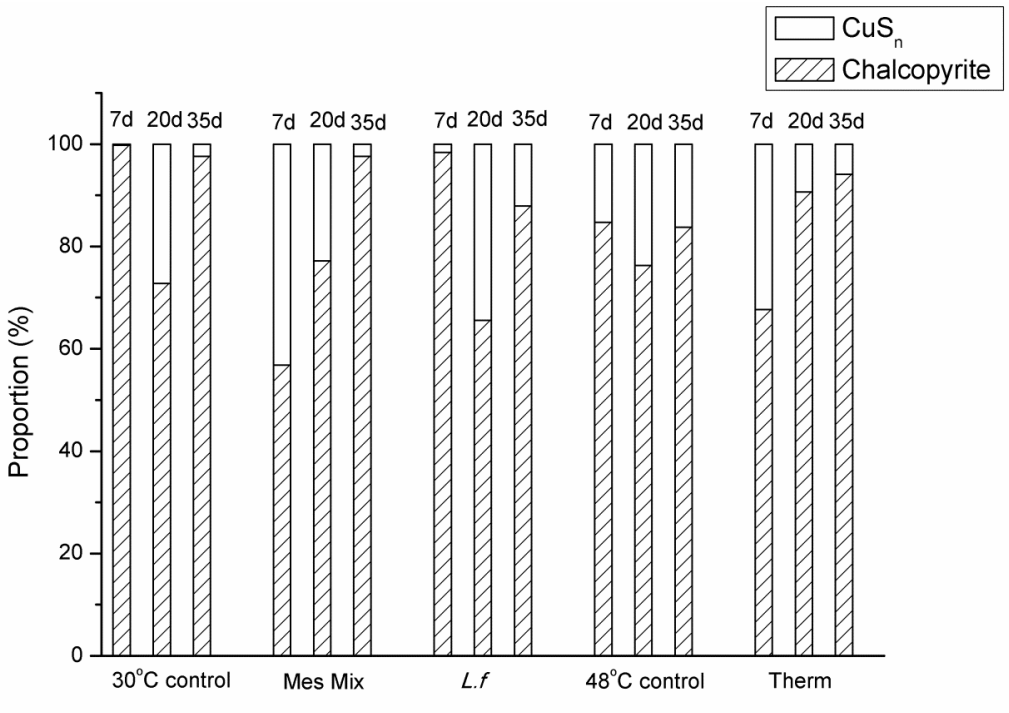

Fig. 3-19 The evolution of CuS_n formed on leached chalcopyrite.

At 30 ^{o}C, the XANES study indicated the leached residue contained chalcopyrite, CuS_n-like species, and some jarosite, but no other iron intermediates. This finding supports the polysulfide pathway proposed by Sand et al. (2001). Furthermore, the changes of Cu XANES spectra could be explained as follows. At the beginning, as the result of rapid dissolution of iron and relatively slow dissolution of copper, a copper-sulfur rich layer accumulated on top of the bulk chalcopyrite and made the spectra shift towards CuS_n. During leaching, copper was removed from the surface as well and a metal-deficient polysulfide layer (S_n^{2-}) was formed (Acres et al., 2010a; Mikhlin et al., 2004). As the Cu K-edge XANES spectra only reflect the local structure of copper atoms, there was no characteristic absorption of any sulfur species and the spectra show the characteristic shape of the chalcopyrite under the polysulfide layer. Therefore, the increasing amount of CuS_n-like species resulted from the preferential dissolution of copper and iron.

3.3.5.2 Iron K-edge studies

The Fe K-edge spectra at 48 ^{o}C are displayed in Fig 3-21. That at 30 ^{o}C resembles the one in Fig. 3-21A. In sterile controls and bioleaching with mesophilic mixture, there were no visible changes in the spectra, and no to little jarosite formed (Fig. 3-22). In contrast, in

bioleaching at 48 ^{o}C, the spectra changed towards that of jarosite in late stages, which is confirmed by 51% of the Fe species in the residue being jarosite.

As shown in Fig. 3-1, copper dissolution gradually slowed down with time. This is typical passivation. However, at 30 ^{o}C, only less than 10% of the Fe species in the residue was jarosite, which definitely cannot fully account for the cessation of copper release. Based on the results of SXPS and Cu K-edge XANES, it is proposed that copper leaching slowed down due to the formation of metal-deficient polysulfide (S_n^{2-}). Therefore, the oxidation rate of inert metal-deficient polysulfide (S_n^{2-}) layer should be the key step in chalcopyrite leaching.

At 48 ^{o}C, only a small amount of jarosite was formed before day 20 of bioleaching. The decrease of copper leaching during that period should at least partially be caused by the formation of metal-deficient polysulfide (S_n^{2-}) layer. However, passivation seems to be attenuated in the presence of thermophiles, possibly because of the faster kinetics of chalcopyrite leaching at higher temperature. More jarosite precipitated on the chalcopyrite surface from day 20 onwards. This could partially account for the decrease of copper release rate in late stages. However, as the passivation could also be caused by the sulfur-rich layer, it is difficult to quantify the contribution of jarosite to passivation.

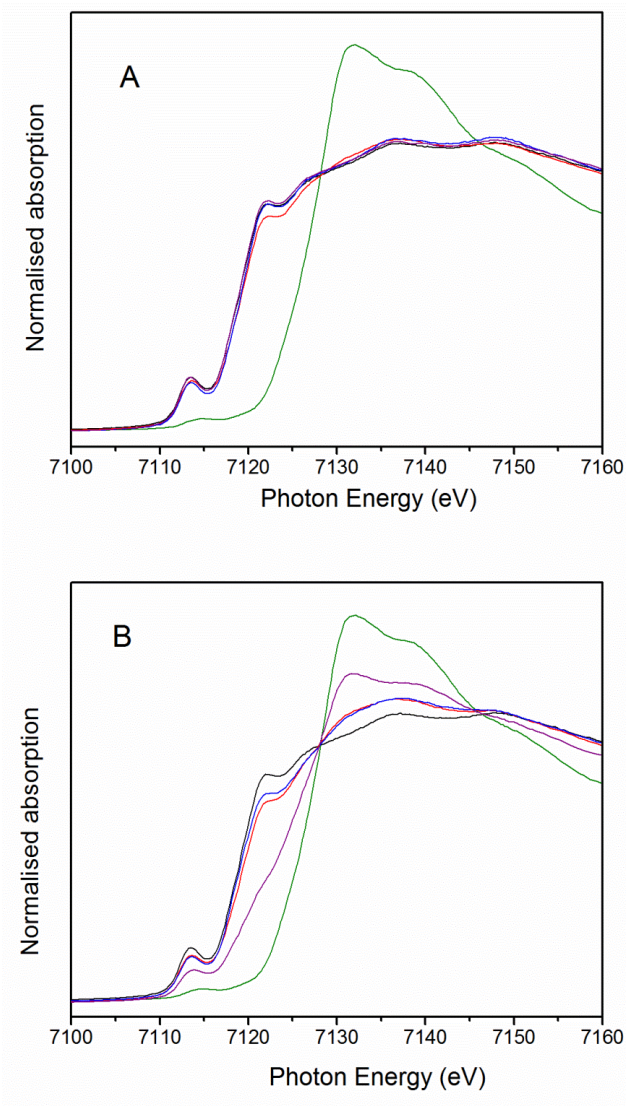

Fig. 3-21 Fe K-edge XANES spectra of chalcopyrite A) chemical leached and B) bioleached at 48 ^{o}C (Original chalcopyrite — black; Jarosite — green; Chalcopyrite leached for 7 d — red, 20 d — blue, 35 d— purple.)

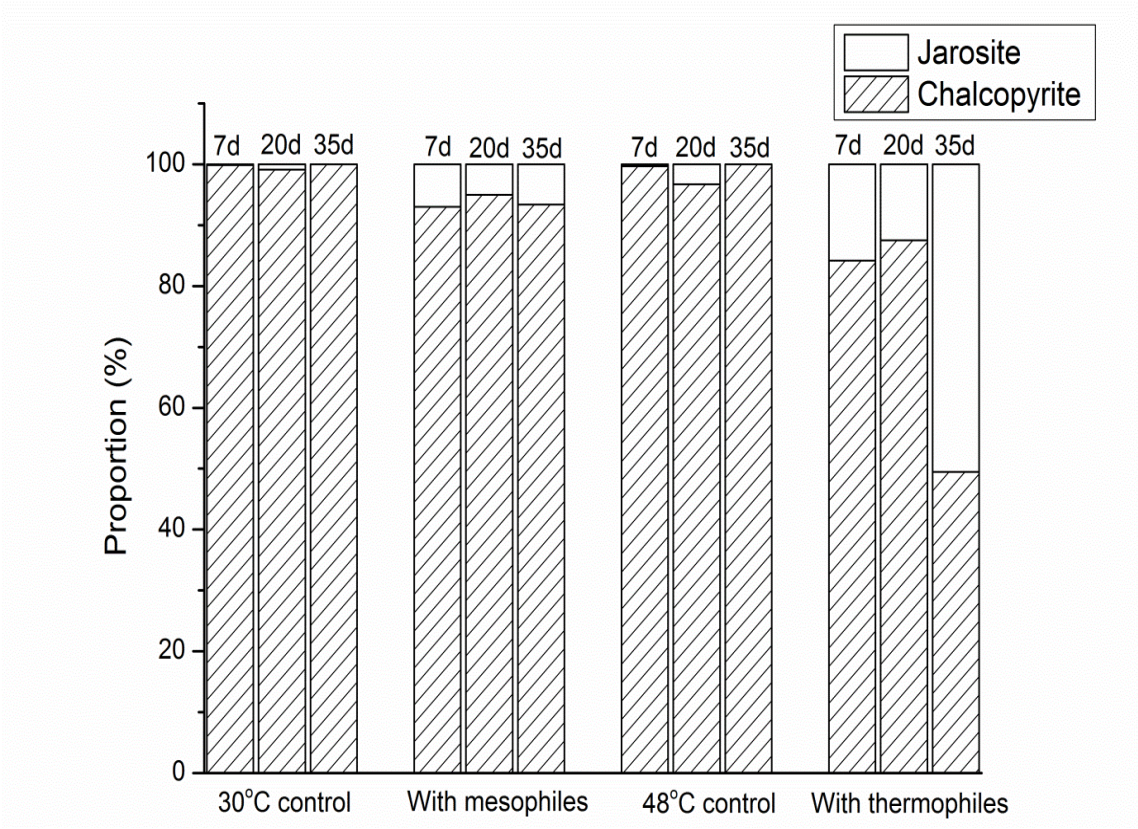

Fig. 3-22 The evolution of iron species formed on the leached chalcopyrite

3.4 Conclusions

Based on the results from this study, following conclusions could be made. In the early stages of leaching, more iron than copper dissolved, leaving on the particle surface CuS_n-like species that identified on a Cu K-edge XANES spectra and SXPS. In the late stages of leaching, copper in CuS_n-like species was leached, leaving behind S_n-like species. The oxidation of S_n^{2-} layer should be the rate-controlling step for the surface oxidation of chalcopyrite and further more the rate-controlling step for bioleaching process. Thermophiles can significantly enhance the leaching efficiency. The high leaching efficiency in presence of thermophiles is caused by the increased abiotical reaction rate as a result of elevated temperature, while there is no significant difference on surface sulfur speciation between the chalcopyrite bioleached at 48 or 30 ^{o}C. The synergistic effect of microorganisms with different metabolic pathways does not play a comparably important role with temperature in bioleaching. Elemental sulfur forms on the chalcopyrite as suggested in the polysulfide pathway (Sand et al., 2001), which could be effectively eliminated by sulfur-oxidizing microorganisms. However, the formation of elemental sulfur does not seem to hinder the leaching significantly.

Chapter 4 chalcopyrite surface chemical species evolution in electrochemical oxidation

4.1 Introduction

Electrochemical studies have been used extensively to study the evolution of chalcopyrite surface species and have revealed some information regarding the mechanism of chalcopyrite dissolution (Mikhlin et al., 2004; Nava et al., 2006; Parker et al., 1981). In a potentiodynamic curve, there are distinct passive and active regions, which are very helpful to understand the nature of the passivation layer (Ghahremaninezhad et al., 2010; Majuste et al., 2012). However, the specific surface chemistry of chalcopyrite in that passive-active-passive region is unclear.

Electrochemical methods only provided indirect evidence of the surface chemistry. Spectroscopic methods like XPS and Raman spectroscopy could provide direct evidence of the surface species.

In this chapter, the electrochemical properties of chalcopyrite electrode were investigated using 9K as electrolyte. The surface chemistry of chalcopyrite modified at particular electrochemical potentials was studied by SXPS, NEXAFS and Raman spectroscopy, to reveal information of chalcopyrite passivation in an electrochemical process.

4.2 Experimental

4.2.1 Electrode preparation

Chalcopyrite electrode were prepared according to the description in section 2.3.4.

4.2.2 Electrochemical studies

Cyclic voltametric, potentiodynamic studies and the potentiostatic modification were performed according to the description in section 2.6.

4.2.3 SXPS and NEXAFS studies

SXPS and NEXAFS studies were preformed according the description in section 2.7 and 2.8.3, respectively.

4.2.4 Raman studies

The Raman data were recorded between 800 and 100 cm^{-1} using the settings described in section 2.10.

4.3 Results and Discussion

4.3.1. Voltametric and potentiodynamic studies

The result of a cyclic voltametric test was shown in Fig. 4-1. Four anodic peaks and three catholic peaks were detected. The peak A1 may indicate a selective dissolution of iron from the crystal lattice of chalcopyrite (Zeng et al., 2011). A2 around 630 mV could be ascribed to partial oxidation of chalcopyrite as shown in Reaction (4-1), where *y>x*. (Lu et al., 2000; Price and Warren, 1986)

$$CuFeS_2 \rightarrow Cu_{1-x}Fe_{1-y}S_{2-z} + xCu^{2+} + yFe^{2+} + zS + 2(x + y)\, e^{-} \quad (4\text{-}1)$$

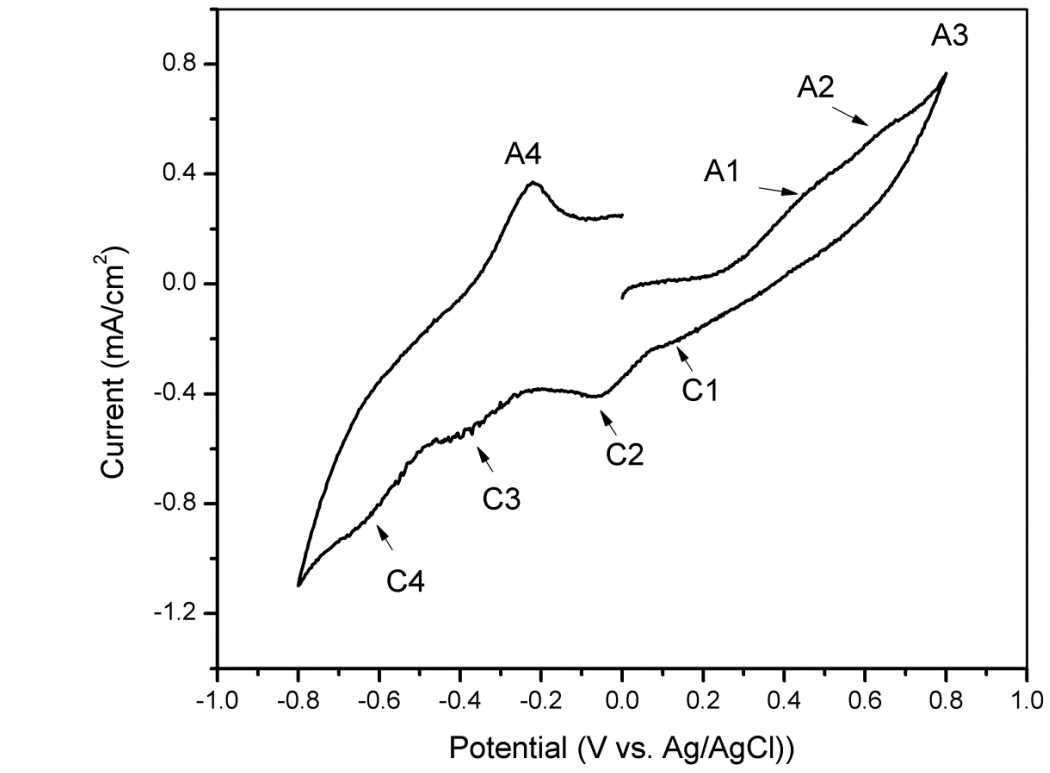

Fig. 4-1 Cyclic voltametry of chalcopyrite in the 9 K basic medium at a scan rate of 5 mV/s

This suggests the preferential release of iron from the chalcopyrite lattice during anodic dissolution. Parker et al. (1981) referred to the $Cu_{1-x}Fe_{1-y}S_{2-z}$ as a polysulfide, which has semi-conducting properties. While some authors further claimed this layer could be just copper-sulfur layer such as covellite or CuS_2 (Yin et al., 1995). When the potential further

increased to over 0.7 V, this layer dissolved with the oxidation of ferrous iron to ferric iron and the oxidation of sulfur to sulfuric acid (Nava et al., 2002).

In the inverse scan, C1 and C2 may be attributed to the reaction of the cupric ions with chalcopyrite, CuS or elemental sulfur, producing chalcocite (Qin et al., 2013). When the potential value was lower than -0.3 V, peaks C3 and C4 were observed. They possibly relate to the reduction of covellite and chalcopyrite, respectively (Arce and Gonzalez, 2002; Biegler and Horne, 1985).

A4 observed in the reverse oxidation scan is very similar to the results of Zeng et al. (2011) and Gomez et al. (1996) as a result of Reaction (4-2).

$$Cu_2S \rightarrow Cu_{1.92}S + 0.08Cu^{2+} + 0.16e^- \quad (4\text{-}2)$$

Fig. 4-2 shows the result of potentiodynamic study at a scan rate of 0.5 mV s^{-1}. The results show the potentiodynamic profile has the similar properties as Ghahremaninezhad et al. (2010). A passive region is evident from the OCP to 570 mV. In this region the current was low and surface reaction was very slow. From 550 to 630 mV, the current rose rapidly with the increase of potential. In this region, the surface reaction was fast. According to the CV curve, it is assumed some non-stoichiometric or secondary metal sulphide mineral formed in this region as showed in Reaction (4-1). The previous EIS studies also suggest in this region following reaction may occur (Ghahremaninezhad et al., 2010):

$$Cu_{1-x}Fe_{1-y}S_2 \rightarrow Cu_{1-x-z}S_2 + zCu^{2+} + (1\text{-}y)Fe^{2+} + 2(z+1\text{-}y)\,e^- \quad (4\text{-}3)$$

From 630 mV to 750 mV, another region of slow current increase was observed, indicating the formation of a passviation layer. When potential increased to approximately 750 mV, another active region appeared, as a result of the dissolution of intermediates and passivation layers (Mikhlin et al., 2004; Ghahremaninezhad et al., 2010; Yin et al., 1995).

$$Cu_{1-x-z}S_2 \rightarrow (1\text{-}x\text{-}z)Cu^{2+} + 2S^0 + 2(1\text{-}x\text{-}z)e^- \quad (4\text{-}4)$$

$$CuFeS_2 + 8H_2O \rightarrow Cu^{2+} + Fe^{3+} + 2SO_4^{2-} + 16H^+ + 17e^- \quad (4\text{-}5)$$

Above studies suggest there was an active region for chalcopyrite dissolution around 600 mV and two passive regions in 500-550 mV and 630-750 mV. It is very important to understand the surface chemistry of chalcopyrite in this passive-active-passive region for understanding the chalcopyrite dissolution mechanisms in electrochemical oxidation. To confirm the chemical species, three critical potentials (530 mV, 600 mV, 650 mV) were selected for the following potentiostastic oxidation and spectroscopic characterization.

Fig. 4-3 displays the current changes with time on the electrode under different potentials. The figure shows that current density was substantially enhanced when potential was raised from 530 mV to 600 mV. At 650 mV, the current was much higher than that at 600 mV at the beginning, however the currents under the two potentials were very similar after 2000 s. This result indicates a passivation film might have formed on the chalcopyrite oxidized at 650 mV, which counteracted the effect of elevated potential. During the potentiostatic modification, 0.108 C/cm^2 charge was transferred through chalcopyrite surface at 530 mV, while 0.37 and 0.528 C/cm^2 charge were transferred via the electrode surface under 600 and 650 mV, indicating the electrode subjected much more significant surface modification under higher potentials. The result also shows that the electrode reached stable surface status after potentiostatic oxidation for 2 hours, and can be used for following spectroscopic characterization.

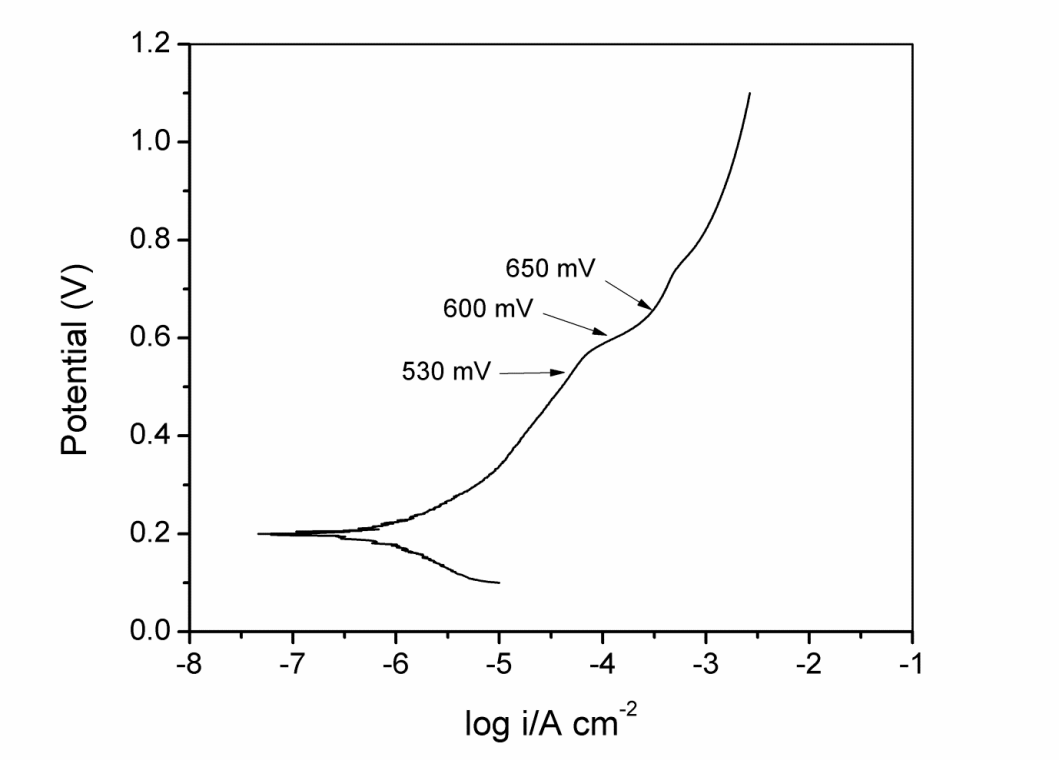

Fig. 4-2 Potentiodynamic curve for chalcopyrite in the 9 K basic medium at a scan rate of 0.5 mV/s

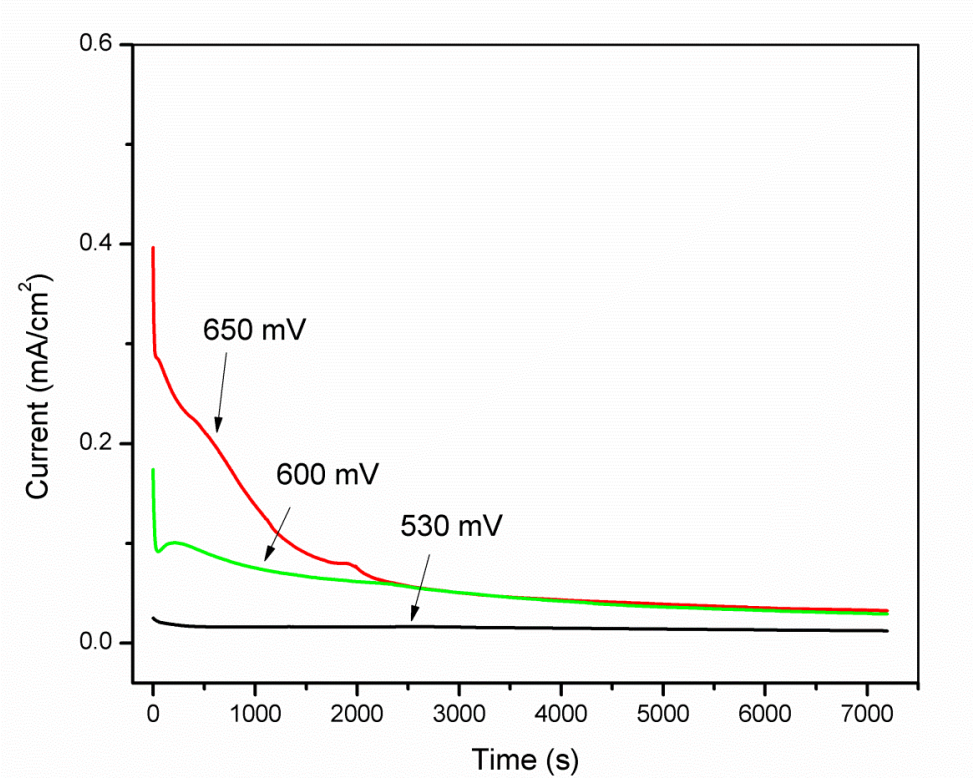

Fig. 4-3 Current–time curves of chalcopyrite electrode at different applied potentials

4.3.2 Spectroscopic studies

4.3.2.1 XPS studies

To verify the analysis based on electrochemical studies, surface sensitive spectroscopic studies have been carried out on three most critical potentials (530 mV, 600 mV, 650 mV) that are related to the formation of passivation layers in chalcopyrite electrochemical oxidation. The surface atomic concentration calculated based on the survey scan was summarized in table 4-1 and the survey scan of electrode oxidized at 650 mV is shown in Fig. 4-4. The most abundant element is carbon, which contributed to 40-65% of the surface elements. Oxygen is the second most abundant element, which may come from various sources including oxides, hydroxides, attached and absorbed water (Harmer et al., 2006). S/(Fe+Cu) ratio increased with potential from 0.95 in the original chalcopyrite to 2.45 in the chalcopyrite oxidized at 650 mV, indicating the surface became increasingly metal-deficient. This phenomenon was also observed by other authors during the chalcopyrite chemical and electrochemical oxidation (Buckley and Woods, 1984; Ghahremaninezhad et al., 2010). Nitrogen was detected on all oxidized chalcopyrite samples. The source of nitrogen may come from ammonia jarosite or from the solution species dried down on the surface. Phosphorus was also detected, which could come from

the solution species dried down on the surface or/and iron phosphate precipitate (Al-Sogair et al., 2002).

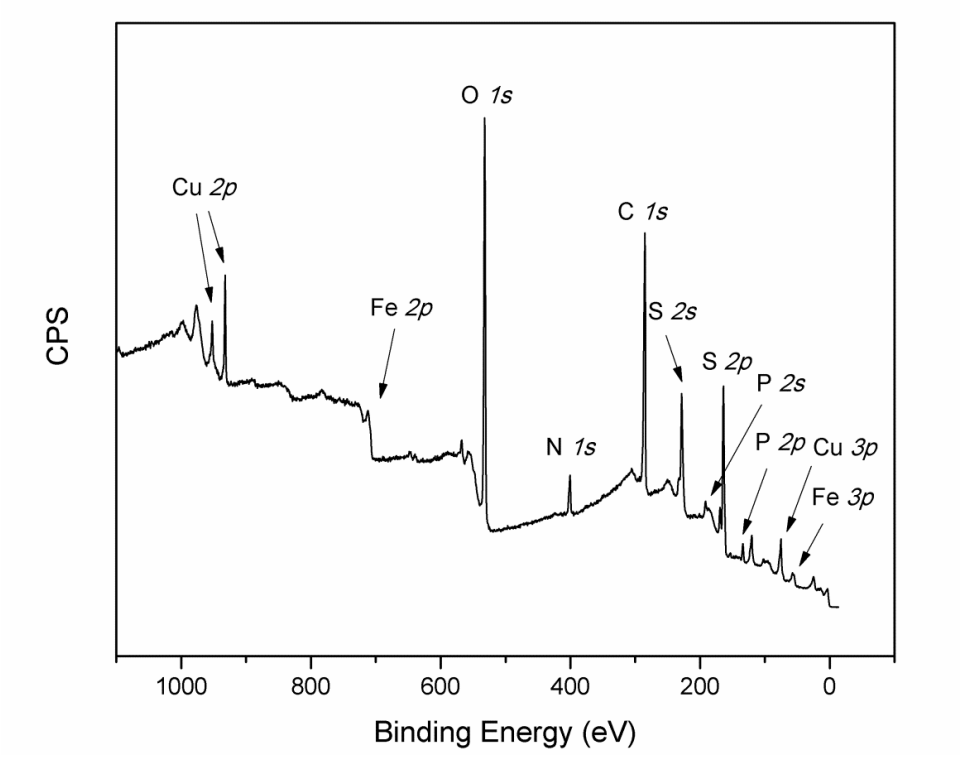

Fig. 4-4 Survey scan spectra of chalcopyrite oxidized at 650 mV

Table 4-1 Atomic concentration (%) of elements on the surface of chalcopyrite oxidized at 530, 600, and 650 mV (*hv* = 1487 eV)

	C	O	N	S	Fe	Cu	P
Original Cp	46.2	22.7	-	15.1	7.2	8.6	-
530 mV	64.8	7.7	3.2	13.4	5.5	5.5	-
600 mV	40.0	29.6	1.8	17.4	3.8	4.6	2.8
650 mV	50.2	23.2	4.2	14.7	3.1	2.9	1.6

The S *2p* XPS spectra collected at photon energy of 1487 eV are displayed in Fig. 4-5. There is no obvious distortion or broadening of any spectra, indicating the samples were not affected by differential charging. Comparing to the original chalcopyrite, it is clear that sulfur species with higher oxidation states formed on the surface of electrode after oxidation. This agrees with the increasing S proportion relative to Cu, Fe and S. The quantitative result of fitting (table 4-2) shows further features. At 530 mV, a moderate increase of S_n^{2-}/S^0 species was found, which is similar to previous XPS studies on an

electrochemically oxidized chalcopyrite (Velásquez et al., 2005) as well as on the (bio)leached ones (Sandström et al., 2005). At 600 mV, an increase of S_2^{2-} was found, which is consensus with the Reaction (4-3). When potential rose to 650 mV, the S_2^{2-} layer decreased dramatically to less than 6%. This result is in very good accordance to reation (4-4), proposed from previous EIS study (Ghahremaninezhad et al., 2010). Contrary to the decreased proportion of S_2^{2-} species, that of S_n^{2-} species stayed at a high level at 650 mV, which may be explained by Reaction (4-1). The detection of an increased amount of S_n^{2-}/S^0 indicates that sulfur polymerization had occurred at the potentials studied, while the explicit composition of the product remains unknown. The XPS S *2p* fits also indicated that the energy of S $2p_{3/2}$ peak of S_n^{2-}/S^0 species increased from 163.35 eV for chalcopyrite oxidized at 530 mV to 163.45 eV for that oxidized at 650 mV. This result suggests the sulfur species became more polymerized with increasing potentials, which could be long chain polysulfides or elemental sulfur. However, as the sublimation of sulfur in the UHV environment at room temperature, most of the oxidized species are likely to be polysulfides. A peak arising from sulfate was also observed from the XPS study. Considering 9K basic medium was used as electrolyte, this may come from the precipitation of jarosite.

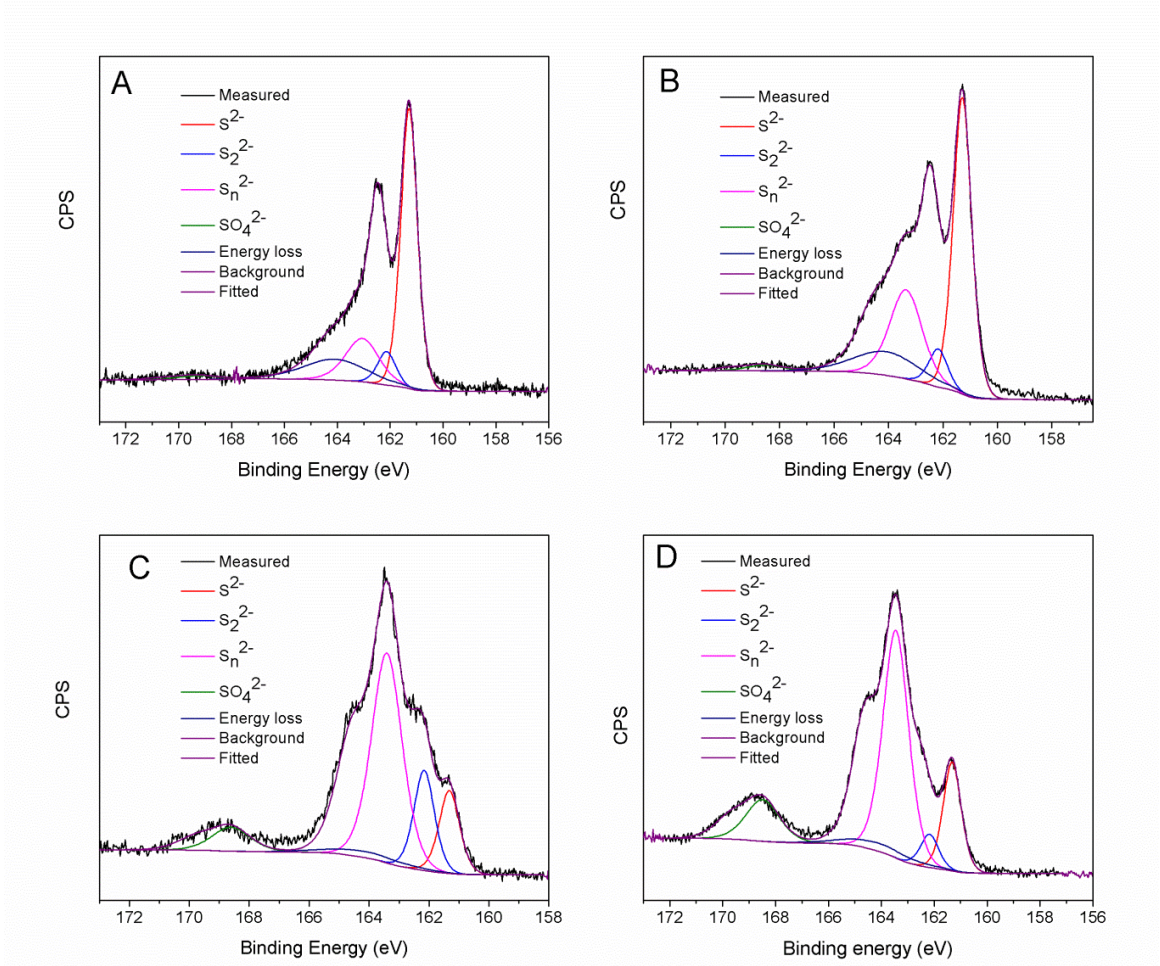

Fig. 4-5 S *2p* XPS spectra of chalcopyrite oxidized under different potentials for two hours (*hv* = 1487 eV)

Table 4-2 Percentages of surface sulfur components in total sulfur on chalcopyrite after potentiostatic oxidized at 530, 600 and 650 mV (*hv* = 1487 eV).

	S^{2-}	S_2^{2-}	S_n^{2-}/S^0	SO_4^{2-}	loss
S $2p_{3/2}$ BE (eV)	161.3	162.4	163..4	168.5	164.1
Original Cp	60.1	7.8	18.7	2.0	11.2
530 mV	53.2	6.8	23.0	2.1	9.9
600 mV	14.3	17.9	57.2	7.9	2.7
650 mV	19.1	5.8	57.8	13.7	3.6

The S *2p* spectra collected at 400 eV is shown in Fig. 4-6 and the fitting results were summarized in table 4-3. Similarly, S_n^{2-}/S^0 species increased moderately at 530 mV, and dominated on the surface of chalcopyrite oxidized at 650 mV, indicating a more severe

oxidation at higher potential. On the other hand, the spectra taken at 400 eV show higher amount of oxidized sulfur species than their counterparts taken at 1487 eV. According to the universal IMFP curve, at 400 eV, the approximate maximum depth probed is 8 monolayers with approximately 40% of the signal originating from the first 3-4 monolayers, which is more sensitive than XPS experiment carried out at photon energy 1487 eV, which collects information from approximately first 15 monolayers (Tanuma et al., 1991; Seah, 1990). This result indicates the oxidized sulfur species were on the surface of bulk chalcopyrite.

Table 4-3 Percentages of surface sulfur components in total sulfur on chalcopyrite oxidized at 530 and 650 mV ($h\nu$ = 400 eV).

	S^{2-}	S_2^{2-}	S_n^{2-}/S^0	SO_4^{2-}	loss
S $2p_{3/2}$ BE (eV)	161.3	162.4	163..4	168.5	164.1
Original Cp	39.7	15.7	36.1	1.1	7.4
530 mV	24.3	10.6	55.5	4.8	4.6
650 mV	5.1	4.2	74.4	15.3	1.0

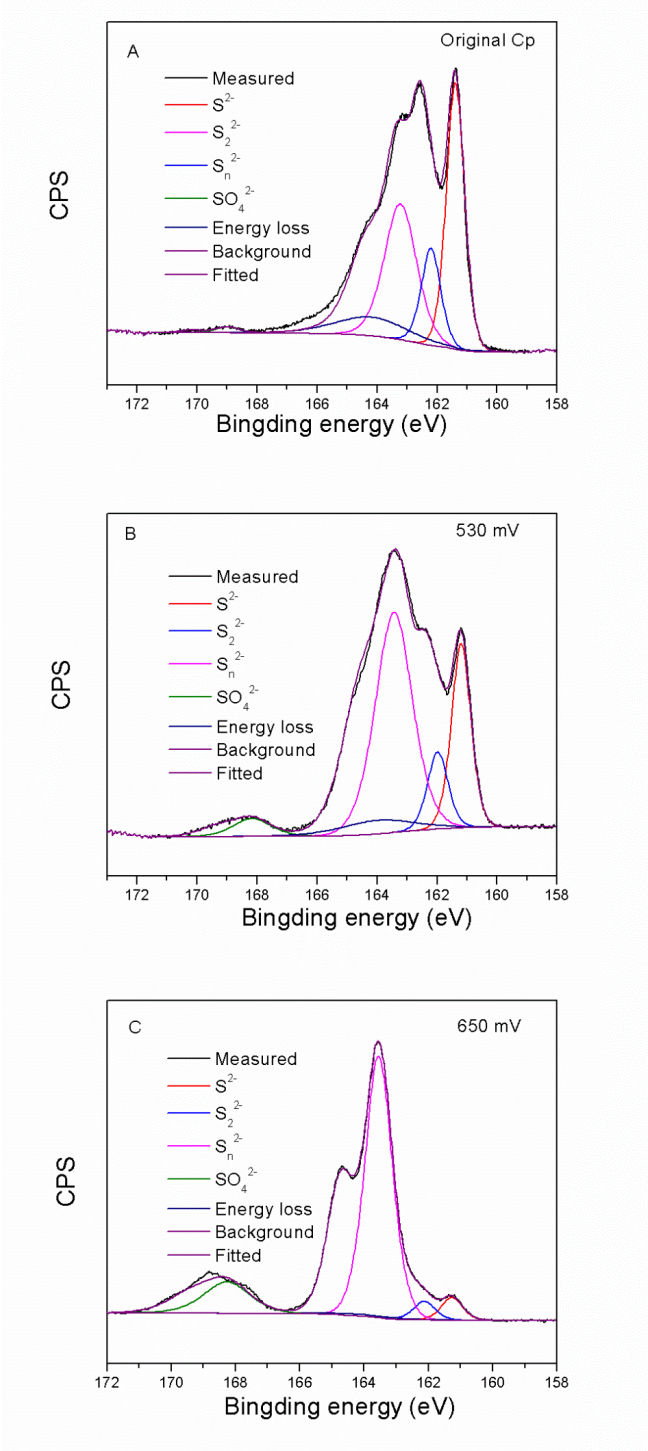

Fig. 4-6 S *2p* XPS spectra of chalcopyrite oxidized under different potentials for two hours ($h\nu$ = 400 eV)

The Cu *2p* XPS study is shown in Fig. 4-7. The Cu $2p_{3/2}$ peak of original chalcopyrite, which is at 932.4 eV, shows only Cu(I) species existed on the chalcopyrite surface (Goh

et al., 2006; Pearce et al., 2006). Similarly in the oxidized electrodes, copper retained the oxidation state +1 since no satellites lines in the range of 940-950 eV were found and the binding energy changed by less than 0.2 eV. However, the slightly lower value of Cu $2p_{3/2}$ peak at 650 mV may be considered as indicative of the formation of covellite or covellite-like surface structure (Mikhlin et al., 2004). The formation of covellite could be explained by Reaction (4-6).

$$CuFeS_2 \rightarrow 0.75CuS + 1.25S^0 + 0.25Cu^{2+} + Fe^{2+} + 2.5e^- \quad (4\text{-}6)$$

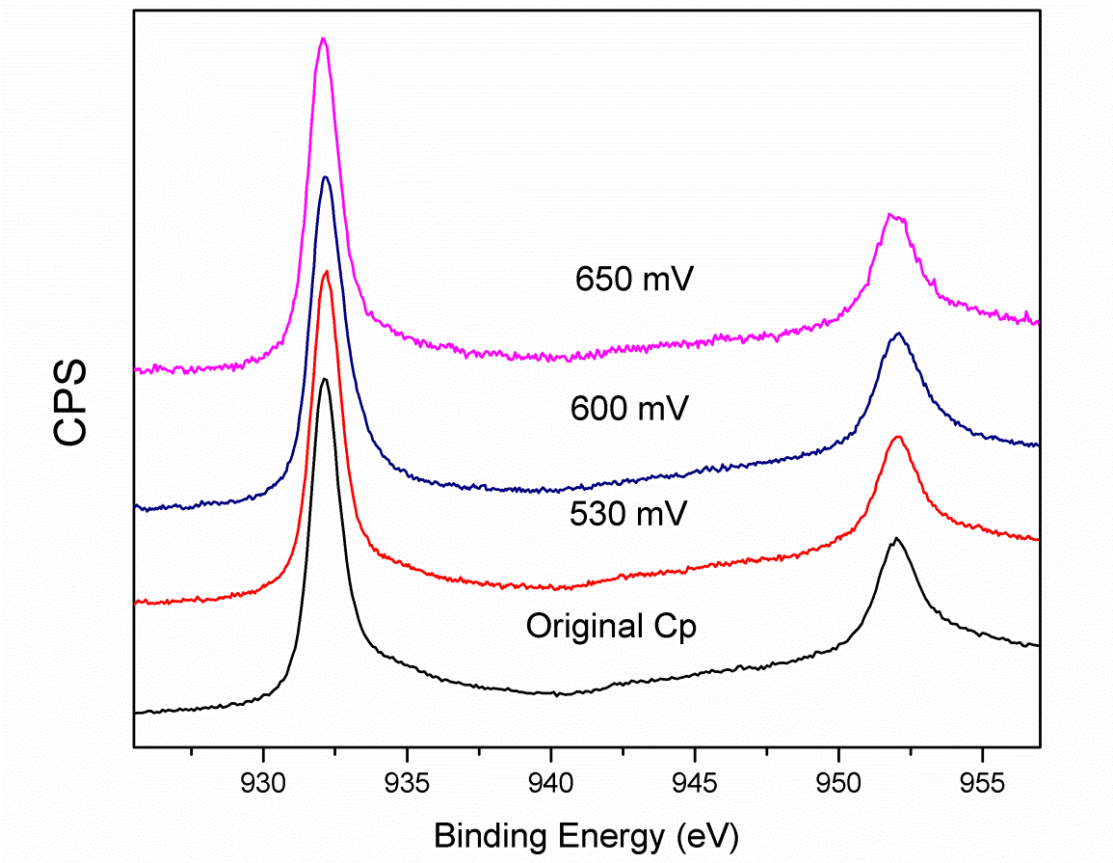

Fig. 4-7 Cu *2p* XPS spectra of chalcopyrite oxidized under different potentials hours (*hv* = 1487 eV)

The Fe 2*p* spectra of the original and oxidized chalcopyrite are displayed in Fig. 4-8. The peak at 708.2 eV could be assigned to Fe(III)-S (McIntyre and Zetaruk, 1977), which represents the bulk chalcopyrite. The Fe *2p* of the sample oxdized at 530 mV shows almost the same feature as original chalcopyrite, which indicate the iron precipitation at this potential was very weak. The spectra of sample oxidized at 650 mV shows an additional feature around 711 eV. According to the standard Fe *2p* spectrum of jarosite, this feature may be an indication of the jarosite (Sandström et al., 2005). As no definitive

evidence of K was found in the XPS survey spectra, it is speculated that ammonia jarosite could be one of the major components of the iron precipitate. This peak could also be assigned to iron(III)-O-OH species such as iron (III) oxyhydroxides (McIntyre and Zetaruk, 1977; Nesbitt and Muir, 1994) or iron(III) phosphate (Annapragada and Gulari, 1990; Yu et al., 2007). However, Fe oxyhyroxides or/and iron phosphate is expected to have a small contribution to the iron precipitation in the 9K solution at pH 1.8 (Al-Sogair et al., 2002).

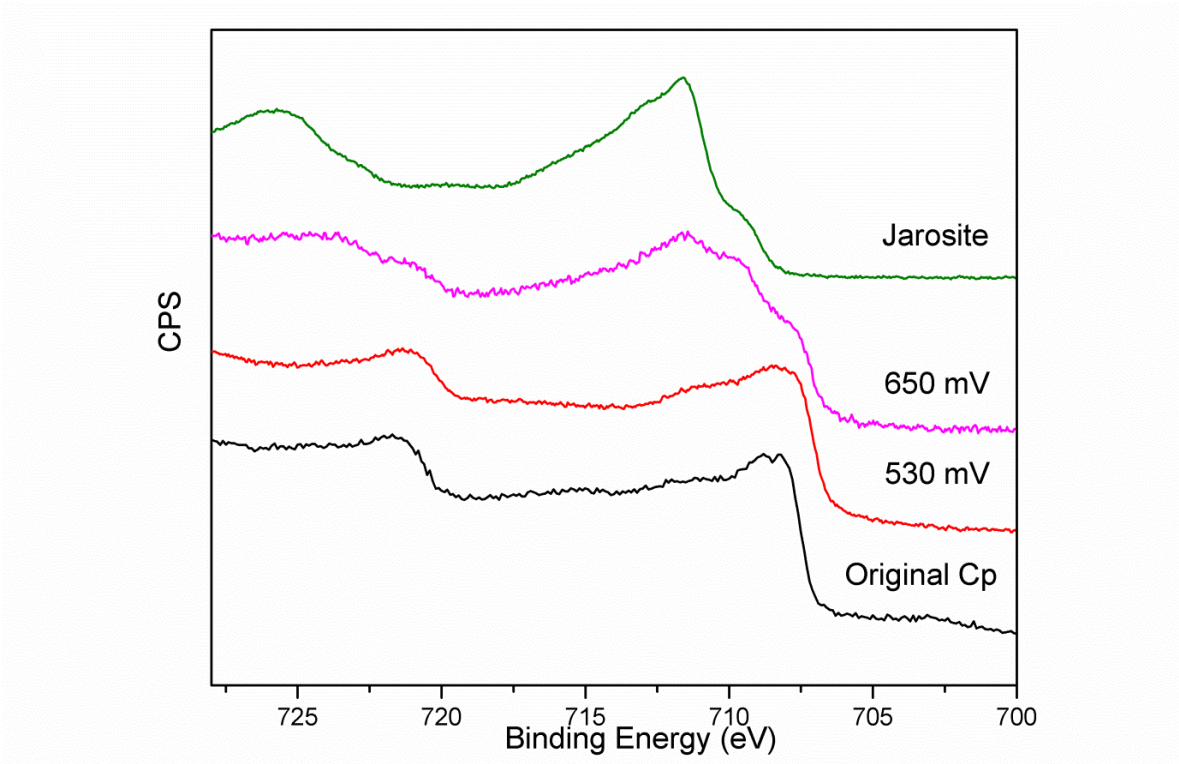

Fig. 4-8 Fe *2p* XPS spectra of chalcopyrite oxidized under different potentials for two hours ($h\nu$ = 1487 eV)

4.3.2.2 NEXAFS studies

The S K-edge, Fe $L_{2,3}$-edge, Cu L_3-edge NEXAFS spectra are shown in Fig. 4-9 A, B, C, respectively. In Fig. 4-9 A, the original chalcopyrite shows a sharp absorption edge at 2468 eV, which decreased dramatically as the increase of potential. On the other hand, a peak at 2469.8 eV, which suggests the oxidation of electrode surface, appeared after potentiostastically modification, and rose with the increasing potential. According to the literature, this peak is higher than that of FeS_2 (S_2^{2-}) but slightly lower than that of elemental sulfur (S_8) (Xia et al., 2010). Coupled with the results of XPS study, it can be inferred that this peak indicates the formation of polysulfide (S_n^{2-}) and/or elemental sulfur.

The result of Fe L-edge NEXAFS spectra show that no obvious change of iron species occurred on the electrode surface at 530 mV. However, at elevated potentials, the spectra show the feature of Fe(III)-O species (Goh et al., 2006). This new feature coupled with the results of XPS suggests a thin film of iron(III) precipitation (oxide, oxyhydroxide or jarosite) formed on the electrode surface.

In Fig. 4-9 C, the Cu L-edge NEXAFS spectra are displayed. The original sample shows a typical spectrum of chalcopyrite with a peak at 932.5 eV, indicating the existence of Cu(I) as reported in literature (Acres et al., 2010). At 530 mV, no change was observed from the spectra. However, at 600 mV an additional peak raised at 935 eV. There is also loss of a contribution at 934-935 eV, which is evident for chalcopyrite. According the literature, the additional peak may indicate the presence of covellite or chalcocite (Goh et al., 2006). As chalcocite forms at a negative potential (Liang et al., 2011; Nava et al., 2008), covellite is more likely to be the product of Reaction (4-6). In a previous study, Nava and Gonz âlez (2006) suggest that covellite forms in the potential range between 863 mV and 943 mV. While Mikhlin et al. (2004) reported the formation CuS at 600 mV mainly based on Cu *2p* XPS spectra, according to the binding energy at 931.8 eV. This study confirmed the result of Mikhlin et al. (2004) with much clearer NEXAFS evidence. At 650 mV, the copper spectra shifted back towards the original chalcopyrite, indicating the formation of covellite in this condition is less favourable.

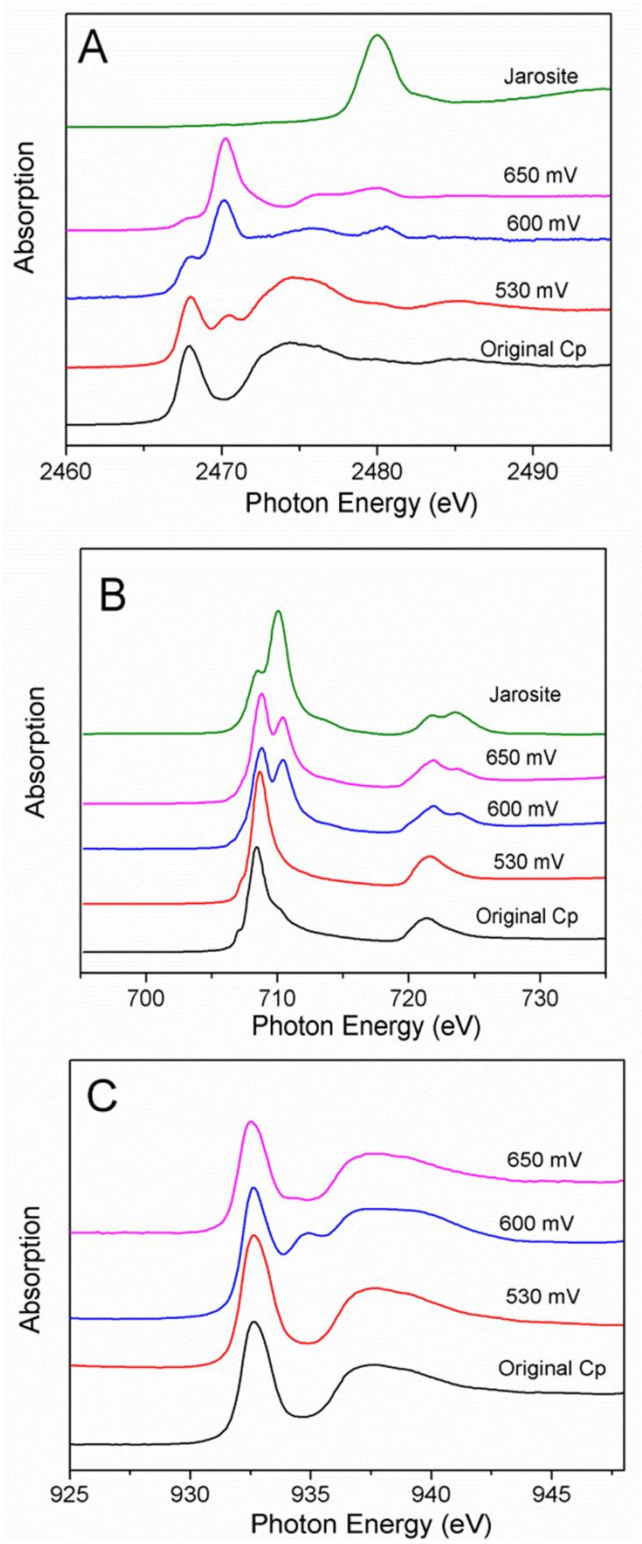

Fig. 4-9 NEXAFS studies of chalcopyrite oxidized under different potentials (A, S K-edge; B, Fe $L_{2,3}$-edge; C, Cu L_3-edge. The spectra of jarosite standard was taken at at BL-4B7A and 4B7B, Beijing National Synchrotron Radiation Facility (BSRF), respectively)

4.3.2.3 Raman studies

Raman spectra of original and oxidized chalcopyrite are shown in Fig. 4-10. The Raman spectra of original mineral only displayed the three peaks of chalcopyrite, which resulted from lattice vibrations (Mernagh and Trudu, 1993; Ohrendorf and Haeuseler, 1999). The electrode oxidized at 530 mV shows almost the feature of original chalcopyrite, rather than any evidence of oxidized sulfur speices or a metal-deficient sulfur-rich layer. This result may be caused by an inferior surface sensitivity of Raman spectroscopy than XPS and NEXAFS, which is not able to detect ultrathin film (<5 nm) and usually has an optical penetration of greater than 100 nanometers using the 514 nm light source (Holtz et al., 2000; Parker, 2005; Ruiz et al., 2013). At 600 mV, the spectra display very weak features of crystalline sulfur (153 cm^{-1} and 218 cm^{-1}) (Sasaki et al., 2009). In XPS studies, no explicit evidence of elemental sulfur was detected, which is primarily due to volitility of elemental sufur in ultra-high vacuum, especially when no sample cooling was available. Raman spectroscopy is sensitive to sulfur species (Eckert and Steudel, 2003; Mycroft et al., 1990). In this study, it provided important complementary evidence for the presence of elemental sulfur. A broad peak around 470 cm^{-1} was also found in the spectra, which could be assigned to a S-S bond of covellite (Sasaki et al., 2009). Majuste et al. (2012) also observed a similar peak on oxidized chalcopyrite electrode using Raman spectroscopy.

Further more, the broad shoulder shows the presence of polysulfides (Mycroft et al., 1990; Janz et al., 1976). The evidence of crystalline sulfur and covellite supported Reaction (4-6). The spectra of electrode oxidized at 650 mV shows a similar feature. A similar but lower peak at 470 cm^{-1} was observed, which suggest less covellite formed in this condition. More intensive peaks at 153 cm^{-1} and 218 cm^{-1} suggest the accumulation of crystalline sulfur (Reaction (4-1)).

Unlike the S *2p*, Fe *2p* XPS and Fe L-edge NEXAFS, there was no evidence of jarosite or other iron precipitates found in Raman, which is explained by the inferior surface sensitivity of Raman spectroscopy. These results suggest only very small amount of the iron precipitated even at 650 mV.

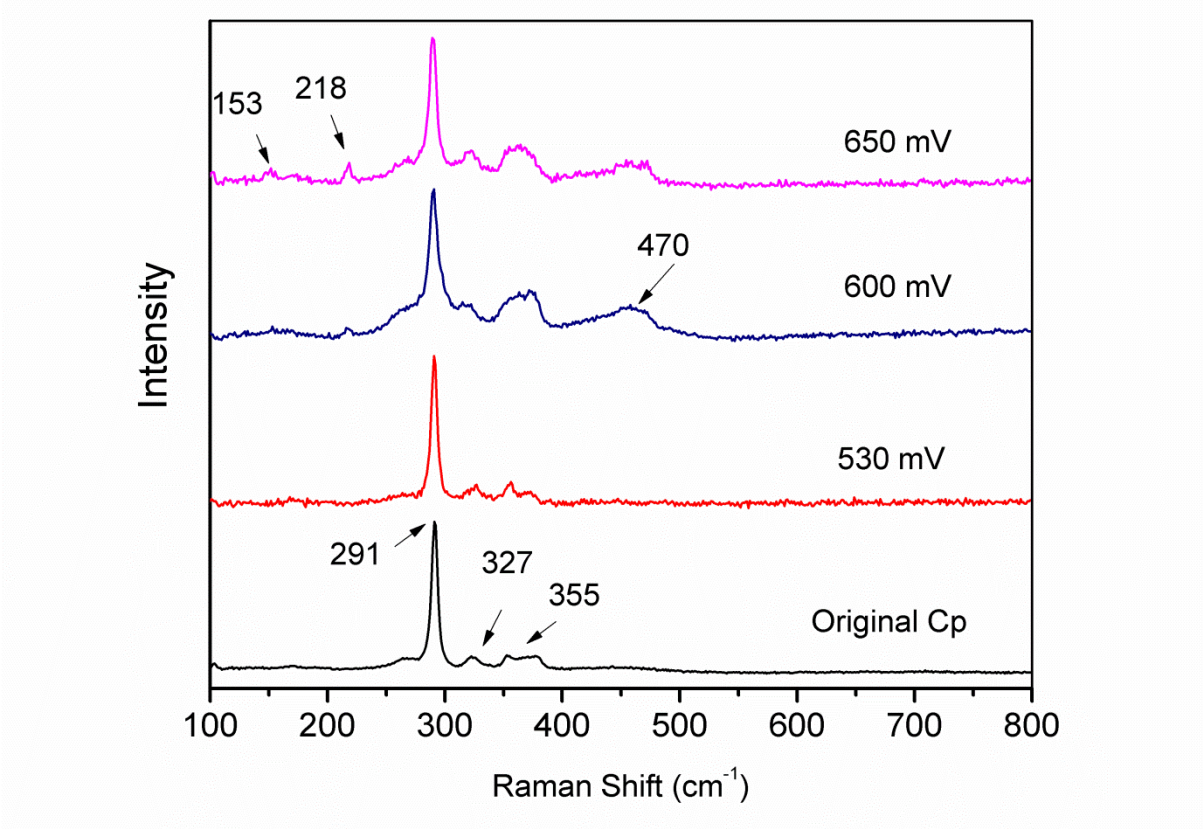

Fig. 4-10 Raman spectra of chalcopyrite oxidized under different potentials

4.3.3 The evolution of chalcopyrite surface at different potentials

According to the spectroscopic studies, it could be inferred that when the potential was lower than 530 mV, the initial chalcopyrite dissolution occurred, which induced the formation of a very thin metal-deficient polysulfide film ($Cu_{1-x}Fe_{1-y}S_{2-z}$). It is reported that the depletion in metals could produce first a disordered surface layer, causing the passivation as suggested by other researchers (Ghahremaninezhad et al., 2010; Mikhlin et al., 2004).

In the potential range between 570 to 630 mV, a surge of anodic current appeared, accompanied by further metal deficiency. In this region, the dissolution of chalcopyrite to metal deficient polysulfide continued, with several other reactions occurring simultaneously to form $Cu_{1-x-z}S_2$ and CuS. The formation of $Cu_{1-x-z}S_2$ and CuS is at least partially responsible for the activation of chalcopyrite, which is also consistent with the finding of others (Yin et al., 1995).

When the potential rose to 630 mV or above, there is another passivation region, evidenced by the slow current rising rate. In this region, $Cu_{1-x-z}S_2$ dissolved and less amount of covellite presented on the chalcopyrite surface according to S *2p* XPS, Cu L-edge NEXAFS and Raman studies. The polysulfide species and elemental sulfur were the

primary products on the electrode surface. The high S/(Cu+Fe) ratio (table 4-1) also suggests the electrode was metal-deficient.

Jarosite is claimed as a passivation factor in (bio)leaching, especially when it forms in large quantities (Córdoba et al., 2008b; Sasaki et al., 2009). However, it was previously found chalcopyrite dissolution is more passivated in bioleaching at 30 ^{o}C than at 48 ^{o}C, coinciding with a larger amount of jarosite formed (Yang et al., 2013), indicating jarosite is not the primary reason of passivation. In this study, the formation of jarosite at 600 mV did not block the chalcopyrite dissolution. In the passive region near 650 mV, a increased amount of jarosite and/or other iron precipitates were found with thick sulfur-rich layer. The potentiodynamic curves in the study of Ghahremaninezhad et al. (2010) shows chalcopyrite was passivated in the same potential region in 0.5M H_2SO_4 electrolyte, which definitely is not caused by jarosite. As only very small amount of iron precipitate formed on the electrode surface, jarosite is unlikely to be the primary reason of passivation in this study.

It has also been suggested in the literature that elemental sulfur can hinder ion transport and the dissolution process (Dutrizac, 1989). On the other hand, some studies indicate elemental sulfur does not passivate leaching because of its porous nature (Hackl et al., 1995; Linge, 1976). In the work of Parker et al. (1981) elemental sulfur on the electrode was removed by dipping the electrode in CS_2. However, the electrode treated with CS_2 behaved similarly with that simply suspended in a nitrogen atmosphere, which indicated the passivating film is not sulfur. In a previous leaching study, the finding indicates chalcopyrite is more passivated when its surface is more metal-deficient (Yang et al., 2013). It may be similarly speculated that in this region the highly metal-deficient sulfur-rich layer (mainly containing polysulfide and elemental sulfur) is the primary reason for the passivation.

4.4. Conclusions

The surface chemical information of massive chalcopyrite electrode species in chalcopyrite electrochemical oxidation was studied by SXPS, NEXAFS and Raman spectroscopy. The electrochemical studies show that there was one active region for chalcopyrite anodic dissolution between 550 to 630 mV, companied by two passive regions nearby. The Current–time curves of chalcopyrite electrode indicate a passivation film might have formed on the chalcopyrite oxidized at 650 mV, which counteracted the effect of elevated potential.

Further spectroscopic studies show in the first passive region a thin film of non-stoichiometric polysulfides, which may be responsible for the passivation. In the active region, besides polysulfides, S_2^{2-} species and covellite were found, which may be the cause of the potential surge. When the potential increased to 650 mV, S_2^{2-} species and covellite started to dissolve, leaving a highly metal deficient polysulfide on the chalcopyrite surface, which may cause the passivation of chalcopyrite anodic dissolution.

Chapter 5 Cell initial attachment and to chalcopyrite surface and Biofilm formation

5.1 Introduction

Bacterial initial attachment is an important process for bioleaching. The physical attachment of bacteria to mineral surfaces has also been proposed to accelerate leaching. Selective attachment of bacteria to defective surfaces, such as cracks, of mineral was reported previously (Sand et al., 2001).

The objective of this chapter is to obtain a fundamental understanding of the population behaviour of *Acidithiobacillus ferrooxidans* at chalcopyrite surfaces. The use of single strain microorganism greatly simplifies the technique used to follow bacteria population behaviour. Bacteria population from two hours to six days of bioleaching will be investigated. The attached bacteria will be preserved using well established methodology (Erlandsen et al., 2004) and the attached bacteria can be observed using an optical microscopy. The selectivity in bacterial attachment to mineral sites, and the crystal orientation, the biofilm formation was also investigated.

5.2 Experimental

5.2.1 Sample preparations

Test samples were prepared according to the details in section 2.3.3 and 2.3.4.

5.2.2 Leaching tests

The leaching test was carried out by according to section 2.4.3.

5.2.3 Bacterial coverage tests

Bacterial attachment at the mineral surfaces was monitored using an optical microscope (Olympus BX51). To study the bacteria coverage at mineral surfaces, Image J (NIH) was used to quantify the surface area of mineral and the number of attached bacteria at the surfaces was counted manually (Abramoff, 2004). The average mineral surface occupied per bacterium in each sample was determined from tracking at least 600 bacteria on each

sample. The surface area occupied by per bacterium was approximated as a rectangle with dimension of 0.5 μm x 1.5 μm.

5.2.4 Raman studies

Raman study was carried out according to the description in section 2.10.

5.2.5 AFM studies

Chalcopyrite coupons before and after bioleaching for 72 hours were characterized according to the description in section 2.13.2.

5.2.6 Electron Backscatter Diffraction (EBSD) studies

The EBSD study were carried out according to the description in 2.12.

5.3 Result and discussion

5.3.1 Optical microscopic studies

Fig. 5-1 shows the original chalcopyrite and samples bioleached for 24, 72 and 96 hours. In the first 24 hours of leaching, the bacterial population at polished mineral surfaces is primarily attributed to bacterial attachment from the bulk solution. Significant cell attachment was observed with the first 24 hours, and a film started to develop on the mineral surface after bioleaching for 72 hours. After leaching for 96 hours, the thin film further developed to cover more area of the mineral.

Besides the cell attachment and film formation, selective attachment of bacteria at area of defects has also been observed (Fig. 5-2) where higher cell concentration was found near the defects on the mineral surfaces. Fig. 5-3 A, B shows a depth profile of chalcopyrite mineral sample when a microscope was used to observe the surface and inside the areas of defects. The bacteria concentration was higher inside the fractured area (indicated by arrows). This observation provides evidence that contact leaching is an important mechanism.

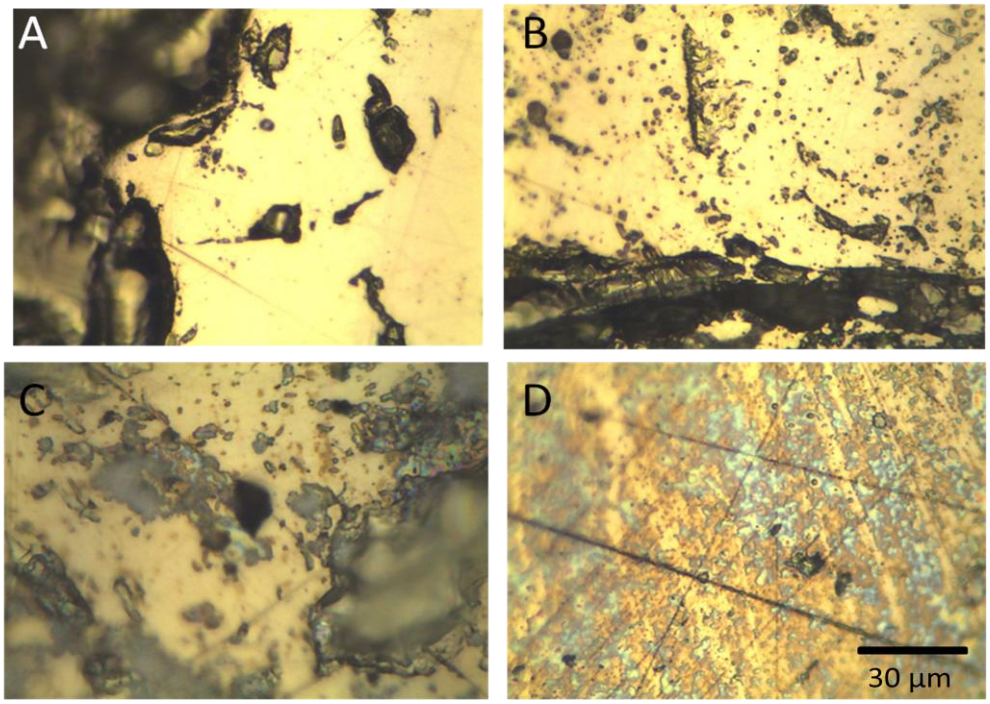

Fig. 5-1 The formation of biofilm on chalcopyrite (chalcopyrite leached for A, 0; B, 24; C, 72 and D, 96 hours by *A. ferrooxidans* by *A. ferrooxidans*)

Preferential attachment of bacteria at defective sites has been reported (Andrews, 1988; Gehrke et al., 1998). The reason for the selective attachment is still not clear yet. The adhesion to defective area might be partially explained by increased contact area enhancement and surface roughness (Vera et al., 2013). At the same time, it is also proposed that attachment to specific sites on the mineral surface is principally related to different attractants, most likely caused by charge imbalances (Vera et al., 2013). Andrews' analysis of diffusion process of sulfur in pyrite matrix show that relative rates of sulfur diffusion is faster along the dislocation than through pyrite crystals. The faster sulfur diffusion rate in the former is a likely explanation for the preferred adsorption of bacteria at areas of defect/dislocation (Andrews, 1988).

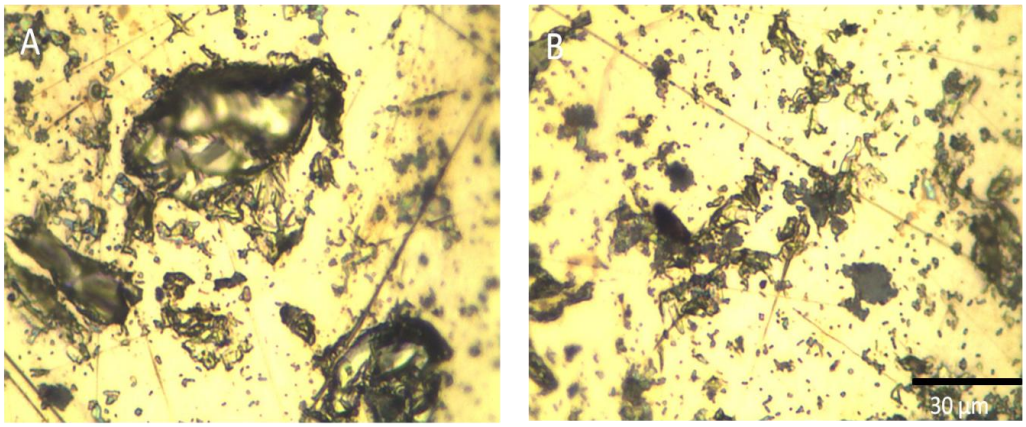

Fig. 5-2 Selective attachment of bacteria to the defects of sample after 48 hours of leaching by *A. ferrooxidans*

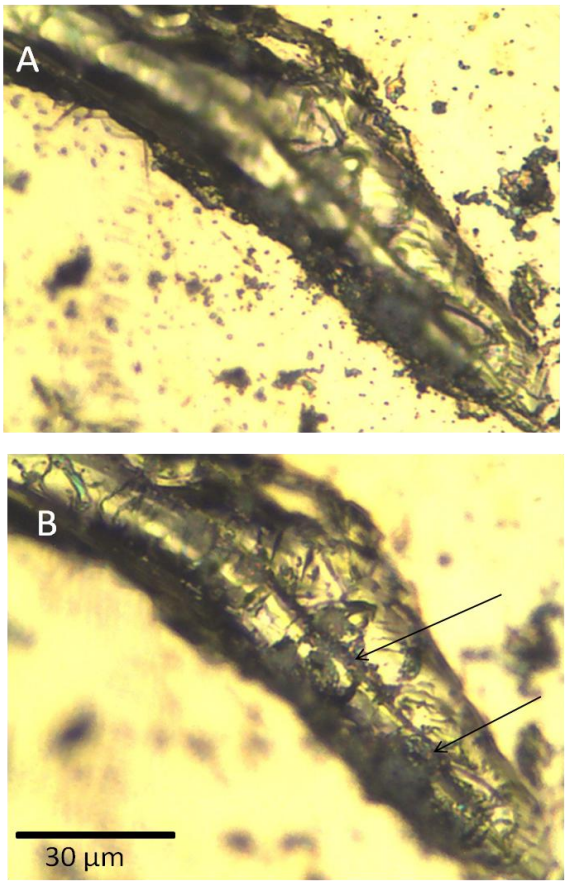

Fig. 5-3 Depth profile of two chalcopyrite surfaces after 48 hours of leaching by *A. ferrooxidans*

5.3.2 AFM studies

The AFM images of chalcopyrite before and after bioleaching for 72 hours are displayed in Fig 5-4. The unleached chalcopyrite shows a clean and flat surface, and the height

difference in a 5X5 μm^2 area was less than 40 nm. However, after bioleaching for 72 hours, the AFM image shows the formation of biofilm on the mineral surface. Similar observation of the formation of EPS layer was reported previously (Zeng et al., 2011). The roughness of the surface also significantly increased after bioleaching as indicated by the height difference, which is also an indicative of the formation of EPS layer. EPS can create a miro-environment with higher concentration of ferric ions and facilitate the oxidation of chalcopyrite, where uronic acid and other unidentified compounds in the EPS complex with ferric ion (Gehrke et al., 1998; Sand et al., 2001).

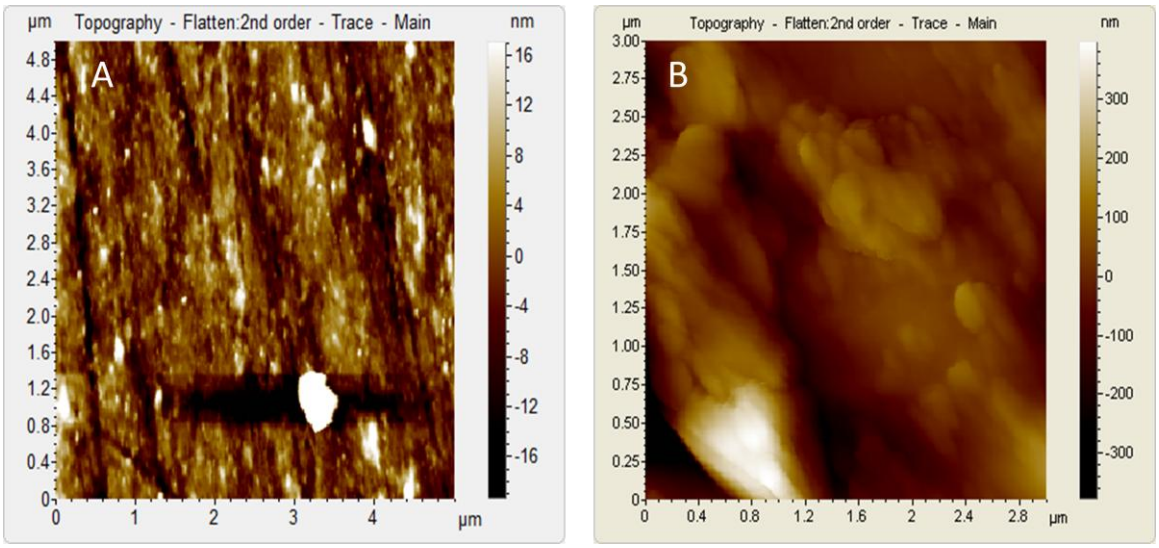

Fig. 5-4 AFM images of chalcopyrite before (A) and after (B) bioleaching for 72 hours.

5.3.3 Raman studies

To understand the type of film formed on the coloured areas after 72 hours of bioleaching (Fig. 5-1C&D), Raman spectroscopy was used to study the mineral surfaces and selective spectra are displayed in Fig. 5-5. The Raman spectra do not show evidence of the formation of any leaching product, which indicates that the film formed on the chalcopyrite surface did not result from mineral oxidation. The film formed after 72 hours of leaching was likely a biofilm as Raman spectroscopy showed presence of peaks in the range of 1200 to 1800 cm^{-1}, in agreement with the peaks from *A. ferrooxidans* cells. For instance, the peak at 1337 cm^{-1} characterizes the N–H vibrations of the amide III peptide bond of proteins and the peak at 1522 cm^{-1} could be assigned to –NH bending of the secondary amide group (–CONH) (Sharma et al., 2003).

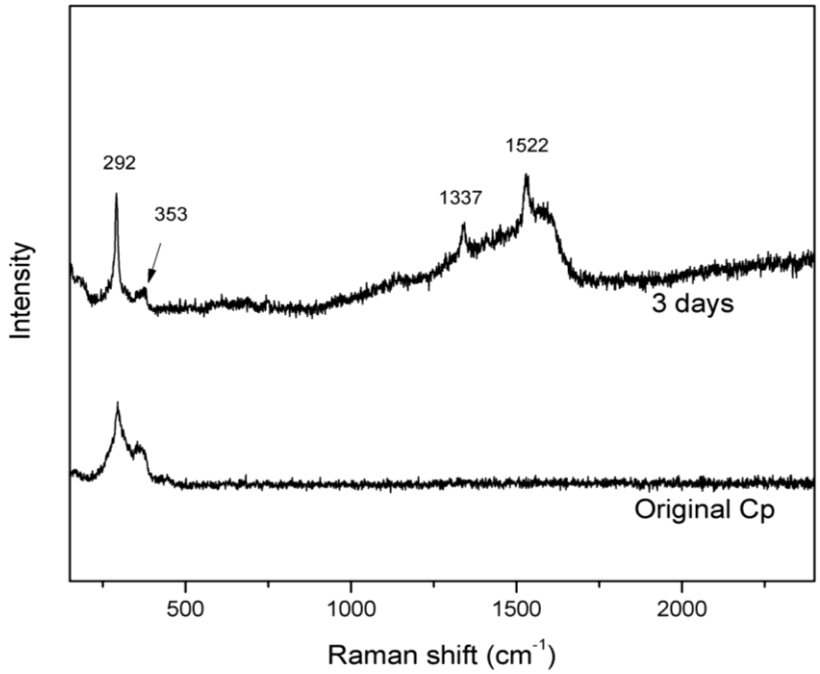

Fig. 5-5 Raman spectroscopy of chalcopyrite before and after 3 days bioleaching

5.3.4 Initial cell attachment and crystal orientation of chalcopyrite

From morphology and Raman studies (Fig. 5-1 and Fig. 5-5) it can be seen that biofilm of *A. ferrooxidans* preferentially formed on certain chalcopyrite surfaces. Because Cai et al. (2012) previously reported the extent of chemical oxidation of chalcopyrite to be sensitive to crystal orientation, the relationship of crystal orientation to cell attachment and population size was studied in this thesis. The EBSD IFP-Z pattern is shown in Fig. 5-6. In the IFP-Z figure, different crystal planes are represented by different colours, such as dark blue for (111) plane, red for (001) plane and green for (101) plane. The IFP-Z figure shows that the sample contained a variety of crystal planes and could be used in a study of bacterial attachment.

Different crystal orientations have different surface atomic arrangements. Some orientations contain more than one termination. For instance, in S-terminated ((001)-S) surface, there are eight S atoms in the first atomic layer and four Fe and four Cu atoms in the second layer in a two unit super cell. By contrast, in the metal-terminated ((001)-M) surface, considering a two-unit cell model, there are four Fe and four Cu atoms in the first layer with eight S atoms in the next layer (de Oliveira and Duarte, 2010). In the (111)-M surface, there are two Fe and two Cu in the first layer in the one unit cell model, although these four metal atoms are not exactly in the same plane (de Oliveira et al., 2012). In contrast, the (012) plane represents the only surface with an equal number of metal atoms

(Cu and Fe) and S atoms (Von Oertzen et al., 2006). Similarly, The (112) and the (101) planes exhibit a stepped surface with superficial atoms in different attitudes, the sulfur and metal atoms occurring in alternate positions (de Oliveira et al., 2012).

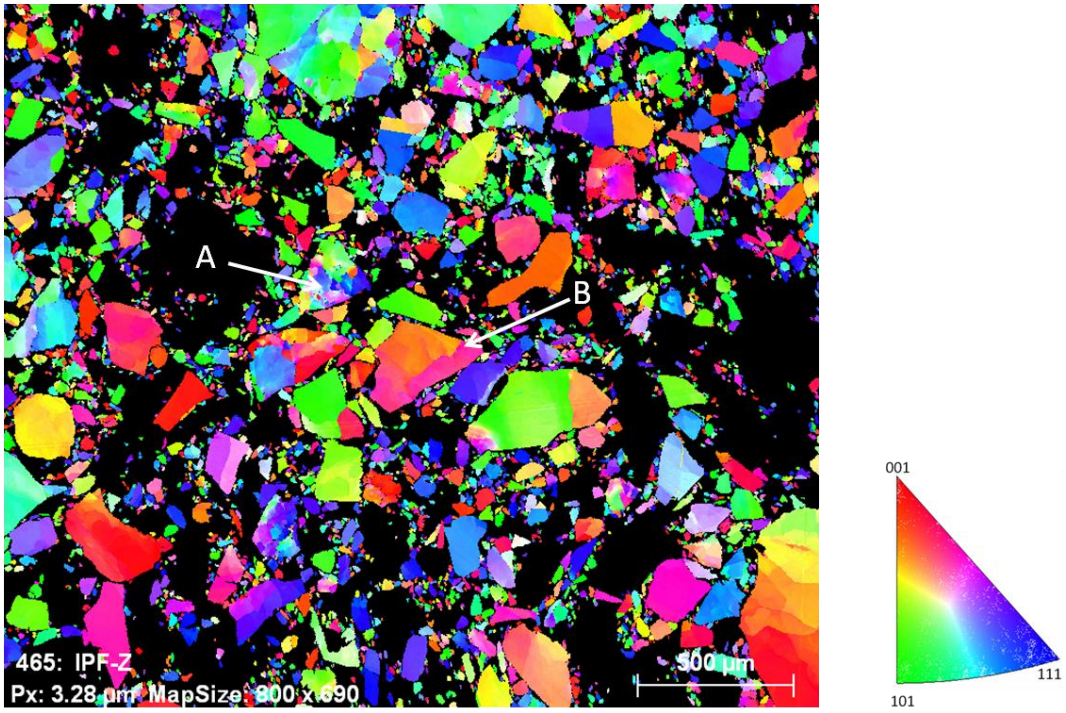

Fig. 5-6 EBSD IFP-Z map of polished chalcopyrite particles

In Fig. 5-7, the optical images of two different areas before and after 24 hours of bioleaching are displayed. The locations of the two areas are indicated by A and B, respectively, in Fig. 5-6. It is clear that bacteria attached to the area rather randomly, despite a range of planes could be identified there. Results from enumeration of the bacteria attached to the major planes are shown in Table 5-1. The results show that the average coverage for each plane was similar after 24 hours. Initial attachment of the cells with respect to crystal orientation seemed irrelevant in the case of chalcopyrite. As the poor cleave of chalcopyrite, it is assumed there were both metal terminated and sulfur terminated surfaces for the planes presented in Fig. 5-6, however, the bacteria coverage on the chalcopyrite surface did not show clear difference between particles of the same orientation as well. This result suggests the cell initial attachment may not have been directly affected by the difference in atomic arrangement of the upmost surface layer in the very initial stage.

On the contrary, a distinctive population of bacteria on the (110) and (100) faces of pyrite reported previously was observed accompanied by more significant mineral corrosion and much higher pit densities (Edwards et al., 1998; Edwards and Rutenberg, 2001; Ndlovu and Monhemius, 2005). Because it is well known that bacteria tend to attach to rough and defective surfaces, the higher bacterial concentration observed on the (110) and (100) faces in those studies may be related to the more significant corrosion on those faces. The work of Cai et al. (2012) suggests the corrosion of chalcopyrite sulfate ions proceeded preferentially in the (112) or (001) planes. However, this may not significantly affect the behaviour of cell attachment in the very initial stage, because the crystallographic effect on bacterial attachment was not observed.

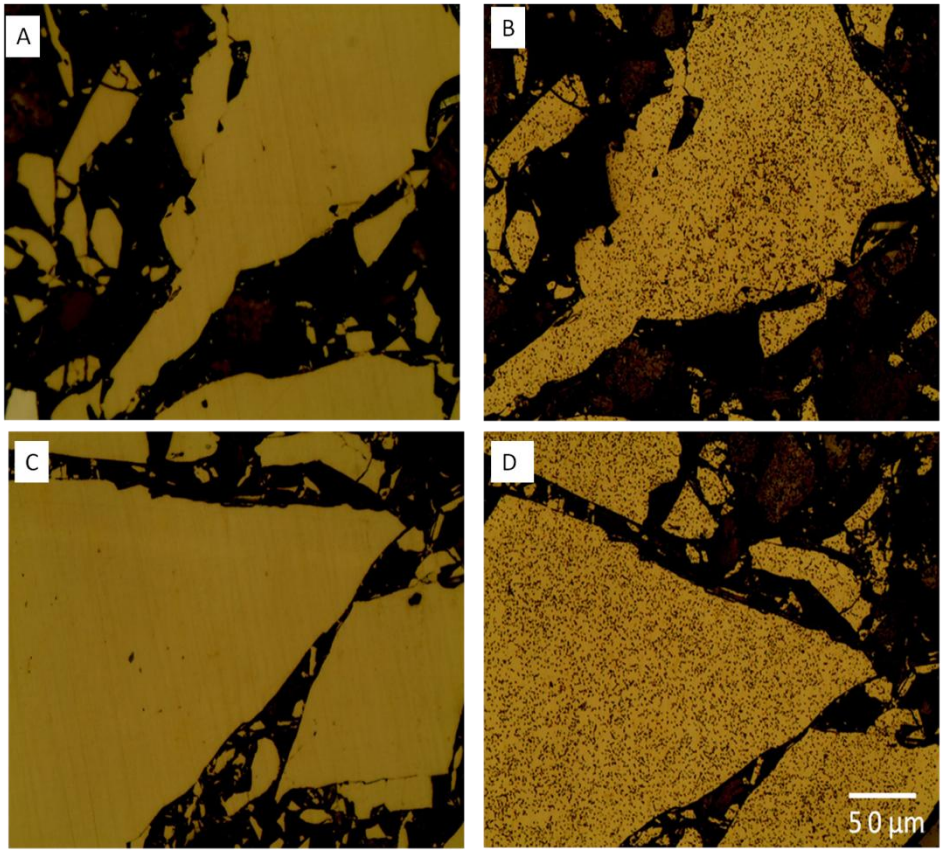

Fig. 5-7 The attachment behavior of *A. ferrooxidans* to the different faces of chalcopyrite crastal. (A and C: before bioleaching; B and D: after bioleaching for 24 hours.)

Table 5-1 Percent coverage of minerals by bacteria on different crystal planes of chalcopyrite

Nominal plane No.	Colour in IPF-Z Map	Bacteria coverage, %	Error, % [a]
101	Green	6.8	18.4
103	Orange	6.1	17.7
001	Red	6.4	11.3
548	Blue	6.3	13.8
213	Light blue	7.0	12.4
102	Yellow	6.6	8.7
438	Purple	7.0	13.5
113	Pink	6.8	10.4

a: Error = SD/Average X 100%

5.4 Conclusions

The microbial population behaviour of *Acidithiobacillus ferrooxidans* on polished chalcopyrite was studied up to 96 hours. In the first 24 hours, *A. ferrooxidans* started to attach onto the chalcopyrite surface. The bacterial population in the defects was significantly higher than that on the polished surfaces. After 72 hours of leaching, biofilm formation occurred. The AFM studies indicate abundant EPS was produced on the mineral surface after 72 hours of leaching. The formation of biofilm was further supported by the Raman. From EBSD and optical images analysis, no significant difference in selectivity of bacterial attachment was found on crystal orientation of chalcopyrite.

Chapter 6 The effect of ferrous and ferric ions on chalcopyrite bioleached at 30 and 48 ^{o}C

6.1 Introduction

Iron ions have significant impact on chalcopyrite dissolution. As discussed in chaper 1, Fe^{3+} is the primary impetus of chalcopyrite dissolution in current theory, thus the presence of Fe^{3+} will be favourable to the leaching kinetics (Sand et al., 2001). However, some studies show that the addition of ferrous ion can significantly improve the chalcopyrite dissolution kinetics over the addition of ferric ion (Hiroyoshi et al., 1997; Hiroyoshi et al., 2001; Third et al., 2000; Third et al., 2002). This phenomenon may relate to the low solution potentials as a result of Fe^{2+} addition (Sandström et al., 2005; Vilcáez and Inoue, 2009). However, the mechanism of the promotion of chalcopyrite leaching kinetics by low redox potential is not clear yet.

Jarosite is a common leaching by-product, which is proposed to be a possible passivation factor (klauber, 2008). Efforts have been made by the researchers to evaluate its passivating nature, yielding controversial results (Sasaki et al., 2009; Córdoba et al., 2008a; Córdoba et al., 2008b; D'Hugues et al., 2002; Stott et al., 2002). Therefore, it is helpful to study the how the formation of jarosite affects the leaching kinetics to reveal the passivation effect of jarosite.

In this work, the impact of Fe^{2+}/Fe^{3+} ratio to the chalcopyrite leaching behaviour was studied. At the same time, XANES, XRD and Raman were employed to characterize the changes of the mineralogy in bacterial and chemical leaching.

6.2 Experimental

6.2.1 Leaching experiments

For the 30 ^{o}C leaching study, the chalcopyrite was leached by mixed mesophilic culture. Modified 9K basic medium containing 3 g/L iron in different Fe^{2+}/Fe^{3+} ratio (1:0, 5:1, 1:1, 1:5, 1:20, 0:1) was used as the basic salt medium in this study. The bacteria were inoculated into 250 mL flasks which containing 150 mL 9K medium and 2.25 g chalcopyrite and the initial bacteria concentration was adjusted to 10^{7} cell/mL. The initial

pH was adjusted to 1.8 and maintained between 1.7-1.9 by adding sulfuric acid or potassium hydroxide. The flask was agitated at 170 rpm and kept at 30 ^{o}C. The leaching experiment with moderate thermophiles was carried out as described above but at 48 ^{o}C. Chemical leaching at 30 ^{o}C with the same solid to liquid ratio was also conducted for comparison to the bioleaching experiment.

6.2.2 Solution studies

Solution studies were performed as per the description in section 2.5.

6.2.3 Raman studies

Raman spectroscopic study was performed according to the description in section 2.10.

6.2.4 XRD studies

Powder XRD data were collected according to the description in section 2.9.

6.2.5 Cu and Fe K-edge XANES studies

X-ray absorption spectra were recorded at BL-20B beamline (Australian National Beamline Facility, ANBF) beam-line using synchrotron radiation Photon Factory, High Energy Accelerator Research Organization (KEK), Japan. The experimental details could be found in section 2.8.2 and 3.2.3.

6.3 Result and discussion

6.3.1 Solution studies

The change of copper concentrations for three sets of experiments is shown in Fig. 6-1. In the bioleaching experiments (Fig. 6-1A&B), it is clear that leaching at 48 ^{o}C profoundly enhances copper leaching rate. At 30 ^{o}C, only 0.45 g/L copper was release at the optimal condition in 28 days, while at 48 ^{o}C 3.5 g/L copper was released in the same period and 4.2 g/L copper was released at the end of experiment. It is clear that higher initial ferrous concentration can promote chalcopyrite dissolution. The increase of copper dissolution rate was not linear with the increase of Fe^{2+}/Fe^{3+} ratio. The curves were apparently divided into a high Fe^{2+}/Fe^{3+} ratio group and a low Fe^{2+}/Fe^{3+} ratio group. A significant increase of copper leaching rate was seen when the initial Fe^{2+}/Fe^{3+} ratio was higher than 20:1 for leaching at 30 ^{o}C and 1:1 for that at 48 ^{o}C. In chemical leaching (Fig. 6-1C), the results of copper dissolution at 30 ^{o}C also fell into two groups like those in bioleaching but with 2-3 times higher copper concentration than their counterparts in bioleaching.

Fe^{2+} concentration changes for the different experiments are displayed in Fig. 6-2. In bioleaching experiments (Fig. 6-2A&B), the changes of ferrous concentration were very similar. In almost every case, the ferrous concentration dropped sharply to 0 within 5-10 days. In chemical leaching experiments at 30 ^{o}C (Fig. 6-2C), the ferrous concentrations increased by about 0.2 to 1.6 g/L, with the increment negatively correlated to the initial ferrous concentration.

The total iron concentration in bioleaching experiments at 30 ^{o}C and 48 ^{o}C changed in a similar way (Fig. 6-3A&B). Generally, the iron concentration decreased with time due to precipitation losses. Exceptions were seen in the cases where significantly more copper was released (Fig. 6-1A&B), where an increase of total iron concentration in first 5-15 days was detected. In chemical leaching at 30 ^{o}C, the total iron concentration increased slightly to moderately.

The cell growth curves are displayed in Fig. 6-4. In general, the mesophiles and thermophiles had similar cell densities and growth cycles, despite the copper concentration in 48 ^{o}C bioleaching being about 8-10 times higher. At the same time, bacteria grew better in experiments with higher ferrous concentration, and this is more obvious for the mesophiles. This result suggests ferrous iron promoted bacteria growth, which may partially explain the higher copper recovery in experiments with high Fe^{2+}/Fe^{3+} ratios. This in turn promotes leaching and the formation of sulfur which is another source of energy for some of the bacteria.

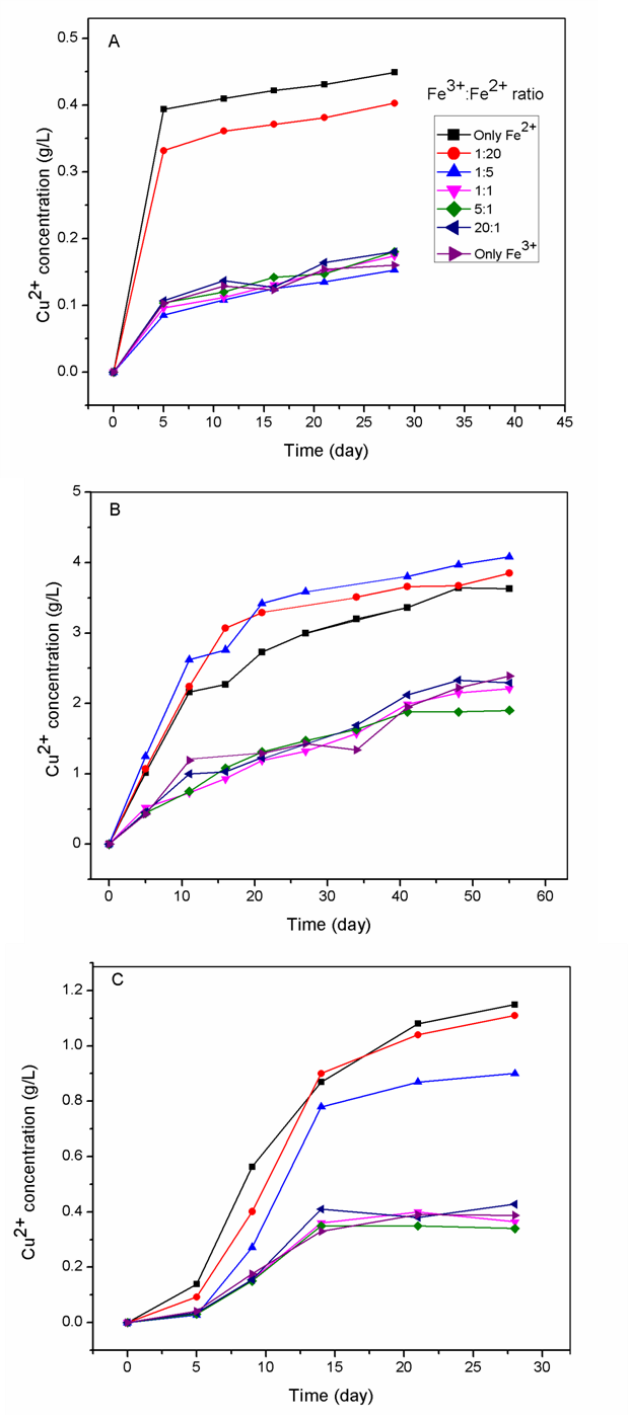

Fig. 6-1 Copper ion concentration as a function of time during leaching of chalcopyrite with different initial ratio of Fe^{2+}/Fe^{3+} (A, bioleaching at 30 ^{o}C; B, bioleaching at 48 ^{o}C; C, chemical leaching at 30 ^{o}C)

.

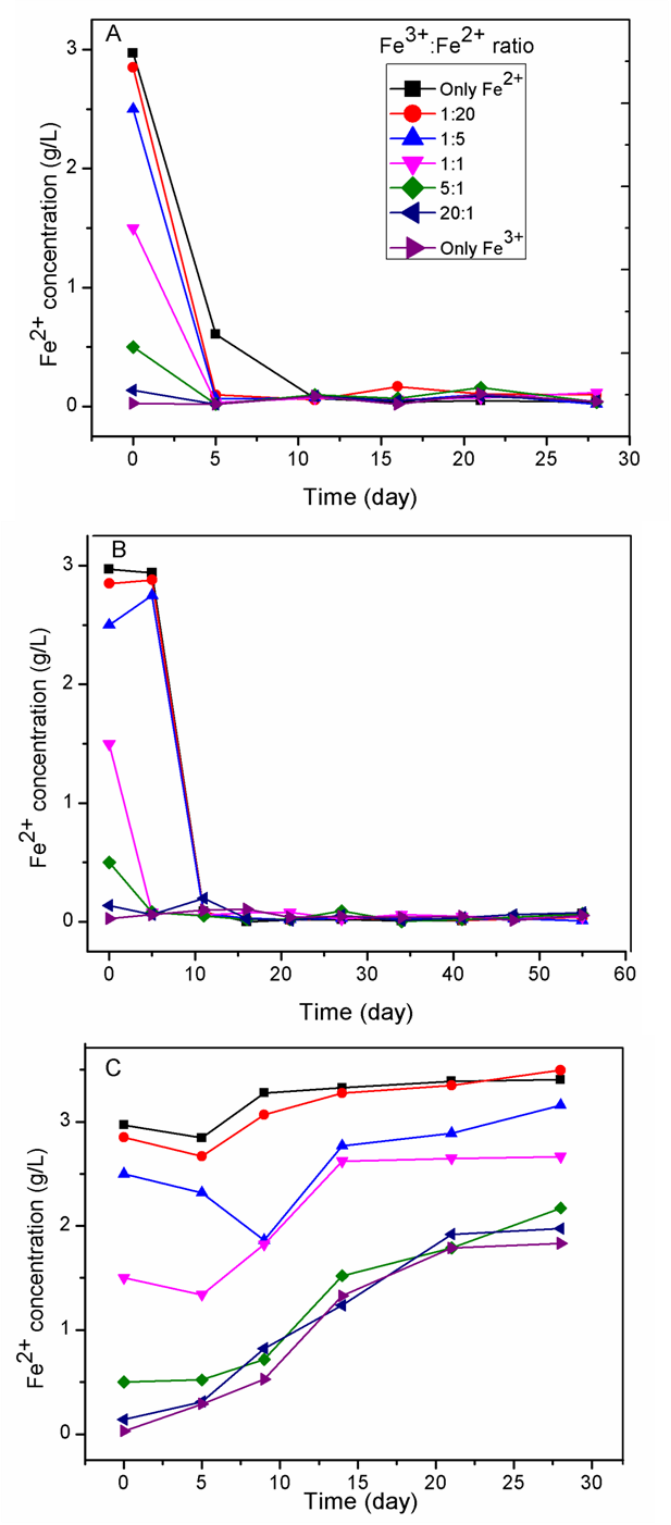

Fig. 6-2 Ferrous ion concentration as a function of time during leaching of chalcopyrite with different initial ratio of Fe^{2+}/Fe^{3+} (A, bioleaching at 30 ^{o}C; B, bioleaching at 48 ^{o}C; C, chemical leaching at 30 ^{o}C)

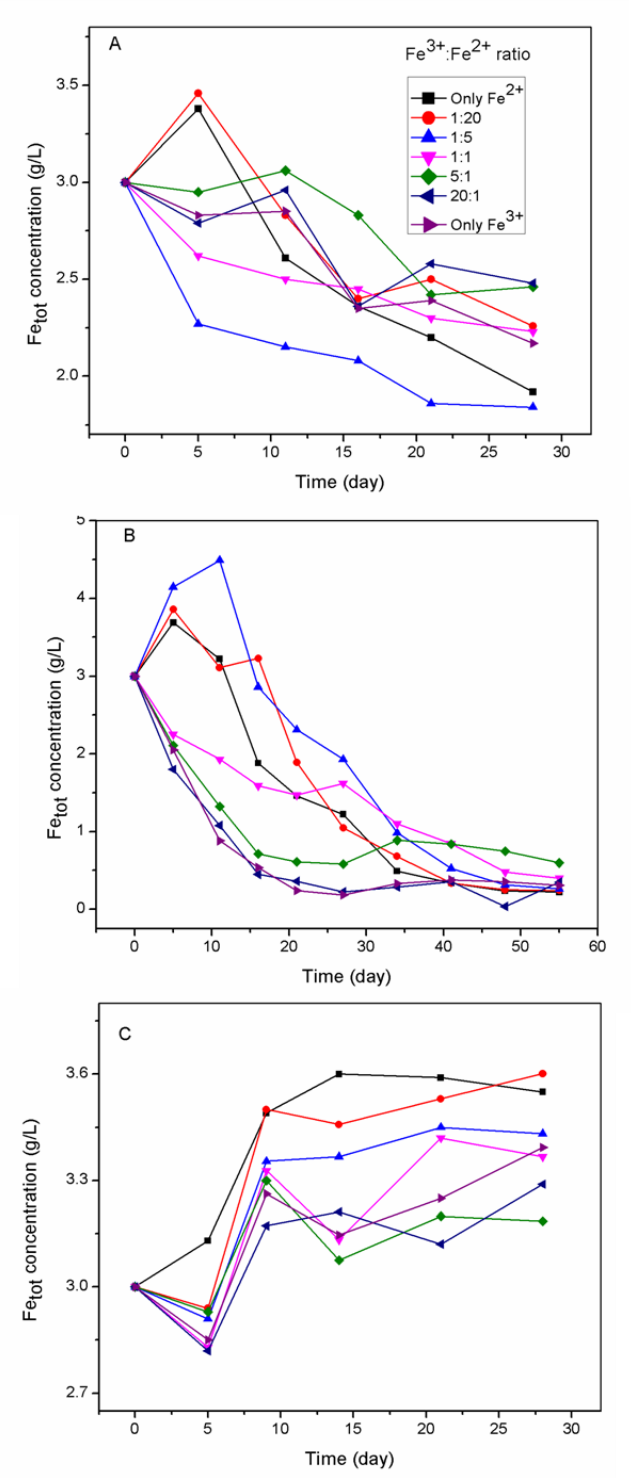

Fig. 6-3 Total iron concentration as a function of time during leaching of chalcopyrite with different initial ratio of Fe^{2+}/Fe^{3+} (A, bioleaching at 30 ^{o}C; B, bioleaching at 48 ^{o}C; C, chemical leaching at 30 ^{o}C)

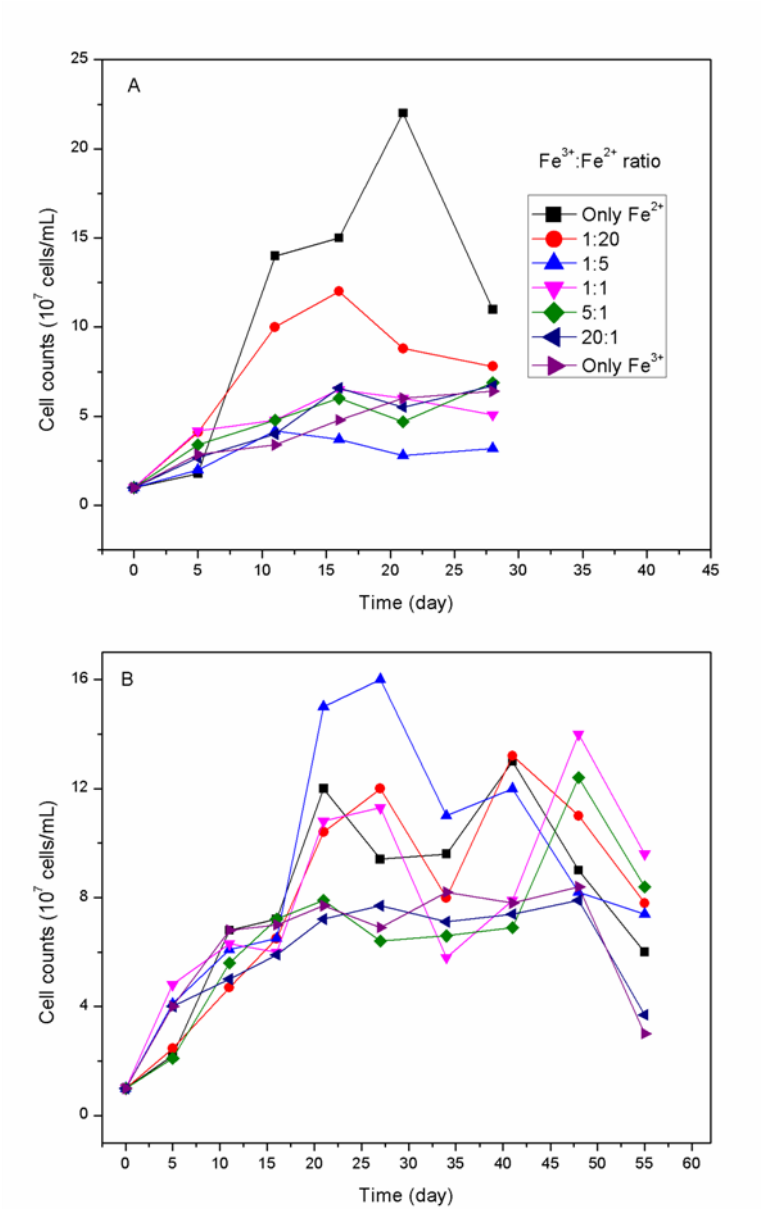

Fig. 6-4 Cell growth curves during chalcopyrite bioleaching with different initial ratio of Fe^{2+}/Fe^{3+} (A, bioleaching at 30 ^{o}C; B, bioleaching at 48 ^{o}C)

The solution Eh changes are displayed in Fig. 6-5. The initial Eh value is in accord with the corresponding Fe^{2+}/Fe^{3+} ratio, where lower Eh values were found for higher Fe^{2+}/Fe^{3+} ratios. In 30 ^{o}C bioleaching, the Eh increased rapidly to approximately 700 mV. On the other hand, during bioleaching at 48 ^{o}C the increase of Eh values was slower at the beginning, especially for the high ferric concentration experiments. This may be explained by the rapid precipitation of soluble iron as shown in Fig. 6-3.

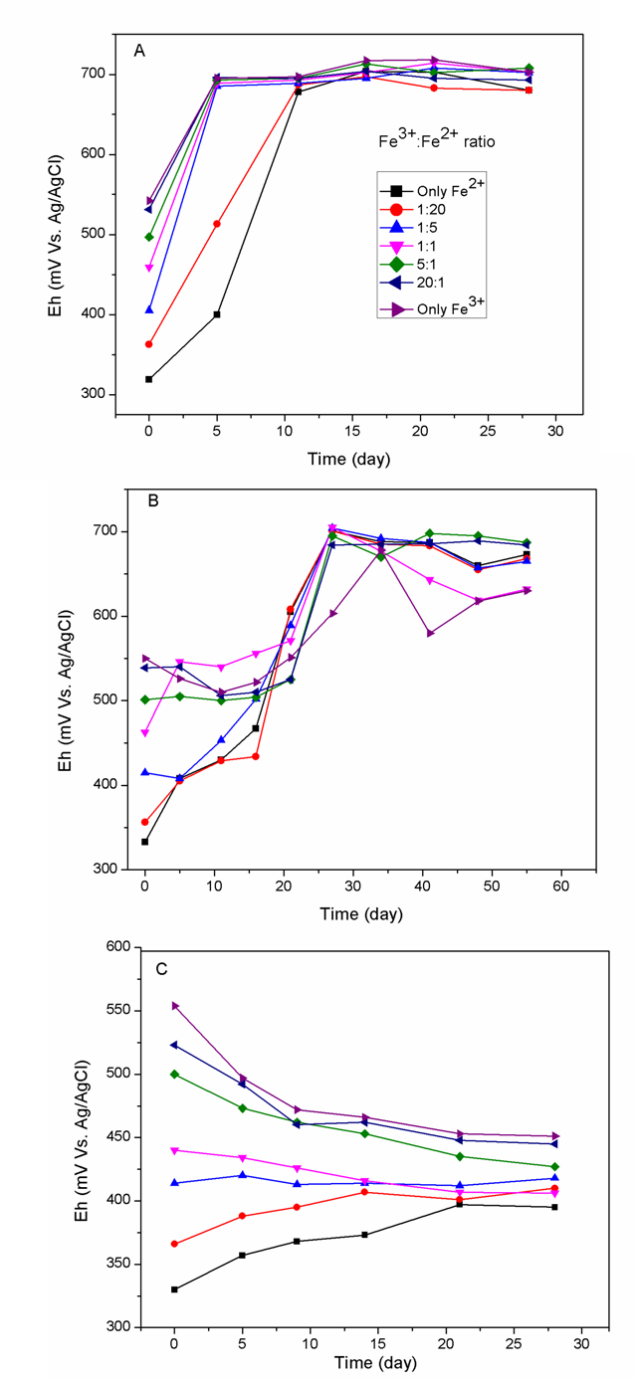

Fig. 6-5 Eh changes as a function of time during leaching of chalcopyrite with different initial ratio of Fe^{2+}/Fe^{3+} (A, bioleaching at 30 ^{o}C; B, bioleaching at 48 ^{o}C; C, chemical leaching at 30 ^{o}C)

In chemical leaching experiments at 30 ^{o}C, the Eh tended toward an equilibrium value of approximately 450 mV. The Eh curves coupled with copper leaching results confirmed that a lower Eh value is more favorable for the chalcopyrite leaching. Leaching of chalcopyrite was clearly hindered when the Eh was higher than 700 mV especially during

bioleaching at 30 ^{o}C, which is consistent with previous results (Hiroyoshi et al., 1997; Sandström et al., 2005; Third et al., 2002).

It is worth to be noticed that in Chaper 4, the active region for chalcopyrite dissolution was 550-630 mV, according to the result of electrochemical study, and the active region for chalcopyrite was found 350-480 mV during bioleaching. In the electrochemical study, the potential (E) is applied externally to the electrode and forms an over-potential (E-E_{OCP}). The sum of cathodic and anodic current is not zero and the system is not in the equilibrium. On the other hand, in a real leaching experiment the redox potential is a mixed potential in an equilibrium system (no net current). Its value lies between the value of equilibrium potential of oxidation and reduction reactions, and depends on the nature of the system (Ahmad, 2006). Therefore, the active and passive region in anodic polarization curve indicates the response of chalcopyrite to different over-potentials. This may be different to the active and passive region in leaching, which indicates the response of chalcopyrite to different mixed potential.

It is important to note the maximum copper recovery was always less than 80% in this work and oxidation never progressed to completion. In all cases, a parabolic copper leaching curve was observed in spite of the Eh changes. This is more obvious for chemical leaching at 30 ^{o}C, during which the leaching of chalcopyrite ceased after 28 days even though the potential values were in the previously reported optimal range (Sandström et al., 2005). This result indicates that high Eh is not the only reason for a decrease in chalcopyrite leaching and the parabolic leaching curve may be due to passivation layers formed in leaching.

6.3.2 Raman studies

The Raman results are displayed in Fig. 6-6 A and B for leaching experiments conducted at 30 ^{o}C and 48 ^{o}C, respectively. In the Raman spectra, the peak at approximately 291 cm^{-1} is assigned to chalcopyrite (Mernagh et al., 1993); peaks at 151 cm^{-1}, 220 cm^{-1}, can be assigned to elemental sulfur (Eckert and Steudel, 2003); and peaks at 138 cm^{-1}, 429 cm^{-1}, 625 cm^{-1}, 1007 cm^{-1} and 1102 cm^{-1} can be assigned to jarosite (Sasaki et al., 2009). The peak at 472 cm^{-1} could be assigned to either elemental sulfur or covellite (Sasaki et al., 2009). For 30 ^{o}C chemical leaching the amount of jarosite was much less than for bioleaching, which is in accord with the lower Eh and high soluble iron concentration found in solution. Elemental sulfur was also detected in chemically leached samples and

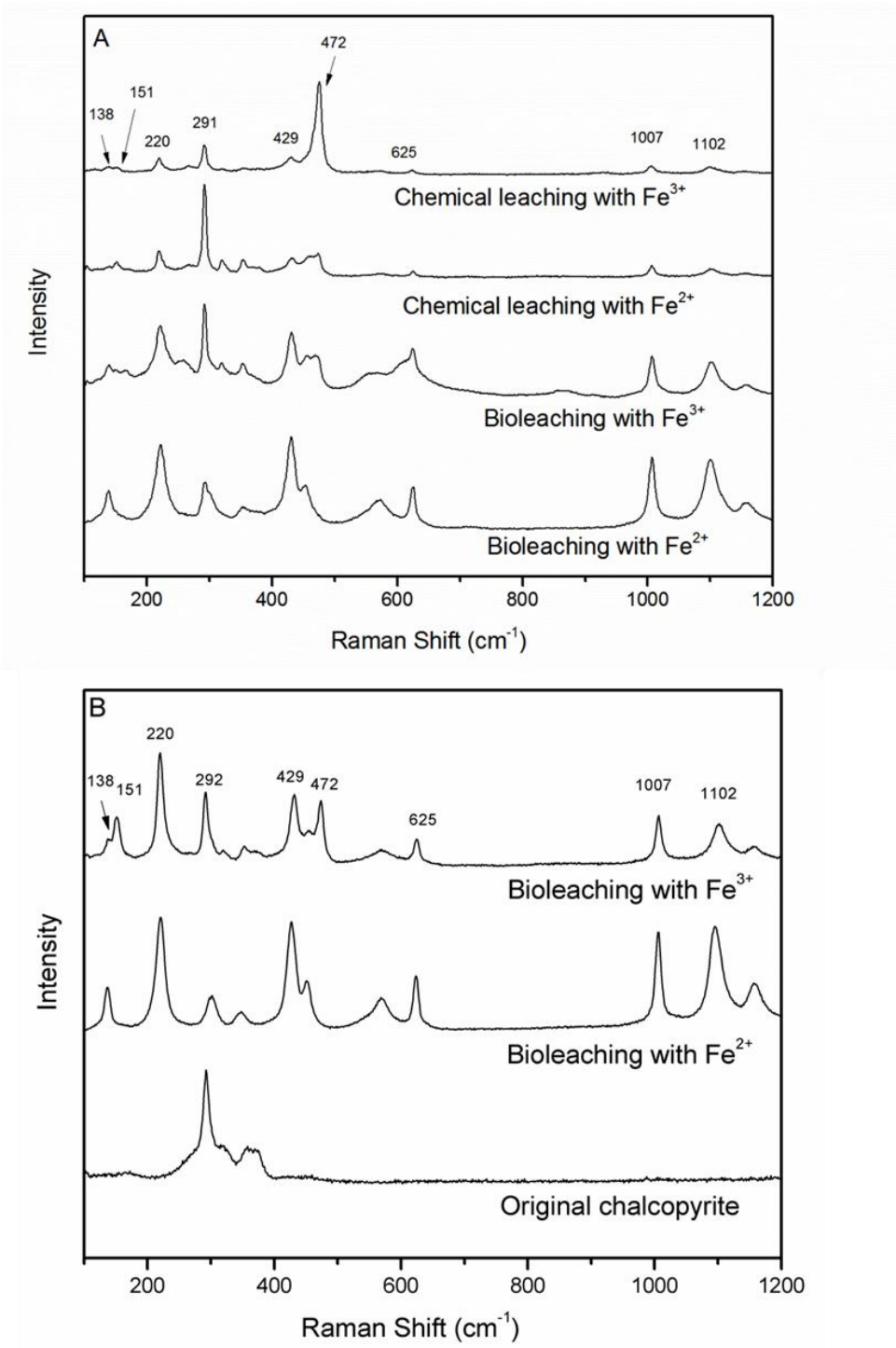

Fig. 6-6 Raman spectra of chalcopyrite leached with 3 g/L ferrous or ferric addition (A, bacterial and chemical leaching at 30 ^{o}C for 28 days; B, bioleaching at 48 ^{o}C for 55 days)

bioleached ones in the presence of Fe^{3+}. As the only peak for covellite overlaps with the peak of elemental sulfur, the presence of covellite could not be unambiguously confirmed by Raman spectra. However, in samples chemically leached by ferric ion, a strong peak at 472 cm^{-1} was detected, which is not in proportion to the other peaks for elemental sulfur, and which may therefore indicate the presence of covellite. For 48 ^{o}C bioleaching, and similar to that at 30 ^{o}C, jarosite and elemental sulfur were detected in the sample leached

with just ferric ion. On the other hand, elemental sulfur was not detected in the sample leached with just ferrous ion, and this may also be linked to the better cell growth in that experiment.

6.3.3 XRD studies

XRD analysis was conducted for samples leached with just ferrous or ferric ion additions. XRD patterns from chalcopyrite leached at 30 ^{o}C are displayed in Fig. 6-7. The bioleached samples were composed mostly of jarosite and chalcopyrite while in the cases of chemical leaching, the residue was mainly composed of chalcopyrite especially when Fe^{3+} was initially added, although the copper recovery in chemical leaching was much higher. Besides chalcopyrite and jarosite, there were also weak peaks that could be assigned to elemental sulfur and mooihoekite ($Cu_9Fe_9S_{16}$).

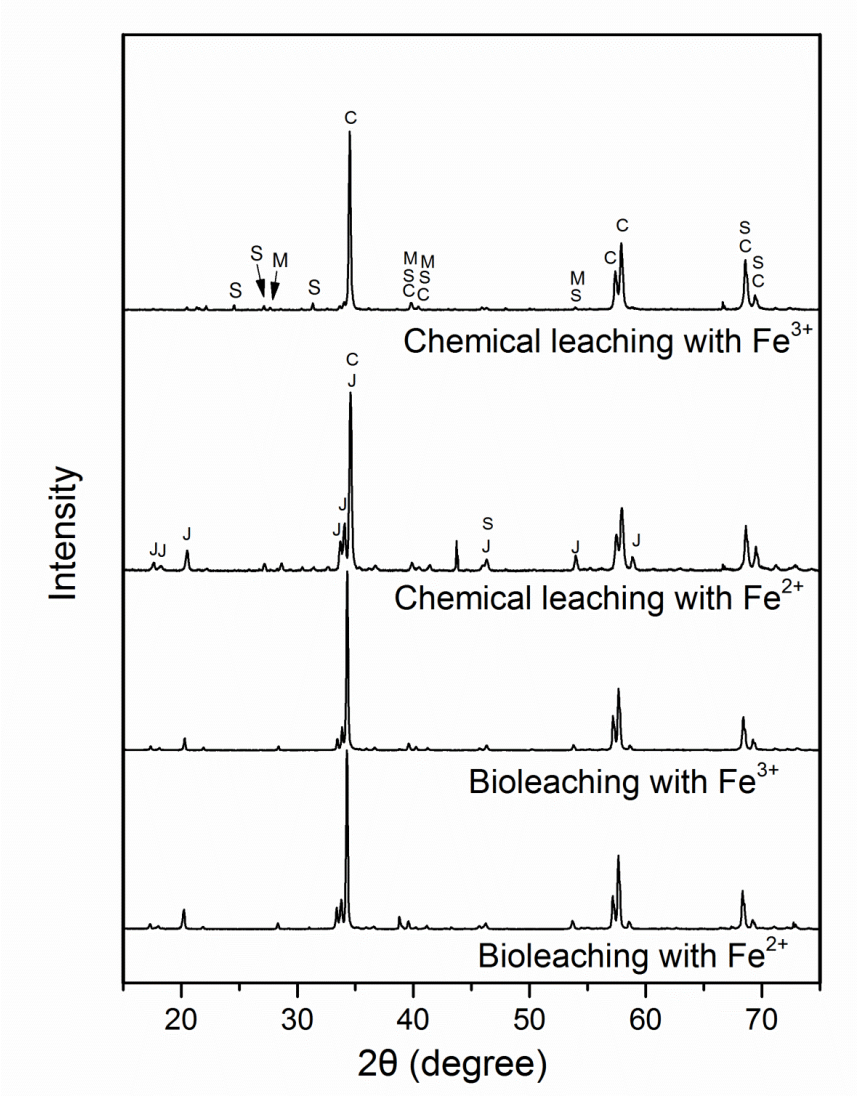

Fig. 6-7 XRD patterns of chalcopyrite chemically or bacterially leached with 3 g/L ferrous or ferric addition for 28 days. (C: chalcopyrite; J: jarosite; S: S_8; M: Mooihoekite)

The quantitative results of XRD are shown in table 6-1 and table 6-2 for leaching conducted at 30 ^{o}C and 48 ^{o}C, respectively. In chemical leaching at 30 ^{o}C, only minor to modest amounts of jarosite were detected under all conditions, while in bioleaching a significant amount of jarosite precipitated in 20 days. In bioleaching, more jarosite formed in leaching with ferrous ion than with ferric, which accounted 70.9% of the residue in the former one but only 33.1% in the later one at day 28.

During bioleaching at 48 ^{o}C, jarosite precipitation occurred much earlier and for a greater extent compared to leaching at 30 ^{o}C. More than 60% of jarosite was found in the leaching product in the first 10 days and over 80% of the leaching residue was composed of jarosite after 20 days in bioleaching with ferrous ion. In the experiment with ferric ion, the formation of jarosite was slower, with 47.2 % of the residue was composed of jarosite after 20 days.

Jarosite is a common leaching by-product and has been reported as passivation factor previously (klauber, 2008; Córdoba et al., 2008a; Córdoba et al., 2008b). However, in this study it was found that leaching with Fe^{2+} gave a better copper extraction at both 30 ^{o}C and 48 ^{o}C (Fig. 6-1), while more jarosite was precipitated. This result indicates Eh was the driving force for extraction and that the extent of jarosite precipitation did not appear to be important in the current set of experiments. In addition, from the kinetics of chalcopyrite dissolution and that of jarosite formation, it can be inferred that the passivation of the chalcopyrite is not mainly caused by the jarosite formation. For instance, during bioleaching with Fe^{2+} at 48 ^{o}C, the highest leaching kinetics was found in the first 10 days when the formation of jarosite was rapid. The chalcopyrite leaching rate decreased dramatically from day 10 to day 20 (Fig. 6-1B) and the leaching further slowed down afterwards when the jarosite precipitation was much slower (table 6-1). On the other hand, in bioleaching with Fe^{3+} at 48 ^{o}C, 27% jarosite was detected at day 10 when the copper dissolution kinetics decreased considerably. From day 10 onwards, the copper dissolution was almost linear while the jarosite content increased to 86.5% after 55 days leaching. It seems that the change of the copper dissolution kinetics is not related to the jarosite precipitation in this study. This observation suggests jarosite is not the dominant factor dictating chalcopyrite dissolution behaviour, and jarosite precipitates have no significant effect (if any) to the inhibition of chalcopyrite dissolution.

Table 6-1 Summary of quantitative XRD analysis of chalcopyrite bacterially or chemically leached at 30 ^{o}C (wt%)

	Time (day)	Fe^{2+} (g/L)	Fe^{3+} (g/L)	Cp	Py	Qz	J	S	Mh
Original Cp				94.6	2.1	3.3			
Bioleaching	10	3	0	96.0	0.8	0.1	2.9	-	0.1
	10	0	3	97.6	1.2	0.4	0.8	-	-
	20	3	0	29.1	3.3	1.5	66.1	-	-
	20	0	3	67.8	0.7	0.1	31.1	0.5	-
	28	3	0	19.9	3.9	1.1	75.1	-	-
	28	0	3	66.3	0.5	0.1	33.1	-	-
Chemical leaching	10	3	0	70.8	1.2	0.2	27.4	0.4	-
	10	0	3	96.3	1.4	0.1	1.6	0.5	-
	20	3	0	64.6	1.1	0.1	33.4	0.8	-
	20	0	3	94.8	0.6	0.1	3.3	1.1	-
	28	3	0	51.7	1.3	0.2	46.3	0.6	-
	28	0	3	88.3	1.0	0.2	8.3	2.0	0.1

Cp: chalcopyrite; Py: pyrite; Qz: quartz; J: jarosite; S: S_8; Mh: Mooihoekite

Table 6-2 Summary of quantitative XRD analysis of chalcopyrite bioleached at 48 ^{o}C (wt%).

Time (day)	Fe^{2+} (g/L)	Fe^{3+} (g/L)	Cp	Py	Qz	J	S	Mh
10	3	0	19.2	2.1	0.1	77.9	0.7	-
10	0	3	65.2	6.1	0.7	27.0	1.0	-
20	3	0	16.4	0.7	0.1	81.7	1.2	-
20	0	3	44.9	5.3	0.8	47.2	1.8	-
55	3	0	12.5	0.6	-	86.5	0.4	-
55	0	3	18.3	0.5	0.1	81.1	-	-

Cp: chalcopyrite; Py: pyrite; Qz: quartz; J: jarosite; S: S_8; Mh: Mooihoekite

Besides jarosite, 0.4-2.0 % of elemental sulfur was present in the solid samples taken from chemical leaching. In the cases of bioleaching, 0.5% and 0.6% elemental sulfur was found in samples leached with ferric and ferrous ions after 20 days, respectively. This finding is in accord with the Raman study and suggests elemental sulfur is largely eliminated by the sulfur-oxidizing bacteria present in the cultures. The amount of elemental sulfur after bioleaching at 48 ^{o}C was more than that at 30 ^{o}C, which indicated more significant oxidation of the chalcopyrite.

It has been suggested in the literature that elemental sulfur can hinder ion transport and the dissolution process (Dutrizac, 1989). Dutrizac reported that the surface of chalcopyrite was enveloped by a layer of elemental sulfur which became progressively thicker with leaching time. In this study, when chalcopyrite was leached at 30 ^{o}C, higher copper recovery was found for chemical leaching, for which a higher amount of elemental sulfur was found. At the same time, the bioleaching at 48 ^{o}C was more efficient than that

at 30 ^{o}C, but more elemental sulfur was produced. The results suggest that removal of sulfur during chalcopyrite leaching did not improve copper recovery. This suggests that sulfur formed during chalcopyrite leaching did not decrease the copper recovery.

According to the above analysis, neither jarosite nor elemental sulfur should be considered as the primary factor causing chalcopyrite passivation. It is proposed that metal deficient polysulfide is the most likely passivation layer which dictates the copper recovery. Polysulfide is a polymeric form of metal sulfide, generally in the form of M_xS_n where n>2. Current literature suggests the formation of metal deficient polysulfide during chalcopyrite leaching. XPS analysis of bacterially and chemically leached chalcopyrite residue show preferential dissolution of iron and copper concentration and the formation of sulfur-rich layer in the early stage of leaching (e.g. (Buckley and Woods, 1984; Hackl et al., 1995; Harmer et al., 2006). Hackl et al. (1995) suggested that sulfur species on the oxidized chalcopyrite is more inert than copper or iron and the surface species could be the rate-controlling step in the chalcopyrite oxidation process. It was proposed that the passivation layer subsequently formed is further enriched in sulfur and has the form of Cu_xS_n. This layer further hindered the dissolution of the bulk chalcopyrite (Hackl et al., 1995).

Another interesting finding from XRD is that trace amount of mooihoekite was detected in several samples. The formation of non-stoichiometric compounds in chalcopyrite oxidation has been proposed previously by electrochemical and XPS studies (Hackl et al., 1995; Mikhlin et al., 2004). Compared to an electrochemical study which is an indirect method to study chalcopyrite bioleaching and XPS which provides evidence of non-stoichiometric compounds based on the elemental concentration analysis, the evidence from XRD is a more direct way to confirm the formation of non-stoichiometric crystalline materials.

6.3.4 XANES studies

6.3.4.1 Copper K-edge XANES

A copper K-edge XANES study was conducted to study the chalcopyrite copper species evolution during leaching experiment. In all 30 samples leached with different Fe^{2+}/Fe^{3+} ratios at 30 or 48 ^{o}C for 4 days, 10 days and 22 days, no evidence of chalcocite was found. Selected Cu K-edge XANES spectra are shown in Fig. 6-8. After bioleaching with Fe^{2+} or Fe^{3+} for 22 days the copper spectra changed slightly, indicating the formation of new

copper species. It is clear that the spectra of the oxidized samples did not indicate the presence of chalcocite, but rather covellite to some extent, which is in agreement with the result of the Raman study. The copper spectra for residue samples are either unchanged or similar to those in Fig. 6-8. The results of linear combination fitting for all copper K-edge XANES spectra are displayed in table 6-3. The results of this analysis show that no chalcocite was present in those samples, however minor to modest amounts (up to 15%) of covellite-like species may exist in a number of samples. As covellite-like species were not found in XRD, it is suggested that this may be some amorphous species, or the crystal size was too small to be identified by XRD under these conditions.

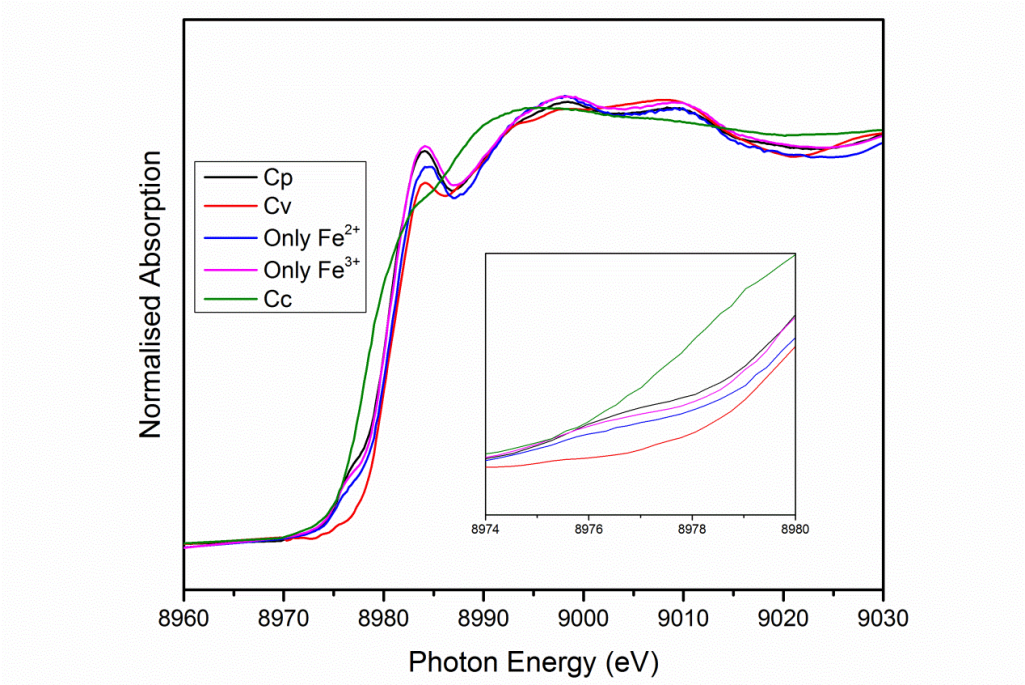

Fig. 6-8 Cu K-edge spectra of chalcopyrite bioleached with 3 g/L ferrous or ferric addition at 48 ^{o}C for 22 days. (Cp: chalcopyrite; Cv: Covellite; Cc: chalcocite)

Table 6-3 Fitting results of Cu K-edge XANES spectra of chalcopyrite leached with different ratio of Fe^{2+}/Fe^{3+} for different times (wt%)

Microorganisms	Time (day)	Fe^{2+} (g/L)	Fe^{3+} (g/L)	Cp	Cv
Meso Mix	4	3	0	100.0	0.0
	4	1.5	1.5	100.0	0.0
	4	0	3	91.2	8.4
	22	3	0	91.5	8.5
	22	1.5	1.5	92.3	7.7
	22	0	3	88.9	11.1
Thermo Mix	4	3	0	100.0	0.0
	4	1.5	1.5	100.0	0.0
	4	0	3	100.0	0.0
	10	3	0	88.4	11.6
	10	1.5	1.5	85.2	14.8
	10	0	3	100.0	0.0
	22	3	0	85.6	14.4
	22	1.5	1.5	90.0	10.0
	22	0	3	96.5	3.5

Cp: chalcopyrite; Cv: Covellite

The detection of CuS or CuS-like structure by Raman and Cu K-edge XANES in the leaching products suggests that chalcopyrite dissolves in a stepwise manner, as suggested in previously studies. In electrochemical studies, evidence for CuS was found in middle to high potential range. For instance, Nava and González (2006) detected covellite in the region of 1.085 V ≤ *E*anod < 1.165 V vs. SHE, while Mikhlin et al. (2004) claimed the detection of covellite at 0.6 V vs. Ag/AgCl, according to the assignment of Cu *2p* XPS spectra. These results indicate covellite is formed in an oxidation process. Chalcopyrite firstly oxidizes, forming CuS as an intermediate product:

$$CuFeS_2 \rightarrow 0.75CuS + 1.25S^0 + 0.25Cu^{2+} + Fe^{2+} + 2.5e^- \qquad (6\text{-}1)$$

Then, covellite is oxidized by ferric sulfate, releasing Cu^{2+} ions:

$$CuS \rightarrow S^0 + Cu^{2+} + 2e^- \qquad (6\text{-}2)$$

The proposed pathway is also in agreement with other leaching studies. Córdoba et al. (2008a) demonstrated the presence of CuS in the leaching products at short times by using XRD. Sasaki et al. (2009) studied the bioleaching of chalcopyrite with *A. ferrooxidans* using Raman spectroscopy and found the presence of covellite when the Eh was above 700 mV.

Chalcocite is an important intermediate for the proposed two-step leaching model, which is used to explain the promotion of chalcopyrite leaching at low Eh (Hiroyoshi et al., 2000; Hiroyoshi et al., 2001). In study, it was not detected by XRD or XANES under any conditions. The absence of any evidence for chalcocite in this study suggests it may just exist in the leach residue as an unstable trace intermediate if the currently proposed two-step leaching model is correct. On the other hand, although the formation of covellite is probably derived from direct oxidation of chalcopyrite, it could arise from from the chalcopyrite initial reduction product – chalcocite, which is oxidized to covellite by ferric sulfate through the formation of copper-deficient intermediate products, as reported by Ferron (2003):

$$Cu_2S + Fe_2(SO_4)_3 \rightarrow CuSO_4 + 2FeSO_4 + CuS \qquad (6\text{-}3)$$

It needs to be noticed that covellite was not found by XRD, which is inconsistence of the results of Raman and XANES. This indicates the covellite-like species is more likely to be some amorphous CuS compounds with similar structure to covellite. Another point need to be explained is CuS_n-like structure was not detected in samples leached with ferrous or ferric ions. This may be linked to different chemical environment in two studies. In chapter 3, it was found that CuS_n-like species almost disappeared in late stages, when chalcopyrite surface was heavily oxidized. In this study, the surface reaction was faster as the addition of extra chemicals, which made the meta-stable CuS_n species were not found even in early stages.

6.3.4.2 Iron K-edge XANES

Chalcopyrite iron species were studied by Fe K-edge XANES and the results are given in Fig. 6-9 and table 6-4. The spectra indicate the iron species of chalcopyrite residue was mostly composed of jarosite and chalcopyrite and there is no evidence of other iron species (Fig 6-9). The fitting results indicate more jarosite formed in the cases with higher Fe^{2+}/Fe^{3+} (table 6-4). The precipitation of jarosite was largely restricted when there was no ferrous addition, which may be due to the poor leaching rate. The addition of Fe^{2+} obviously facilitated the formation of jarosite, the relative weight percentage which increased from 32.3% to 70.3% at 30 ^{o}C and from 39.5% to 77.2% at 48 ^{o}C after 0.5 g/L Fe^{2+} were added. Further increasing of the Fe^{2+}/Fe^{3+} ratio increased the final jarosite/chalcopyrite ratio but in a more modest manner. The results from Fe K-edge XANES spectra are in agreement with XRD analysis and further support the conclusion that jarosite did not passivate the chalcopyrite leaching.

Córdoba et al. (2008b) found more rapid precipitation of Fe^{3+} as jarosite when the initial redox is high. However, in the present study based on the result of XRD and Fe K-edge XANES, the jarosite precipitation in bioleaching was enhanced by high Fe^{2+}/Fe^{3+} ratio in bioleaching. This observation may be due to the precipitation of jarosite being significantly promoted by bacteria in bioleaching (Córdoba et al., 2008a). In this study, more chalcopyrite was dissolved at a high Fe^{2+}/Fe^{3+} ratio, which produced more sulfur. As a result, More H^+ was generated. To keep the pH around 1.8, more KOH was added in the cases with more Fe^{2+}, which promoted the precipitation of jarosite.

In the case of chemical leaching, more chalcopyrite was dissolved in a high Fe^{2+}/Fe^{3+} ratio, which produced more soluble iron for jarosite formation. In addition, faster pH increases because of H^+ consumptions which also favored the formation of jarosite.

Table 6-4 Fitting results of Fe K-edge XANES spectra of chalcopyrite leached with different ratio of Fe^{2+}/Fe^{3+} for 22 days (wt%).

Microorganisms	Fe^{2+} (g/L)	Fe^{3+} (g/L)	Cp	J
Meso Mix	3	0	20.6	79.4
	2.5	0.5	13.2	86.8
	1.5	1.5	19.7	80.3
	0.5	2.5	29.7	70.3
	0	3	67.7	32.3
Thermo Mix	3	0	17.4	82.5
	2.5	0.5	19.1	80.9
	1.5	1.5	22.2	77.8
	0.5	2.5	22.8	77.2
	0	3	60.5	39.5

Cp: chalcopyrite; J: jarosite

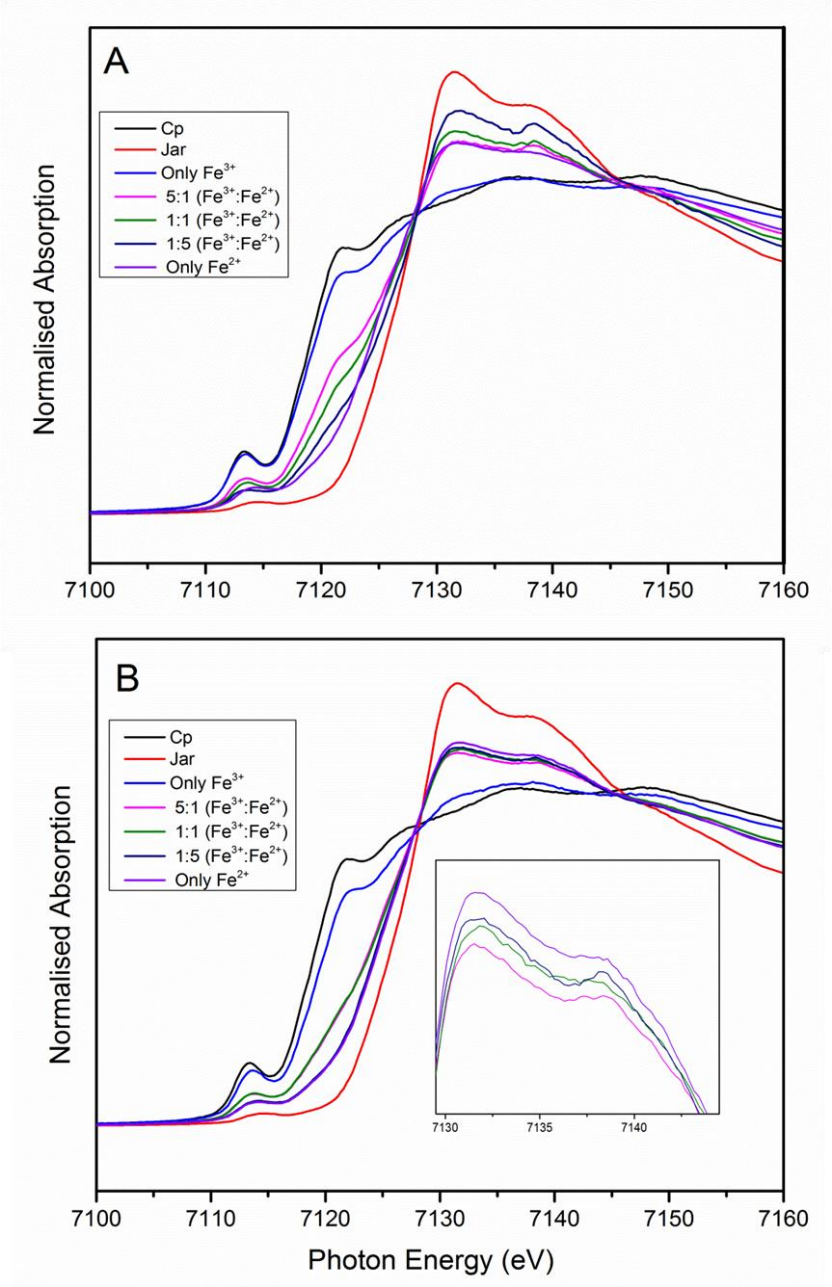

Fig. 6-9 Fe K-edge spectra of chalcopyrite bioleached with 3 g/L ferrous or ferric addition for 22 days at 30 ^{o}C (A) or 48 ^{o}C (B). (Cp: chalcopyrite; Jar: jarosite)

6.4 Conclusions

The results of this study indicate high Fe^{2+}/Fe^{3+}, which keeps the Eh at a relatively low range (350-480 mV), can significantly promote the dissolution of chalcopyrite in either bioleaching and chemical leaching. However, passivation of chalcopyrite was also noted and resulting in a decrease in chalcopyrite dissolution rate in the later stages of experiments. Jarosite was found as the major leaching product which accumulated more rapidly with higher initial Fe^{2+}/Fe^{3+} ratio and at higher temperature. Elemental sulfur was

also found as an intermediate which could be effectively eliminated by the presence of sulfur-oxidizing bacteria. The leaching results in conjunction with quantitative XRD and XANES show that jarosite and elemental sulfur were not the principal factors in the passivation of chalcopyrite. A secondary copper sulfide mineral, covellite, was detected during chalcopyrite dissolution, which is probably an intermediate formed in chalcopyrite direct oxidation. Mooihoekite was also detected by XRD which provided an evidence for the proposed non-stoichiometric species.

Chapter 7 The effect of pyrite on chalcopyrite bioleaching

7.1 Introduction

Chalcopyrite dissolution is enhanced by the addition of pyrite (Li et al., 2013). The effect of pyrite on chalcopyrite leaching is commonly explained as galvanic effect, which results in the preferential leaching of chalcopyrite in a chalcopyrite-pyrite system. In an ideal galvanic leaching scenario, the minerals of interest would be selectively leached while the other minerals can be recovered and recycled to the leaching circuit for further processing. However, the selectivity of chalcopyrite leaching has not been quantified and the link between leaching selectivity, solution properties and mineral surface chemistry has not been established yet.

The motivation of this work is to study and understand the influence of different microbes and temperatures on galvanic leaching behaviour of chalcopyrite concentrates and the corresponding surface chemistry changes on chalcopyrite and pyrite. XFM, Raman spectroscopy, Quantitative XRD and XANES were used to understand the leaching selectivity and the leaching products formation. This may help to understand the role of bacteria and the mechanisms involved more deeply.

7.2 Experimental

7.2.1 Mineral preparation

The mineral powder used in batch leaching was prepared according to the description in section 2.3.1; the Cp/Py coupon for Coupon samples for μ-XRF, μ-XANES and Raman analyses were prepared according to section 2.3.2.

7.2.2 Leaching studies

7.2.2.1 Batch leaching

Batch leaching tests were carried out in 250 ml Erlenmeyer flasks. 150 ml of modified 9K media containing 0.75 g/L Fe^{2+} and 2.25 g/L Fe^{3+} was prepared. The amount of chalcopyrite used was 1.2 g and the amount of pyrite used, when required, was 3.6 g. The minerals were leached with pure *L. ferrooxidans*, a mixed culture of *A. ferrooxidans*, *L.*

ferrooxidans and *A. thiooxidans* with even initial proportion, moderate thermophilic mixture and *S. metallicus*, respectively. The initial bacteria concentration was 1.0 $x10^7$ cells/mL and the initial pH was adjusted to 1.8 and maintained between 1.7-1.9 by adding sulfuric acid or potassium hydroxide. The flasks were agitated at 170 rpm and kept at 30 ^oC for mesophiles, 48 ^oC for moderate thermophiles and 60 ^oC for *S. metallicus*. Chemical leaching at corresponding conditions were performed for comparison. The solid samples were withdrawn at appropriate time interval and then washed with pH 1.8 sulfuric acid three times before further surface analysis was taken to prevent possible contamination of the surface by solution species. Leaching residues were withdrawn in proper time intervals for XRD and Raman tests. The bioleaching samples for XANES study were prepared in a separate experiment using identical conditions as described above.

7.2.2.2 Column leaching

Column leaching was carried out as described in section 2.4.2.

7.2.3 Solution studies

Solution samples were periodically taken from batch leaching and column leaching. The Solution tests were conducted as described in section 2.6.

7.2.4 XFM and μ-XANES

XFM and μ-XANES studies were performed according to section 2.11.

7.2.5 Raman studies

Raman study was performed according to section 2.10.

7.2.6 XRD studies

Powder XRD data were collected according to section 2.9.

7.2.7 Fe K-edge XANES studies

X-ray absorption spectra were recorded at X-ray Absorption Spectroscopy (XAS) beamline at Australian synchrotron. The current of the storage ring was operated in top-up mode with a beam current approximately 200 mA. The XAS beamline is a Wiggler beamline equipped with Si(111) monochromator, with and an energy resolution ($\Delta E/E$) of $1.5x10^{-4}$. The beam size was 0.25×0.25 mm (fully focused) at the sample. The sample chamber was filled with argon to protect the sample from being oxidized when exposed to X-ray. The incident beam intensity I0 was measured with an ionisation chamber using a N_2 fill gas at atmospheric pressure.

Data was acquired in fluorescence mode with a Passivated Implanted Planar Silicon (PIPS) detector. The near edge part of the Fe X-ray absorption spectra that has been used in this study was collected using a step of 0.25 eV and Dwell time of 1 s in appropriate energy range. The Fe K-edge XANES data were then calibrated according to the spectra of Fe foil respectively, and normalized to the edge jump. LC fitting was then carried out according to section 2.8.2 .

7.2.8 X-ray Tomography (CT) studies

The original low grade chalcopyrite ore was characterized by synchrotron X-ray Tomography. The detailed description of the experiment and analysis was in section 2.14.

7.3 Results and discussion

7.3.1 Solution studies

The variation of copper concentration is shown in Fig.7-1. The results show copper leaching efficiency was improved by a factor of 6.8 or 7.7 in galvanic assisted leaching with or without mixed mesophiles. In the absence of pyrite addition, the mesophiles did not show significant impact on copper recovery compared to the abiotic one. These results confirmed the high efficiency of chalcopyrite dissolution when pyrite coexist (Mehta et al., 1982). The copper leaching efficiency with *L. ferrooxidans* was marginally higher than that with mixed mesophiles, but lower than that of chemical leaching at 30 ^{o}C. The leaching at higher temperatures shows a better chalcopyrite dissolution efficiency, more than 2.5 g/L copper was released within 31 days in both chemical leaching and bioleaching at 48 ^{o}C, which accounted for more than 90% of the copper in the initially added chalcopyrite. The increase of temperature from 48 ^{o}C to 60 ^{o}C was further enhanced the leaching rate but in a relatively modest manner, where the leaching progressed to complete within 25 days. Increase temperature leads to faster leaching kinetics and galvanic leaching effect. Copper recovery greater than 90% in chalcopyrite leaching with extreme thermophiles has been reported previously (Konishi et al., 2001). From Fig. 7-1, it is clear that the addition of microorganism negatively affected the leaching efficiency. However, this phenomenon is less obvious at 60 ^{o}C. The copper concentration of bioleaching at 60 ^{o}C was very close to that of chemical leaching after day 16.

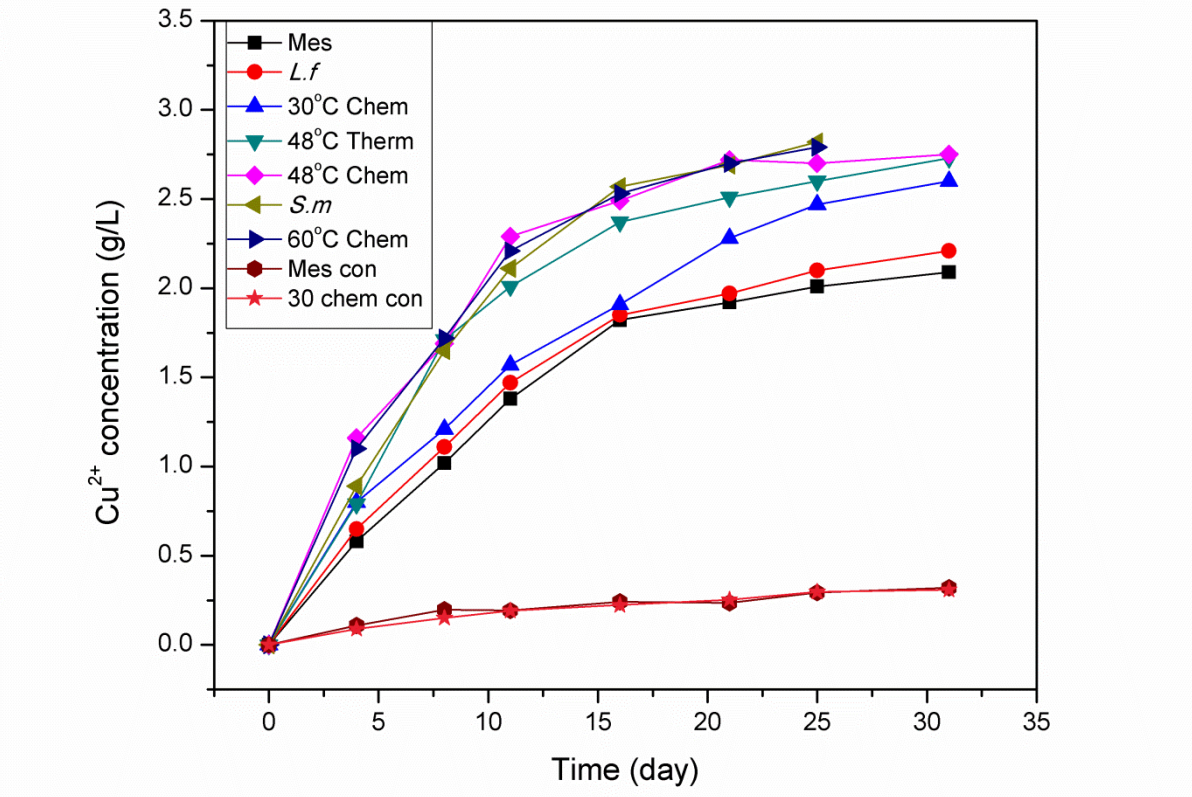

Fig.7-1 Copper ion concentration as a function of time during leaching of chalcopyrite concentrates with or without pyrite

Fig. 7-2 shows the cell concentrations of mixed mesophiles, *L. ferrooxidans* and *S. metallicus*. When no pyrite was added, the mixed mesophiles grew much slower and the final cell concentration was only $1.6x10^8$ cells/mL. In the same time, $6.5x10^8$ cells/mL of mixed mesophiles was found at day 31 when chalcopyrite was leached with pyrite. This result indicates the addition of pyrite provided an extra energy source and was favorable to bacteria growth.

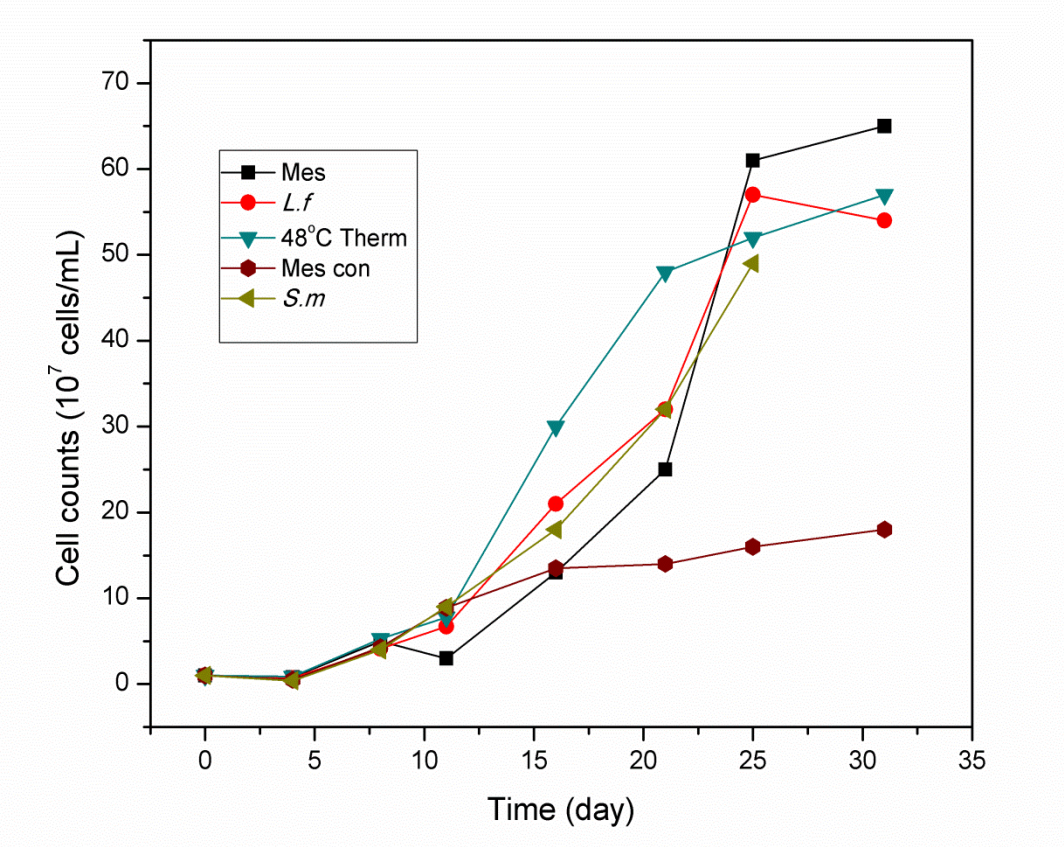

Fig. 7-2 Cell concentration as a function of time leached with or without pyrite.

Fig. 7-3A shows the variation of ferric concentration. A rapid decrease of ferric in all case was observed. Ferric ion could be consumed by the initial oxidizing attack to the minerals and a slight increase of that was found in later stages possibly because of the effect of microorganism or oxygen. Another reason for the decrease of ferric ion concentration is jarosite formation. Compared to the mixed mesophiles, *L. ferrooxidans* had a higher ferrous oxidation activity than mixed mesophiles in this study. At the same time, 0.21 g/L ferric was detected in the solution with *S. metallicus*, which occurred with more significant jarosite precipitation. Only increasing Fe^{3+} detected is in the case of pure chalcopyrite bioleaching. The Fe^{3+} decreased firstly like others and increased because of oxidation of Fe^{2+}. The reason for higher Fe^{3+} concentration in pure chalcopyrite leaching is likely linked to two reasons. Firstly, it was less consumed because of the poor leaching result. In addition, it was found in galvanic leaching the pH dropped much more rapidly. In this study pH was adjusted 1.8-2.0 periodically, which means more KOH was consumed more rapidly, which lead to more serious jarosite precipitation and lower Fe^{3+} concentration in galvanic bioleaching.

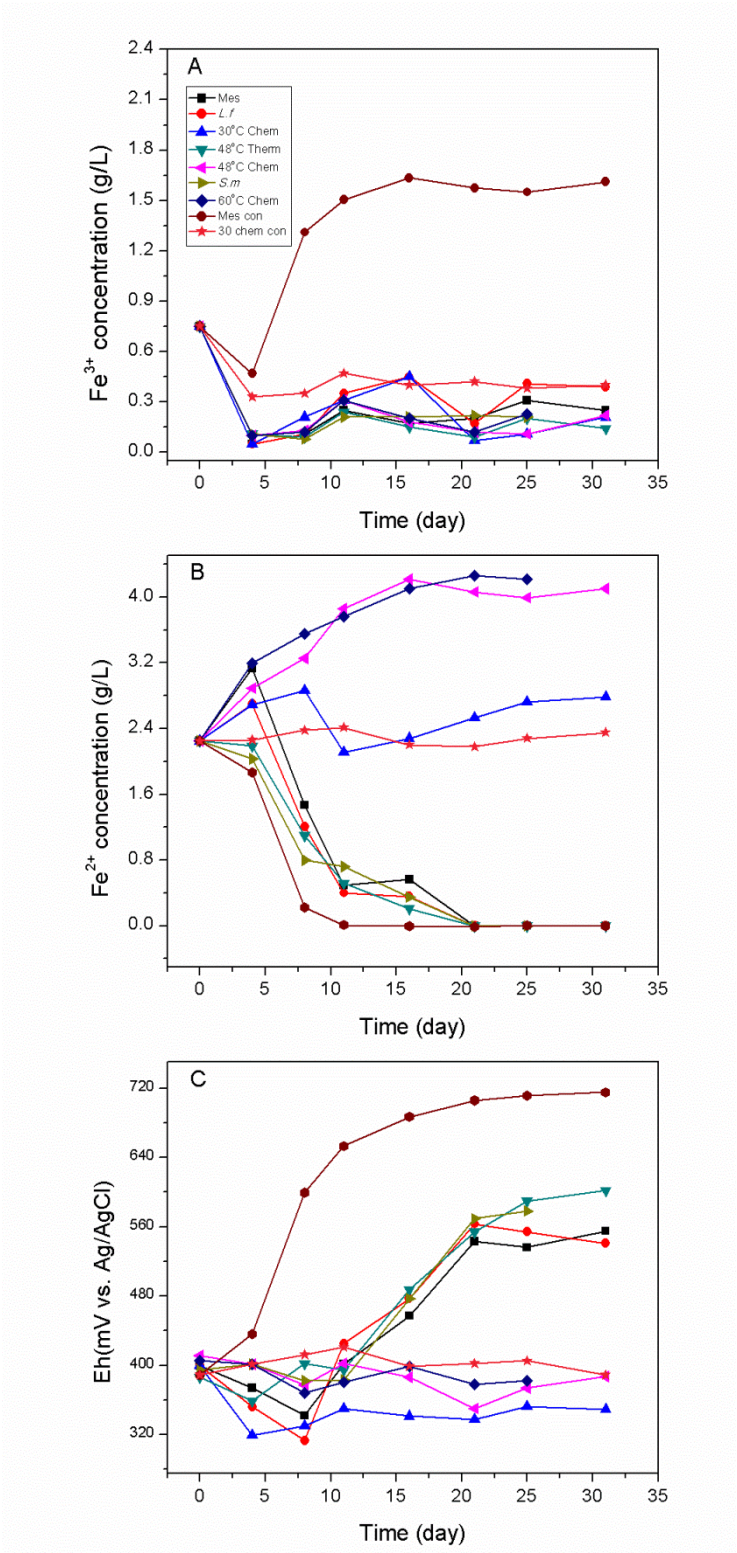

Fig. 7-3 A) ferrous ion, B) ferric ion concentration and C) Redox potential as a function of time during leaching of chalcopyrite concentrates with or without pyrite.

The ferrous concentration was displayed in Fig. 7-3B. In bioleaching groups, a fast decrease of ferrous concentration was observed in the experiment without pyrite addition,

where the ferrous ion dropped to 0 within 11 days. Compared to mixed mesophiles, *L. ferrooxidans* showed higher ferrous oxidation efficiency. In the former one, 0.57 g/L ferrous was detected at day 16, while 0.36 g/L was detected in the latter one, no ferrous ion could be detected after that. The ferrous ions in the abiotic control experiments showed a more modest change. At 30 ^{o}C the ferrous concentration fluctuated between 2 and 2.9 g/L, while a monotonous increase of ferrous ion concentration was observed in leaching at 48 ^{o}C and 60 ^{o}C, which may be a result of faster chalcopyrite and pyrite dissolution at elevated temperatures. The ferrous variation curves also indicate bacteria used in this study had good iron oxidation activity.

The redox potential (Eh) variation is shown in Fig. 7-3C. In the chemical leaching, the Eh value fluctuated between 320 and 420 mV, close to the optimal condition for chalcopyrite leaching (Koleini et al., 2010). The addition of bacteria in a system without pyrite caused a very rapid increase of solution Eh to over 700 mV. While in bioleaching experiments with pyrite, the Eh was significantly lower. In the first 16 days of leaching, the Eh values were maintained lower than 500 mV despite the temperature and microorganism type. However, a rapid increase of that was found after that, when the ferrous ion dropped to a low level.

At 30 ^{o}C, chemical galvanic leaching was found more effective. One of the major differences observed in the comparison between bacterial galvanic leaching and chemical galvanic leaching is that the former has much higher Eh because of bacteria activity (Reaction (7-1)).

$$Fe^{2+} + 2H^{+} + 0.5O_2 \rightarrow 2Fe^{3+} + H_2O \qquad (7\text{-}1)$$

Reaction (7-1) suggests the main role of bacteria in bacterial galvanic leaching is to reproduce Fe^{3+}. According to the indirect mechanism, chalcopyrite dissolution is generally considered to occur via the attack of Fe^{3+} and H^{+} through the formation of polysulfide (Sand et al, 2001). Fe^{3+} is the primary impetus of chalcopyrite dissolution, thus increasing Fe^{3+} concentration will be favourable to chalcopyrite leaching (Reaction(7-2)) (Sand et al, 2001; Klauber, 2008).

$$CuFeS_2 + 4Fe^{3+} \rightarrow Cu^{2+} + 5Fe^{2+} + 2S \qquad (7\text{-}2)$$

However, as described in the chapter 1, a number of studies show that there is an optimal potential range for chalcopyrite dissolution (Hiroyoshi et al., 2002; Sandström et al.,

2005). A high solution Eh has been shown to negatively affect the chalcopyrite leaching rate (Koleini et al., 2010). Third et al. (2000) showed that solution potential is far more important than cell concentration and activity in dictating leaching kinetics of chalcopyrite.

Similarly, a decrease of chalcopyrite leaching rate against the rapid raise of Eh in leaching with mesophiles was also observed in this study. Copper dissolution rate was fast in the cases of bioleaching in first 16 days, which was close to the case of chemical leaching, and the Eh values on day 16 were 450-470 mV (Ag/AgCl), which is close to the reported up-limit of the optimal Eh window for chalcopyrite leaching (Hiroyoshi et al., 2002; Sandström et al., 2005). The Eh values on day 20 were about 550 mV (Fig. 7-3 C), which exceeded the optimal chalcopyrite leaching window and the chalcopyrite slowed down (Fig. 7-1). This is not observed in the abiotic case. Based on the above discussion, it could be concluded that low Eh is the primary reason for the faster leaching of chalcopyrite in chemical galvanic leaching.

In leaching at 60 ^{o}C, the difference is not clear. This is likely link to fast leaching kinetics in both chemical leaching and bioleaching at higher temperature. The fast and complete oxidation of chalcopyrite in both cases (Fig. 7-1) made the impact of Eh not obvious.

The difference of Eh values was also distinct between the cases of non-galvanic bacterial leaching and galvanic bacterial leaching. The Eh of the former raised much faster (Fig. 7-3C). Koleini et al. (2011) indicated that during the dissolution of chalcopyrite, the overall chalcopyrite oxidation reaction at electrochemical anodic could be described as Reaction (7-3):

$$CuFeS_2 \rightarrow Cu^{2+} + Fe^{2+} + 2S + 4e^- \qquad (7\text{-}3)$$

and the cathodic half cell reaction as follows:

$$4Fe^{3+} + 4e^- \rightarrow 4Fe^{2+} \qquad (7\text{-}4)$$

In the absence of pyrite, both reactions occur at chalcopyrite surfaces. With the addition of pyrite, the cathodic half-cell reaction takes place on pyrite surface at a significantly faster rate (Koleini et al., 2011), which helps maintain the solution Eh at a low level. As low Eh is favourable to chalcopyrite leaching, it could be speculated that the favourable

influence of galvanic effect to chalcopyrite leaching is at least partially because of its function on Eh control.

In the studies of Mehta and Murr (1982 and 1983) and Khoshkhoo et al (2014), the authors found bacterial galvanic leaching is more effective than chemical one. At the same time, they found the Eh increased from about 340 mV to about 600 mV in bioleaching, and the Eh was low (below 410 mV) in chemical leaching (Mehta and Murr, 1982 and 1983; Khoshkhoo et al., 2014). This is very similar to the results of this study, in which the Eh ranged between 300-400 mV in chemical leaching and increased to 600 or 700 mV in bioleaching. So, the difference between this study and theirs is not caused by Eh changes.

It needs to be noticed that although redox potential is a critical factor, it is not the only one that influences chalcopyrite leaching. Chalcopyrite leaching is an overall oxidative process, where oxidant is an essential factor. Such as in the two step oxidation pathway by Hiroyoshi et al (2000), Fe^{3+} is still necessary in the final step for oxidizing chalcocite to Cu^{2+}.

In the studies of Mehta and Murr (1982, 1983) and Khoshkhoo et al. (2014), the system was initially iron-free. In their chemical leaching experiments, there was lack of oxidant and iron, which accounts for the slow leaching. On the contrary, the iron concentration was higher in their bioleaching studies.

In the present study, there was 0.75 g/L of Fe^{3+} and 2.25 g/L of Fe^{2+} initially added, which resulted an effective chemical leaching. In the terms of bioleaching the ferrous was rapidly oxidized to ferric and the Eh increased to 500 mV or above, which decreased the leaching rate. Moreover, contrary to the studies of Mehta and Murr (1982, 1983) and Khoshkhoo et al. (2014), the iron concentration in bioleaching is lower than that in chemical leaching because of rapid iron precipitation. However, it also needs to be pointed out that the precipitation of iron in bioleaching is not the primary reason for the slowing down of copper leaching in the present study. In bacteria galvanic leaching, the leaching rate significantly slowed down after day 16, while significant iron precipitation occurred in the very beginning.

7.3.2 XFM and μ-XANES studies

Fig. 7-4 shows the S, Fe and Cu spatial distribution of mixed chalcopyrite/pyrite sample chemically leached for 25 days. In the three-element co-localization map, red represents sulfur (Fig. 7-4a), green represents iron (Fig. 7-4b) and blue represents copper (Fig. 7-4c). The overlay map (Fig. 7-4d) shows μ-XRF mapping can distinguish between chalcopyrite and pyrite very well. The iron was more abundant on pyrite particles, which is accordance

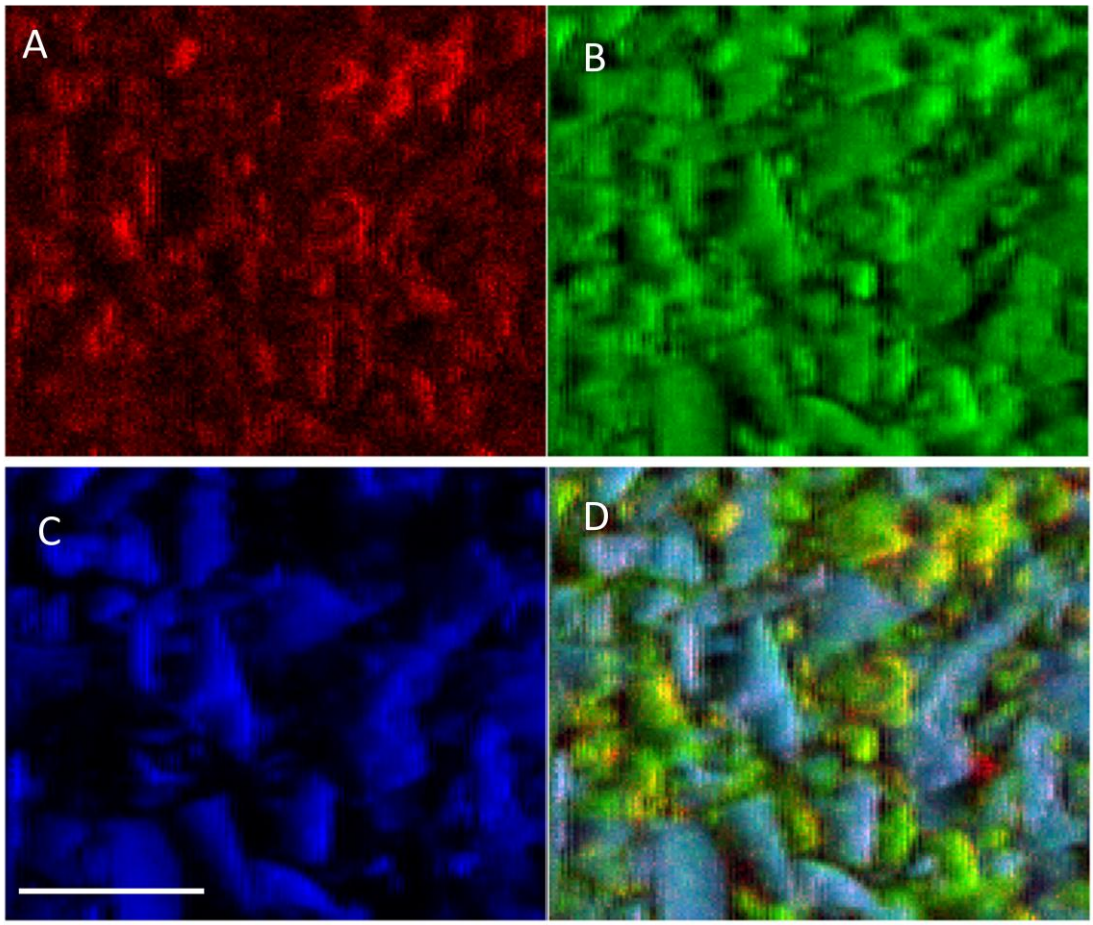

Fig. 7-4 μ-XRF images of cp/py coupon sample chemically leached for 25 days (Red: S, Green: Fe, Blue: Cu. Scale bar 100 μm)

with the high Fe proportion in bulk mineral. This is the same case for sulfur. The chalcopyrite particles were identified by the presence of Cu. It can be seen the right side of particles generally exhibit higher S intensity, which is a result of the self-absorption effect that is more significant for low Z elements. The detector was set on the right of the sample, the signal of sulfur from the left side of a particle can be absorbed by the particle itself.

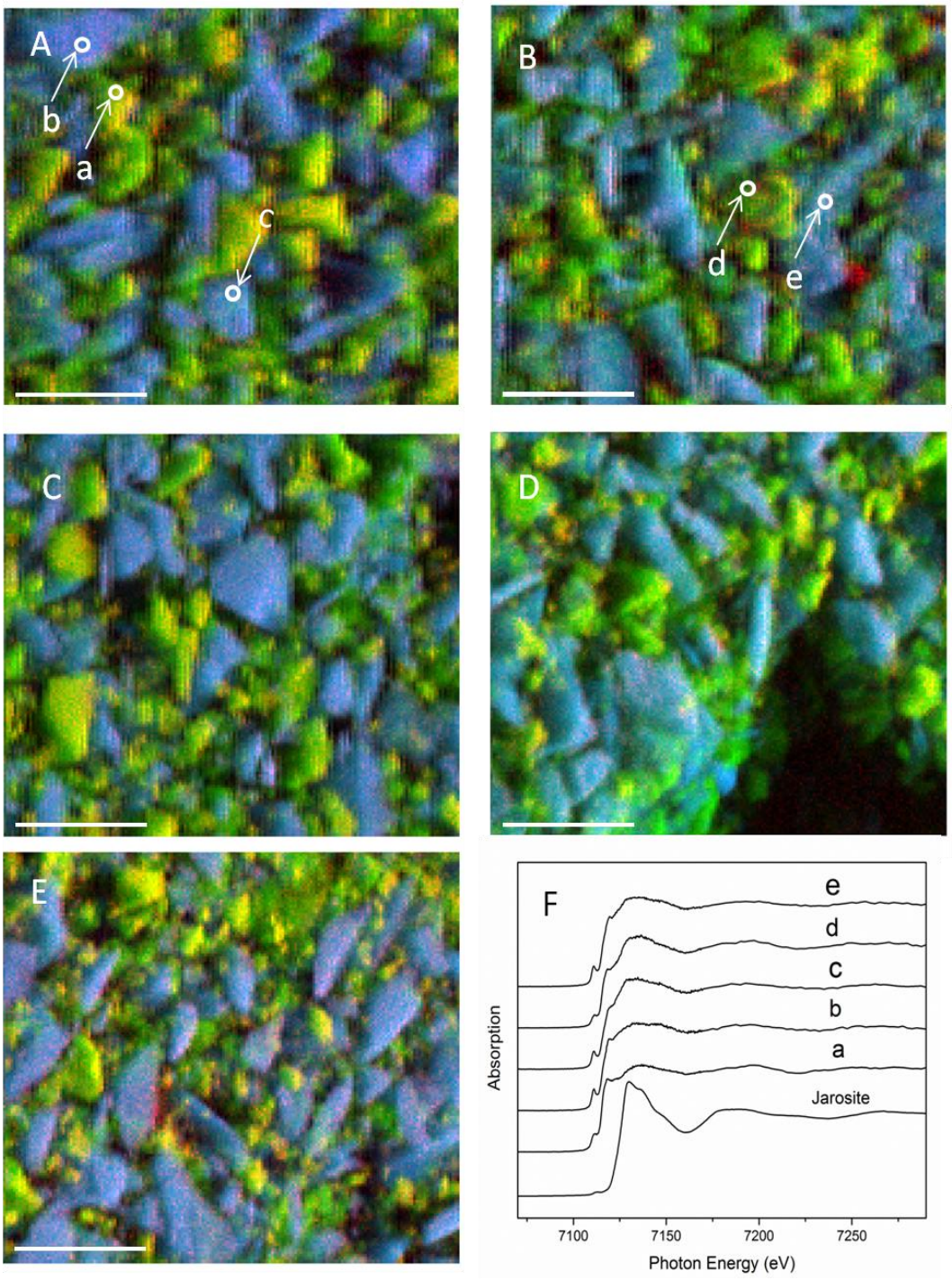

Fig. 7-5 Overlay Cu, Fe, S μ-XRF images and Fe K-edge μ-XANES of cp/py coupon samples leached for 25 days (A: *S. metallicus*, B: abiotic at 60 ^{o}C, C: mixed mesophiles, d: *L. ferrooxidans*, E: abiotic at 60 ^{o}C, F: Fe K-edge μ-XANES for points a-e. Scale bar 100 μm).

The overlaid Cu, Fe and S maps of samples leached 25 days are shown in Fig. 7-5 A-E. μ-XANES analyses were performed on selective spots on either chalcopyrite or pyrite. The spectra from 5 spots of samples leached for 25 days at 60 ^{o}C are displayed in Fig. 7-5F.

The red spots in μ-XRF maps suggest higher S/(Fe+Cu) ratio, which is most obvious in the cases of chemical leaching (Fig. 7-5B and Fig. 7-5E), indicating the accumulation of S in the oxidation of minerals as reported previously (Konishi et al., 1995). In the chalcopyrite region, it is clear that more sulfur formed in the chemical leaching at 30 ^{o}C than in the bioleaching with *L. ferrooxidans* (Fig. 7-5D and Fig. 7-5E). As *L. ferrooxidans* cannot remove elemental sulfur, high S/metal ratio in the chemical leaching is most likely to be the result of better chalcopyrite leaching at low Eh. In addition, compared to the sample leached with mesophilic mixtures (Fig. 7-5C), that leached with *L. ferrooxidans* show more bright spots in the chalcopyrite region (Fig. 7-5D), which may indicate sulfur layer formed on sample leached with mesophiles was at least partial removed. From the Fig. 7-5, it also could be concluded that the sulfur-rich layer was not homogenously deposited on the mineral surface (Parker et al., 2008).

The spectra of spots a and b, which were chosen from pyrite region and chalcopyrite region respectively, show almost unchanged feature of chalcopyrite and pyrite (England et al., 1999). In spectra a, the pre-edge feature at 7111.2 eV is assigned to a transition of electron of pyrite Fe from the Fe 1*s* states to states which are mainly Fe 3d_{eg} in character (with some Fe 4p and S 3*p* contribution) (Mosselmans et al., 1995). The spectra b shows typical characteristics of chalcopyrite, which shows a high pre-edge feature. The stronger pre-edge feature could be explained by the tetrahedral structure of chalcopyrite, which allows 1*s*-3*d* transition. This result confirmed the identification of chalcopyrite and pyrite based on the μ-XRF study. The spectra of spot d are assigned to a mixture of pyrite and jarosite, evidenced by the pyrite feature with a steep increase of absorption between 7119-7129 eV. Similarly, the spectra of spots c and e show additional features of jarosite besides that of chalcopyrite. The spectra of spots c-e show the presence of jarosite with either chalcopyrite or pyrite, which precipitates as Reaction (7-4):

$$3\,Fe^{3+} + 2\,SO_4^{2-} + 6H_2O + M^+ \rightarrow MFe_3(SO_4)_2(OH)_6 + 6\,H^+ \qquad (7\text{-}4)$$

where M represents K^+ or NH_4^+

The μ-XANES on other samples leached for 25 days show similar results (data not shown). A total number of 44 spots were tested and no other iron species were found. This result indicate other intermediate iron species are not likely to be detected by Fe K-edge XANES. Previously, it was found the iron intermediates in chalcopyrite dissolution

are not stable enough to be detected by Fe K-edge XANES (Yang et al., 2013), which is consistent with current study.

7.3.3 Raman studies

The Raman spectra of samples leached for 25 days are shown in Fig. 7-6. The peaks at 292 cm^{-1}, 319 cm^{-1} and 353 cm^{-1} could be assigned to chalcopyrite (Parker et al., 2008), while the peaks at 342 cm^{-1}, 378 cm^{-1} and 430 cm^{-1} could be assigned to pyrite (Xia et al., 2010). Elemental sulfur could be identified from the peaks at 152, 220, 473 cm^{-1} (Parker et al., 2008). Peaks at 137, 220, 429, 1006, 1098 cm^{-1} are assigned for jarosite (Xia et al., 2010).

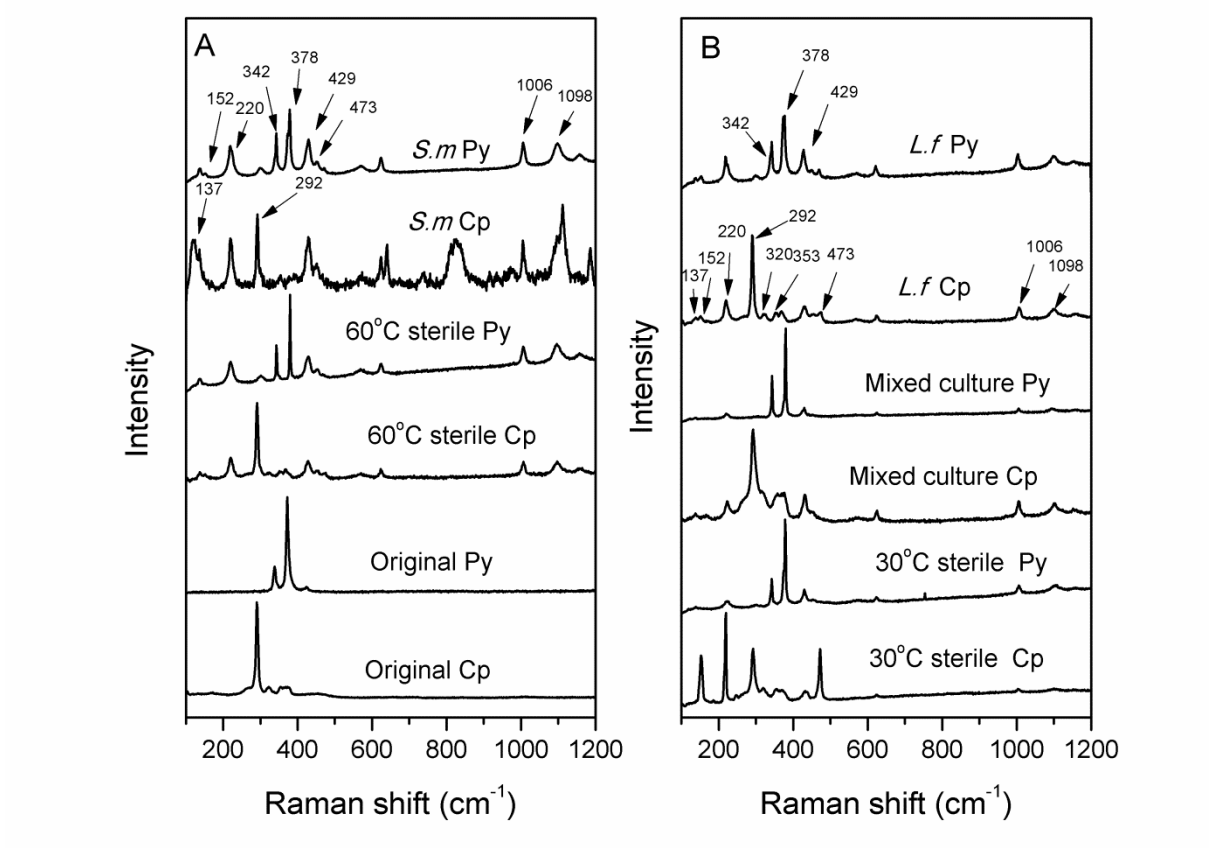

Fig. 7-6 Raman spectra of cp/py coupon samples leached for 25 days

After leaching for 25 days, jarosite and elemental sulfur could be found in most samples (Fig. 7-6). The elemental sulfur was identified on chalcopyrite in chemically leached samples as well as that bioleached by *L. ferrooxidans*. On pyrite surface, the elemental sulfur was found in samples leached by *L. ferrooxidans* and *S. metallicius*. According to the current theory, pyrite dissolves via a thiosulfate pathway, and no elemental sulfur forms directly (Sand et al., 2001). However, the formation of elemental sulfur in pyrite

oxidation has been found in previous studies (Konishi et al., 1995; Pisapia et al., 2007). Elemental sulfur formed on pyrite surfaces could arise from the decomposition of $S_2O_3^{2-}$ according to Reaction (7-5) (Chandra and Gerson, 2010).

$$S_2O_3^{2-} \rightarrow S^0 + SO_3^{2-} \quad (7\text{-}5)$$

As the Raman spectra only give the information of specific points, the lack of Raman evidence of elemental sulfur in some cases did not completely deny the possibility of the presence of it. However, the fact that the absence of evidence of sulfur in at least 4 random points indicates the elemental sulfur in those cases was less abundant.

The Raman results confirmed the finding in μ-XRF. Compared to the chemical leaching at 30 ^oC and bioleaching with *L. ferrooxidans*, no evidence of elemental sulfur has been found in samples leached by mesophiles. This result suggested elemental sulfur produced during the leaching was efficiently oxidised to sulfate by sulfur-oxidizing bacteria *(A. ferrooxidans* and *A. thiooxidans*) as shown in Reaction (7-6).

$$2S^0+3O_2+2H_2O \rightarrow 2SO_4^{2-} + 4H^+ \quad (7\text{-}6)$$

However, the solution studies show leaching with mesophilic mixed culture did not exhibit an better copper recovery over bioleaching with *L. ferrooxidans* or chemical leaching. This suggests that the formation of elemental sulfur did not hinder the galvanic effect.

In chemical leaching, it is noteworthy that in all cases the pyrite surface was almost unchanged except minor amount of jarosite precipitation after leaching for 25 days. This result is also consistent with that observed by Mehta and Murr (1983) using scanning electron microscopy observations and dispersive X-ray analysis which showed no major changes on pyrite surfaces when in contact with chalcopyrite. It result is expected, which indicate the surface reaction preferentially occurred on the chalcopyrite. This may indicate the surface reaction preferentially occurred on the chalcopyrite as is also suggested by the μ-XRF study. On the other hand, in bioleaching, a minor amount of elemental sulfur was identified from the Raman spectra of pyrite leached by *L. ferrooxidans* and *S. metallicius* (Fig. 7-6), which suggest more significant oxidation of pyrite happened in bioleaching.

7.3.4 XRD studies

XRD patterns of leached Cp/Py mixture are displayed in Fig. 7-7. The most distinct differences between the XRD patterns of bioleached and chemical leached samples are the intensity of peaks from jarosite and chalcopyrite. In the XRD pattern of bioleached samples, the major peaks came from jarosite, pyrite and chalcopyrite. However, in chemical leached samples, the intensity of peaks of jarosite was low and the peaks of chalcopyrite almost disappeared. The quantitative analysis of XRD results was summarised in table 7-1. The most abundant species in bioleaching is jarosite, which accounted for more than 60% of the residue. In chemical leaching, jarosite only account for 6.3% in sample leached at 30 ^{o}C and 26.7% in sample leached at 48 ^{o}C. XRD analysis also shows the difference in leaching selectivity between bacterially and chemically leached Py/Cp mixture. After 31 days' leaching, the Py/Cp ratio in bioleaching is 19 for leaching at 30 ^{o}C and 7.9 for that at 48 ^{o}C in the absence of bacteria. While in bacterial leaching, the final Py/Cp ratios are 2.3 and 2.5 for experiments at 30 ^{o}C and 48 ^{o}C, respectively. This result indicated that significant dissolution of pyrite occurred in bioleaching, though the chalcopyrite dissolution was still fast as a result of galvanic leaching (Fig. 7-1). The quantitative XRD analysis indicated there was also minor amount of elemental sulfur formed during leaching, which has been extensively reported previously (klauber, 2008; Li et al., 2013).

7.3.5 Fe K-edge XANES analysis

The Fe K-edge XANES spectra collected from standard compounds of pyrite (FeS), chalcopyrite ($CuFeS_2$), jarosite ($KFe_3(SO_4)_2(OH)_6$) are shown in Fig. 7-8A. In the spectra of chalcopyrite, the strong pre-edge peak at 7111.9 eV indicates the tetrahedral structure of chalcopyrite, which allows 1*s*-3*d* transition (Petiau et al., 1998). In the pyrite FeS_2, iron is sixfold coordinated to the sulphur and forms an octahedral structure. The 1*s*-3*d* transition is dipolar forbidden for pure atomic states. However, the Fe K-edge spectrum of pyrite reveals a small 'pre-edge' feature, which could be explained by the mix of Fe 4*p* states with the Fe 3*d* eg states (with also some S 3*p* contribution) (England et al., 1999). The peak at 7120.7 is assigned to transition from Fe 1*s* to Fe 4*sp* states (Mosselmans et al., 1995). The Fe in jarosite is also octahedral coordinated by six oxygen atoms (four from –OH groups and two from SO_4 groups) with slightly distortion, which is in consensus with the very low pre-edge peak (Kato and Miúra, 1975).

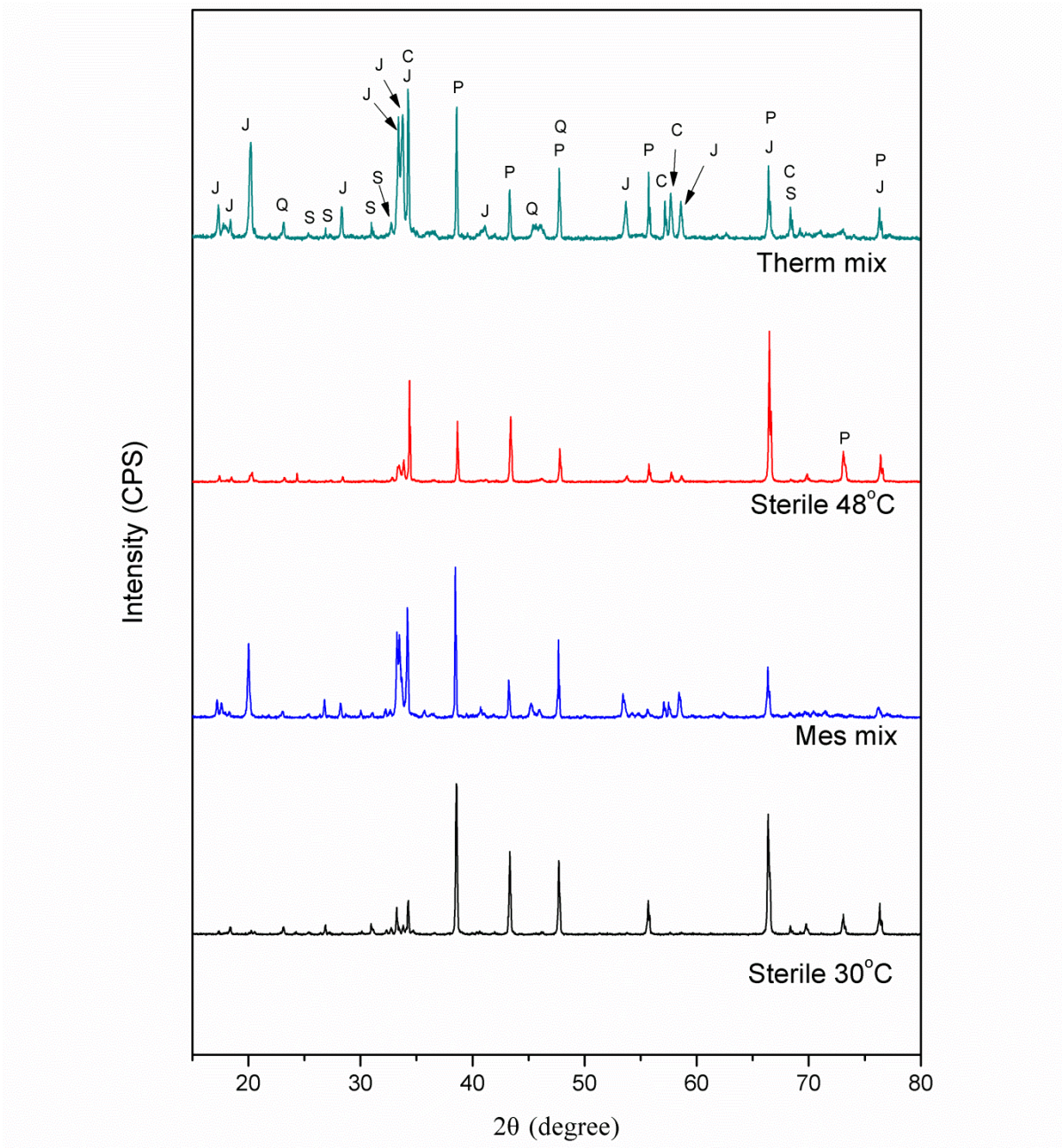

Fig. 7-7 XRD patterns of chalcopyrite chemically or bacterially leached with pyrite addition for 31 days (Mes mix: mesophilic mixture; Therm mix: thermophilic mixture)

Table 7-1 Summary of quantitative XRD analysis of selective leached residue collected after 31 days of leaching (wt%)

Mineral	Bacteria	T (^{o}C)	Cp	Py	Jar	Qz	S_8	Py/Cp
Py/Cp	Mes mix	30	10.1	23.5	59.0	0.8	6.6	2.3
Py/Cp	Sterile	30	4.0	80.8	6.5	4.0	4.7	20
Py/Cp	Therm	48	10.1	24.9	61.1	2.0	1.9	2.5
Py/Cp	Sterile	48	7.5	59.3	26.0	4.8	2.4	7.9

Cp: Chalcopyrite; Py: pyrite;Qz: Quartz; Jar: Jarosite; Mes mix = mesophilic mixed culture; Therm: Thermophiles.

The Fig. 7-8B shows the changes of Fe K-edge XANES spectra of chalcopyrite leaching residual. The spectra of chemically leached chalcopyrite for 14 days and 31 days show almost identical features, which were majorly composed of chalcopyrite with some jarosite. At the same time, spectra of bioleached chalcopyrite show an increasing peak at 7130 eV, which suggested jarosite accumulate with time. The spectra of Py/Cp mixture leached for 31 days are shown in Fig. 7-8C. The most distinct observation from Fig. 7-8B is that more jarosite presented in the bioleached samples, especially for that leached by moderate thermophiles.

To retrieve quantitative information from the spectra, a linear combination fitting was conducted to the spectra and the results were summarised in table 7-2. For pure chalcopyrite leaching, 49.1% jarosite formed after 14 days bioleaching, which was only 20.0% in chemical leaching. After leaching for 31 days the proportion of jarosite increased to 69.8% in bioleaching while that in chemical leaching stayed almost unchanged. Córdoba et al. (2008a) also reported that the addition of iron-oxidizing bacteria could profoundly promote the formation of jarosite.

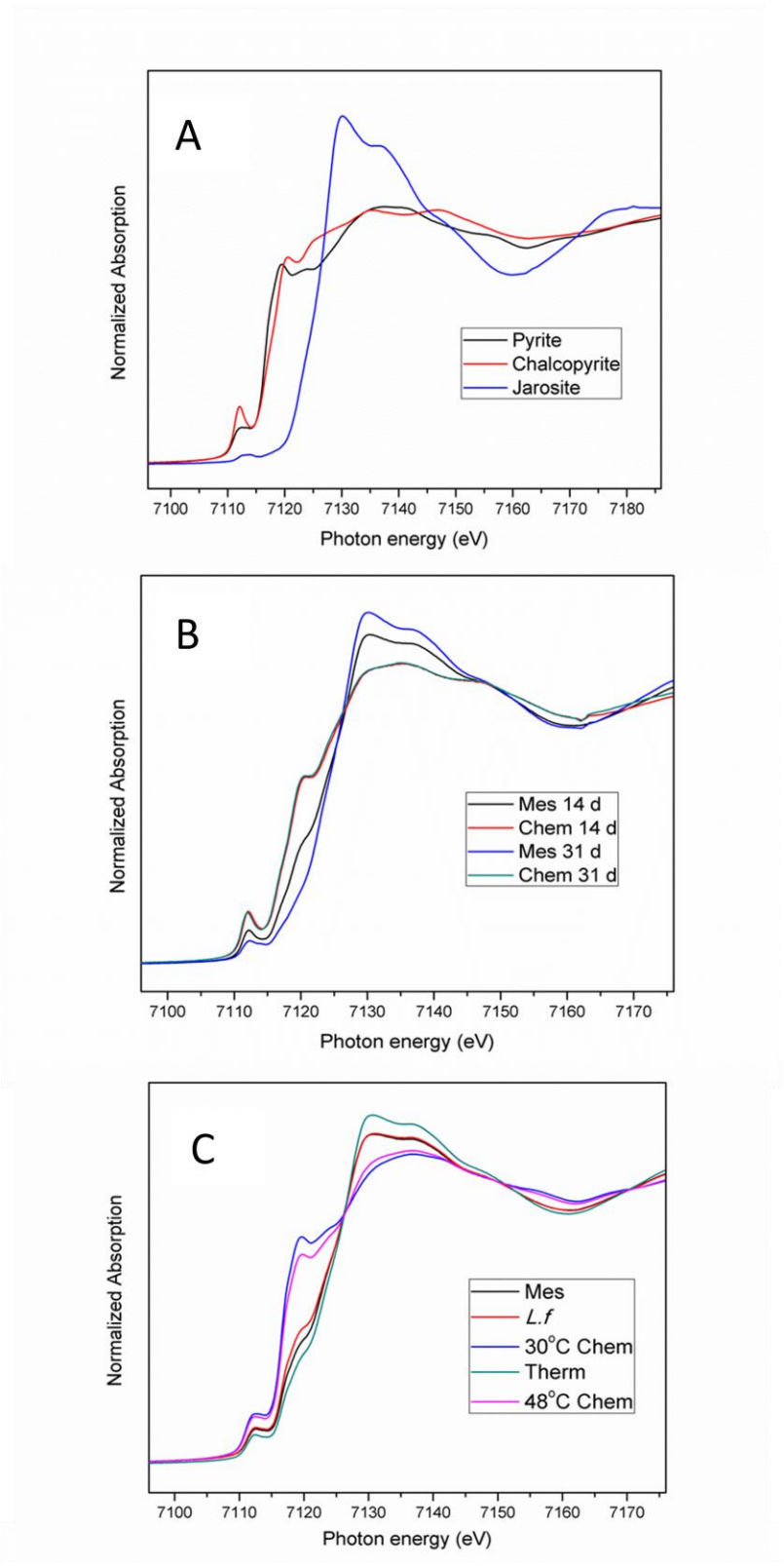

Fig. 7-8 Fe K-edge spectra of standards iron compounds (A), residue of pure chalcopyrite bacterially or chemically leached for 14 and 31 days (B) and residue of chalcopyrite and pyrite mixture at a ratio of 1:3 (C) (Mes: mesophilic mixture; Chem: chemical leaching; Therm: thermophilic mixture)

The above observations could be explained by the difference of the solution Eh in different experiments. In this study, the Eh of chalcopyrite chemical leaching was much lower than bioleaching and the solution Eh in the case with Cp/Py mixture was lower than that with pure chalcopyrite (Fig. 7-3C). The precipitation of iron, and the formation of jarostie, is directly related to the redox potential of the solution (Córdoba et al, 2008a&b). Bigham et al. (1996) reported that the stable potential of potassium jarosite is higher than 563 mV vs. Ag/AgCl, when pH is lower than 2. Therefore, jarosite precipitation will be more rapid when solution potential is closer to 563 mV (Córdoba et al, 2008b).

Table 7-2 The fitting results of Fe K-edge XANES analysis of leached residue collected after 14 and 31 days of leaching (wt%)

Time (days)	Mineral	Bacteria	Temp. (^{o}C)	Cp	Py	Jarosite	Py/Cp
14	Cp	Mes mix	30	50.9	-	49.1	-
14	Cp	Sterile	30	80.0	-	20.0	-
14	Py/Cp	Mes mix	30	9.5	27.6	62.9	2.9
14	Py/Cp	*L.f*	30	16.4	31.3	52.3	1.9
14	Py/Cp	Sterile	30	19.5	78.1	2.4	4.0
14	Py/Cp	Therm	48	14.1	18.1	67.7	1.3
14	Py/Cp	Sterile	48	15.0	74.2	10.8	4.9
31	Cp	Mes mix	30	30.2	-	69.8	-
31	Cp	Sterile	30	80.2	-	19.8	-
31	Py/Cp	Mes mix	30	16.0	41.2	42.8	2.6
31	Py/Cp	*L.f*	30	16.8	37.8	45.4	2.3
31	Py/Cp	Sterile	30	8.1	90.5	1.4	11
31	Py/Cp	Therm	48	19.0	19.0	62.0	1.0
31	Py/Cp	Sterile	48	11.3	76.9	11.9	6.8

Cp: Chalcopyrite; Py: pyrite; Mes mix: mesophilic mixed culture; Therm: Thermophiles

In the chemical leaching of Py/Cp mixed ore, it can be found that the weight ratio of Py/Cp increased with leaching time. The final Py/Cp ratio was 8.9 at 30 ^{o}C and 6.8 at 48 ^{o}C. This result suggests the preferential leaching of pyrite as a result of galvanic leaching. On the contrary, in the case of bioleaching Py/Cp ratio was low than the original mixture,

indicating pyrite was preferentially oxidized in the presence of bacteria. This result is in consensus with the Raman and XRD analysis and the previous reports (Petersen and Dixon, 2006). A high solution E_h has been shown to adversely affect the chalcopyrite leaching rate has been extensively reported (Koleini et al., 2010). While, the dissolution rate of pyrite is significant at redox potential above 500 mV (Tshilombo, 2004). In a study of heap bioleaching of copper-gold using Geocoat^{TM} technology, Petersen and Dixon (2006) also suggested that significant pyrite dissolution occurred during bioleaching at 30 ℃, which was attributed to the high solution redox potential.

Therefore, the low chalcopyrite leaching selectivity in biotic leaching compared to abiotic leaching is likely linked to the high solution E_h in the former whereby pyrite leaching kinetic is enhanced. When chalcopyrite was leached abiotically, the solution E_h maintained at <430 mV, which is the optimal condition for chalcopyrite leaching and the leaching of pyrite is slow. The dissolution of pyrite at high Eh is also possibly linked to the inferior copper leaching efficiency in bacterial galvanic leaching. The study of Dixon et al. (2008) showed the pyrite-to-chalcopyrite ratio is very important to galvanic leaching. In that study, the efficiency of galvanic leaching was significantly enhanced by increasing the py/cp mass ratio from 0.8 to 2.7.

7.3.6 Column leaching

The solution parameters of column leaching of low grade ore were shown in Fig. 7-9. When chalcopyrite was not leached with pyrite, the copper leaching kinetics was low. At 30 ^{o}C, the copper concentration slowly increased to 0.5 g/L in 110 days and the leaching ceased after that. Surprisingly, the leaching at 48 ^{o}C did not show a better kinetics compared to that at 30 ^{o}C. In the case of non-galvanic leaching at 48 ^{o}C, the copper concentration was 0.46 g/L after 172 days, compared to 0.42 in leaching at 30 ^{o}C. This result is not consistent with the results from the shaking-flask studies with chalcopyrite concentrate in chapter 3. The ineffective leaching by thermophiles in this study may be caused by the temperature control. Although the temperature inside the column was control approximately 48 ^{o}C throughout the experiment, the temperature in the reservoir was near room temperature (25 ^{o}C) though it had been wrapped with insulating layers. This caused the thermophiles were not always under their optimal temperature and were not active as in shaking-flask leaching.

Compared to the non-galvanic leaching, the leaching with pyrite addition was much more rapid. At 30 ^{o}C, a rapid increase of copper concentration was detected between day 40 and 120, which resulted a final copper concentration of 1.2 g/L. The galvanic assisted leaching at 48 ^{o}C generally show same features as the 30 ^{o}C leaching with a higher leaching kinetics, whose final copper concentration was about 1.5 g/L, which equals 62.5% of copper extraction

The iron concentration is more complicated probably because of jarosite precipitation. Fig. 7-9B shows the concentration of ferric ion. Compared to copper, the concentration of iron was much lower. For instance, the iron concentration in the case of galvanic leaching at 48 ^{o}C was 0.6 g/L and that of copper was 1.5 g/L, which probably because of iron precipitation. The ore used in this study contained basic gangue, which caused a relative higher pH (up to 2.5) in the process and further facilitated the iron precipitation. On the other hand, there were much more ferric ions in the solution of galvanic leaching, which may be a result of better chalcopyrite leaching or pyrite dissolution at high solution redox potential. The concentration of ferrous ions was low and cannot be detected accurately, which is supported by the Eh variation. From Fig. 7-9C, it is clear that the Eh was higher than 550 mV in most of the time and the highest Eh was over 600 mV for each column, which indicated the ferric concentration was 2-5 orders higher than that of ferrous ions (Hiroyoshi et al., 2001). The promotion of chalcopyrite leaching by pyrite is mostly explained as galvanic effects. In this study, the Eh values were higher than the proposed optimal Eh range for chalcopyrite leaching in most of the times and they are similar in different columns, which indicate the pyrite promoted the chalcopyrite dissolution mostly by the galvanic effect. The high Eh values observed in all the cases could be explained by the slow kinetics of column leaching, where the ferrous generated from mineral dissolution is slow and could be effectively oxidized to ferric by bacteria.

The bacteria growth in the first 40 days was very slow, which is in accordance with the copper dissolution rate. The log phase of bacteria in columns loaded with pyrite and low grade chalcopyrite ores came first, which may result from the ferrous ions provided by the pyrite dissolution. The cell concentrations stabilized at $2X10^{8}$ cells/mL after about 90 days' leaching, which is also in accordance with the change of Eh. As Eh values mainly reflect the Fe^{3+}/Fe^{2+} levels, the results suggest the activity of bacteria significantly affected the iron oxidation and the solution redox potentials.

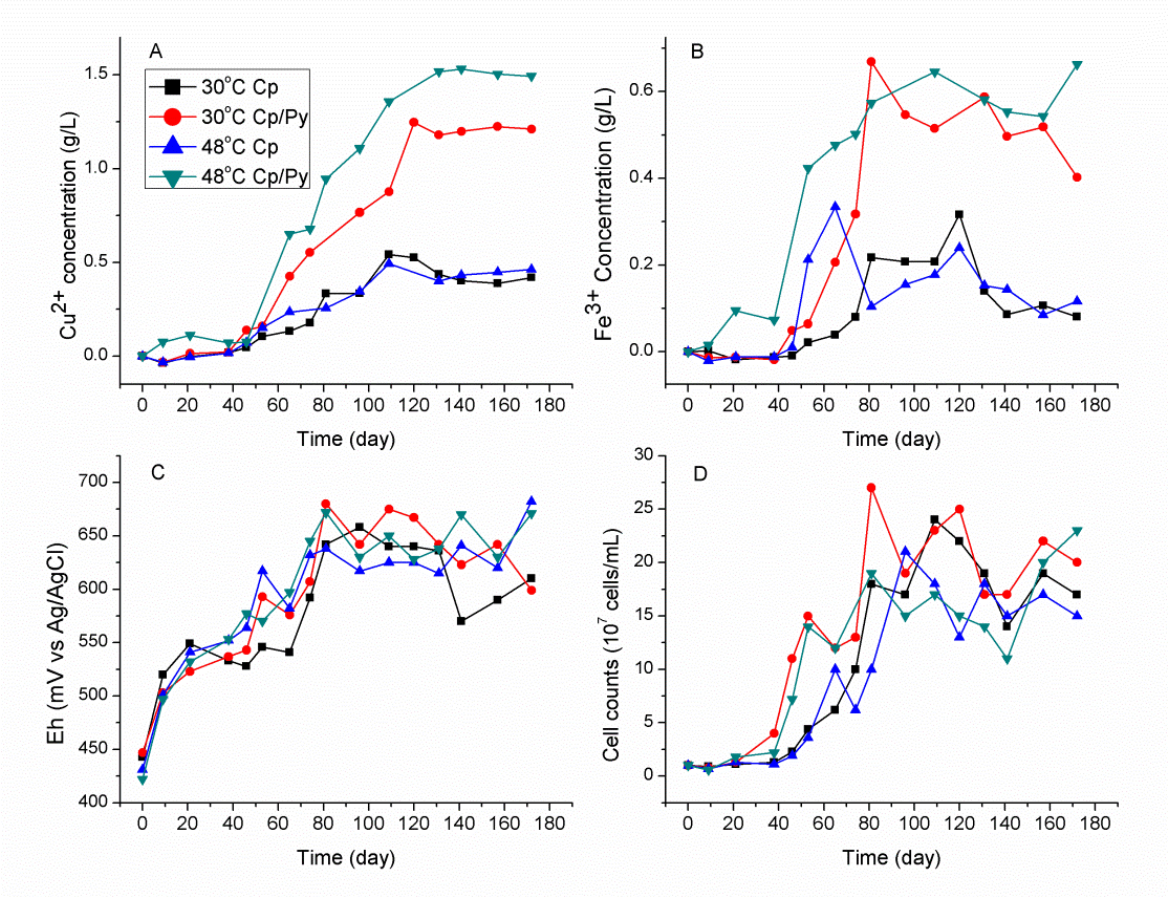

Fig. 7-9 solution studies of column leaching with and without pyrite (A, Copper concentration; B, Ferric ion concentration; C, Redox potential; D, Cell concentration)

Another point needs to be noted is the chalcopyrite dissolution ceased in spite of the initial conditions in the late stages, with highest copper recovery of 62.5%. This could be caused by the formation of passivation layers. In addition, for column leaching, the particle size and chalcopyrite grain size are also factors need to be taken into consideration. A CT reconstruction of a section of the low grade ore particle is shown in Fig. 7-10. The CT analysis shows some of the chalcopyrite grains are less than 0.5 um in diameter and completely embed in the gangue, which is likely to be orthoclase. The CT reconstruction also indicates the porosity of the particle is very low, which would result a poor permeability of the mineral. The CT results proved that the incomplete leaching of the low grade ores is at least partially caused by the incomplete liberation of chalcopyrite grain especially in galvanic leaching at 48 ^{o}C.

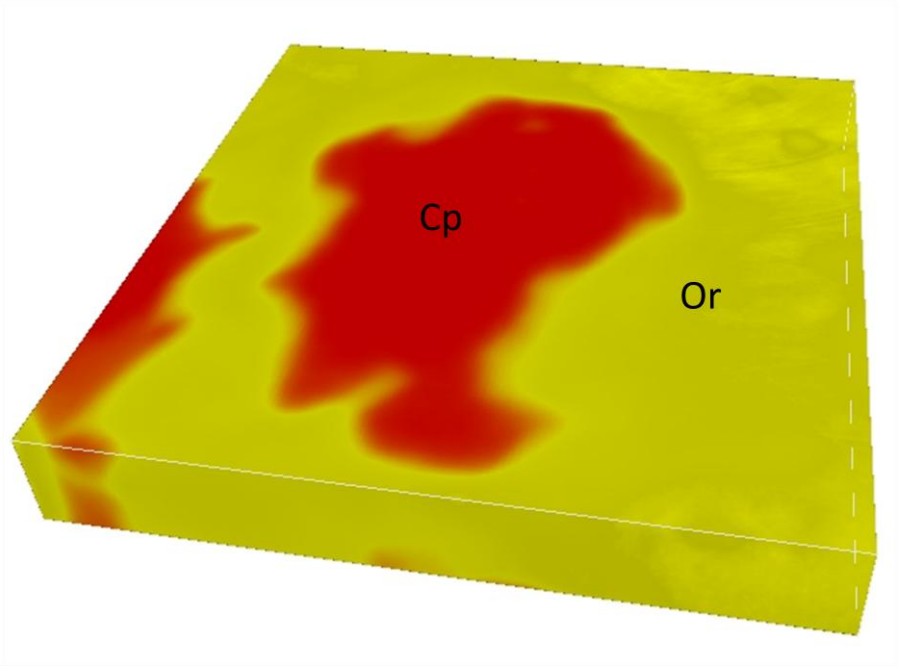

Fig. 7-10 CT reconstruction of low grade chalcopyrite from Rio Tinto (Cp: chalcopyrite; Or: orthoclase. The approximate dimension for the displayed section is 0.455x0.455x0.065 mm^3)

In column and heap leaching, particle size is a very important parameter. The results of Ahonen and Tuovinen (1995) show that the leaching rates for all metals increased with a smaller particle size fraction, which is attributed to a geometric increase in the available surface area. They found copper and nickel leaching rates approximately doubled when the particle diameter was decreased from 5-10 mm to 1.68-5 mm. The model of Neuburg et al. (1991) also indicate the smaller particles present a significantly higher copper leaching rate in comparison with the larger particle sizes in the early stages of the process. However, once the exposed minerals have been mostly leached out, the process becomes practically controlled by intraparticle diffusion, and the rate of copper recovery decreases to very low values, which could be the case of present study. To further increase copper yield, it is necessary to further crush the low grade ore. At the same time, as the utilization of small particle sizes may course plugging of the ore bed (Neuburg et al., 1991), agglomeration is also necessary to be performed prior to the leaching experiment.

7.4 Conclusions

Based on the studies made in this paper, following conclusions could be drawn. The addition of pyrite significantly enhanced the chalcopyrite leaching rate as a result of galvanic effect. Raman and μ-XRF indicate a sulphur-rich layer developed

inhomogenously on mineral particles after leaching. The XRD and iron K-edge XANES and Raman studies indicate the presence of microorganism decreased the chalcopyrite leaching efficiency and selectivity in spite of the temperature and bacteria in use, likely linked to the increased solution potential with the biooxidation ability of the bacteria. The XRD and iron K-edge XANES analysis also indicate significant jarosite precipitation in bacterial leaching, which is also the result of increased solution potential. The galvanic effect was also verified in column leaching with low grade chalcopyrite ore, which increased the yield of copper by a factor of about 3 at bioleaching at either 30 ^{o}C or 48 ^{o}C. More than 60% copper was leached out in 172 days in galvanic assisted column leaching with moderate thermophiles, though the chalcopyrite grains were not completely liberated.

Chapter 8 The effect of silver ions on chalcopyrite bioleaching by moderate thermophiles

8.1 Introduction

Silver ions have been proven to have positive impact on the bioleaching of chalcopyrite with mesophiles, however, there are only few reports on the effect of silver ions to thermophiles (Ballester et al., 2007).This chapter investigated the effect of silver ions on the leaching behaviours of a moderate thermophilic mixture enriched from Acid mine drainage (AMD) from several chalcopyrite mines in China, which has shown high leaching efficiency in previous studies (Zhou et al., 2009; Zeng et al., 2010). The chalcopyrite oxidation mechanisms in the presence of silver ions have also been investigated by electrochemical methods.

8.2 Experimental

8.2.1 Leaching experiment

For bioleaching, the thermophiles which had been adapted to silver ions were inoculated into the 250 ml flasks which containing 150 ml 9K medium and 1.5 g of chalcopyrite. The initial bacteria concentration was adjust to 10^7 cell/mL and the initial pH was adjusted to 1.8. 0, 2, 5, 10 mg silver ions per gram chalcopyrite ore was added into different flasks before the experiment in the form of $AgNO_3$. The flask was agitated at 130 rpm and kept at 48 ^oC. Chemical leaching was also conducted as comparison to the bioleaching experiment.

8.2.2 Electrochemical studies

The chalcopyrite electrode was prepared according to the description in section 2.3.4 and the electrochemical studies were carried out according to the description in section 2.6.

8.2.3 Raman studies

The Raman data were recorded between 100 and 1200 cm^{-1} for the bioleached chalcopyrite and between100 and 800 cm^{-1} for electrochemically oxidized electrodes.

8.2.4 XRD studies

Powder XRD patterns of bioleached chalcopyrite were collected according to section 2.9.

8.3 Results and discussion

8.3.1 The effect of silver ions in chalcopyrite leaching

8.3.1.1 Solution studies

The changes of copper concentration during bacterial and chemical leaching are shown in Fig. 8-1A and Fig. 8-1B. The results of chemical leaching indicate the chalcopyrite leaching was ineffective in sterile controls. This result suggests that the addition of silver ions could improve the copper leaching rate, but this requires sufficient amount of oxidant such as Fe^{3+}.

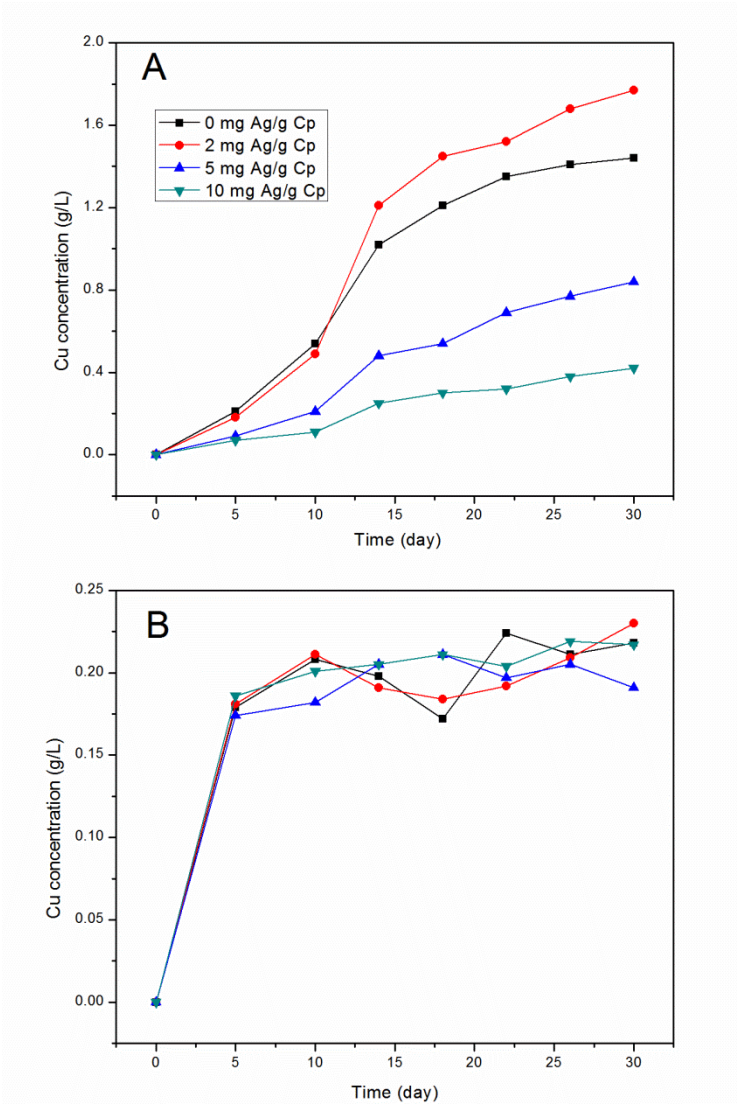

Fig. 8-1 Copper dissolution curves in chalcopyrite bacterial (A) or chemical (B) leaching at 48 ^{o}C in the presence of different amount of silver ions.

Compared to the sterile control, the copper concentration was significantly higher in bioleaching and the impact of silver ions is clear. The highest leaching rate was obtained at 2 mg silver ions per gram chalcopyrite addition (referred as mg/g in the following text). 1.8 g/L copper was leached out within 31 days in that case. The second rapid chalcopyrite dissolution was obtained when bioleaching was conducted without silver ion, where 1.3 g/L copper was released. The addition of high concentration of silver ions adversely impacted the chalcopyrite dissolution. About 0.75 g/L copper was dissolved into the solution with 5 mg/g silver ions, while only 0.33 g/L copper was leached out with 10 mg/g silver ions.

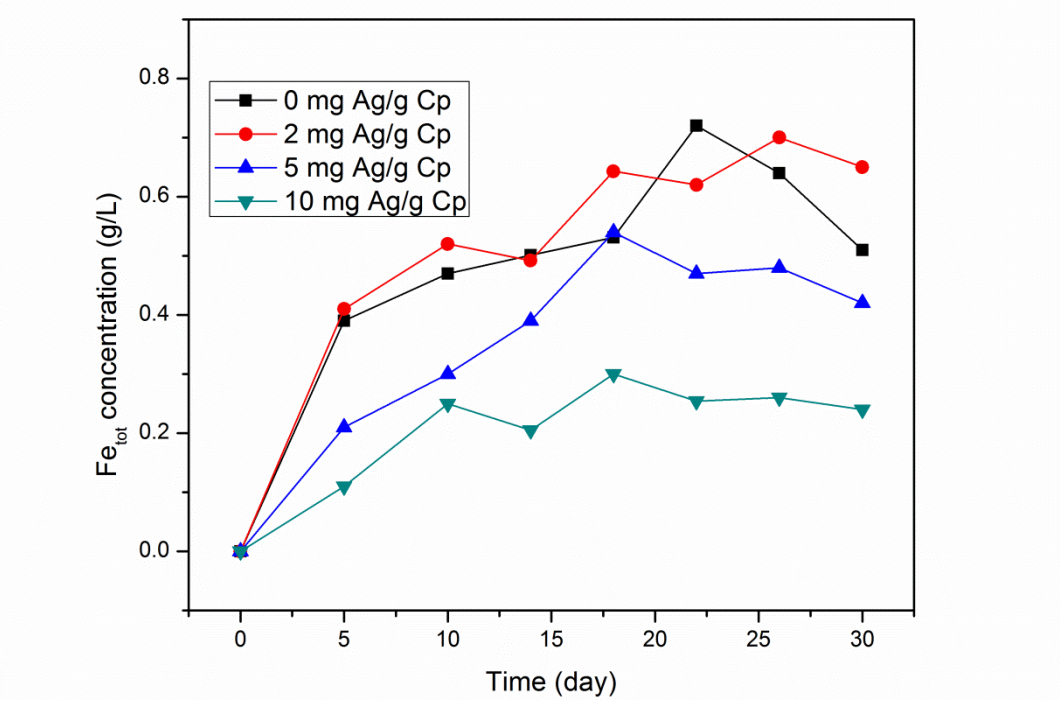

Fig. 8-2 Total iron concentration changes in chalcopyrite bioleaching at 48 ^{o}C in the presence of different amount of silver ions

The changes of total Fe concentration in bioleaching are shown in Fig. 8-2. Similar to the changes of copper concentration, significant lower Fe concentration was found when 5 or 10 mg/g silver ions were added in the solution, which is a result of inefficient chalcopyrite leaching. The total iron concentration increased more rapidly than copper in first the 5 days as a result of the preferential removal of Fe atoms in chalcopyrite. However, the iron concentration was much lower than that of chalcopyrite after 15 days of leaching, which is caused by the iron precipitation.

The changes of Eh and pH are shown in Fig. 8-3 and Fig. 8-4, respectively. In all cases, the Eh increased rapidly (Fig. 8-3) in the initial stages of leaching as observed in the results of previous chapters as a result of bacterial oxidation. In general, the solution Eh value decreased with increased amount of silver ions. These results may be related to the toxic effect of the silver ions to bacteria. The pH curves increased in the initial stages of leaching as the Reaction (8-1) and decreases after day 10 when elemental sulfur was oxidized in to sulfuric acid according to Reaction (8-2). It is noteworthy that a significant increase of pH was observed in the experiment when 10 mg/g silver ions was added, the reason of which is still unclear (no pH change was observed in chemical leaching with the same amount of silver ion addition). It is still not clear what caused the significant pH increase in the case of high silver concentration. A possible explanation is that the S bio-oxidation was severely inhibited by the silver ions, and no H^+ could be generated into the leaching system. The increase of pH with 10 mg/g silver ion is consistent with the decrease of Eh, which is linked to rapid ferric ion precipitation at higher pH.

$$CuFeS_2 + 4H^+ + 0.5O_2 \longrightarrow Cu^{2+} + 2S + Fe^{2+} + H_2O \qquad (8\text{-}1)$$

$$2S + 3O_2 + 2H_2O \xrightarrow{\text{bacteria}} 2SO_4^{2-} + 4H^+ \qquad (8\text{-}2)$$

The cell concentration was displayed in Fig. 8-5. The cell concentration curves indicate this thermophilic mixture could tolerant up 5 mg/g silver ion without its growth being significantly inhibited. However, as shown in Fig. 8-1A, its copper leaching efficiency at this silver concentration was considerably impaired. It is suspected that the iron oxidation ability of the thermophilic mixture was inhibited.

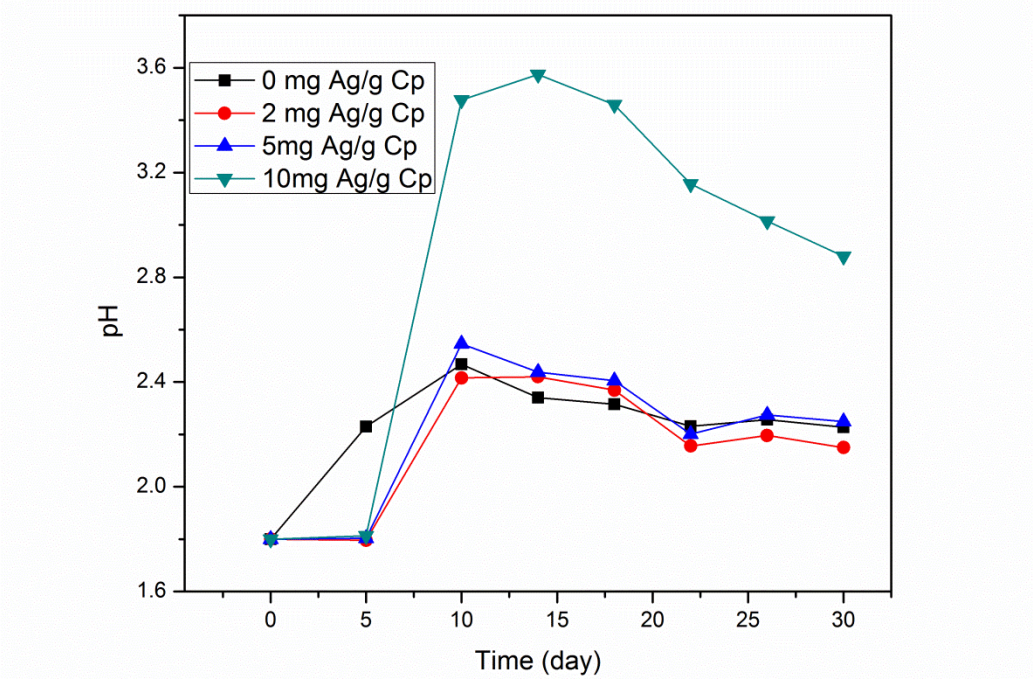

Fig. 8-3 pH changes in chalcopyrite bioleaching at 48 ^{o}C in the presence of different amount of silver ions

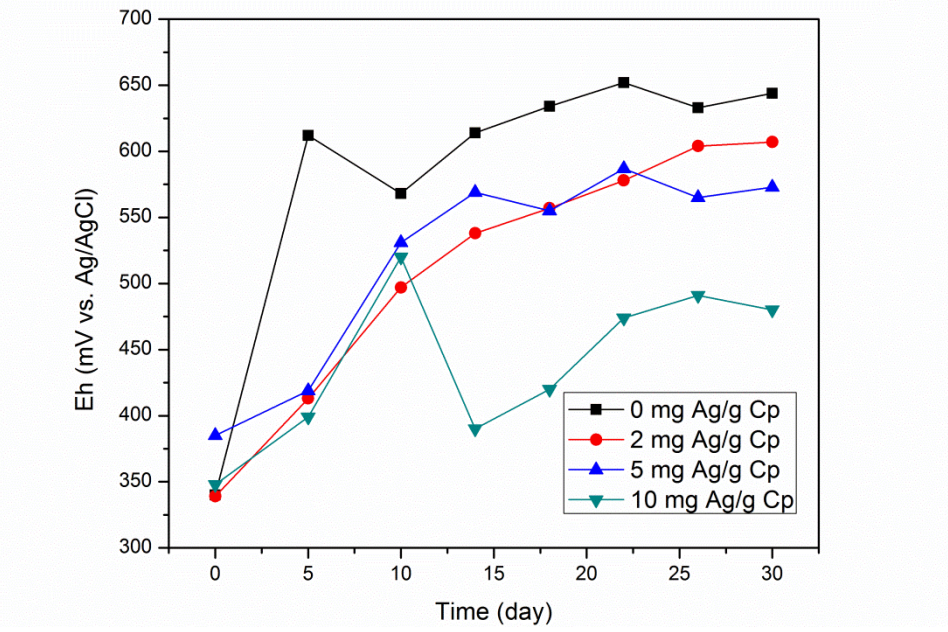

Fig. 8-4 Eh changes in chalcopyrite bioleaching at 48 ^{o}C in the presence of different amount of silver ions

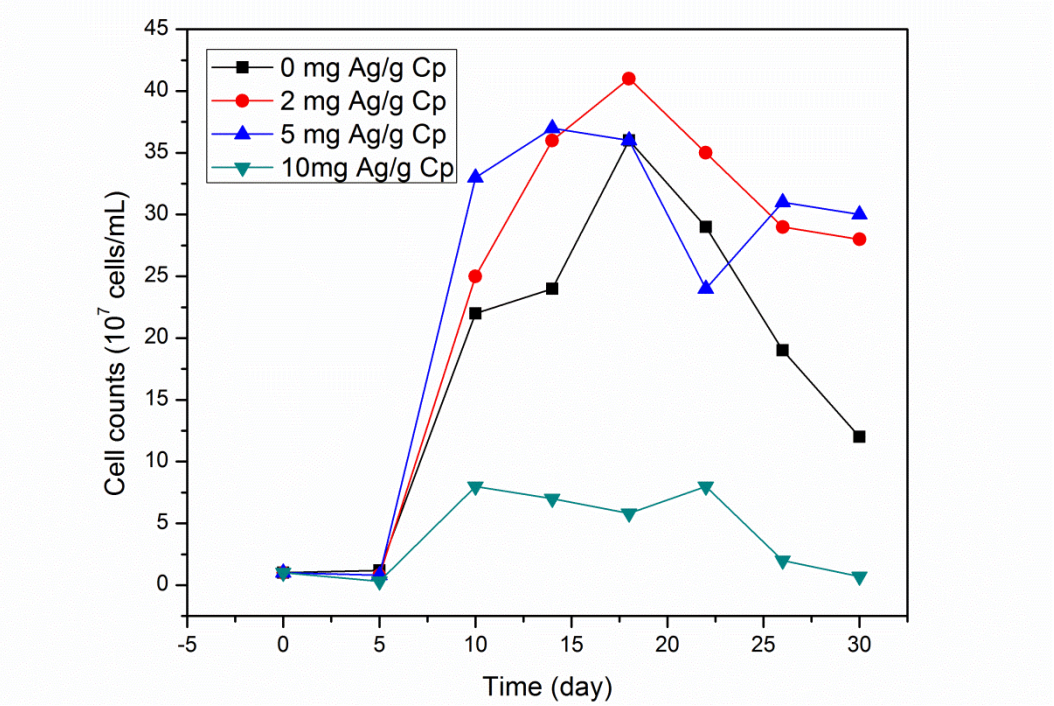

Fig. 8-5 Cell concentration changes in chalcopyrite bioleaching at 48 ^{o}C in the presence of different amount of silver ions

There are a numbers of case studies for silver-catalysed bioleaching with mesophiles, however, only few papers discussed the effect of silver on bioleaching with moderate or extreme thermophiles (Blázquez et al., 2007; Muñoz et al., 2007a; Muñoz et al., 2007b). Blázquez et al. (2007) indicated that non-adapted *Sulfolobus* culture only extracted less than 35% of copper from chalcopyrite ores, while the adapted culture extracted less than 60% of the copper. At the same time, the copper yield without silver ions increased to 90% during the same period of time. The silver inhibited the oxidation of ferrous ion to ferric and also the oxidation of elemental sulfur to sulfate. Therefore, the main problems associated to the effectiveness of catalysis in bioleaching are the silver availability and silver toxicity (Blázquez et al., 2007).

Compared to the extreme thermophiles, moderate thermophiles show a better silver tolerance as shown in the results of this study. Gomez et al. (1999) studied the effect of silver on the bioleaching of a chalcopyrite concentrate with mixed cultures of moderate thermophiles isolated from a drainage water of Rio Tinto mines and reached similar results. They adapted the culture to different concentrations of silver (0.1–0.5 g of silver per kg of concentrate). The results showed the important role of silver in the chalcopyrite leaching process carried out at 45 ^{o}C. Copper yields increased around 3-fold over the

control experiment without silver. At 50 ^{o}C, the amount of copper extracted using the catalyst was double than that obtained without it despite the effect of silver was masked by strong jarosite precipitation. The iron precipitation increased with the amount of silver used which may be avoid by using more diluted media. Based on the results of this study and the previous reports, the use of moderate thermophiles in silver-catalysed leaching is potentially promising, since chalcopyrite is better attacked at high temperatures and these bacteria are more resistant to silver than thermophiles.

8.3.1.2 XRD analysis

The mineralogy of the leaching residue was characterized by XRD and the results are displayed in Fig. 8-6. In bioleaching without silver or with 2 mg/g silver, chalcopyrite was the main component of the residue accompanied with jarosite and possibly a minor amount of elemental sulfur. In bioleaching with 5 mg/g silver, there was possibly a small amount of hematite formed in the residue, as a result of higher pH (Fig. 8-4). The evidence of the formation of hematite is clearer in bioleaching with 10 mg/g silver ions, which is also consistent with the high pH value.

There is no strong evidence for the presence of any silver species in the residue even in the case with 10 mg/g silver. The XRD patterns indicate there is no detectable amount of Ag_2S in the residue. There was possibly some stromeyerite in some samples, however, as the peaks overlap with other species, the presence of stromeyerite could not be fully confirmed by XRD.

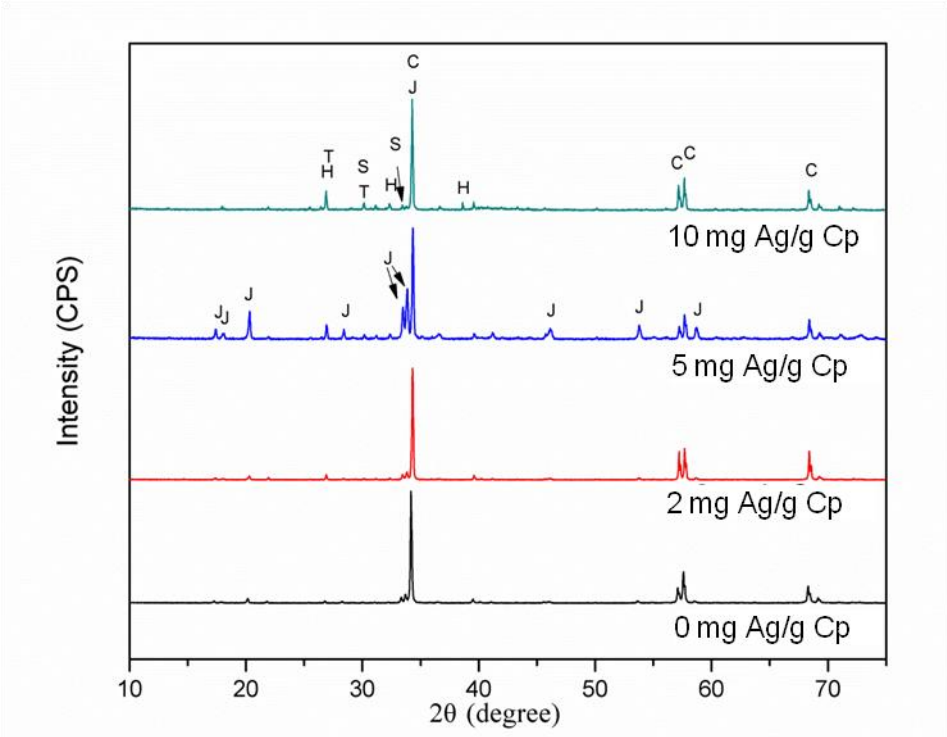

Fig. 8-6 XRD patterns of chalcopyrite bioleached in the presence of different amount of silver ions for 31 days (C: Chalcopyrite; J: Jarosite; S: elemental sulfur; H: Hematite; T: stromeyerite)

8.3.1.3 Raman studies

The results of Raman characterization of the samples are shown in Fig. 8-7. In the Raman spectra, the peak at approximately 291 cm^{-1} is assigned to chalcopyrite (Mernagh et al., 1993); peaks at 151 cm^{-1}, 218 cm^{-1}, could be assigned to elemental sulfur (Eckert and Steudel, 2003); peaks at 138 cm^{-1}, 429 cm^{-1}, 625 cm^{-1}, 1007 cm^{-1} and 1102 cm^{-1} could be assigned to jarosite (Sasaki et al., 2009) and peaks at 227 cm^{-1}, 245 cm^{-1}, 292 cm^{-1}, 411 cm^{-1} are from hematite (de Faria et al., 1997). The Raman results indicate there were elemental sulfur and jarosite formed during the leaching in bioleaching without or with only 2 mg/g silver ions. When 5 mg/g silver ions were added in to the solution, hematite appeared in the leaching residue with elemental sulfur and jarosite. When the silver concentration was increased into 10 mg/g, jarosite disappeared from the residual, at the same time more hematite presented on the chalcopyrite surface.

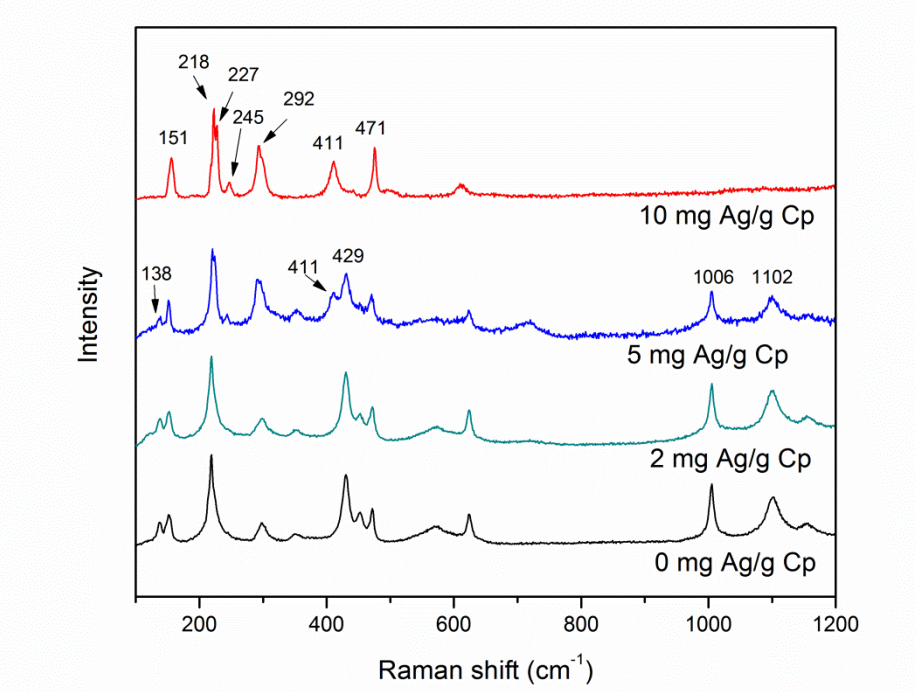

Fig. 8-7 Raman spectra of chalcopyrite bioleached in the presence of different amount of silver ions for 31 days

The Raman results indicated iron precipitated to form hematite in the presence of high concentration of silver ions and to form jarosite in the presence of low concentration of silver ions. The formation of jarosite is more concerned because it forms in the normal pH range for the operation of bioleaching. The iron precipitation is also jarosite in cases when high leaching efficiency was reached. It may negatively affect the bioleaching by reducing soluble Fe^{3+} or the effective of passivation, although the previous chapters indicate this impact may be just slight. The formation of jarosite is favoured by the presence of cations such as silver and, especially by high temperatures. The results of Gomez et al. (1999) indicated jarosite precipitation increased with increasing amounts of silver. In present study, the situation is similar when silver concentration increased up to 5 mg/g. The problem can be overcome by using more diluted culture media, although this could lead to a lower bacterial growth in initial stage; later on, it would be possible to maintain a higher concentration of iron in solution preventing the ore from being covered with a layer of jarosite which hinders bacterial attack and consumes silver to form argentojarosites (Gomez et al., 1999).

8.3.2 The effect of silver in chalcopyrite electrochemical oxidation

8.3.2.1 Cyclic voltametric studies

Fig. 8-8 and Fig. 8-9 show the results of cyclic voltametric curve of chalcopyrite in 9k basic salt solution with 5 mg/L and 20 mg/L silver ions. The CV curve with 5 mg/L silver shows very similar properties to chalcopyrite CV curve without silver in chapter 4 (Fig. 4-1). The peak A1 may indicate a selective dissolution of iron from the crystal lattice of chalcopyrite (Zeng et al., 2011). A2 around 630 mV could be ascribed to partial oxidation of chalcopyrite as shown in Reaction (1), where $y>x$. (Lu et al., 2000; Price and Warren, 1986). A3 observed could be assigned to the oxidation of copper and chalcocite (Zeng et al., 2011 and Gomez et al., 1996).

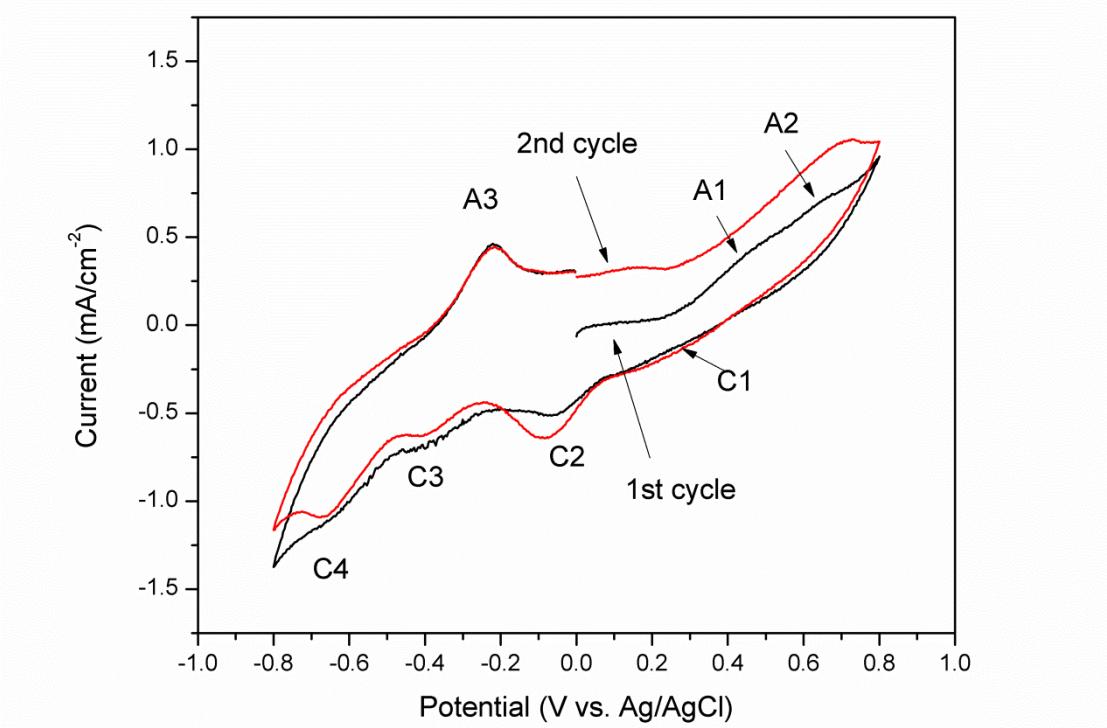

Fig. 8-8 Cyclic voltametry of chalcopyrite in the 9 K basic medium with 5 mg/L silver ions at a scan rate of 5 mV/s

In the inverse scan, C1 and C2 may be attributed to the reaction of the cupric ions with chalcopyrite, CuS or elemental sulfur, producing chalcocite (Qin et al., 2013). When the potential value was lower than -0.3 V, peak C3 and peak C4 were observed. They possibly related to the reduction of covellite and chalcopyrite, respectively (Arce and Gonzalez, 2002; Biegler and Horne, 1985).

The most remarkable change in the CV curve of chalcopyrite with the addition of 20 mg/L silver ions is a stronger oxidation peak at 0.35 V, which indicate the chalcopyrite dissolution was more rapid. At the same time, the addition of 20 mg/L silver ions enhanced the current density.

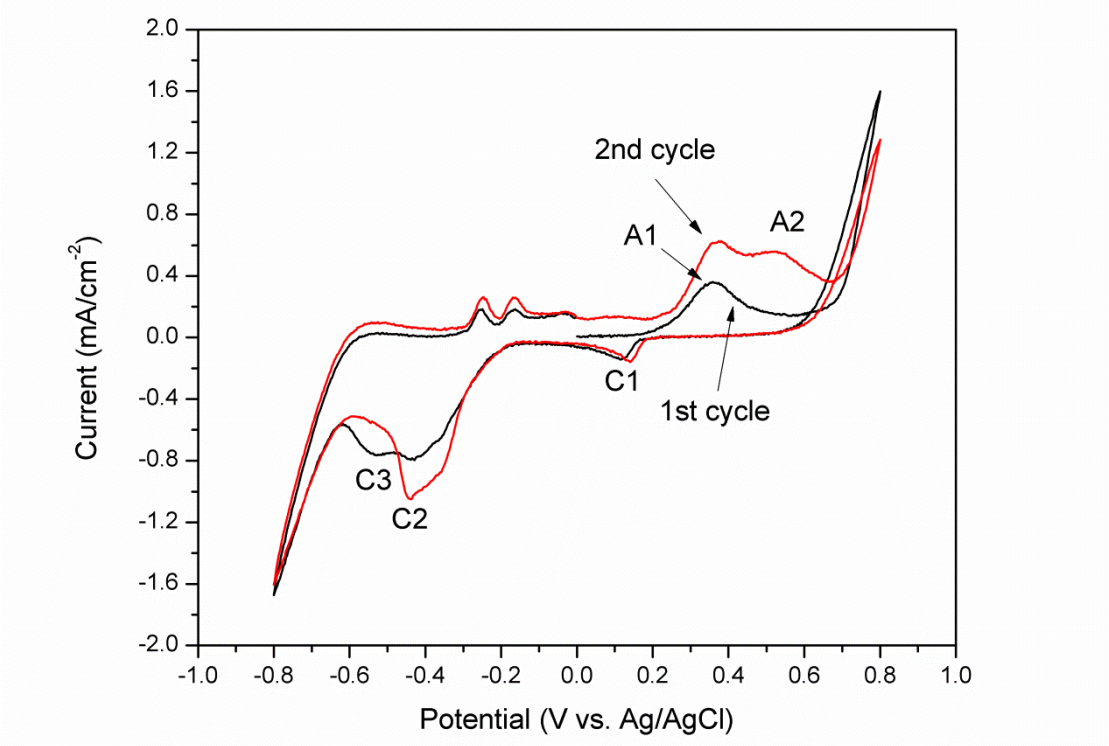

Fig. 8-9 Cyclic voltametry of chalcopyrite in the 9 K basic medium with 20 mg/L silver ions at a scan rate of 5 mV/s

8.3.2.2 Potentiodynamic studies

Fig. 8-10 shows the result of the potentiodynamic study at a scan rate of 0.5 mV s^{-1} with 20 mg/L silver ions. A passive region is evident from the OCP to 570 mV. In this region the current was low and surface reaction was very slow. From 550 to 630 mV, the current rose rapidly with the increase of potential. In this region, the surface reaction was fast. It is assumed some non-stoichiometric or secondary metal sulphide mineral formed in this region. From 630 mV to 750 mV, another region of slow current increase was observed, indicating the formation of a passivation layer. When potential increased to approximately 750 mV, another active region appeared which could be regarded as the dissolution of intermediates and passivation layers (Mikhlin et al., 2004; Ghahremaninezhad et al., 2010; Yin et al., 1995). This potentiodynamic profile has very

similar properties to the one without silver ions (Fig 4-2), indicating the addition of silver ions did not change the chalcopyrite passivation mechanism.

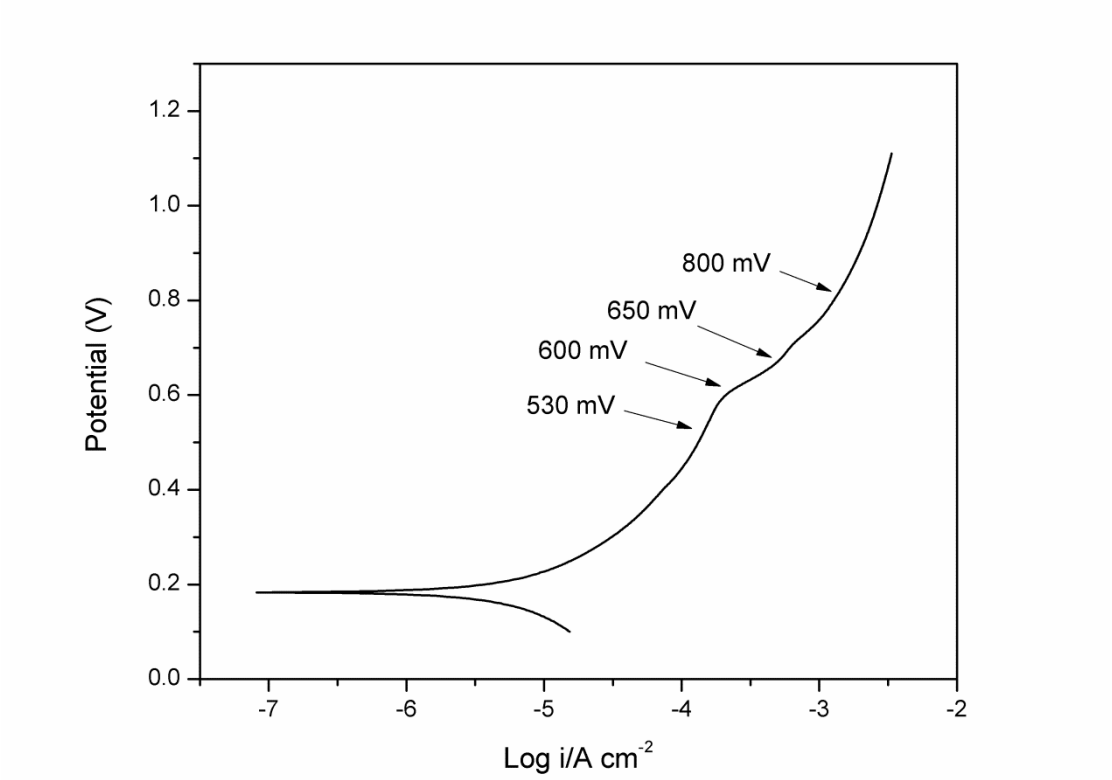

Fig. 8-10 Potentiodynamic curve for chalcopyrite in the 9 K basic medium with 20 mg/L silver ions at a scan rate of 0.5 mV/s

8.3.2.3 Raman studies

To study the surface species of chalcopyrite electrode in different potential ranges, Raman studies were carried out and the results are shown in Fig. 8-11. In accordance with the linear potentiodynamic curve, the surface species indicated by Raman spectra also show similar changes with the chalcopyrite oxidized in the absence of silver ions (Fig. 4-7). The electrode oxidized at 530 mV shows almost the feature of original chalcopyrite, with a strong peak at 292 cm^{-1} (Parker et al., 2008). At 600 mV, besides the chalcopyrite features, a strong peak around 473 cm^{-1} appeared, which is assigned to the S-S bond of covellite (Sasaki et al., 2009). At 650 mV, additional peaks at 153 cm^{-1} and 218 cm^{-1} appeared, suggesting the formation of crystalline sulfur (Sasaki et al., 2009). The intensity of peak assigned to covellite decreased as also observed in the absence of silver ion, which suggests less covellite formed in this condition. At 800 mV, more elemental sulfur presented on the electrode sulfur as evidenced by the stronger peaks at 151 and 218 cm^{-1}. A very strong peak at 473 cm^{-1} appeared with a shoulder at 460 cm^{-1}. This peak indicates

the formation of covellite at this potential as reported previously. The shoulder near 460 cm^{-1} is likely come from polysulfide species (Janz et al., 1976).

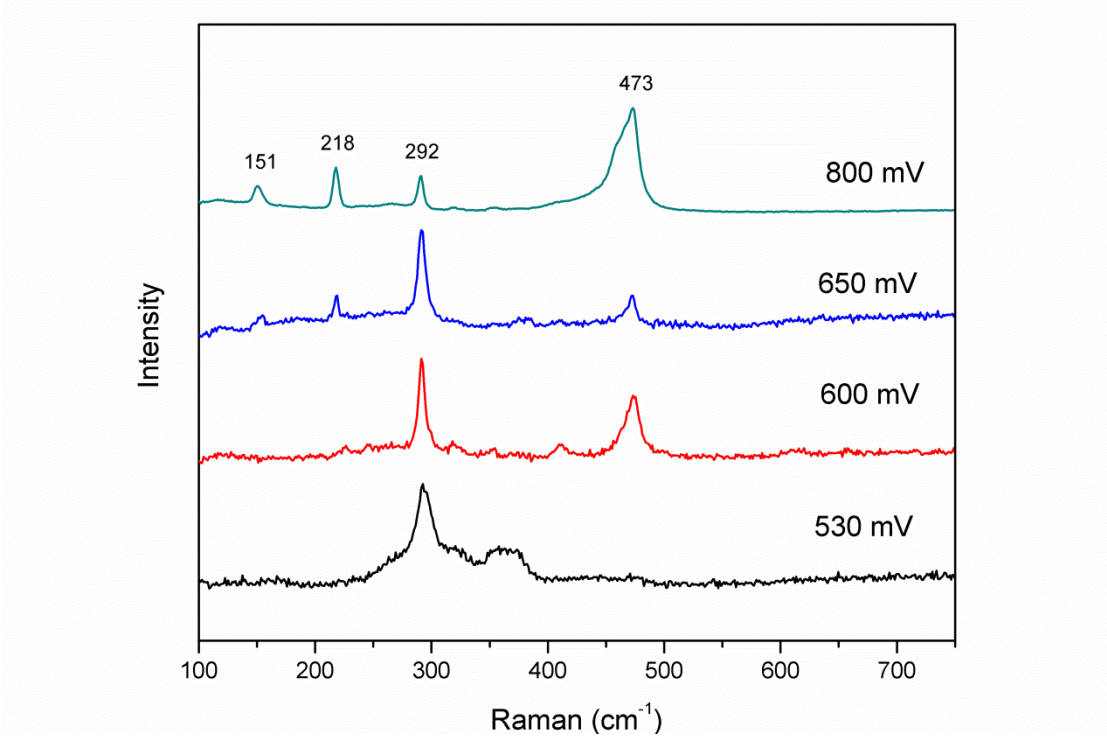

Fig. 8-11 Raman spectra of chalcopyrite oxidized in the 9 K basic medium with 20 mg/L silver ions under different potentials

8.4 Conclusions

The bioleaching efficiency of chalcopyrite by thermophiles was enhanced by low concentration of Ag^+ but decreased by high concentration of Ag^+. The solution pH increased significantly in bioleaching when high concentration of Ag^+ was added, but this phenomenon was not observed in chemical leaching. The increase of pH caused the formation of hematite in bioleaching experiments with high concentration of Ag^+. Electrochemistry indicates the addition of Ag^+ did not shift the passive region, but increased the current density. The Raman spectra of the electrochemically oxidized chalcopyrite also indicate there were no changes in the chalcopyrite dissolution pathway.

9 Summary of the thesis and future work

In this thesis, the effect of several environmental factors on chalcopyrite bioleaching has been studied and the changes of surface species and mineralogy in bioleaching and electrochemical oxidation have been characterized. The major findings were summarised as follows:

9.1 Chalcopyrite dissolution pathways in (bio)leaching

In chalcopyrite bioleaching iron was preferentially leached out, leaving on the particle surface CuS_n-like and covellite-like species. The copper was removed slower than iron but faster than sulfur, which left an inert polysulfide and elemental sulfur on the chalcopyrite surface. The oxidation of sulfur rich layer should be the rate-controlling step for the surface oxidation of chalcopyrite.

The electrochemical studies show that there was an activated region in the middle of two passive regions for chalcopyrite electrochemcial oxidation. In the active region, between 550 to 630 mV (vs. Ag/AgCl), S_n^{2-}/S^0, S_2^{2-} species and covellite were found by XPS and Raman. XPS study suggested a thin sulfur rich layer formed in the first passive region (530 mV). At 650 mV, S_2^{2-} species and covellite started to dissolve, leaving a highly metal deficient polysulfide layer.

9.2 Bacteria initial attachment

In the first 24 hours, *A. ferrooxidans* started to attach onto the chalcopyrite surface. The bacterial population in the defects was significantly higher than that on the polished surfaces. After 72 hours of leaching, a layer of biofilm formed on chalcopyrite. The AFM study indicated abundant EPS was produced on the mineral surface after 72 hours of leaching. The formation of biofilm was further supported by the Raman analysis. From EBSD and optical images analysis, no significant difference in selectivity of bacterial attachment was found on crystal orientations of chalcopyrite.

9.3 Effect of temperature and bacteria type on chalcopyrite bioleaching

Thermophiles can significantly enhance the leaching efficiency. The high leaching efficiency in presence of thermophiles is caused by the increased abiotical reaction rate

as a result of elevated temperature, while there is no significant difference on surface sulfur speciation between the chalcopyrite bioleached at 48 or 30 ^{o}C. The synergistic effect of microorganisms with different metabolic pathways does not play a comparably important role with temperature in bioleaching, evidenced by the similar leaching efficiency between *L. ferrooxidans* and a mesophilic mixture. Elemental sulfur forms on the chalcopyrite as suggested in the polysulfide pathway (Sand et al., 2001), which could be effectively eliminated by sulfur-oxidizing microorganisms. However, the formation of elemental sulfur does not seem to hinder the leaching significantly.

9.4 Effect of Eh on chalcopyrite bioleaching

Low Eh (350-480 mV vs. Ag/AgCl) significantly promoted the chalcopyrite (bio)leaching. Jarosite was found as one major leaching product which accumulated more rapidly with higher initial Fe^{2+}/Fe^{3+} ratio and at higher temperatures. The leaching results and quantitative XRD and XANES show jarosite and elemental sulfur did not primarily account for the passivation of chalcopyrite. Secondary mineral covellite was detected in chalcopyrite dissolution.

9.5 Effect of pyrite on chalcopyrite bioleaching

Chalcopyrite leaching was significantly enhanced by pyrite. Chalcopyrite was selectively leached in chemical leaching as a result of galvanic effect. However, the chalcopyrite leaching efficiency decreased in bioleaching when a large amount of pyrite dissolved. The disolution of pyrite is likely linked to the increased solution potential because of the biooxidation ability of the bacteria. The XRD and iron K-edge XANES analysis also indicate significant jarosite precipitation in bacterial leaching, which is also the result of increased solution potential. μ-XRF and Raman studies suggest a sulfur-rich layer developed inhomogenously on mineral. The galvanic effect was also verified in column leaching of low grade chalcopyrite. More than 60% copper was leached out in 172 days in galvanic assisted column leaching with moderate thermophiles, though the chalcopyrite grains were not completely liberated.

9.6 Effect of silver ions on chalcopyrite bioleaching

The bioleaching efficiency of chalcopyrite by thermophiles was enhanced by low concentration of Ag^{+} but decreased by high concentration of Ag^{+}. Iron precipitated as jarosite in experiment with low silver concentration but hematite in experiment with high silver concentration. Electrochemistry indicates the addition of Ag^{+} increased the current

density, which indicates a faster oxidation rate. However, there is no evidence of the shift of the passive region. The Raman spectra collected on the electrochemically oxidized chalcopyrite also indicate there were no changes in dissolution pathway.

9.7 Future work

In the industrial practice of metal sulfide leaching, heap leaching is a widely applied technology (Dhawan et al., 2012). However, the attempt to use this technology on low grade chalcopyrite is still very challenging (Pradhan et al., 2008). Besides temperature, microorganism, Eh, galvanic effect etc., the leaching kinetics of metal sulfide in heap leaching is also significantly impacted by ore type (both metal-bearing ore and gangue), particle size, mineral permeability and pore network structure (Dhawan et al., 2012). To further understand the bioleaching of chalcopyrite in industrial conditions, further work will focus on the bioleaching of low grade chalcopyrite ore. The impact of pH, Eh, temperature, particle size, gangue and impurities on low grade chalcopyrite bioleaching will be investigated. The leaching products will be characterized by XPS, XAS, XRD and Raman spectroscopy. In particular, X-ray CT will play a key role in this work to investigate the mineralogy and 3D structure changes of bulk low grade mineral during long-term leaching. The interparticle and intraparticle fluid distribution will also be investigated and modelled based on the CT data.

Chapter 10 references

Abramoff, M.D., Magalhaes, P.J., Ram, S.J., 2004. Image processing with ImageJ. Biophotonics International, 11, 36-42.

Acres, R.G., Harmer S.L., Beattie, D.B., 2010a. Synchrotron XPS, NEXAFS, and ToF-SIMS studies of solution exposed chalcopyrite and heterogeneous chalcopyrite with pyrite. Minerals Engineering 23,928-936.

Acres, R.G., Harmer, S.L., Beattie, D.A., 2010b. Synchrotron XPS studies of solution exposed chalcopyrite, bornite, and heterogeneous chalcopyrite with bornite. International Journal of Mineral Processing 94, 43-51.

Acuña., J., Rojas, J., Amaro, A.M., Toledo, H., Jerez, C.A., 1992. Chemotaxis of *Leptospirillum ferrooxidans* and other acidophilic chemolithotrophs: comparison with the Escherichia coli chemosensory system. FEMS Microbiology Letters 75, 37–42.

Ahonen, L., Tuovinen O.H., 1995. Bacterial leaching of complex sulfide ore samples in bench-scale column reactors. Hydrometallurgy 37, 1-21.

Akcil, A., Ciftci, H., Deveci, H., 2007. Role and contribution of pure and mixed cultures of mesophiles in bioleaching of a pyritic chalcopyrite concentrate. Minerasl Engineering 20, 310-318.

Al-Harahsheh, M., Kingman, S., Bradshaw, S., 2006. Scale up possibilities for microwave leaching of chalcopyrite in ferric sulphate. International Journal of Mineral Processing 80, 198-204.

Al-Harahsheh, M., Rutten, F., Briggs, D., Kingman, S., 2006. Preferential oxidation of chalcopyrite surface facets characterized by ToF-SIMS and SEM. Applied Surface Science 252, 7155-7158.

Al-Sogair, F., Marafie, H.M., Shuaib, N.M, Youngo, H.B, El-Ezaby M.S., 2002. Interaction of phosphate with iron(III) in acidic medium, equilibrium and kinetic studies Journal of Coordination Chemistry 55, 1097-1109.

Ahmad, Z. Chapter 3 - Corrosion Kinetics, In Principles of Corrosion Engineering and Corrosion Control, edited by Zaki Ahmad, Butterworth-Heinemann, Oxford, 2006, 57-119.

Andrews, G.F., 1988. The selective adsorption of Thiobacilli to dislocation sites on pyrite surfaces. Biotechnology and bioengineering, 31, 378-381.

Annapragada, A.V., Gulari, E., 1990. Fe-P-O Catalysts for Methane Utilization--Catalyst development and identification. Journal of Catalysis 123, 130-146.

Arce, E.M., González, I., 2002. A comparative study of electrochemical behavior of chalcopyrite, chalcocite and bornite in sulfuric acid solution. International Journal of Mineral Processing 67, 17-28.

Baker, B.J., Banfield, J.F., 2003. Microbial communities in acid mine drainage. FEMS Microbiology Ecology 44, 139–152.

Ballester, A., Blázquez, M.L, González, F., Muñoz, J.A. catalytic role of silver and other ions on the mechanism of chemical and biological leaching. In: Microbial Processing. Donati, E.R., Sand, W., Eds, 2007. Springer, pp. 77-101.

Battaglia-Brunett, F., d'Hugues, P., Cabral, T., Cezac, P., Garcia, J.L., Morin, D., 1998. The mutual effect of mixed *Thiobacilli* and *Leptosprilli* populations on pyrite bioleaching. Minerasl Engineering 11, 195-205.

Berry, V.K., Murr, L.E., Hiskey, J.B., 1978. Galvanic interaction between chalcopyrite and pyrite during bacterial leaching of low grade waste. Hydrometallurgy 3, 309-326.

Bertsch, P.M., Hunter, D.B., 2001. Applications of synchrotron-based X-ray microprobes. Chemical Reviews 101, 1809-1842.

Bevilaqua, D., Acciari, H. A., Benedetti, A. V., Garcia, O. Electrochemical Techniques Used To Study BacteriaL-Metal Sulfides Interactions In Acidic Environments, in Microbial Processing of Metal Sulfides. Donati E.R. Sand W, eds. Springer, 2007, 59-76.

Bevilaqua, D., Leite, A.L.L.C., Garcia, Jr O., Tuovinen, O.H.,2002. Oxidation of chalcopyrite by *Acidithiobacillus ferrooxidans* and *Acidithiobacillus thiooxidans* in shake flasks. Process Biochemistry 38, 587-592.

Biegler, T., Swift, D.A., 1979. Anodic electrochemistry of chalcopyrite. Journal of Applied Electrochemistry 9, 545-554.

Bigham, J.M., Schwertmann, U., Traina, S.J., Winland, R.L., Wolf, M., 1996. Schwertmannite and the chemical modeling of iron in acid sulfate waters. Geochimica et Cosmochimica Acta 60, 2111–2121.

Blake, R.C., Griff, M.N., 2012. In situ spectroscopy on intact Leptospirillum ferrooxidans reveals that reduced cytochrome 579 is an obligatory intermediate in the aerobic iron respiratory chain. Frontiers in Microbiology 3, 136–146.

Blázquez, M.L., Álvarez, A., Ballester, A., González, F., Muñoz, J. A., Amils, R., Ballester, A., 1999. Bioleaching behaviour of chalcopyrite in the presence of silver at 35^{o}C and 68^{o}C. Process Metallurgy 9, 137-147.

Bonnefoy, V., Holmes, D.S., 2011. Genomic insights into microbial iron oxidation and iron uptake strategies in extremely acidic environments. Environmental Microbiology 14, 1597–1611.

Bowden, W.L, Baraette, L.H., DeMuth, D.L., 1984. Insoluble heavy metal polysulfide cathodes. US patent 4481267.

Brierley, C.L., 1978. Bacterial leaching. Critical Reviews in Microbiology 6, 207– 262.

Brierley, C.L., 1982. Microbiological mining. Scientific American 247, 42-51.

Brierley, C.L., 2010. Biohydrometallurgical prospects. Hydrometallurgy 104, 324-328.

Brierley, J.A., 2008. A perspective on developments in biohydrometallurgy. Hydrometallurgy 94, 2-7.

Brierley, J.A., Brierley, C.L., 2001. Present and future commercial applications of biohydrometallurgy. Hydrometallurgy 59, 233-239.

Brierley, J.A., Le Roux, N.W.,1977. A facultative thermophilic Thiobacillus-like bacterium: oxidation of iron and pyrite. In: Schwartz, W. (Ed.), Conference Bacterial Leaching 1977. Verlag Chemie, New York, pp. 55–66.

Brock, T.D., Brock, K.M., Belly, R.T., Weiss, R.L, 1972. A new genus of sulfur-oxidizing bacteria living at low pH and high temperature. Archives of Microbiology 84, 8454-68.

Bruker (2009). TOPAS. Version 4.2. Bruker AXS Inc., Madison, Wisconsin, USA.

Buckley, A., 1994. A survey of the application of X-ray photoelectron spectroscopy to flotation research. Colloids and Surfaces A: Physicochemical and Engineering Aspects. 93, 159-172.

Buckley, A.N., Woods, R., 1984. An X-ray photoelectron spectroscopic study of the oxidation of chalcopyrite. Australian Journal of Chemistry 37, 2403-2413.

Butt, H., Cappella, B., Michael, K., 2005. Force measurements with the atomic force microscope:Technique, interpretation and applications. Surface Science Reports 59, 1–152.

Cai, Y.F., Chen, X.M., Ding, J.Y. and Zhou, D.S., 2012. Leaching mechanism for chalcopyrite in hydrochloric acid. Hydrometallurgy, 113, 109-118.

Carneiro, M.F.C., Leão, V.A., 2007. The role of sodium chloride on surface properties of chalcopyrite leached with ferric sulphate. Hydrometallurgy 87, 73–82.

Chandra, A.P., Gerson, A.R., 2010. The mechanisms of pyrite oxidation and leaching: A fundamental perspective. Surface Science Reports 65, 293-315.

Coram, N.J., Rawlings, D.E., 2002. Molecular relationship between two groups of the genus *Leptospirillum* and the finding that *Leptospirillum ferriphilum* sp. nov. dominates South African commercial biooxidation tanks that operate at 40 degrees C. Applied and Environmental Microbiology 68, 838–845.

Córdoba, E.M., Muñoz, J.A., Blázquez, M.L., González, F. and Ballester, A., 2008a. Leaching of chalcopyrite with ferric ion. Part IV: The role of redox potential in the presence of mesophilic and thermophilic bacteria. Hydrometallurgy, 93, 106-115.

Córdoba, E.M., Muñoz, J.A., Blázquez, M.L., González, F. and Ballester, A., 2008b. Leaching of chalcopyrite with ferric ion. Part II: Effect of redox potential. Hydrometallurgy 93, 88-96.

Córdoba, E.M., Muñoz, J.A., Blázquez, M.L., González, F., Ballester, A., 2008c. Leaching of chalcopyrite with ferric ion. Part III: effect of redox potential on the silver-catalyzed process. Hydrometallurgy 93:97-105.

Córdoba, E.M., Muñoz, J.A., Blázquez, M.L., González, F., Ballester, A., 2009. Comparative kinetic study of the silver-catalyzed chalcopyrite leaching at 35 and 68 °C. International Journal of Mineral Processing. 92, 137-143.

Darezereshki, Schaffie, E.M., Lotfalian, M., Seiedbaghery, S.A., Ranjbar, M., 2011. Use of mesophilic and thermophilic bacteria for the improvement of copper extraction from a low-grade ore. International Journal of Minerals, Metallurgy and Materials18, 138-143.

de Faria, D.L.A., Venâncio Silva, S., de Oliveira M.T., 1997. Raman microspectroscopy of some iron oxides and oxyhydroxides. Journal of Raman Spectroscopy 28, 873-878.

de Oliveira, C., de Lima, G.F., De Abreu, H.A., Duart,e H.A., 2012. Reconstruction of the chalcopyrite surfaces — a DFT study. The Journal of Physical Chemistry C, 116, 6357-6366.

de Oliveira, C., Duarte, H.A., 2010. Disulphide and metal sulphide formation on the reconstructed surface of chalcopyrite: a DFT study. Applied Surface Science. 257, 1319-1324.

Dhawan, N.M., Safarzadeh, S., Miller, J.D., Moats, M.S., Rajamani, R.K., Lin, C.L., 2012. Recent advances in the application of X-ray computed tomography in the analysis of heap leaching systems. Minerals Engineering 35, 75-86

D'Hugues, P., Foucher, S., Gallé-Cavalloni, P., Morin, D., 2002. Continuous bioleaching of chalcopyrite using a novel extremely thermophilic mixed culture. International Journal of Mineral Processing 66, 107-1019.

Dinnebier, R.E., Billinge S.L.. Principles of Powder Diffraction. In powder diffraction Theory and practice, Dinnebier, R.E., Billinge S.L. Eds; RSC publishing, 2008, 1-19.

Dixon, D.G., Mayne, D.D. and Baxter, K.G., 2008. Galvanox (TM) - A novel galvanically-assisted atmospheric leaching technology for copper concentrates. Canadian Metallurgy Quarterly 47, 327-336.

Dopson, M., Lindstrom, E.B., 2003. Potential Role of *Thiobacillus caldus* in Arsenopyrite Bioleaching. Applied Environment Microbiology 71, 31-36.

Dutrizac, J., 1981. The dissolution of chalcopyrite in ferric sulfate and ferric chloride media. Metallurgical and Materials Transactions B 12, 371-378.

Dutrizac, J.E., 1976. Synthesis and properties of jarosite-type compounds. The Canadian Mineralogist 14, 151-158.

Dutrizac, J.E., 1983. Factors affecting alkali jarosite precipitation. Metallurgical Transactions B-Process Metallurgy, 14, 531-539.

Dutrizac, J.E., 1989. Elemental sulfur formation during the ferric sulfate leaching of chalcopyrite. Canadian Metallurgical Quarterly, 28, 337-344.

Dutrizac, J.E., Jambor, J.L., 2000. Jarosites and their application in hydrometallurgy. In: C.N. Alpers and J.L. Jambor (Editors), Sulfate Minerals - Crystallography, Geochemistry and Environmental Significance. Reviews in Mineralogy & Geochemistry, pp. 405-452.

Dutrizac, J.E.,1978. The kinetics of dissolution of chalcopyrite in ferric ion media Metallurgical Transactions B 9B, 431-439.

Dutrizac, J.E., 2008 Factors affecting the precipitation of potassium jarosite in sulfate and chloride media. Metallurgical Transactions B-Process Metallurgy 39, 771-783.

Eckert, B., Steudel, R., 2003. Molecular spectra of sulfur molecules and solid sulfur allotropes. Topics in Current Chemistry 231, 31-98.

Edwards, K.J., Rutenberg, A.D., 2001. Microbial response to surface microtopography: the role of metabolism in localized mineral dissolution. Chemical Geology. 180 , 19-32.

Edwards, K.J., Schrenk, M.O.,Hamers, R., Banfield, J. F., 1998. Microbial oxidation of pyrite: experiments using micro-organisms from an extreme acidic environment. American Mineralogist 83, 1444-1453.

Ekmekqi, Z., Demirel, H., 1997. Effects of galvanic interaction on collectorless flotation behaviour of chalcopyrite and pyrite. International Journal of Mineral Processing 52, 31-48.

Elisabeth, U., Fittschen, A., Falkenberg, G., 2011. Trends in environmental science using microscopic X-ray fluorescence. Spectrochimica Acta Part B 66, 567-580

England, K., Charnock, J., Pattrick, D., Vaughan D., 1999. Surface oxidation studies of chalcopyrite and pyrite by glancing-angle X-ray absorption spectroscopy (REFLEXAFS) Mineralogical Magazine 63, 559-566.

Fahrni, C.J., 2007. Biological applications of X-ray fluorescence microscopy: exploring the subcellular topography and speciation of transition metals. Current Opinion in Chemical Biology 11,121–127.

Fairley, N, 2009. CasaXPS Manual, version 2.3.15. Casa Software Ltd. http://www.casaxps.com.

Falco, L., Pogliani, C., Curutchet, G., Donati, E., 2003. A comparison of bioleaching of covellite using pure cultures of Acidithiobacillus ferrooxidans and *Acidithiobacillus thiooxidans* or a mixed culture of *Leptospirillum ferrooxidans* and *Acidithiobacillus thiooxidans*. Hydrometallurgy 71, 31-36.

Ferron, C.J., 2003. Leaching of secondary copper minerals using regenerated ferric sulphate. In: Riveros, P.A., Dixon, D., Dreisinger, D.B., Menacho, J. (Eds.), COPPER 2003, Vol. VI — Hydrometallurgy of Copper (Book 1), pp. 337-352. Santiago, Chile

Fuchs, T., Huber, H., Burggraf, S., 1996. 16S rDNA-based phylogeny of the archaeal order *Sulfolobales* and reclassification of *Desulfurolobus ambivalens* as *Acidianus ambivalens* comb. nov. Systematic and Applied Microbiology 19, 56-60.

Fujisawa, M., Suga, S., Mizokawa, T., Fujimori, A., Sato, K., 1994. Electronic structures of $CuFeS_2$ and $CuAl_{0.9}Fe_{0.1}S_2$ studied by electron and optical spectroscopies. Physical Review B 49, 7155-7164.

Garcia-Meza, J. V., Lara, R. H., Navarro-Contreras, H. R., 2011. Application of Raman spectroscopy to the biooxidation analysis of sulfide minerals. International Journal of Spectroscopy, 2012, 1-7.

Gehrke, T., Telegdi, J., Thierry, D., Sand, W., 1998. Importance of extracellular polymeric substances from Thiobacillus ferrooxidans for bioleaching. Applied and environmental microbiology, 64, 2743-2747.

Ghahremaninezhad, A., Asselin, E., Dixon, D., 2010. Electrochemical evaluation of the surface of chalcopyrite during dissolution in sulfuric acid solution. Electrochim. Acta. 55, 5041-5056.

Goh, S.W., Buckley, AN, Lamb, R. N., Rosenberg, R. A., Moran, D., 2006. The oxidation states of copper and iron in mineral sulfides, and the oxides formed on initial exposure of chalcopyrite and bornite to air. Geochimica et Cosmochimica Acta 70, 2210-2228.

Golovacheva, R.S., Karavaiko, G.I., 1978. A new genus of thermophilic spore-forming bacteria, Sulfobacillus. Mikrobiologiya 47, 815-822 (English translation pp. 658–665).

Golyshina, OV, Pivovarova, T.A., Karavaiko G.I., Kondratéva, T.F., Moore, E.R., Abraham, W.R., Lünsdorf, H., Timmis, K.N., Yakimov, M.M., Golyshin, P.N, 2000. Ferroplasma acidiphilum gen. nov., sp. nov., an acidophilic, autotrophic, ferrous-iron-oxidizing, cell-wall-lacking, mesophilic member of the Ferroplasmaceae fam. nov., comprising a distinct lineage of the Archaea. International Journal of Systematic and Evolutionary Microbiology 50, 997-1006.

Gomez, C., Figueroa, M., Muñoz, J., Blázquez, M.L., Ballester, A., 1996. Electrochemistry of chalcopyrite. Hydrometallurgy 43, 331-344.

Gu, G., Hu, K., Zhang, X., Xiong, X., Yang, H., 2013. The stepwise dissolution of chalcopyrite bioleached by *Leptospirillum ferriphilum*. Electrochim. Acta 103, 50-57.

Hackl, R.P, Dreisinger, D.B., Peters, E., King, J.A., 1995. Passivation of chalcopyrite during oxidative leaching in sulfate media Hydrometallugy 39, 25-48.

Hall, S.R., Stewart, J.M., 1973. The crystal structure refinement of chalcopyrite, $CuFeS_2$. Acta Crystallogr B 29, 579-85.

Hallberg, K.B., Johnson, D.B., 2001. Biodiversity of acidophilic prokaryotes. Advances in Applied Microbiology 49, 37-84.

Harmer, S.L., Thomas, J.E., Fornasiero, D., Gerson, A.R., 2006. The evolution of surface layers formed during chalcopyrite leaching. Geochimica et Cosmochimica Acta 70, 4392-4402.

Harneit, K., Göksel, A., Kock, D., Klock, J.H., Gehrke, T., Sand, W., 2006. Adhesion to metal sulphide surfaces by cells of *Acidithiobacillus ferrooxidans*, *Acidithiobacillus thiooxidans* and *Leptospirillum ferrooxidans*. Hydrometallurgy 83, 245-254.

He, H., Xia, J.L., Yang, Y., Jiang, H.C., Xiao, C.,Q., Zheng, L., Ma, C.Y., Zhao, Y.D, Qiu, G.Z., 2009. Sulfur speciation on the surface of chalcopyrite leached by *Acidianus manzaensis*. Hydrometallurgy 99, 45-50.

Hippe, H., 2000. Leptospirillum gen. nov. (ex Markosyan 1972), nom. rev., including *Leptospirillum ferrooxidans* sp. nov. (ex Markosyan 1972), nom. rev. and *Leptospirillum thermoferrooxidans* sp. nov. (Golovacheva et al. 1992). International Journal of Systematic and Evolutionary Microbiology 50, 501-503.

Hiraishi, A., Nagashima, K.V., Matsuura, K., Shimada, K., Takaichi, S., Wakao, N., Katayama, Y., 1998. Phylogeny and photosynthetic features of *Thiobacillus acidophilus* and related acidophilic bacteria: its transfer to the genus *Acidiphilium* as *Acidiphilium acidophilum* comb. nov. International Journal of Systematic and Evolutionary Microbiology 48, 1389-1398.

Hiroyoshi, N., Arai, M., Miki, H., Tsunekawa, M., Hirajima, T., 2002. A new reaction model for the catalytic effect of silver ions on chalcopyrite leaching in sulfuric acid solutions. Hydrometallurgy 63, 257- 267.

Hiroyoshi, N., Hirota, M., Hirajima, T.,Tsunekawa, M., 1997. A case of ferrous sulfate addition enhancing chalcopyrite leaching. Hydrometallurgy 47, 37-45.

Hiroyoshi, N., Miki, H., Hirajima, T., Tsunekawa, M., 2001. Enhancement of chalcopyrite leaching by ferrous ions in acidic ferric sulfate solutions. Hydrometallurgy 60, 185-197.

Hiroyoshi, N., Miki, H., Hirajima, T.,Tsunekawa, M., 2000. A model for ferrous-promoted chalcopyrite leaching. Hydrometallurgy 57, 31-38.

Hiroyoshi, N., Tsunekawa, M., Okamoto, H., Nakayama, R., Kuroiwa, S., 2008. Improved chalcopyrite leaching through optimization of redox potential. Canadian Metallurgy Quarterly 47, 253-258.

Holmes, P.R., Crundwell, F.K., 1995. Kinetic aspects of galvanic interactions between minerals during dissolution. Hydrometallurgy 39, 353-375.

Holtz, M., Duncan, W. M., Zollner, S., Liu, R., 2000. Visible and ultraviolet Raman scattering studies of $Si_{1-x}Ge_x$ alloys. Journal of Applied Physics 88, 2523-2528.

Hu, Y., Qiu, G., Wang, J., Wang, D., 2002. The effect of silver-bearing catalysts on bioleaching of chalcopyrite. Hydrometallurgy, 64, 81-88.

Itoh, Y.H, Kurosawa, N., Uda, I., Suga, A., Tanoue, S., Itoh, T., Horiuchi, T., Itoh, T., 2001 *Metallosphaera sedula* TA-2, a calditoglycerocaldarchaeol deletion strain of a thermoacidophilic archaeon. Extremophiles 5, 241-245.

Janz, G. J., Coutts, J. W., Downey, J. R., Roduner, E., 1976. Raman studies of sulfur-containing anions in inorganic polysulfides: potassium polysulfides. Inorganic Chemistry 15, 1755 -1758.

Johnson, D.B., 1998. Biodiversity and ecology of acidophilic microorganisms. FEMS Microbiology Ecology 27, 307-317.

Johnson. D.B., Hallberg, K.B. Carbon, Iron and Sulfur Metabolism in Acidophilic Micro-Organisms. Advances in Microbial Physiology. 54, 201-255.

Jones RT. Electronic structures of the sulfide minerals sphalerite, wurtzite, pyrite, marcasite, and chalcopyrite. PhD thesis University of South Australia; 2006.

Kametani, H., Aoki, A., 1985. Effect of suspension potential on the oxidation rate of copper concentrate in a sulphuric acid solution. Metallurgical Transactions B 16B, 695-705.

Kato, T, Miúra, Y., 1975. The crystal structures of jarosite and svanbergite. Mineralogical Journal 8, 419-430.

Keeling, S.E., Palmer, M.L., Caracatsanis, F.C., Johnson, J.A., Watling, H.R., 2005. Leaching of chalcopyrite and sphalerite using bacteria enriched from a spent chalcocite heap. Miner. Eng. 18, 1289–1296

Kelly, D.P., Wood, A.P. , 2000. Reclassification of some species of Thiobacillus to the newly designated genera Acidithiobacillus gen. nov., Halothiobacillus gen. nov., and

Thermithiobacillus gen. nov. International Journal of Systematic and Evolutionary Microbiology 50, 511–516.

Khoshkhoo, M., Dopson, M., Shchukarev, A., Sandström, Å., 2014. Electrochemical simulation of redox potential development in bioleaching of a pyritic chalcopyrite concentrate. Hydrometallurgy 144-145, 7-14

Kinnunen, P.H.M., Puhakka, J.A., 2004. Chloride-promoted leaching of chalcopyrite concentrate by biologically-produced ferric sulfate. Journal of Chemical Technology and Biotechnology 79, 830-834

Klauber, C., 2008. A critical review of the surface chemistry of acidic ferric sulphate dissolution of chalcopyrite with regards to hindered dissolution. International Journal of Mineral Processing 86, 1-17.

Klauber, C., Parker, A., Bronswijk, W.V., Watling, H., 2001. Sulphur speciation of leached chalcopyrite surfaces as determined by X-ray photoelectron spectroscopy. International Journal of Mineral Processing 62, 65-94.

Koleini, S.M.J., Aghazadeh, V., Sandström, Å., 2011. Acidic sulphate leaching of chalcopyrite concentrates in presence of pyrite. Mineral. Engineering 24, 381-386.

Koleini, S.M.J., Jafarian, M., Abdollahy, M., Aghazadeh, V., 2010. Galvanic Leaching of Chalcopyrite in Atmospheric Pressure and Sulfate Media: Kinetic and Surface Studies. Industrial & Engineering Chemistry Research 49, 5997-6002.

Koningsberger, D.C, Mojet, B.L., van Dorssen, G.E., Ramaker, D.E., 2000. XAFS spectroscopy fundamental principles and data analysis. Topics in Catalysis 10, 143-155.

Konishi, Y., Asai, S, Tokushige, M., 1999. Kinetics of the Bioleaching of Chalcopyrite Concentrate by Acidophilic Thermophile *Acidianus brierleyi*. Biotechnology Progress 15, 681-688.

Konishi, Y., Tokushige, M., Asai, S., Suzuki, T., 2001. Copper recovery from chalcopyrite concentrate by acidophilic thermophile Acidianus brierleyi in batch and continuous-flow stirred tank reactors. Hydrometallurgy 59, 271-282.

Konishi, Y., Yoshida, S., Asai, S. ,1995. Bioleaching of pyrite by acidophilic thermophile Acidianus-Brierleyi. Biotechnology and Bioengineering 48, 592-600.

Kurosawa, N., Itoh, Y.H., Iwai, T., 1998. *Sulfurisphaera ohwakuensis* gen. nov., sp. nov., a novel extremely thermophilic acidophile of the order *Sulfolobales.* International Journal of Systematic Bacteriology 48, 451-456.

Laajalehto, K., Kartio, I., Suoninen, E., 1997. XPS and SR-XPS techniques applied to sulphide mineral surfaces. International Journal of Mineral Processing. 51, 163-170

Lazaro, I., Nicol, M.J., 2003. The mechanism of the dissolution and passivation of chalcopyrite: an electrochemical study. In: Young, C., Eds, Hydrometallurgy 2003, Proceedings of the International Symposium honoring Professor Ian M. Ritchie, 5th, Vancouver, BC, Canada, Aug. 24–27, vol. 1. Minerals, Metals & Materials Society, Warrendale PA, pp. 405-417.

Le Roux, N.W., Wakerley, D.S., Hunt, S.D., 1977. Thermophilic Thiobacillus-type bacteria from Icelandic thermal areas. Journal of General Microbiology 100, 197-201.

Li, Y., Kawashima, N., Li, J., Chandra, A.P., Gerson, A.R., 2013. A review of the structure, and fundamental mechanisms and kinetics of the leaching of chalcopyrite. Advances in Colloid and Interface Science. 197-198, 1-32.

Liang, C., Xia, J., Nie, Z., Yang, Y., Ma, C., 2012 Effect of sodium chloride on sulfur speciation of chalcopyrite bioleached by the extreme thermophile *Acidianus manzaensis*. Bioresource Technology 110, 462-467.

Liang, C., Xia, J., Yang, Y., Nie, Z., Zhao, X., Zheng, L., Ma, C., Zhao, Y., 2011 Characterization of the thermoreduction process of chalcopyrite at 65 ℃ by cyclic voltam metryand XANES spectroscopy. Hydrometallurgy 107, 13-21.

Liang, C., Xia, J., Zhao, X., Yang, Y., Gong, S., Nie Z., Ma C., Zheng L., Zhao Y, Qiu G., 2010. Effect of activated carbon on chalcopyrite bioleaching with extreme thermophile *Acidianus manzaensis*. Hydrometallurgy 105, 179-185.

Linge, H.G., 1976. A study of chalcopyrite dissolution in acidic ferric nitrate by potentiometric titration. Hydrometallurgy 2, 51-64.

Liu, Q., Li, H., Zhou, L., 2007. Study of galvanic interactions between pyrite and chalcopyrite in a flowing system: implications for the environment. Environmental Geology, 52, 11-18.

López-Juárez, A., Gutiérrez-Arenas, N., Rivera-Santillán, R.E., 2006. Electrochemical behavior of massive chalcopyrite bioleached electrodes in presence of silver at 35 °C. Hydrometallurgy 83, 63-68.

Lu, Z.Y., Jeffrey, M.I., Lawson, F., 2000. The effect of chloride ions on the dissolution of chalcopyrite in acidic solutions. Hydrometallurgy 56, 189-202.

Lundgren, D.G., Silver, M., 1980. Ore Leaching By Bacteria. Annual Reviews in Microbiology 34, 263-283.

Madsen, I.C., Scarlett N.Y. Quantitative Phase Analysis. in powder diffraction Theory and practice, Dinnebier, R.E., Billinge S.L. Eds; RSC publishing, 2008, 298-331.

Majuste, D., Ciminelli, V.S.T., Osseo-Asare, K., Dantas, M.S.S., Magalhães-Paniago, R., 2012. Electrochemical dissolution of chalcopyrite: Detection of bornite by synchrotron small angle X-ray diffraction and its correlation with the hindered dissolution process. Hydrometallurgy 111-112, 114-123.

McIntyre, N. S., Zetaruk, D. G., 1977. X-ray photoelectron spectroscopic studies of iron oxides. Analytical Chemistry 49, 1521-1529.

Mehta, A.P., Murr, L.E. 1983. Fundamental-Studies of the Contribution of Galvanic Interaction to Acid-Bacterial Leaching of Mixed Metal Sulfides. Hydrometallurgy 9, 235-256.

Mehta, A.P., Murr, L.E., 1982. Kinetic Study of Sulfide Leaching by Galvanic Interaction between Chalcopyrite, Pyrite, and Sphalerite on the Presence of *T. ferrooxidans* (30 °C) and a Thermophilic Microorganism (55 °C). Biotechnology and Bioengineering 24, 919-940.

Mernagh, T.P., Trudu, A.G., 1993. A laser Raman microprobe study of some geologically important sulphide minerals. Chemical Geology 103, 113-127.

Metson, J.B., 1999. Charge compensation and binding energy referencing in XPS analysis. Surface and Interface Analysis 27, 1069-1072.

Meyer, G., Schneider-Merck, T., Böhme, S., Sand, W., 2002. A simple method for investigations on the chemotaxis of *A. ferrooxidans* and *D. vulgaris*. Acta Biotechnologica 22, 391-399.

Mikhlin, Y., Tomashevich, Y., Tauson, V., Vyalikh, D., Molodtsov, S., Szargan, R. A., 2005. comparative X-ray absorption near-edge structure study of bornite, Cu_5FeS_4, and chalcopyrite, $CuFeS_2$. Journal of Electron Spectroscopy and Related Phenomena 142, 83-88.

Mikhlin, Y.L., Tomashevich, Y.V., Asanov, I.P., Okotrub, A.V., Varnek, V.A., Vyalikh, D.V., 2004. Spectroscopic and electrochemical characterization of the surface layers of chalcopyrite ($CuFeS_2$) reacted in acidic solutions. Applied Surface Science 225, 395-409.

Miller, A., MacKinnon, A., Weaire, D., 1982. Beyond the Binaries—The Chalcopyrite and Related Semiconducting Compounds Solid State Physics, 36, 119-175.

Miller, J.D., Portillo, H.Q.,1979. Silver catalysis in ferric sulphate leaching of chalcopyrite. In: Lawskosky, A.J. (Ed.), 13th International Mineral Processing Congress. Part A. Elsevier, Amsterdam, pp. 851-901.

Mosselmans, J.F.W., Pattrick, R.A.D., van der Laan, G., Charnock, J.M., Vaughan, D.J., Henderson, C.M.B., Garner, C.D., 1995. X-ray absorption near-edge spectra of transition metal disulfides FeS_2 (pyrite and marcasite), CoS_2, NiS_2,and CuS_2 and their isomorphs FeAsS and CoAsS. Physics and Chemistry of Minerals 22, 311-317.

Muñoz, J., Dreisinger, D., Cooper, W., Young, S, 2007a. Silver-catalyzed bioleaching of low-grade copper ores.: Part I: Shake flasks tests. Hydrometallurgy, 88, 3-18.

Muñoz, J.A., Dreisinger, D.B., Cooper, W.C., Young, S.K., 2007b. Silver catalyzed bioleaching of low-grade copper ores. Part III: Column reactors. Hydrometallurgy 88, 35-51.

Muñoz, P.B., Miller, J.D., Wadsworth, M.E.,1978. Reaction mechanism for the acid ferric sulfate leaching of chalcopyrite Metallurgical and Materials. Transactions B 10B, 149-158

Mussel, W. N., Murad, E., Fabris, J. D., Moreira, W.S., Barbosa, J.B.S., Murta, C.C., Abrahão, W.P., Mello, J.W.V., Garg, V.K., 2007. Characterization of a chalcopyrite from Brazil by Mössbauer spectroscopy and other physicochemical techniques. Physics and Chemistry of Minerals 34, 383-387.

Mycroft, J.R., Bancroft, G.M., McIntyre, N.S., Lorimer, J.W., Hill, I.R., 1990. Detection of sulfur and polysulfides on electrochemically oxidized pyrite surfaces by X-ray photoelectron spectroscopy and Raman spectroscopy Journal of Electroanalytical Chemistry 292, 139-152

Nakai, I., Sugitani,Y., Nagashima, K., Niwa, Y., 1978. X-ray photoelectron spectroscopic study of copper minerals. Journal of Inorganic and Nuclear Chemistry. 40, 789-791.

Nakazawa, H., Fujisawa, H., Sato, H., 1998. Effect of activated carbon on the bioleaching of chalcopyrite concentrate. International Journal of Mineral Processing 55, 87-94.

Nava, D., Gonzalez, I., 2006. Electrochemical characterization of chemical species formed during the electrochemical treatment of chalcopyrite in sulfuric acid. Electrochimica Acta 51, 5295-5303.

Nava, D., Gonzalez, I., Leinen, D., Jose, R., Barrado, R., 2008. Surface characterization by X-ray photoelectron spectroscopy and cyclicvoltammetry of products formed during the potentiostatic reduction of chalcopyrite. Electrochimica Acta 53, 4889-4899.

Nava, J.L., Oropeza, M.T., Gonzalez, I., 2002. Electrochemical characterisation of sulfur species formed during anodic dissolution of galena concentrate in perchlorate medium at pH 0. Electrochimica Acta 47, 1513-1525.

Nazari, G., Dixon, D.G., Dreisinger, D.B., 2011. Enhancing the kinetics of chalcopyrite leaching in the Galvanox (TM) process. Hydrometallurgy, 105, 251-258.

Nazari, G., Dixon, D.G., Dreisinger, D.B., 2011. Enhancing the kinetics of chalcopyrite leaching in the Galvanox™ process. Hydrometallurgy 105, 251-258.

Ndlovu, S. and Monhemius, A.J., 2003. Correlations between reaction rates and evolution of corrosion pits in bacterial leaching of pyrite. Transactions of the Institution of Mining and Metallurgy Section C-Mineral Processing and Extractive Metallurgy, 112, 102-108.

Ndlovu, S., Monhemius, A.J., 2004. The role of orientation of crystal lattice on the development of bacterial leaching patterns on pyrite single crystals. Journal of the South African Institute of Mining and Metallurgy, 104, 573-578.

Ndlovu, S., Monhemius, A.J., 2005. The influence of crystal orientation on the bacterial dissolution of pyrite. Hydrometallurgy, 78, 187-197.

Nesbitt, H. W., Scaini, M., Hochst, H., Bancroft, G. M., Schaufuss, A. G., Szargan, R., 2000. Synchrotron XPS evidence for $Fe2^{+}$-S and Fe^{3+}-S surface species on pyrite fracture-surfaces, and their 3D electronic states. American Mineralogist 85, 850-857.

Nesbitt, H.W., Muir, I.J., 1994. X-ray photoelectron spectroscopic study of a pristine pyrite surface reacted with water vapour and air. Geochimica et Cosmochimica Acta 58, 4667-4679.

Ohrendorf, F.W., Haeuseler, H., 1999. Lattice dynamics of chalcopyrite type compounds. Part I. Vibrational frequencies. Crystal Research and Technology 34, 339-349.

Nesbitt, H.W., Muir, I.J., 1998. Oxidation states and speciation of secondary products on pyrite and arsenopyrite reacted with mine waste waters and air. Minerals and Petroleum 62, 123-144.

Neuburg, H. J., Castillo, J.A., Herrera, M.N., Wiertz, J.V., Vargas, T., Badilla-Ohlbaum, R., 1991. A model for the bacterial leaching of copper sulfide ores in pilot-scale columns. International Journal of Mineral Processing 31, 247-264.

Newville, M. 2001. IFEFFIT: interactive XAFS analysis and fitting. Search ResultsJournal of Synchrotron Radiation 8, 322-324.

Norris, P. R., 1983. Iron and mineral oxidation with Leptospirillum- like bacteria. In Recent Progress in Biohydrometallurgy, pp. 83-96. Edited by G. Rossi & A. E. Torma. Iglesias, Italy: Associazione Mineraria Sarda.

Norris, P. R., Barr, D. W., Hinson, D., 1988. Iron and mineral oxidation by acidophilic bacteria: affinities for iron and attachment to pyrite. In: Biohydrometallurgy, Proceedings of the International Symposium, pp. 43-59. Edited by P. R. Norris & D. P. Kelly. Kew: Science and Technology Letters.

Norris, P. R., Parrot, L., Marsh, R. M., 1986. Moderately thermophilic mineral-oxidizing bacteria. Biotechnology and bioengineering symposium 16, 253-262.

Norris, P.R., Barr, D.W., 1985. Growth and iron oxidation by acidophilic moderate thermophiles. FEMS Microbiology Letters 28, 221-224.

Norris, P.R., Brierley, J.A., Kelly, D.P., 1980. Physiological characteristics of two facultatively thermophilic mineral-oxidizing bacteria. FEMS Microbiology Letters 7, 119–122.

Norris, P.R., Calvo-Bado, L.A., Brown, C.F., Davis-Belmar, C.S., 2012. Ore column leaching with thermophiles: I, copper sulfide ore. Hydrometallurgy 127-128, 62-69.

Ohmura, N., Tsugita, K., Koizumi, J., Saiki, H.,1996. Sulfur binding protein of flagella of *Thiobacillus ferrooxidans*. Journal of Bacteriology 178, 5776-5780.

Ohrendorf, F.W., Haeuseler, H., 1999. Lattice dynamics of chalcopyrite type compounds. Part I. Vibrational frequencies. Crystal Research and Technology 34, 339-349.

Parker, A., Klauber, C., Kougianos, A., Watling, H.R., Bronswijk, W.V., 2003. An X-ray photoelectron spectroscopy study of the mechanism of oxidative dissolution of chalcopyrite. Hydrometallurgy 71, 265-276.

Parker, A.J., Paul, R.L., Power, G.P., 1981. Electrochemistry of the oxidative leaching of copper from chalcopyrite. Journal of Electroanalytical Chemistry and Interfacial Electrochemistry 118, 305-316.

Parker, G.K., 2005. Spectroelectrochemical investigation of chalcopyrite leaching 2005 PhD thesis, Faculty of Fcience, Griffith University.

Parker, G.K., Woods, R., Hope, G.A. 2008. Raman investigation of chalcopyrite oxidation. Colloids and Surfaces A: Physicochemical and Engineering Aspects 318, 160-168.

Paterson, D., Jonge, M.D.D., Howard, D.L., Lewis, W., Mckinlay, J., Starritt, A., Kusel, M., Ryan, C.G., Kirkham, R., Moorhead, G., Siddons, D.P., 2011. The X-ray Fluorescence Microscopy Beamline at the Australian Synchrotron. AIP Conference Proceedings, 1365, 219-222.

Pattrick, R.A.D., Mosselmans, J.F.W., Charnock, J.M., England, K.E.R., Helz, G.R., Garner, C.D., Vaughan, D.J., 1997. The structure of amorphous copper sulfide precipitates: An X-ray absorption study. Geochimica et Cosmochimica Acta 61, 2023-2036.

Pawlek, F., 1976. Hydrometallurgical process for extracting copper from chalcopyrite or bornite concentrates. April. US Patent. 3,949,051..

Pearce, C.I, Pattrick, R.A.D., Vaughan, D.J, Henderson, C.M.B, van der Laan, G., 2006. Copper oxidation state in chalcopyrite: Mixed Cu d 9 and d10 characteristics. Geochimica et Cosmochimica Acta 70, 4635-4642.

Penner-hahn, J. X-ray Absorption Spectroscopy In Comprehensive coordination chemistry II, Volume 2; McCleverty J., Meyer T. Eds.; Elsevier, 2004, 159-186

Petersen, J., Dixon, D.G. 2006. Competitive bioleaching of pyrite and chalcopyrite. Hydrometallurgy 83, 40-49.

Petersen, J., Dixon, D.G., 2002. Thermophilic heap leaching of a chalcopyrite concentrate. Minerals Engineering 15, 777-785.

Petiau, J, Sainctavit, P., Calas, G., 1988. K X-ray Absorption Spectra and Electronic Structure of Chalcopyrite $CuFeS_2$. Materials Science and Engineering B-Solid State Materials for Advanced Technology, 237-249.

Pireaux, J.J., Liehr, M, Thiry, P.A., Delrue, J.P., Caudano, R., 1984. Electron spectroscopic characterization of oxygen adsorption on gold surfaces: II. Production of gold oxide in oxygen DC reactive sputtering. Surface Science 141, 221-232.

Pisapia, C., Chaussidon, M., Mustin, C.,Humbert, B., 2007. O and S isotopic composition of dissolved and attached oxidation products of pyrite by *Acidithiobacillus ferrooxidans*: Comparison with abiotic oxidations. Geochimica et Cosmochimica Acta 71, 2474-2490.

Pradhan, N., Nathsarma, K.C., Srinivasa Rao, K., Sukla, L.B., Mishra, B.K., 2008. Heap bioleaching of chalcopyrite: A review. Minerals Engineering 21, 355-365.

Price, D.W., Warren, G.W., 1986. The influence of silver ion on the electrochemical response of chalcopyrite and other mineral sulfide electrodes in sulfuric acid. Hydrometallurgy 15, 303-324.

Qin, W., Yang, C., Lai, S., Wang, J., Liu, K., Zhang, B., 2013. Bioleaching of chalcopyrite by moderately thermophilic microorganisms. Bioresource Technology 129, 200-208.

Qiu, G.Z., Fu, B., Zhou, H.B., Liu, X., Gao, J., Liu, F.F., Chen, X.H., 2007. Isolation of a strain of *Acidithiobacillus caldus* and its role in bioleaching of chalcopyrite. World Journal of Microbiology and Biotechnology. 23, 1217-1225.

Raj, D., Chandra, K., Puri, S.P., 1968. Mössbauer studies of chalcopyrite. Journal of the Physical Society of Japan. 24, 39–41.

Rawlings, D. E., Tributsch, H., Hansford, G, 1999. Reasons why ' *Leptospirillum* '-like species rather than *Thiobacillus ferrooxidans* are the dominant iron-oxidizing bacteria in many commercial processes for the biooxidation of pyrite and related ores. Microbiology 145, 5-13.

Rawlings, D.E., 2005 Characteristics and adaptability of iron- and sulfur-oxidizing microorganisms used for the recovery of metals from minerals and their concentrates. Microbial Cell Factories 2005, 4, 13.

Rehr, J., Albers, R., 2000. Theoretical approaches to x-ray absorption fine structure. Reviews of Modern Physics 72, 621-654

Rodríguez, Y., Ballester, A., Blázquez, M.L., González, F., Muñoz, J.A., 2003. New information on the chalcopyrite bioleaching mechanism at low and high temperature. Hydrometallurgy 71, 47-56.

Rohwerder, T., Gehrke, T., Kinzler, K., Sand, W., 2003. Bioleaching review part A: Progress in bioleaching: fundamentals and mechanisms of bacterial metal sulfide oxidation. Applied Microbiology and Biotechnology 63, 239-248.

Rohwerder, T., Sand, W., 2003. The sulfane sulfur of persulfides is the actual substrate of the sulfur-oxidizing enzymes from *Acidithiobacillus* and *Acidiphilium* spp. Microbiology 149, 1699-1709.

Rohwerder, T., Sand, W., 2003. The sulfane sulfur of persulfides is the actual substrate of the sulfur-oxidizing enzymes from Acidithiobacillus and Acidiphilium spp. Microbiology 149, 1699-1709.

Rohwerder, T., Sand, W., 2007. Oxidation of inorganic sulfur compounds in acidophilic prokaryotes. Engineering in Life Sciences 7, 301-309.

Ruiz, C. M., Fontané, X., Fairbrothe,r A., Izquierdo-Roca, V., Broussillou, C., Bodnar, S., Pérez-Rodríguez, A., Bermúdez, V., 2013. Impact of electronic defects on the Raman spectra from electrodeposited Cu(In,Ga)Se2 solar cells: Application for non-destructive defect assessment. Appl. Phys. Lett. 102, 091106-1-091106-4Sampson, M.I., Phillips, C.V., Blake, R.C., 2000. Influence of the attachmentof acidophilic bacteria during the oxidation of mineral sulfides. Mineral Engineering13, 373–389.

Sand W, Gehrke T, Jozsa P, Schippers A. (Bio)chemistry of bacterial leaching--direct vs. indirect bioleaching. Hydrometallurgy, 2001, 59, 159-175.

Sandström, Å., Shchukarev, A., Paul, J., 2005. XPS characterisation of chalcopyrite chemically and bio-leached at high and low redox potential. Minerasl Engineering 18, 505-515.

Sartz W.E. , Wynne K.J., Hercules D.M., 1971. X-ray photoelectron spectroscopic investigation of Group VIA elements. Analytic Chemistry 1971, 43, 1884–1887

Sasaki, K., Nakamuta, Y., Hirajima, T., Tuovinen, O.H., 2009. Raman characterization of secondary minerals formed during chalcopyrite leaching with *Acidithiobacillus ferrooxidans*. Hydrometallurgy 95, 153-158.

Schaufuss, A.G., Nesbitt H.W., Kartio, I., Laajalehto, K., Bancroft, G.M, Szargan R., 1998. Reactivity of surface chemical states on fractured pyrite. Surf. Sci. 411, 321-328.

Schippers, A., Jozsa, P., Sand, W., 1996. Sulfur chemistry in bacterial leaching of pyrite. Applied and Environmental Microbiology 62, 3424-3431.

Seah, M.P., 1990. Quantification of AES and XPS. In: Briggs, D., Seah, M.P. (Eds.), Practical Surface Analysis 1. Wiley, Salle + Sauerlander, Chichester, New York, pp. 201–255.

Segerer, A., Neuner, A., Kristjansson, J.K., Stetter, K.O., 1986. Acidianus infernus gen. nov., sp. nov., and Acidianus brierleyi comb. nov.: Facultatively aerobic, extremely acidophilic thermophilic sulfur-metabolizing archaebacteria. International Journal of Systematic Bacteriology 36, 559-564.

Segerer, A.H., Trincone, A., Gahrt,z M., Stetter, K.O, 1991., *Stygiolobus azoricus* gen. nov., sp. nov. represent a novel genus of anaerobic, extremely thermoacidophilic

archaebacteria of the order *Sulfolobale*s. International Journal of Systematic Bacteriology, 49, 495-501.

Sharma, P.K., Das, A., Rao, K.H, Forssberg, K.S.E, 2003. Surface characterization of *Acidithiobacillus ferrooxidans* cells grown under different conditions. Hydrometallurgy, 71, 85–292.

Shirley, D.A., 1972. High-resolution X-ray photoemission spectrum of the valence bands of gold. Physical Review B 5, 4709-4714.

Silverman, M.P. and Lundgren, D.G., 1959. Studies on the chemoautotrophic iron bacterium *Ferrobacillus-ferrooxidans*.1. An improved medium and a harvesting procedure for securing high cell yields. Journal of Bacteriology 77, 642-647.

Smart, R.S.C., Skinner W. M., Gerson, A.R., 1999. XPS of sulphide mineral surfaces: metal-deficient, polysulphides, defects and elemental sulphur. Surface and Interface Analysis 28, 101-105.

Smart, R.S.C.,1991. Surface layers in base metal sulphide flotation. Minerasl Engineering 4, 891-909.

Sokic, M.D., Markovic, B., Zivkovic, D., 2009. Kinetics of chalcopyrite leaching by sodium nitrate in sulphuric acid. Hydrometallurgy 95, 273–9.

Stevenson, A.W., Hall, C. J., Mayo, S. C., Häusermann, D., Maksimenko, A., Gureyev, T.E., Nesterets, Y.I., Wilkins, S.W., Lewis, R.A., 2012. Analysis and interpretation of the first monochromatic X-ray tomography data collected at the Australian Synchrotron Imaging and Medical beamline. Journal of Synchrotron Radiation **19**, 728-750

Stott, M.B., Sutton, D.C., Watling, H.R.,Franzmann, P.D., 2003. Comparative Leaching of Chalcopyrite by Selected Acidophilic Bacteria and Archaea. Geomicrobiology Journal 20, 215-230.

Stott, M.B., Watling, H.R., Franzmann, P.D., Sutton ,D., 2000. Role of iron-hydroxy precipitates in the passivation of chalcopyrite during bioleaching. Minerasl Engineering 13, 1117-1127.

Sugio, T., Suzuki, H., Oto, A., Inagaki, K., Tanaka, H., Tano, T., 1991. Purification and some properties of a hydrogen sulfidebinding protein that is involved in sulfur oxidation of *Thiobacillus ferrooxidans*. Agricultural Biology and Chemistry 55, 2091-2097.

Tamura, H., Goto, K., Yotsuyanagi, T., Nagayama, M., 1974. Spectrophotometric determination of iron(II) with 1,10-phenanthroline in the presence of large amounts of iron(III). Talanta 21, 314-318.

Tan, S.N., Chen, M., 2012. Early stage adsorption behaviour of Acidithiobacillus ferrooxidans at mineral interfaces. Hydrometallurgy 119-120, 87-94.

Tanuma, S., Powell, C.J, Penn, D.R., 1991. Calculations of electron inelastic mean free paths II Data for 27 elements over the 50-2000 eV range. Surface and interface analysis, 17, 911-920.

Third, K.A., Cord-Ruwisch, R.,Watling, H.R., 2000. The role of iron-oxidizing bacteria in stimulation or inhibition of chalcopyrite bioleaching. Hydrometallurgy 57, 225-233.

Third, K.A., Cord-Ruwisch, R.,Watling, H.R., 2002. Control of the redox potential by oxygen limitation improves bacterial leaching of chalcopyrite. Biotechnology and Bioengineering 78, 433-441.

Todd, E.C., Sherman, D.M., Purton, J.A., 2003. Surface oxidation of chalcopyrite ($CuFeS_2$) under ambient atmospheric and aqueous (pH 2–10) conditions: Cu, Fe L- and O K-edge X-ray spectroscopy. Geochimica et Cosmochimica Acta 67, 2137–2146.

Tributsch, H.,2001. Direct versus indirect bioleaching. Hydrometallurgy 59, 77-185

Tshilombo, A.F., 2004. Mechanism and kinetics of chalcopyrite passivation and depassivation during ferric and microbial leaching, University of British Columbia, Vancouver.

Valdés, J., Pedroso, I., Quatrini, R., Dodson, R.J., Tettelin, H., Robert B., Eisen, J.A., Holmes D.S., 2008. Acidithiobacillus ferrooxidans metabolism: from genome sequence to industrial applications. BMC Genomics 2008, 9, 597

Vargas, T., Diaz, P., Escobar, B., 2009. Reductive action of activated carbon on ferric iron interferes on the determination of the oxidative activity of *Acidithiobacillus ferrooxidans* on ferrous iron. In: Donati, E.R., Viera, M.R., Tavani, E.L., Giaveno, M.A.,

Lavalle, T.L., Chiacchiarini, P.A. (Eds.), Biohydrometallurgy: a meeting point between microbial ecology, metal recovery processes and environmental remediation. Trans Tech Publications, Zurich, pp. 291–294.

Velásquez, P., Leinen, D., Pascual, J., Ramos-Barrado, J.R., Grez, P., Gómez, H., Schrebler, R., Del Río, R., Córdova, R., 2005. A Chemical, Morphological, and Electrochemical (XPS, SEM/EDX, CV, and EIS) Analysis of Electrochemically Modified Electrode Surfaces of Natural Chalcopyrite ($CuFeS_2$) and Pyrite (FeS_2) in Alkaline Solutions. The Journal of Physical Chemistry B 109, 4977-4988.

Velásquez-Yévenes L, Nicol M, Miki H., 2010. The dissolution of chalcopyrite in chloride solutions: part 1. The effect of solution potential. Hydrometallurgy 103, 108-113.

Vera, M., Schippers, A., Sand, W., 2013. Progress in bioleaching: fundamentals and mechanisms of bacterial metal sulfide oxidation-part A. Applied Microbiology and Biotechnology. 97, 7529-7541.

Vilcáez, J., Inoue, C., 2009. Mathematical modeling of thermophilic bioleaching of chalcopyrite. Minerasl Engineering 22, 951-960.

Vilcaez, J., Suto, K., Inoue, C., 2008. Bioleaching of chalcopyrite with thermophiles: Temperature–pH–ORP dependence. Int. J. Miner. Process. 88, 37-44.

Vogt, S. 2003. MAPS : A set of software tools for analysis and visualization of 3D X-ray fluorescence data sets. Journal de Physique IV 104, 635-638.

Von Oertzen, G., Harmer, S., Skinner, W.M., 2006. XPS and ab initio calculation of surface states of sulfide minerals: pyrite, chalcopyrite and molybdenite. Molecular Simulation 32, 1207-1212.

Wan, R.Y., Miller, J.D., Foley, J., Pon, S., 1984. Electrochemical features of the ferric sulfate leaching of CuFeS2/C aggregates. In: Richardson, P.E., Srinivasan, S., Woods, R. (Eds.), Electrochemistry in Mineral and Metal Processing. Electrochemical Society, Pennington, NJ, pp. 391-416.

Warner, S., Butle, I. Raman and FT-Raman Spectroscopy In Comprehensive coordination chemistry II, Volume 2; McCleverty J., Meyer T. Eds.; Elsevier, 103-112

Watling, H.R. The bioleaching of sulphide minerals with emphasis on copper sulphides — A review. Hydrometallurgy 84, 81-108.

Xia, J.L., Yang, Y., He, H., Liang, C.L., Zhao, X.J., Zheng, L., Ma, C.Y., Zhao, Y.D., Nie, Z.Y., Qiu, G., 2010. Investigation of the sulfur speciation during chalcopyrite leaching by moderate thermophile *Sulfobacillus thermosulfidooxidans*. International Journal of Mineral Processing 94, 52-57.

Xia, J.L., Yang, Y., He, H., Zhao, X.J., Liang, C.L., Zheng, L., Ma, C.Y., Zhao, Y.D., Nie, Z.Y., Qiu, G.Z., 2010. Surface analysis of sulfur speciation on pyrite bioleached by extreme thermophile Acidianus manzaensis using Raman and XANES spectroscopy. Hydrometallurgy 100, 129-135.

Yang D. Photoelectron Spectroscopy. in Comprehensive coordination chemistry II, Volume 2; McCleverty J., Meyer T. Eds.; Elsevier, 2004: 187-196

Yang, Y., Liu, W, Chen, M., 2013. A copper and iron K-edge XANES study on chalcopyrite leached by mesophiles and moderate thermophiles. Minerals Engineering 48, 31-35.

Yang, Y., Diao, M., Liu, K., Qian, L., Nguyen, A.V., Qiu, G., 2013. Column bioleaching of low-grade copper ore by *Acidithiobacillus ferrooxidans* in pure and mixed cultures with a heterotrophic *acidophile Acidiphilium* sp. Hydrometallurgy, 131-132, 93-98.

Yang, Y.S., Furman, S. Tulloh, A., 2008. Adata-constrained 3D model for material compositional microstructures Advanced Materials Research vol 32: Frontiers in Materials Science & Technology J Bell et al., eds. 267-270.

Yarzábal, A., Brasseur, G., Appia-Ayme, C., Ratchouchniak, J., Lund, K., Lemesle-Meunier, D., DeMoss, J.A., Bonnefoy, V., 2002. The high molecular weight cytochrome c Cyc2 of Acidithiobacillus ferrooxidans is an outer membrane protein. Journal of Bacteriology, 184, 313-317.

Yin, Q., Kelsall, G.H., Vaughan, D.J., England, K.E.R., 1995. Atmospheric and Electrochemical Oxidation of the Surface of Chalcopyrite ($CuFeS_2$). Geochimica et Cosmochimica Acta 59, 1091-1100.

Yu, D., Wu, C., Kong, Y., Xue, N., Guo, X., Ding, W., 2007. Structural and catalytic investigation of mesoporous iron phosphate. The Journal of Physical Chemistry C 111, 14394-14399.

Yu, R.L., Zhong, D.L., Miao, L., Wu, F.D., Qiu, G.Z., Gu, G.H., 2011. Relationship and effect of redox potential, jarosites and extracellular polymeric substances in bioleaching chalcopyrite by *Acidithiobacillus ferrooxidans*. Transactions of Nonferrous Metals Society of China 21, 1634-1640.

Zeng, W., Qiu, G., Zhou H., Chen M.,2011. Electrochemical behaviour of massive chalcopyrite electrodes bioleached by moderately thermophilic microorganisms at 48℃. Hydrometallurgy 105, 259-263.

Zeng, W., Tan S.N., Chen, M., Qiu G., 2011. Detection and analysis of attached microorganisms on the mineral surface during bioleaching of pure chalcopyrite with moderate thermophiles. Hydrometallurgy 106, 46–50.

Zeng,W.M, Qiu, G.Z, Zhou, H.B., Peng, J.H, Chen, M, Tan, S.N, Chao, W.L, Liu, X.D, Zhang Y.S., 2010. Community structure and dynamics of the free and attached microorganisms during moderately thermophilic bioleaching of chalcopyrite concentrate. Bioresource Technology 101, 7068-7075.

Zhang, W.M., Gu, S.F., 2007. Catalytic effect of activated carbon on bioleaching of lowgradeprimary copper sulfide ores. Transactions of Nonferrous Metals Society of China 17, 1123-1127.

Zhou, H.B., Zeng, W.M., Yang, Z.F., Xie, Y.J., Qiu, G.Z., 2009. Bioleaching of chalcopyrite concentrate by a moderately thermophilic culture in a stirred tank reactor. Bioresource Technology 100, 515-520.

Zhu, W, Xia, J.L., Yang, Y., Nie, Z.Y., Zhen,g L., Ma, C.Y., Zhang, R.Y, Peng A.A, Tang, L., Qiu, G.Z., 2011. Sulfur oxidation activities of pure and mixed thermophiles and sulfur speciation in bioleaching of chalcopyrite. Bioresource Technology 102, 3877-3882.